Analytical Fragility Curves for Highway Bridges in Moderate Seismic Zones

A Thesis
Presented to
The Academic Faculty

by

Bryant G. Nielson

In Partial Fulfillment
of the Requirements for the Degree
Doctor of Philosophy

School of Civil and Environmental Engineering
Georgia Institute of Technology
December 2005

Analytical Fragility Curves for Highway Bridges in Moderate Seismic Zones

Approved by:

Dr. Reginald DesRoches, Advisor
School of Civil and Environmental Engineering
Georgia Institute of Technology

Dr. Barry J. Goodno
School of Civil and Environmental Engineering
Georgia Institute of Technology

Dr. Bruce R. Ellingwood
School of Civil and Environmental Engineering
Georgia Institute of Technology

Dr. Glenn J. Rix
School of Civil and Environmental Engineering
Georgia Institute of Technology

Dr. Steven P. French
College of Architechture
Georgia Institute of Technology

Date Approved: November 23, 2005

I would like to dedicate this work to my wife Kimberly and my four children Andrew, Heidi, Tyler and Alex.

ACKNOWLEDGEMENTS

At the end of every journey there lies a road behind, built and defined by those around us. My graduate tenure at Georgia Tech has been no different. This has been a positive experience upon which I will often reflect with great fondness. I would like to thank all those people who have made it so.

Great thanks go to my advisor Dr. Reginald DesRoches who has shown an undeserved degree of patience and council to, what many would call, a less than conventional graduate student. He has ensured that I have had experiences and opportunities that will provide a solid foundation for my future.

I would also like to thank my thesis committee Dr. Bruce Ellingwood, Dr. Barry Goodno, Dr. Glenn Rix and Dr. Steven French. They have provided encouragement, praise and guidance throughout this process. I know Dr. Ellingwood must have felt like a second advisor considering the many hours I spent his office discussing reliability and probability. I also greatly appreciate his willingness to be my mentor as I taught my first college level class.

No graduate experience is complete without developing a camaraderie with fellow graduate students. Much of the education I received, both technical and nontechnical, came through long and detailed discussions with office mates and others. I would like to give thanks to Leonardo, Bassem, Jason, Jamie, Joonam, Peeranan, Susendar, Sean, Matthew, Junwon and the many other students with whom I've been associated.

When Nathan began commuting with me to school every day, I don't think he realized the cost of his decision. Many of the commutes were spent with him answering and helping me address the countless questions and problems I encountered throughout my research. I offer my sincerest thanks for the help.

I would be remiss if I didn't acknowledge the contribution and support I have received from my parents and my in-laws. Over the years they have expressed confidence in my abilities and let me know that I can accomplish anything to which I set my mind. My deep love and appreciation is extended to them.

Finally, I would like to express by deepest and most heart felt gratitude to my wife, Kimberly, and my four children Andrew, Heidi, Tyler and Alex. No road is void of stumbling block and pot holes, but my family has always been there to pull me up whenever I fell. This experience has required a lot of personal sacrifice from Kimberly, including financial, physical and emotional. It was more than I had right to ask but something she was willing to give. To her and the kids I not only give my thanks but also my love.

TABLE OF CONTENTS

LIST OF TABLES

LIST OF FIGURES

SUMMARY

Historical seismic events such as the San Fernando earthquake of 1971 and the Loma Prieta earthquake of 1989 did much to arouse an awareness of the vulnerabilities that many existing highway bridges possess. However, it was not until 1990 that this awareness and concern extended past the highly seismic regions of California and settled on moderate seismic regions such as the Central and Southeastern United States (CSUS). This relatively long neglect of seismic issues pertaining to bridges in these moderate seismic zones has resulted in a portfolio of existing bridges with seismic deficiencies which must be assessed and addressed.

An emerging decision tool, whose use is becoming ever increasingly popular in the assessment of this seismic risk, is that of seismic fragility curves. Fragility curves are conditional probability statements which give the probability of a bridge reaching or exceeding a particular damage level for an earthquake of a given intensity level. As much research has been devoted to the implementation of fragility curves in risk assessment packages, a great need has arisen for bridge fragility curves which are reliable, particularly for those in moderate seismic zones. The purpose of this study is to use analytical methods to generate fragility curves for nine bridge classes which are most common to the CSUS. This is accomplished by first considering the existing bridge inventory and assessing typical characteristics and details from which detailed 3-D analytical models are created. The bridges are subjected to a suite of synthetic ground motions which were developed explicitly for

the region. Probabilistic seismic demand models (PSDM) are then generated using these analyses. From these PSD models, fragility curves are then generated by considering specific levels of damage which may be of interest. The fragility curves show that the most vulnerable of all the bridge nine bridge classes considered are those utilizing steel girders. Concrete girder bridges appear to be the next most vulnerable followed by single span bridges of all types. Various sources of uncertainty are considered and tracked throughout this study, which allows for their direct implementation into existing seismic risk assessment packages such as HAZUS and REDARS.

CHAPTER I

INTRODUCTION

1.1 Problem Description

An emerging tool in seismic risk assessment (SRA) is the use of fragility curves. A fragility curve is a conditional probability that gives the likelihood that a structure will meet or exceed a certain level of damage for a given ground motion intensity. Currently, fragility curves are derived using empirical data from past earthquakes, expert opinions or via analytical methods. Empirical fragility curves often lack adequate data and are only applicable to limited regions. Also, their refinement is highly dependent on the bridge inventory of the seismically affected region. Fragility curves based on expert opinion are also very subjective in that they rely heavily upon the experts' seismic experience with the bridges under consideration. Previously developed analytical fragility curves are based on simplified models and simplified methodologies, which by their very nature include a significant amount of epistemic uncertainty, and therefore do not completely represent the performance of most bridges. To adequately represent the fragility of a bridge and to improve the reliability and effectiveness of seismic risk assessment tools, improved fragility curves for highway bridges are needed.

Reliable bridge fragility curves are needed for more than just seismic risk assessment. They have uses in other activities such as bridge retrofit prioritization and post-earthquake emergency response. The retrofit prioritization procedure put forth by the

Federal Highway Administration in 1995 utilized a subjective vulnerability rating system for their bridges (FHWA, 1995b). However, it was recognized that a more objective approach should be made available to prioritize highway bridges for retrofit. In a draft of the newest retrofit manual, an alternative seismic vulnerability rating procedure, which utilizes fragility curves, is recommended (MCEER, 1999). This now permits fragility curves for as-built and retrofitted bridges to be used for retrofit prioritization by highlighting the most vulnerable bridge types in a particular highway transportation network. Thus, the impact of various retrofit strategies on both bridge and network performance is estimated.

As mentioned previously, fragility curves can also be used in the post-earthquake response and evaluation of bridge structures. Immediately following an earthquake, a rapid assessment and assignment of functional levels must be assigned to all bridges in an affected network. Using fragility curves to help streamline reconnaissance efforts has been shown to effectively reduce the duration of the functional assessment stage of recovery (Ranf et al., 2003). This application for fragility curves is currently being formalized in a post earthquake response assessment package for California named ShakeCast Wald et al. (2004).

As shown, bridge fragility curves have many important uses in both pre-earthquake and post-earthquake activities. However, if they are to be effectively and actively used in these activities, it is imperative that reliable fragility curves are available. Engineers, politicians and other decision makers must have confidence in the data before they will use it. To this end, this study looks at developing analytical fragility curves for bridge classes typical to the Central and Southeastern United States (CSUS) region also referred to as the Mid-America region. These curves are developed using detailed non-linear bridge models and

time history analyses in Monte Carlo type simulations with the use of variance reduction techniques. All vulnerable major bridge components are considered in the fragility curve development.

1.2 Objectives and Scope of Research

The goal of this study is to refine an exiting methodology for the development of analytical seismic fragility curves for bridge classes that are typical to the CSUS region. The CSUS is a moderate seismic zone in which the seismic risk mitigation effort has lagged the effort made by the states located in the Western United States. Although there have been a number of studies to develop fragility curves, the majority have focused on the bridge classes typical to high seismic zones in the Western US and Japan. More focus is now being placed upon the CSUS because of the recognition of potential for large ground shaking. To aid in the assessment of seismic risk for the region, nine typical bridge classes have been selected for the development of seismic fragility curves. The level of detail that is used and the refinement of the analytical methodology will aid in generating more reliable fragility curves than what are currently available.

The specific tasks that will be completed as part of this research are as follows:

1. Identify the most common bridge types to the Central and Southeastern United States and statistically describe some of their major structural parameters. The identified bridge classes should represent a majority of the overall inventory for the region.

2. Identify a suite of synthetic ground motions that is representative of the seismic hazard for the region.

3. Generate 3-D non-linear analytical models of the selected bridge classes using detailed analytical models of the various bridge components.

4. Identify the most significant structural parameters in the bridge models though a statistically based screening study.

5. Generate probabilistic seismic demand models (PSDM's) for the bridge components in each bridge class.

6. Explore the impact of using various earthquake intensity measures on the probabilistic seismic demand models.

7. Identify the appropriate capacities and limit states for the components of each bridge type.

8. Generate seismic fragility curves for each of the bridge classes and their individual components.

1.3 Outline of Thesis

This thesis is organized into nine chapters with the following contents:

Chapter 2 summarizes previous research in the area of bridge fragility curves.

Chapter 3 examines the seismic hazard and earthquake history of the Central and Southeastern United States. Two suites of synthetic ground motions for the CSUS are presented.

Chapter 4 presents an in-depth look of the bridge inventory for the Central and Southeastern United States. This is done using the National Bridge Inventory (NBI) and includes statistical data on a number of different geometric parameters.

Chapter 5 presents detailed analytical models for the major bridge components of bridge types found in the Central and Southeastern United States. 3-D analytical bridge models are subjected to a scenario earthquake to illustrate the typical seismic response of each bridge class.

Chapter 6 looks at the various structural parameters that are used in the analytical models of the subject bridges. Screening studies are performed and presented to highlight the significance of the various modeling parameters.

Chapter 7 evaluates the seismic demand on the subject bridge types through the use of probabilistic seismic demand analyses. Two intensity measures, peak ground acceleration (PGA) and spectral acceleration (S_a), are considered and investigated for their influence on the degree of uncertainty in the resulting PSDMs.

Chapter 8 presents the results of the fragility analyses for the various bridge components and bridge types. These fragility curves are compared with those which are used in the current edition of the Federal Emergency Management Agency's (FEMA) risk assessment package, HAZUS.

Finally, in Chapter 9, a summary and conclusions are drawn from the research and future research needs are outlined.

CHAPTER II

OVERVIEW OF BRIDGE FRAGILITY WORK

With the occurrence of every major earthquake an increase social awareness of society's seismic vulnerability is witnessed. As a result of this increased awareness, much research has been conducted to help quantify the potential social and economic losses of communities across the nation. Bridge fragility curves have grown from this surge in research as they are an essential component to the risk assessment methodology. It is difficult to talk about the origin of bridge seismic fragility curves without first outlining seismic risk assessment of networks.

2.1 Seismic Risk Assessment

Seismic risk describes the potential for damage or losses that a region is prone to experience following a seismic event. This is in contrast to seismic hazard, which quantifies the recurrence rates of different ground motions. Seismic risk can also be defined as the spatially and temporally integrated product of the seismic hazard, the value of assets and the fragility of assets (Jacob, 1992).

In Figure 2-1, Basoz and Kiremidjian (1996) present a seismic event time-line which illustrates the events that take place before and after a seismic event. The first of these events is to assess the seismic risk, which estimates the potential losses that may occur as a result of the remainder of the events on the time-line. The assessment of these potential

losses is done through the use of seismic risk assessment tools such as HAZUS (FEMA, 2003) and REDARS (Werner et al., 2003) which can be conducted on large and small scale regions. Highway transportation systems play a significant role in the overall impact that a seismic event has on a region because it interconnects with the other infrastructure in the region.

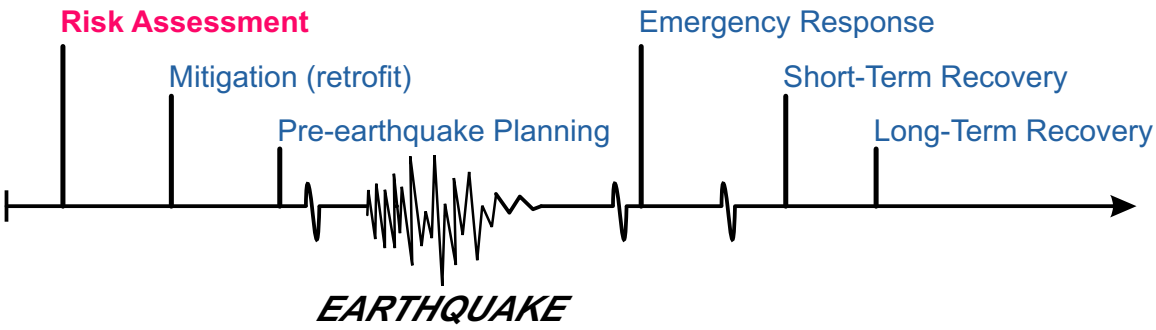

Figure 2-1: Seismic event time-line (Basoz and Kiremidjian, 1996).

A system, such as a highway system, is configured into a network which will consist of a large number of links and nodes (Chang and Nojima, 1998; Kameda, 2000). The disruption of any of these links (e.g. roadway) or nodes (e.g. bridge or tunnel) can disrupt a section of the network, the impact of which is dependent on the redundancy in the system (Rojahn et al., 1992). Thus, a systems or network analysis of a highway system is required to be able to link structural damage of a bridge or roadway to social and economic impacts (Chang and Nojima, 1998; Werner and Taylor, 2002). This network distribution is what sets highway systems and other lifelines (e.g electrical, water and communications) apart from other facilities and functions in a community and warrants special attention.

2.2 Transportation Network Risk Assessment

The risk assessment of a transportation network, which is the first item in the earthquake time-line, is interrelated with the rest of the events on the time-line. This assessment has a circular dependency with the other events on the time-line in that it plays a key role in determining how the rest of the events in the earthquake time-line unfold. However, an analysis and forecast of the other events is necessary to make an assessment of the seismic risk.

Seismic risk assessment methodologies for transportation systems have been proposed and performed by many people since the inception of lifeline earthquake engineering back in the 1970's (ATC, 1985, 1991; King et al., 1997; Shinozuka et al., 1997; Veneziano et al., 2002; Werner et al., 1997). All of the methodologies that have been proposed are conceptually the same and are represented by the lifeline risk assessment flow chart that is given in Figure 2-2. The basic process is to assess the seismic hazard followed by the estimation of physical damage to the lifeline components as a result of that seismic hazard. Fragility curves for the network components are essential inputs into the damage estimation algorithm. In the case of highway networks this would include highway bridge fragility curves. These fragility curves are then used to estimate the physical damage to the bridge which in turn is used to estimate the cost to repair the damage. In addition to repair cost, this damage estimate is also used to estimate post-earthquake functionality and restoration times of the individual network components. Once the component functionality information is obtained it can be used in a network analysis to assess the functionality and restoration time of the

entire network. The loss of functionality of the network system is directly related to the social and economic losses experienced following an earthquake.

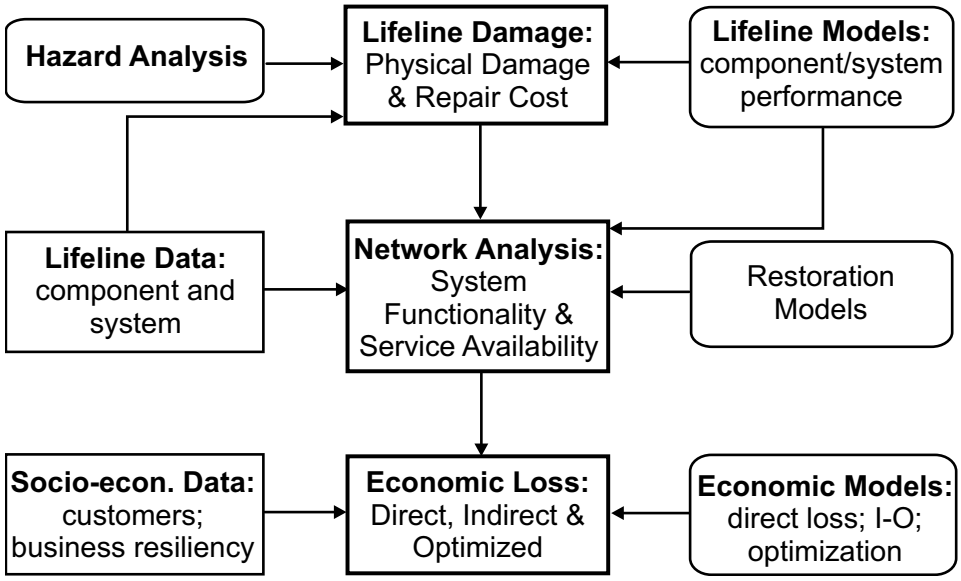

Figure 2-2: Network risk assessment framework (King et al., 1997)

One of the first attempts to formalize this seismic risk methodology is found in the seminal work by Whitman et al. (1975). The methodology they proposed, which is called "Seismic Design Decision Analysis" (SDDA), provided an organized systematic framework for considering the effects of seismic hazard, building damage, direct costs and incident costs. This study really provided the intellectual foundation for subsequent seismic risk assessment studies. In 1985, the Applied Technology Council (ATC) built upon the work of Whitman et al. (1975) to assemble a package for seismic risk assessment of the infrastructure in California (ATC, 1985). This study required the generation of the vulnerability functions for many different building types, facilities and lifeline components, in the

form of damage probability matrices. Because there had been very little data gathered from previous earthquakes, these damage matrices had to be generated based on expert opinion. The experts that participated in the surveys not only had to give their best guess as to the probability of a certain amount of damage, but also were required to use their best judgment in assessing the post-earthquake functionality and restoration time for the various buildings and lifeline components.

The ATC study offered a first step in the implementation of an earthquake risk assessment program, but it was deficient in several areas. First, the damage matrices and restoration times that were developed were only good for California's inventory and second, there was a shortage of information and understanding concerning the assessment of lifelines. In 1991, the Applied Technology Council attempted to remedy this by putting together another report that focused solely on the disruption of lifelines following a seismic event. This program was valid not only for California but for the conterminous United States (ATC, 1991).

Some of the changes that were implemented in the ATC-25 report were modifications to the damage matrices and restoration functions. The damage matrices for the individual lifeline components were changed into continuous damage functions known as fragility curves. These fragility curves were generated by a regression of the discrete values of the various damage probability matrices. There was also a methodology presented whereby these damage functions could be modified for use anywhere in the conterminous United States. In addition to the changes made to damage estimation, the restoration functions were also refined. These restoration functions were initially presented in the ATC-13 report as the time to achieve 30 percent, 60 percent and 100 percent functionality but they were

further discretized in the ATC-25 report to generate more detailed step functions for the various components (ATC, 1991).

In an attempt to push forward the earthquake risk assessment methods, the Federal Emergency Management Association (FEMA) put together a panel of experts to generate a geographical information system (GIS) based risk assessment software package. The first edition of this software was released in 1997 and was called "HAZards US" or HAZUS. This software package, which was written to incorporate the damage to buildings, facilities and lifelines, relied heavily upon the methodology and data that was presented in the ATC-13 report. Regressions of the damage probability data as well as the restoration data were performed and implemented into HAZUS. It was recognized at the time that these damage and restoration functions were based on expert opinion and would need to be updated and modified as more earthquakes occurred, more data was gathered and better estimation methodologies were developed. Some of these improvements, as they apply to both the Eastern and Western US, were implemented in the 1999 and 2003 versions of HAZUS.

2.3 Fragility Functions

The risk assessment of lifelines presented in Figure 2-2 shows that one of the key links in the assessment methodology is to estimate the damage to the lifeline components. This is done by estimating the performance of the various highway bridges in the network as a function of a ground motion intensity parameter. This bridge performance is commonly represented in either a damage probability matrix or a fragility function.

A fragility function is a conditional probability that gives the likelihood that a structure will meet or exceed a specified level of damage for a given ground motion intensity measure. This conditional probability is given in Equation 2.1.

$$Fragility = P[LS|IM = y] \tag{2.1}$$

where LS is the limit state or damage level of the bridge or bridge component, IM is the ground motion intensity measure and y is the realization of the chosen ground motion intensity measure. One can see from this formulation that given an earthquake of a specific intensity, a prediction of the damage level may be made for each bridge for which a fragility function is defined. Figure 2-3 gives a graphical representation of the continuous form of this function.

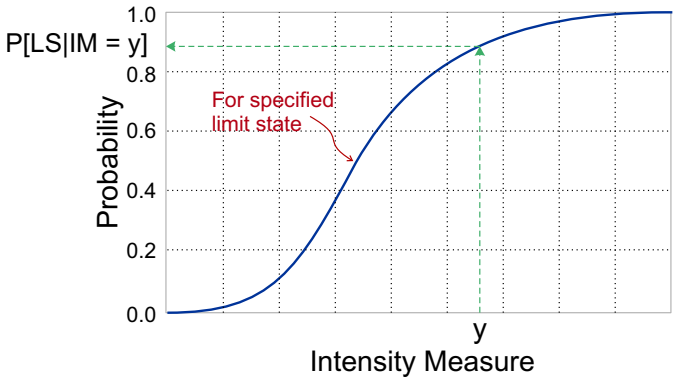

Figure 2-3: Fragility Curve Example.

This probabilistic way of estimating structural damage was used in the evaluation of nuclear facility vulnerabilities in the late 1970s and early 1980s and since then has expanded

into other areas of structural engineering. There are a number of different methodologies that have been employed in the determination of these structural fragilities, a synopsis of which is given in the following sections.

2.3.1 Expert Based Fragility Functions

When the Applied Technology Council (ATC) developed the ATC-13 report, there was a relatively small amount of recorded data available for use in the generation of damage probability matrices. The data shortage was present for various types of structures and facilities including various types of lifeline components. This lack of information necessitated the use of expert opinion for the generation of these damage matrices. The ATC put together a panel of 42 experts whom they could query concerning the various components of a typical Californian infrastructure (ATC, 1985). Only four of the 42 experts were chosen to provide information for highway bridges.

The questionnaires that were created queried the experts on the probability of a bridge being in one of seven damage states for a given Modified-Mercalli Intensity (MMI) value. They also asked the experts to rate themselves on their experience in the field using a scale from zero to ten. After the questionnaires were completed and analyzed, the results were given back to the experts for a second look. They were permitted to consider the overall results and compare them with their initial responses and make any modifications they felt were necessary. These results were then compiled and reported as the damage probability matrices (DPM) for bridges in the ATC-13 report and were subsequently used in the ATC-25 report (ATC, 1991).

There are several major concerns with this methodology, one of which is the subjectivity of the procedure. There is little, if any, correlation to actual earthquake damage reports and is based solely on the experience and number of experts queried. Another concern is that the DPMs were created for only two classes of bridges, major (spans over 500 feet) and conventional (spans under 500 feet). Thus, a high level of uncertainty is present but not quantified in these results. This uncertainty comes as a consequence of human judgment and also the coarseness of the bridge classes.

2.3.2 Empirical Fragility Functions

Following the 1989 Loma Prieta and 1994 Northridge earthquakes, empirical bridge fragility curves became more common as a direct result of more complete ground motion and bridge damage data. Empirical fragility curves are generated from actual earthquake data. This methodology has been presented and demonstrated by several groups of people for the Loma Prieta and Northridge earthquakes such as Basoz and Kiremidjian (1997), Der Kiureghian (2002), Shinozuka et al. (2003) and Elnashai et al. (2004) and by Shinozuka et al. (2000) and Yamazaki et al. (1999) for the 1995 Kobe earthquake.

Although there are some slight variations in the methods used by the aforementioned groups they are conceptually the same. The procedure requires that a post-earthquake assessment be performed where a damage state would be assigned to all the bridges that belong to the bridge class being considered. A shake map, that geographically defines the ground motion in terms of some intensity measure, such as peak ground acceleration (PGA) is used to assign each bridge to a damage state and a given ground motion intensity in a damage frequency matrix. Table 2-1 is an example of a damage frequency matrix that was

Table 2-1: Damage Frequency Matrix for Multi-Span Bridges (Basoz and Kiremidjian, 1997).

	USGS Peak Ground Acceleration (g)						
Observed Damage	**0.15-0.2**	**0.2-0.3**	**0.3-0.4**	**0.4-0.5**	**0.5-0.6**	**0.6-0.7**	**0.7-0.8**
None	194	262	150	31	10	15	17
Minor	2	8	16	2	6	4	2
Moderate	1	8	8	9	6	5	1
Major	0	6	0	5	5	3	1
Collapse	0	0	0	0	0	0	0
Total	197	284	174	47	27	27	21

	USGS Peak Ground Acceleration (g)						
Observed Damage	**0.8-0.9**	**0.9-1.0**	**1.0-1.1**	**1.1-1.2**	**1.2-1.3**	**1.3-1.4**	**Total**
None	18	7	9	1	0	1	717
Minor	0	5	1	1	0	0	47
Moderate	4	7	3	0	0	0	52
Major	1	9	0	0	0	0	30
Collapse	2	1	1	0	0	0	4
Total	25	29	14	2	0	1	848

assembled by Basoz and Kiremidjian (1997) for all multi-span bridges damaged during the 1994 Northridge earthquake. Thus, a percentage of the overall bridge class inventory may be displayed for each damage state and at each ground motion intensity level as shown in Table 2-2.

This information can be used in any number of ways. Basoz and Kiremidjian (1997) used a logistic regression analysis to generate the fragility curves, shown in Figure 2-4, from the damage matrices shown in Tables 2-1 and 2-2. Shinozuka et al. (2000) recommended using the Maximum Likelihood method in conjunction with hypothesis and goodness-of-fit tests to estimate the parameters of the two parameter lognormal probability distribution while Der Kiureghian (2002) used a Bayesian approach and the Likelihood function to accomplish this task.

Table 2-2: Damage Probability Matrix for Multi-Span Bridges (%) (Basoz and Kiremidjian, 1997).

	USGS Peak Ground Acceleration (g)						
Observed Damage	**0.15-0.2**	**0.2-0.3**	**0.3-0.4**	**0.4-0.5**	**0.5-0.6**	**0.6-0.7**	**0.7-0.8**
None	98.5	92.3	86.2	66.0	37.0	55.6	81.0
Minor	1.0	2.8	9.2	4.3	22.2	14.8	9.5
Moderate	0.5	2.8	4.6	19.2	22.2	18.5	4.8
Major	0.0	2.1	0.0	10.6	18.5	11.1	4.8
Collapse	0.0	0.0	0.0	0.0	0.0	0.0	0.0

	USGS Peak Ground Acceleration (g)					
Observed Damage	**0.8-0.9**	**0.9-1.0**	**1.0-1.1**	**1.1-1.2**	**1.2-1.3**	**1.3-1.4**
None	72.0	24.1	64.3	50.0	0.0	100.0
Minor	0.0	17.2	7.1	50.0	0.0	0.0
Moderate	16.0	24.1	21.4	0.0	0.0	0.0
Major	4.0	31.0	0.0	0.0	0.0	0.0
Collapse	8.0	3.5	7.1	0.0	0.0	0.0

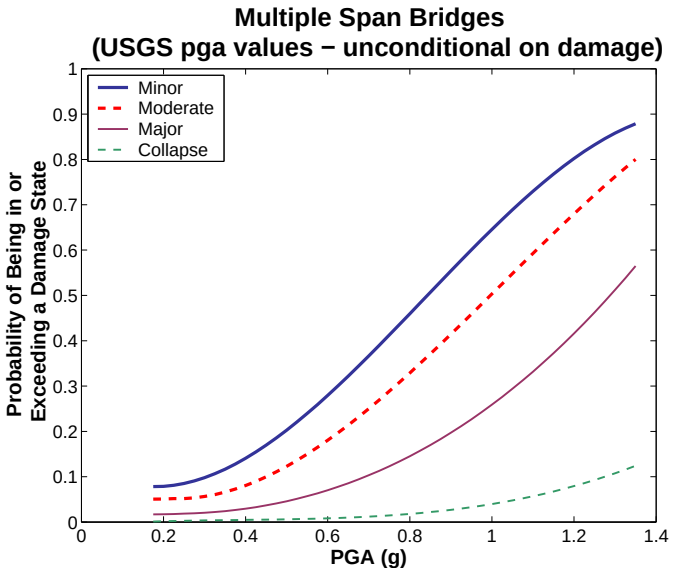

Figure 2-4: Empirical fragility curves for Multi-Span Bridges (Basoz and Kiremidjian, 1997)

Although this method is relatively straight forward it has some drawbacks and limitations. The first limitation is that it is difficult to get an adequate number bridges belonging to one bridge class that lie in a particular damage state. When this is the case it is difficult to get statistically significant results (Shinozuka, 1998). Thus, it is often required to group classes together to get enough bridges in a given damage state and hence reduces the usefulness of the fragility curves.

A second limitation that Basoz and Kiremidjian noted in their generation of fragility curves for several classes of bridges, in both the Loma Prieta and Northridge earthquakes, was that the ground motion intensity (Shakemaps) were different depending on who generated them. They received two different maps with different values for the Northridge earthquake (USGS and WCFS).

A third limitation of empirical fragility curves is that when post-earthquake assessments of bridges are made and damage levels assigned, there is often a discrepancy between the damage levels that any two different inspectors would assign (Basoz and Kiremidjian, 1997). Thus another significant source of uncertainty is entered into the curves.

2.3.3 Analytical Fragility Functions

When actual bridge damage and ground motion data are not available, analytical fragility curves must be used to assess the performance of highway bridges. There have been many researchers that have developed analytical fragility curves for bridges using a variety of different methodologies. Since damage states are related to structural capacity (C) and the ground motion intensity parameter is related to structural demand (D), the fragility or

probability of failure (p_f), can then be described as in Equation 2.2. This specifically gives the probability that the seismic demand will exceed the structural capacity.

$$p_f = P\left[\frac{D}{C} \geq 1\right] \tag{2.2}$$

This probability is generally modeled as a lognormal probability distribution. It is chosen because is has shown to be a good fit in the past and is convenient for manipulation using conventional probability theory (Wen et al., 2003). In addition, when the structural capacity and demand roughly fit a normal or lognormal distribution, using the central limit theorem, it can be said that the composite performance will be lognormally distributed (Kottegoda and Rosso, 1997) . Thus the fragility curve can be represented by a lognormal cumulative distribution function which is given in Equation 2.3 (Melchers, 2001)

$$P_f = \Phi\left(\frac{\ln S_d/S_c}{\sqrt{\beta_d^2 + \beta_c^2}}\right) \tag{2.3}$$

where S_c is the median value of the structural capacity defined for the damage state, β_c is the dispersion or lognormal standard deviation of the structural capacity, S_d is the seismic demand in terms of a chosen ground motion intensity parameter, β_d is the logarithmic standard deviation for the demand and $\Phi[\cdot]$ is the standard normal distribution function.

Referring to Equation 2.3, it can be seen that the structural demand and capacity must be modeled to generate analytical fragility curves. There are a number of methodologies which have been used by researchers to accomplish this task. The methodologies they have employed range from simplistic to fairly rigorous. The following sections introduce some of these methodologies.

2.3.3.1 Elastic Spectral Response

Generating a seismic fragility curve by looking at the elastic spectral response of a bridge is perhaps one of the simplest and least time consuming approaches available. Yu et al. (1991) illustrated the use of this approach when they where trying to assess the seismic vulnerability of highway bridges in Kentucky . They modeled each of the bridge piers as single degree of freedom (SDOF) structures and then estimated their response using an elastic response spectrum. Although the work here was very simplistic, the methodology was further developed and applied by Jernigan and Hwang (2002) with the intent of providing a way for practicing engineers to be able to assess bridge fragilities.

In this methodology, Capacity/Demand (C/D) ratios are generated for the various bridge components. The capacities of the bridge components are calculated according to the Federal Highway Administration's (FHWA) *Seismic Retrofitting Manual for Highway Bridges* (FHWA, 1995b). Following a statistical sampling of various structural parameters (e.g. concrete strength and steel strength), the FHWA's procedure for calculating component capacities was performed for 50 bridge samples.

The demand on the bridges was determined by performing an elastic spectral analysis of the bridge models using a computer program. Uncertainty is included from the demand side by introducing a seismic force factor, SFF. This factor is assumed to follow a lognormal distribution with a mean value of one and a coefficient of variation of 0.5. Calculation of the seismic response coefficient (C_s), as provided by AASHTO (1998), is given in Equation 2.4, where A is the peak ground acceleration, T is the fundamental period of the bridge, S is a term accounting for the site soil condition and SFF is a randomizing term.

$$C_s = (SFF)\frac{1.2AS}{T^{\frac{2}{3}}} \tag{2.4}$$

Once the capacities and demands are calculated for the components in each of the earthquake-bridge samples, the C/D ratio is determined and correlated to a particular damage state. This is done for varying levels of peak ground acceleration. The results from all of these simulations are then put into damage frequency matrix. Fragility curves are then calculated much the same way they are done for empirical fragility curves. In the work by Jernigan and Hwang (2002), the authors asserted that the results from this methodology compare reasonably well to those generated using more rigorous methods.

2.3.3.2 Non-Linear Static Analysis

An improvement upon the elastic spectral analysis can be made by considering the non-linear response of the bridge. However, a full non-linear time history analysis can be very time consuming. A simplified methodology has been developed that benefits from a non-linear analysis but does not incur the computational cost of a time history analysis. This method is a non-linear static procedure and is commonly called the Capacity-Spectrum method. The basic methodology uses a converted non-linear static pushover curve in concert with a reduced response spectrum. Due to time savings, this methodology has already been used by a number of researchers to generate seismic fragility curves for bridges. Dutta (1999) and Mander and Basoz (1999) used this methodology to create seismic fragility curves for standard classes of bridges across the United States. Shinozuka et al. (2000) used this methodology on a three-span continuous concrete girder bridge in the Memphis,

TN area. This has even been the methodology that was adopted in the generation of seismic bridge fragility curves for HAZUS (FEMA, 2003).

The capacity spectrum is developed by first generating a non-linear static pushover curve for the bridge. This pushover is generated by incrementally loading the bridge with a loading pattern that is consistent with its dominant response mode. A slight variation to this would be to use an adaptive pushover which adjusts the load distribution based on the structure's updated modal properties at each increment (Rossetto and Elnashai, 2004). The static pushover curve is a plot of force versus displacement which can then be converted to a capacity spectrum whose x and y axes are in terms of spectral displacement and spectral acceleration respectively as shown in Figure 2-5 (Dutta, 1999).

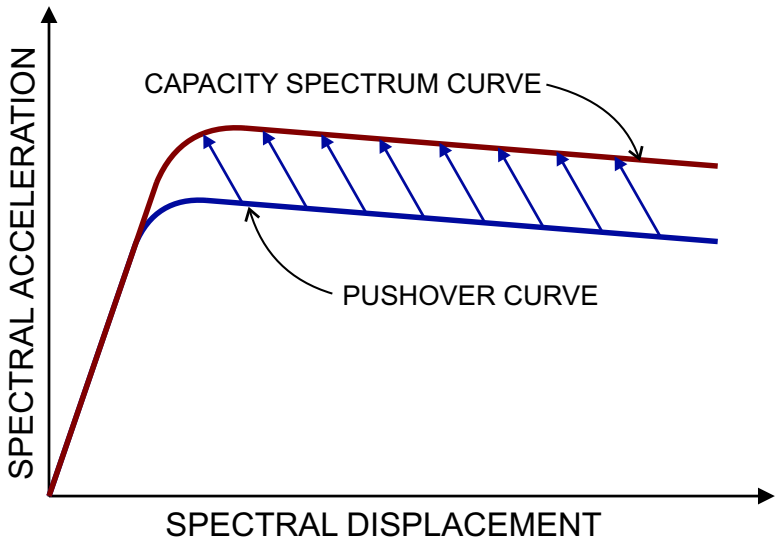

Figure 2-5: Conversion of the Pushover Curve to the Capacity Spectrum (Dutta, 1999).

The demand side of the problem is modeled by a reduced response spectrum plotted as an acceleration-displacement response spectrum (ADRS). The traditional S_a versus T coordinate system can be transformed into a S_a versus S_d coordinate system by observing the relationship between S_a and S_d as shown in Equation 2.5. As seen in Figure 2-6 the period, T, is represented by lines originating from the origin.

$$S_d = S_a g \left(\frac{T}{2\pi}\right)^2 \tag{2.5}$$

This response spectrum can then be adjusted from an elastic response spectrum to an inelastic response spectrum to account for the non-linear behavior of the structure. This can generally be handled by generating the response spectrum at a high damping ratio (Dutta, 1999).

The capacity and demand spectra can be placed on the same plot to determine the maximum response of the bridge. For a deterministic analysis this maximum response would be determined by locating the intersection of the two curves. However, when uncertainty in the capacity and demand are considered, each curve is then represented by a probabilistic distribution as seen in Figure 2-7.

Seismic fragility curves can then be generated from these spectra by evaluating them at predefined limit states. The probability of failure is calculated as the intersection of the demand and capacity distributions. This is done for various levels of a chosen intensity measure (e.g. PGA, S_a).

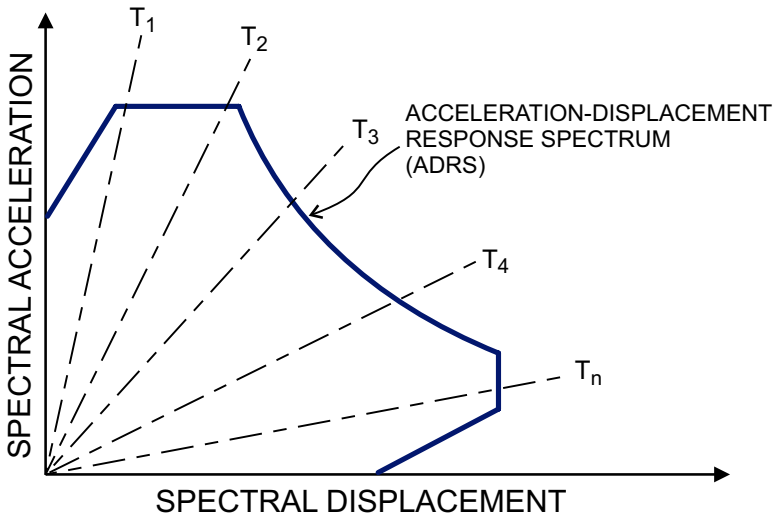

Figure 2-6: Acceleration-Displacement Response Spectrum.

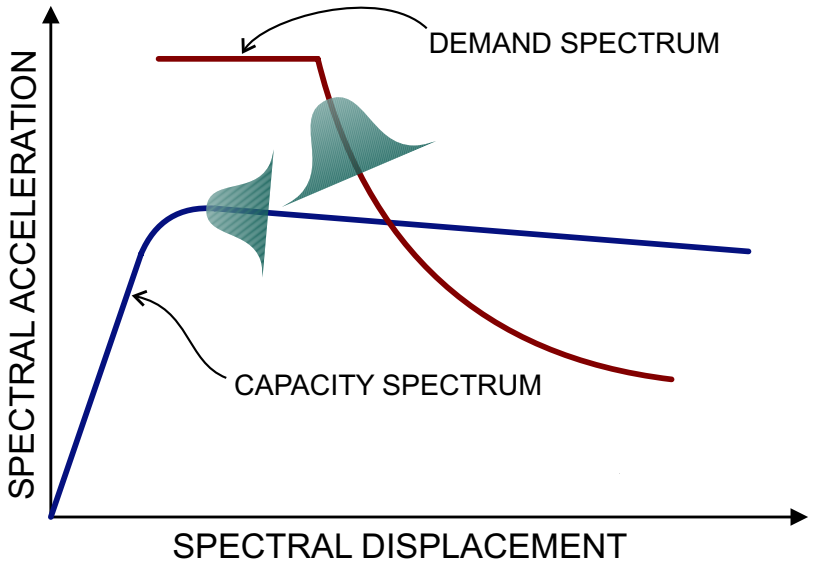

Figure 2-7: Probabilistic Representation of Capacity and Demand Spectra (Mander and Basoz, 1999).

2.3.3.3 Non-Linear Time History Analysis

Seismic fragility curves can also be generated using a non-linear time history (NLTH) approach. Although this type of approach tends to be the most computationally expensive it is also one of the most reliable methodologies available (Shinozuka et al., 2000). For this reason there have been many researchers that have used a methodology rooted in NLTH analysis to generate fragility curves. Although the actual application of the analyses may vary, all applications follow the basic approach outlined in Figure 2-8.

The first step is to obtain a suite of ground motions that is appropriate and representative of the target geographic area and captures the uncertainty inherent in ground motions such as the magnitude and epicentral distances. Next, the structural properties (material strengths and geometric values) are probabilistically sampled from an analytically formulated bridge model. This is done N times thus generating N nominally identical but statistically different bridge samples. Then the ground motions are paired with the bridge simulations and a non-linear time history analysis for each earthquake-bridge sample is performed. For each simulation, the peak structural responses for key elements (e.g. column ductilities, bearing deformation, abutment displacement, etc.) is collected. Using the peak bridge component responses, a probabilistic seismic demand model can then be generated by using a regression analysis of the ground motion parameters and the peak structural response or by using some other parameter estimation technique such as the Maximum Likelihood method. The capacity or limit state of each component is determined using expert based, experimentally based and/or analytically based methods. Finally, the seismic

demand and structural capacity models are combined assuming a lognormal distribution as given in Equation 2.2.

As previously mentioned, although the general framework of the methodology used by researchers is fairly consistent to that outlined in Figure 2-8, there are some differences in the actual tools employed to accomplish each step. When modeling the seismic demand side of the problem, a sampling technique is often employed. Cornell et al. (2002) outlined a methodology using regression analysis to generate a probabilistic seismic demand model for structures as seen in Figure 2-9. This approach was used by Mackie and Stojadinovic (2001) to generate probabilistic seismic demand models for typical California over-pass bridges that are subjected to excitation in both the longitudinal and transverse direction. In their study, they used a suite of ground motions that were acquired from the PEER strong motion database and took the column curvature and displacement ductilities as representative of the overall demand on their bridge.

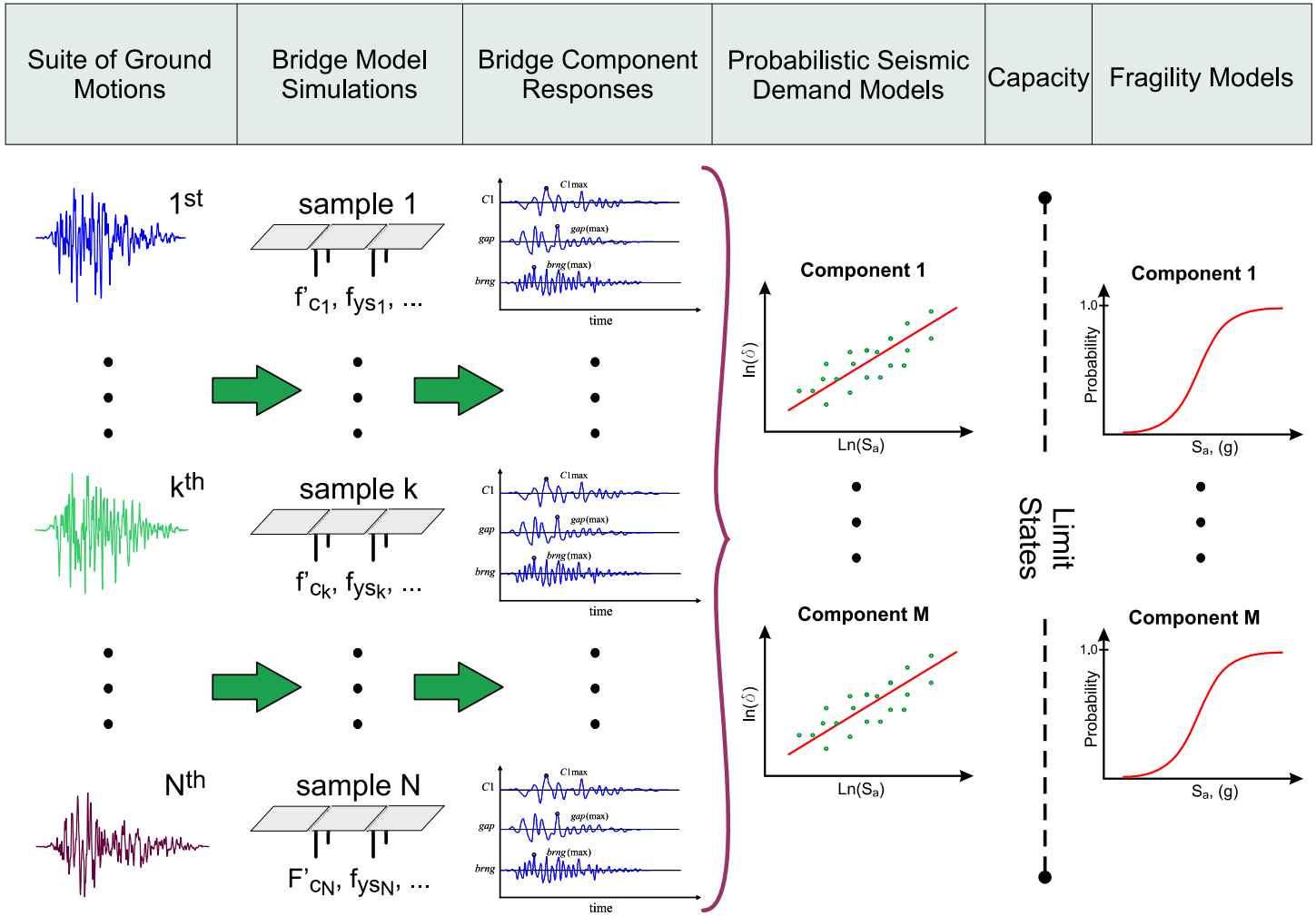

Figure 2-8: Analytical Fragility Curve Generation Using Non-linear Time History Analyses.

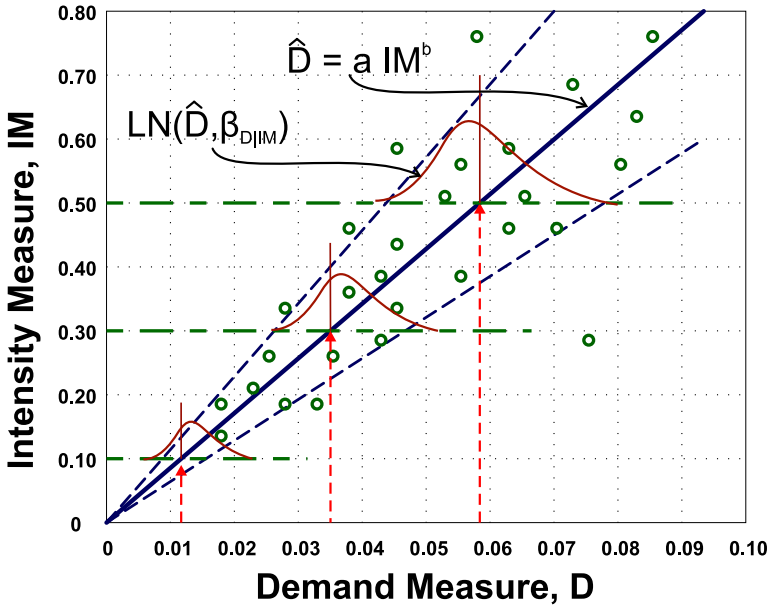

Figure 2-9: Probabilistic Seismic Demand Model (Cornell et al., 2002).

Similar work was done by Hwang et al. (2000) for a four span concrete girder bridge utilizing a suite of synthetic ground motions they generated that were site specific. Once again they looked at column deformations from seismic loading in the longitudinal and transverse directions to model the demand upon the bridge. Other researchers have used the same approach for similar bridges (Bignell et al., 2004; Choi et al., 2004). Other variations to this include the use of a logistic regression analysis of the response simulation (Hwang and Huo, 1998) and the Maximum Likelihood Method (MLE) to model the column responses to the chosen earthquake intensity measure (Shinozuka et al., 2003).

The capacity or limit states of the bridge can be described using a number of different techniques. One such approach is to look at the physics of the bridge using experimental tests. Analytical approaches, such as static pushover, adaptive pushover and incremental

dynamic analyses, can also be used to describe the capacity of the bridges and/or their components. These evaluations can be performed using either a sampling technique (Vamvatsikos and Cornell, 2002) or a first order reliability method (FORM) (Mackie and Stojadinovic, 2004). These types of approaches are more prescriptive in nature in that they prescribe the damage state of the bridge. Another approach is more descriptive in nature and attempts to map specific demand values (ductility, deformation, etc.), to functionality decisions made by bridge inspectors. This is a more subjective approach but may give a more realistic representation of post-earthquake field conditions.

2.4 Closure

Fragility curves, which are probabilistic tool used to assess potential seismic damage to highway bridges, are a fundamental component of seismic risk assessment methodologies. Basic methodologies for the generation of these curves have been developed using both simplistic and complex approaches. Researchers in the field must continue to look at ways of improving upon these methodologies and thus create more reliable fragility information.

The research in this study adapts some of the existing nonlinear time-history analysis approaches to create a more robust and more discretized suite of bridge fragility curves. Specifically, existing methods are adapted such that the effects of more than one bridge component may be incorporated into the determination of the system (bridge) fragility. Additionally, 3-D models are used to, not only capture the variability in ground motion intensity, but also to include the effects of bridge orientation. Thus, these fragility curves will be more representative of a wider class of bridges. The following chapters will specifically address the various aspects of seismic bridge fragility generation.

CHAPTER III

SEISMIC HAZARD AND GROUND MOTIONS IN THE CENTRAL AND SOUTHEASTERN UNITED STATES

3.1 Historical Earthquakes in the Central and Southeastern United States

In the winter of 1811-1812 several large earthquakes rocked the Central and Southeastern United States (CSUS) originating from the Missouri/Tennessee region . Later that same century, in 1886, another large earthquake that originated in South Carolina rocked the region once again. These notable earthquakes, amongst others, have highlighted the seismic hazard and the associated seismic risk that exists in this part of the United States.

The earthquakes of 1811-1812, also known as the New Madrid earthquakes, were characterized by three large earthquakes and several hundred moderate to large earthquakes in a six month period of time. The first of the three main shocks occurred on December 16, 1811 with an estimated moment magnitude of 8.1. The other two occurred on January 23, 1812 and March 15, 1812 with moment magnitudes of 7.8 and ~8.0 respectively (USGS, 2004). It should be noted that the estimates for these earthquakes range from 7.2 to 8.7. However, using the magnitudes published by the United States Geological Survey, two of these earthquakes rank in the top ten largest earthquakes in the United States, as seen in Table 3-1. The losses incurred from these earthquakes were small because the region was underdeveloped at the time.

Table 3-1: Ten Largest Recorded Earthquakes in the United States (USGS, 2004).

No.	Location	Magnitude (M_w)	Date
1	Prince William Sound, AK	9.2	Mar 3, 1964
2	Andreanof Islands, AK	9.1	Mar 3, 1957
3	Rat Islands, AK	8.7	Feb 4, 1965
4	East of Shumagin Islands, AK	8.2	Nov 10, 1938
5	New Madrid, MO	8.1	Dec 16, 1811
6	Yakutat Bay, AK	8.0	Sep 10, 1899
7	Andreanof Islands, AK	8.0	May 7, 1986
8	New Madrid, MO	≈ 8	Feb 7, 1812
9	Near Cape Yakataga, AK	7.9	Sep 4, 1899
10	Fort Tejon, CA	7.9	Jan 9, 1857

The earthquake of 1886 occurred in Charleston, South Carolina and had a moment magnitude estimated at 7.3. This magnitude places this seismic event as the eleventh largest earthquake in the contiguous United States. It is believed to be the most damaging earthquake in the Southeast United States with property damage being estimated at $5-$6 million and the loss of life around 60 persons (USGS, 2004).

Since the Charleston earthquake of 1886, there have been a number of moderate earthquakes in the region. In 1895 both Charleston and New Madrid experienced earthquakes larger than 6.0. Figure 3-1 shows the earthquakes that have occurred in the New Madrid region. The dark or red colored circles indicate earthquakes that have occurred from 1974 to 2002 with magnitudes greater than 2.5. The light or green circles denote earthquakes that occurred prior to 1974. The magnitude of the earthquake is indicated by the size of the circle, keeping in mind that the largest of the green circles represent the earthquakes of 1811 and 1812 (USGS, 2002). This figure shows that this area was and currently is a seismically active region.

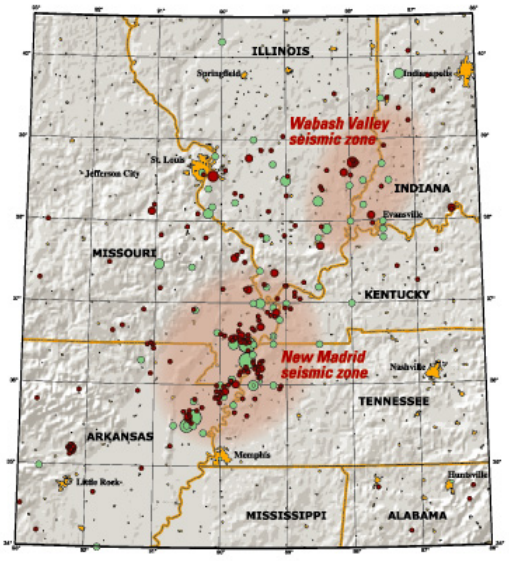

Figure 3-1: Map of the New Madrid and Wabash Valley Seismic Activity (USGS, 2002).

3.2 Seismic Hazard in the Central and Southeastern United States

Given the seismic nature of the CSUS, it has been classified as a moderate seismic zone or a zone with a moderate seismic hazard. Seismic hazard is defined as the potential that the region has of experiencing a certain level of ground shaking or ground deformation and the recurrence thereof. Therefore, this moderate seismic zone classification comes because the earthquakes in this region are infrequent.

Earthquakes in the CSUS generally have more far reaching effects as compared to those in West. This is because the geological make-up of the regions are considerably different. The make-up of the eastern part of the United States is characterized by hard intact rock

with an overlay of soft sediments. The hard rock in the region results in large attenuation distances. By way of illustration, Figure 3-2 compares the attenuation distances of several earthquakes in the East with several earthquakes in the West. It can be seen that the attenuation distances in the East are much longer and therefore the affected areas are much larger. A clearer comparison of this difference between the East and West is illustrated in Figure 3-3. In this figure, two earthquakes of similar magnitudes are compared from the two regions, the 1994 Northridge earthquake with a magnitude of 6.7 and the 1895 New Madrid earthquake with an estimated magnitude of 6.0. Here, it is illustrated that attenuation distances in the East can be as much as two to three times those in the West.

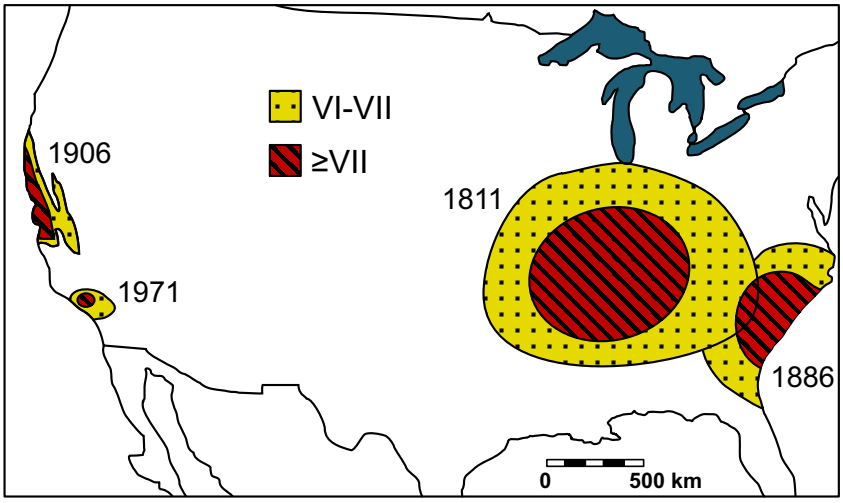

Figure 3-2: Comparison of Attenuation Distances of Several Earthquakes in the Eastern and Western United States (USGS, 2002).

As previously mentioned, the geological make-up in the East is also characterized by soft sediments overlaying the hard rock. These soft soils generally cause an amplification of

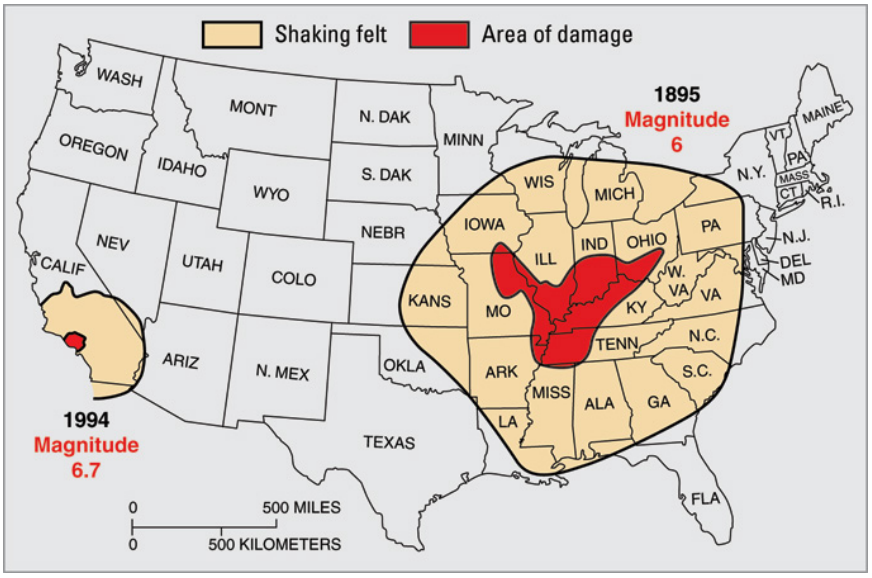

Figure 3-3: Comparison of Attenuation Distances of 1994 Northridge and 1895 New Madrid earthquakes (USGS, 2002).

the ground shaking intensity. For example, the New Madrid seismic zone is characterized by a region of deep sediments which range from 30 m up to 1 km deep. This can cause spectral acceleration values at a period of 2 seconds to range from 0.65 g to 1.5 g for a 2% in 50 years hazard level (Park and Hashash, 2005). This increase in intensity can cause an increase in the amount of damage that is realized as a direct result of an earthquake.

The CSUS is different than the West Coast in another aspect. Unlike the faults on the West Coast, which fall on plate boundaries, the faults in the Mid-West are intra-plate faults. One of theimajor tasks faced by seismologists and other researchers is to estimate the re-currence interval of major earthquakes for the region. Typically, the frequency of small to moderate earthquakes are used to estimate the likelihood of larger events. Unfortunately, the regular seismic activity for the CSUS is relatively small and therefore makes recurrence estimates difficult using this method (USGS, 2002). Another technique used to estimate the

recurrence interval is by using historical earthquakes. Examination of sand blows, in addition to other indicators, has resulted in the determination that major earthquakes occurred approximately 900 A.D. and 1450 A.D. Extrapolating this information, it is estimated that earthquakes with magnitudes similar to those of 1811-1812 should recur every 550-1100 years on average (Johnston and Schweig, 1996; Tuttle et al., 2002).

In recent years, much effort has gone into characterizing the seismic hazard for the United States in a probabilistic manner. In 1996, the United States Geological Survey published seismic hazard maps for the entire U.S. These maps show the hazard for a particular location in a probabilistic sense. These maps, updated in 2002, were generated by considering all seismic sources that could affect the region. The published hazard maps for the region are shown in Figures 3-4 and 3-5. These figures show the peak ground accelerations with a 10% probability of exceedance and 2% probability of exceedance in 50 years respectively. Using these published hazard levels, it is estimated that in the next 50 years a repeat of the 1811-1812 earthquakes has a probability of 7-10% and an earthquake with a magnitude greater than 6.0 has a probability of 25-40% (USGS, 2002).

3.3 Ground Motions in the Central and Southeastern United States

When assessing the vulnerability of civil infrastructure to the associated seismic hazard of a particular region, it is helpful to have ground motion time histories that are representative of the area. Since strong ground motions records for the CSUS do not exist, synthetic acceleration time histories can be used instead. There have been a number of research efforts that have focused on developing appropriate ground motion suites for the New Madrid

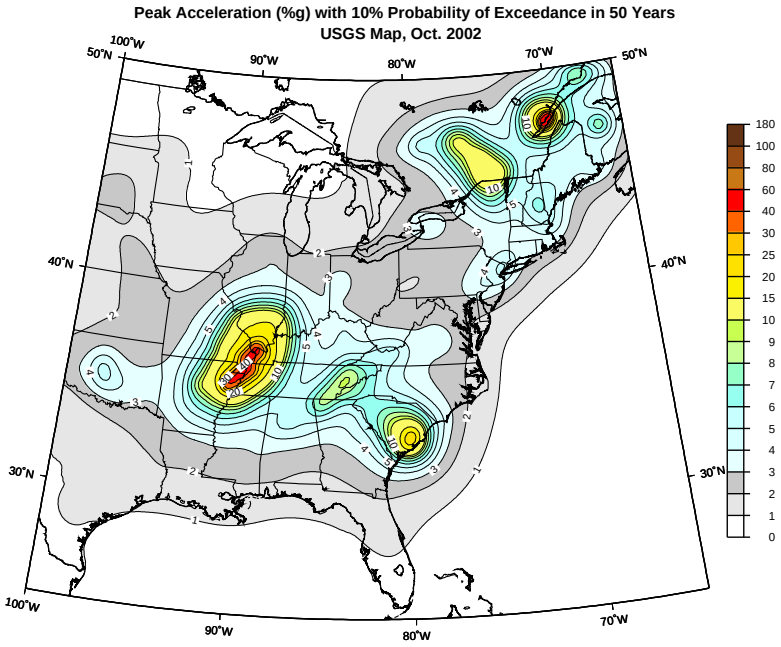

Figure 3-4: Peak Ground Acceleration with a 10% Probability of Exceedance of in 50 years (USGS, 2002).

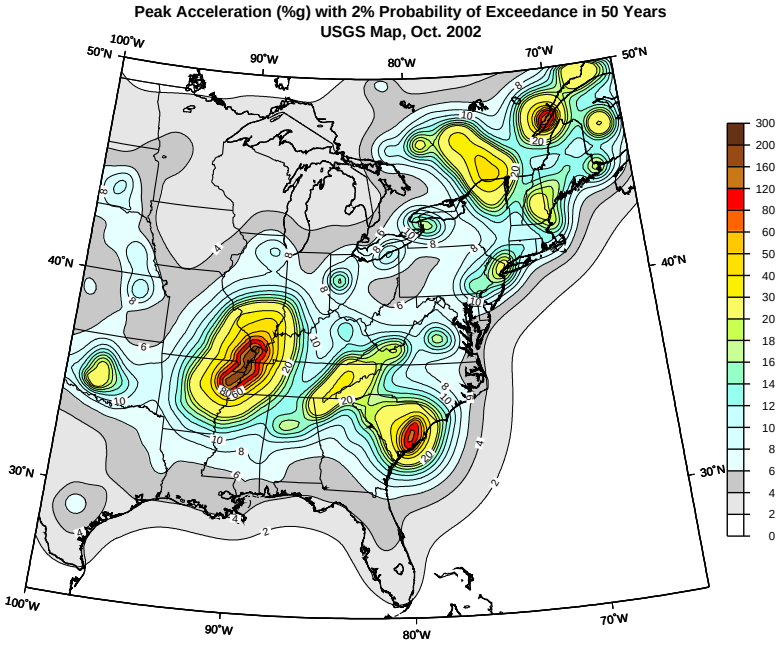

Figure 3-5: Peak Ground Acceleration with a 2% Probability of Exceedance of in 50 years (USGS, 2002).

Seismic Zone. Two of these ground motion suites are used in this study for which a brief introduction is given hereafter.

3.3.1 Orthogonal Ground Motion Components

Before introducing the two ground motion suites, the issue of 3-D analysis must be addressed. The ground motions presented in this section are often considered to be the geometric mean of two orthogonal components. However, when dealing with 3-D structures, as is the case in this study, it is essential that each ground motion be represented in its two orthogonal components (Baker and Cornell, 2005c). Since the synthetic ground motions are not generated in component pairs, an approximate method for creating components from the original ground motions is developed and used in this study.

The basic procedure used to generate ground motion components from existing ground motion records, is as follows:

1. Calculate the acceleration response spectrum for the original (seed) ground motion record using the procedure as outlined in Chopra (2000). The seed ground motions are single component synthetic time histories obtained from published sources.

2. Simultaneously simulate the response spectra for two new orthogonal ground motion components using the method outlined in Baker and Cornell (2005a).

3. Spectrally match the original ground motion to each component of the simulated response spectra. (Some random phase is added.)

4. Pass each new component through a cosine window so that the duration of the components is the same as the original ground motion.

5. Calculate the response spectra again to ensure compatibility with the targeted response spectra.

3.3.1.1 Simulate Orthogonal Component Response Spectra

Simulating the acceleration response spectrum requires knowledge pertaining to the distribution of the spectral acceleration at each period. Performing statistical studies of recorded ground motions, Abrahamson (1988) determined that the distribution of spectral acceleration values for a specified period is modeled well as a two-parameter lognormal distribution. This study assumes that the response spectrum for the seed ground motion is representative of the median which provides one of the two parameters. The second parameter, the lognormal standard deviation, is assumed to be 0.5, following the recommendations of Sewell et al. (1996).

This lognormal model describes the distribution of spectral acceleration at one specific period. However, it has been shown that a significant correlation exists between the spectral accelerations at different periods along the same orientation, which must be addressed. A study of numerous recorded ground motions showed that this correlation is approximated by Equation 3.1 (Baker and Cornell, 2005a).

$$\rho_{Sa_x,Sa_x} = 1 - \cos\left(\frac{\pi}{2} - \left(0.359 - 0.163 \cdot I_{(T_{min}<0.189)} \ln\frac{T_{min}}{0.189}\right)\ln\frac{T_{max}}{T_{min}}\right) \tag{3.1}$$

where $I_{(T_{min}<0.189)}$ is an indicator function equal to 1 if $T_{min} < 0.189$ seconds and equal to 0 otherwise. T_{min} and T_{max} are used to label the smaller and larger periods being considered, respectively.

The correlation between the spectral accelerations of periods at different orientations is also needed to be able to simulate component spectra. In the same study, the correlation of the acceleration were estimated as Equation 3.2 (Baker and Cornell, 2005a). This correlation function is identical to Equation 3.1 other than it has some pre-multiplier function that reduces the overall correlation values. The composite correlation matrix for the spectral acceleration of both *x* and *y* components is represented in Equation 3.3.

$$\rho_{Sa_x,Sa_y} = \left(0.79 - 0.023 \cdot \ln \sqrt{T_{min}T_{max}}\right) \cdot \left(1 - \cos\left(\frac{\pi}{2} - \left(0.359 - 0.163 \cdot I_{(T_{min}<0.189)} \ln \frac{T_{min}}{0.189}\right) \ln \frac{T_{max}}{T_{min}}\right)\right) \tag{3.2}$$

$$\rho_{i,j} = \left(\begin{array}{c|c} \rho_{Sa_x,Sa_x} & \rho_{Sa_x,Sa_y} \\ \hline \rho_{Sa_y,Sa_x} & \rho_{Sa_y,Sa_y} \end{array}\right) \tag{3.3}$$

The simulations of the response spectra components are carried out recognizing that the acceleration values are jointly distributed. An example of one such simulation is given in Figure 3-6 where both the original (mean) spectrum and the component spectra are given.

3.3.1.2 Spectrally Match Response Spectra

Following the simulation of the component response spectra, the seed ground motion record is scaled to match them. This scaling is done in the frequency domain so that the frequency content of the new ground motions will match the spectra which were generated. The iterative procedure for this is outlined in the work by Keaton et al. (2000). The basic procedure is to first calculate the ratio between the actual spectrum and the target spectrum

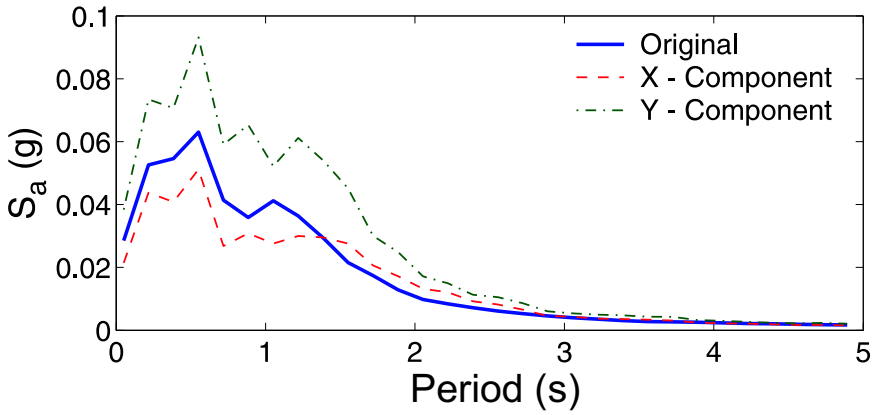

Figure 3-6: Example of Response Spectrum and Its Simulated Component Spectra.

for a specific frequency. The Fourier amplitude spectrum of the record is then multiplied by the spectrum ratios after which the inverse Fourier transform is taken. The resulting spectrum is then compared to the target spectrum indicating if another iteration is required. The spectral matching in this study is accomplished using a Matlab (Mathworks, 2004) script that was coded by Rix (2003).

This spectral matching procedure is purely an amplitude scaling. It is essential that some random phase be added to the seed ground motion prior to matching. This will ensure that the two components are not always in phase which is highly unrealistic.

3.3.1.3 Cosine Window

The spectral matching procedure can also slightly change the duration of the ground motion. To remedy this, the new ground motion components are passed through a cosine taper window. The basic form of this window is presented numerically in Equation 3.4 and graphically in Figure 3-7 (Rix and Fernandez-Leon, 2004).

$$w(t) = \begin{cases} \frac{1-\cos\left(\frac{\pi(t-t_o)}{t_b}\right)}{2} & \text{if } t_o < t < t_{0.5} \\ 1 & \text{if } t_{0.5} < t < t_{99.5} \\ \frac{1+\cos\left(\frac{\pi(t-t_{99.5})}{t_e}\right)}{2} & \text{if } t_{99.5} < t < t_{99.5} + t_e \end{cases} \tag{3.4}$$

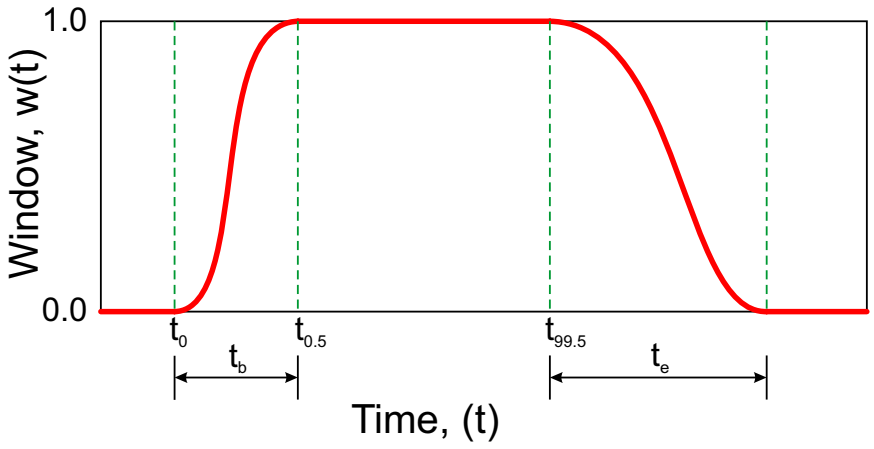

Figure 3-7: Cosine Taper Function for Windowing Ground Motions (Rix and Fernandez-Leon, 2004).

where $t_{0.5}$ and $t_{99.5}$ are the times corresponding to 0.5% and 99.5% of Arias intensity of the seed ground motion respectively. The values for t_b and t_e assume values of 2.0 and 3.0 seconds respectively.

Using the response spectra given in Figure 3-6, the seed ground motion is sampled to give the *x* and *y* components shown in Figure 3-8. Thus, this procedure is used for each of the ground motions in the two ground motion suites presented hereafter.

3.3.2 Wen and Wu Ground Motions

In 2001, Y. K. Wen and C. L. Wu generated synthetic ground motion records for three cities in the CSUS, namely Memphis, Tennessee; Carbondale, Illinois and St. Louis, Missouri.

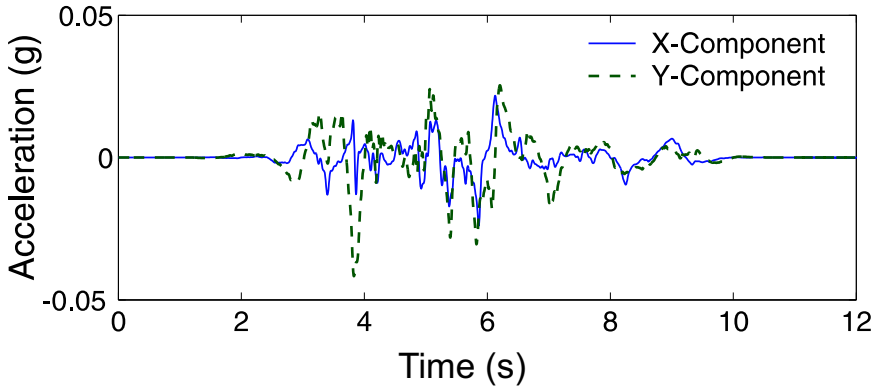

Figure 3-8: Example of Component Ground Motion Generated Through Spectral Matching.

Their objective was to generate ten ground motions that fit well to two different levels of hazard for each city. The two levels they targeted are both 10% and 2% probabilities of exceedance in 50 years (Wen and Wu, 2001). What resulted was a suite of 60 ground motions for the CSUS. A brief description of suite characteristics is given in Appendix A.

Of the 60 ground motions generated, 48 were selected for use in this study because this number works well with the number of bridge samples used which is also a multiple of eight (see Appendix A). It should be noted, however, that by eliminating some of the time histories from the original suite, the remaining suite is no longer representative of uniform hazards which is of little consequence for the purposes of this study. The resulting suite selects eight ground motions from each of the three cities at two hazard levels ($10\%/50 years, 2\%/50 years$). As mentioned previously, each of these ground motions is used as a seed to simulate an associated pair of orthogonal ground motion components following the procedure outlined in the previous section.

The modified ground motion suite is given in terms of orthogonal components. Figure 3-9 shows the components of three sample ground motions – one from each city. The

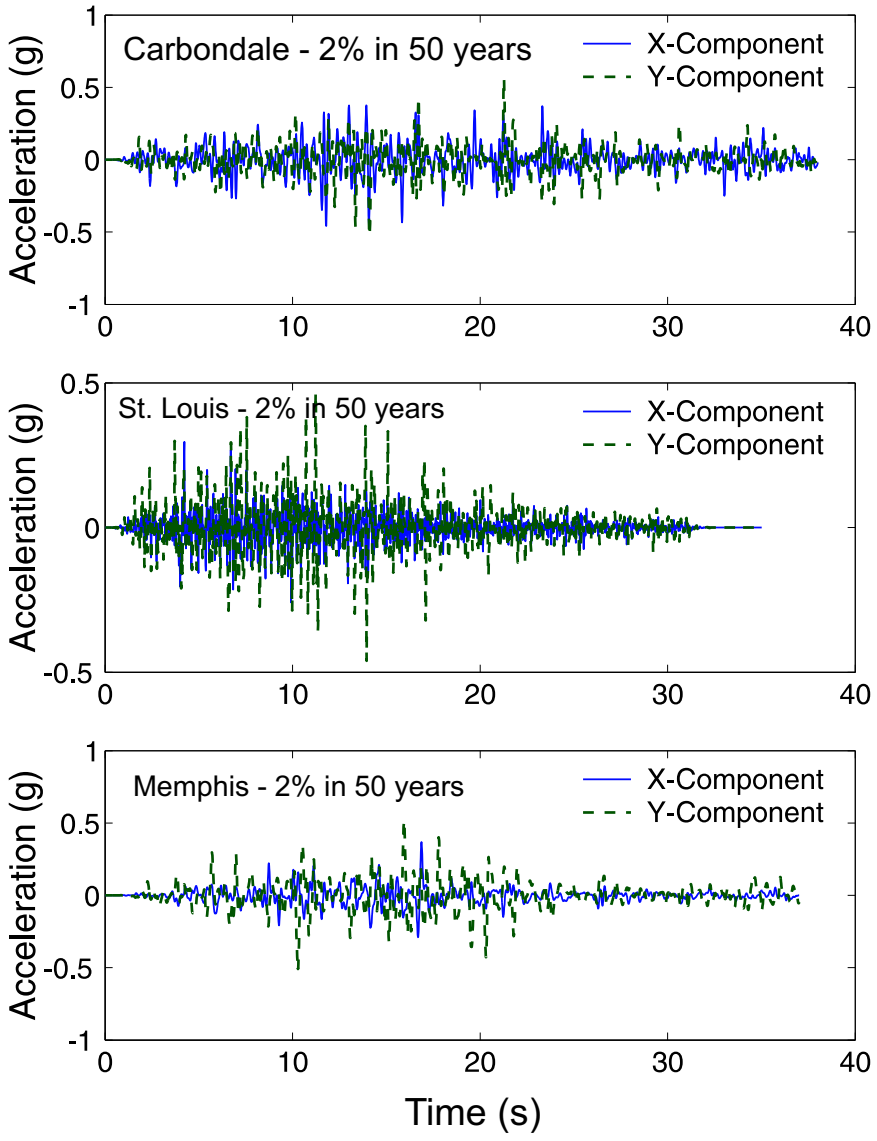

Figure 3-9: Orthogonal Components of Sample Ground Motions - Wen.

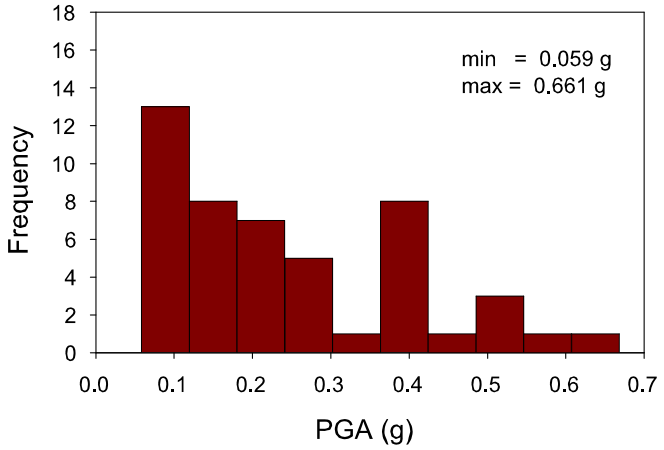

Figure 3-10: Histogram of PGA Values of Wen and Wu Ground Motion Suite.

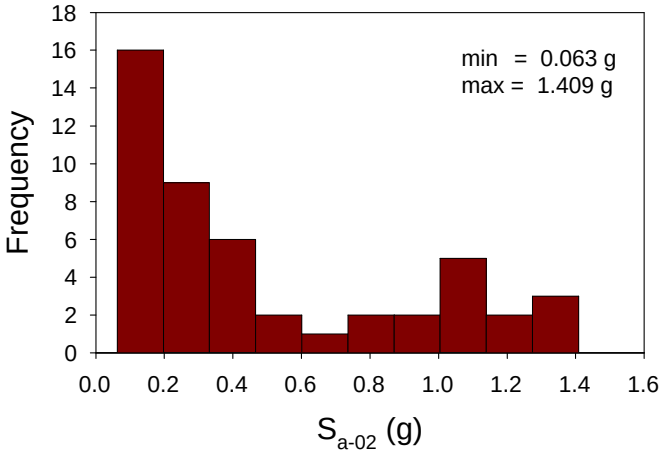

Figure 3-11: Histogram of S_a Values of Wen and Wu Ground Motion Suite at 0.2 Seconds.

distribution of PGA values and spectral acceleration values (0.2 sec) for these 48 ground motions are presented in Figures 3-10 and 3-11 respectively. The acceleration values are calculated as the geometric mean of the two orthogonal components.

It is seen that the PGA values range from 0.06 g to 0.66 g and the spectral accelerations at 0.2 seconds range from 0.06 g to 1.41 g. In both cases, the distributions are left skewed giving more weight to smaller accelerations. The frequency content of the final suite is given in Figure 3-12. This figure gives the mean and mean plus/minus one standard deviation of the response spectra for the geometric means of each ground motion pair. It is clear to see that the concentration of energy in this suite of ground motions is in the short period range from 0.2 to 0.5 seconds. As will be seen later, the frequency content in this suite is noticeably different from the other suite considered in this study.

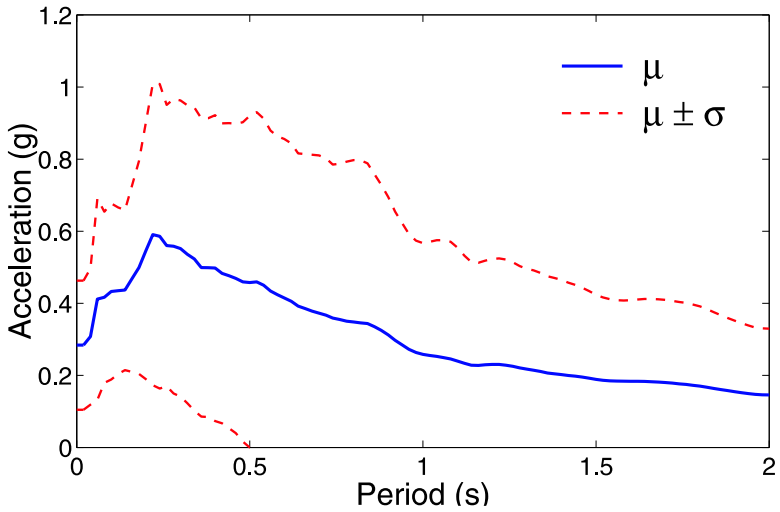

Figure 3-12: Mean and Mean ± One Standard Deviation of Response Spectra - Wen and Wu.

One may also see that there is a significant degree of variability in the spectra based on the width of the standard deviation bounds. This is not surprising when one considers that half of the ground motions are for 10 % in 50 years hazard and the other half are for 2 % in 50 years hazard. One of the characteristics which sets the CSUS apart from the Western US is the stark difference between the intensities of the two hazard levels. As will be shown later in Chapters 7 and 8, the content of this ground motion suite is apparent in the seismic demand and fragility analyses of the highway bridges.

3.3.3 Rix and Fernandez Ground Motions

The second suite of synthetic ground motions used throughout this study was developed by G. J. Rix and J. A. Fernandez-Leon as part of the research program organized out of the Mid-America Earthquake (MAE) Center (Rix and Fernandez-Leon, 2004). They generated ground motions for scenario earthquakes for the Memphis, TN region. Using two different source models these researchers simulated 20 ground motions for each of 11 magnitude-distance bins (M_w: 5.5, 6.5, 7.5; R: 10 km, 20 km, 50 km, 100 km). This resulted in 220 time histories for each source model. The effects of the deep sediments of the Mississippi embayment were also included. A brief description of the characteristics of this ground motion suite is given in Appendix A.

The 48 ground motions which are used in this study were selected from the 220 ground motions developed using Frankel's model (see Appendix A). Since these are scenario earthquakes, the ground motions were selected such that a well balanced cross-section of PGA and S_a values would be attained. Following the generation of orthogonal components, the PGA and S_a value distributions are as shown in Figures 3-13 and 3-14 respectively. The

geometric mean PGA values range from 0.022 g to 0.764 g. The spectral accelerations at 0.2 seconds range from 0.047 g to 0.963 g.

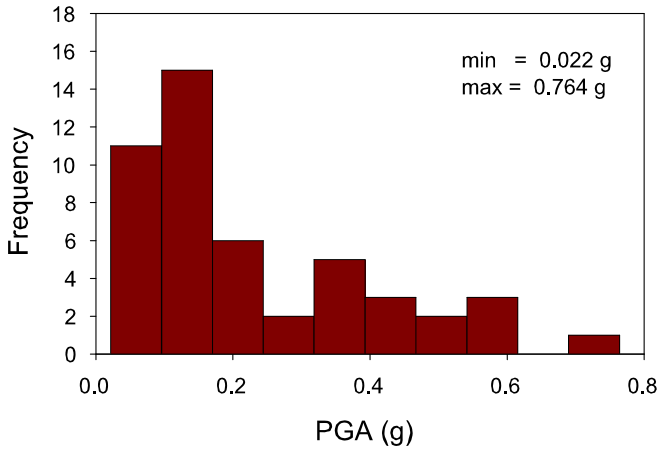

Figure 3-13: Histogram of PGA Values of Rix and Fernandez Ground Motion Suite.

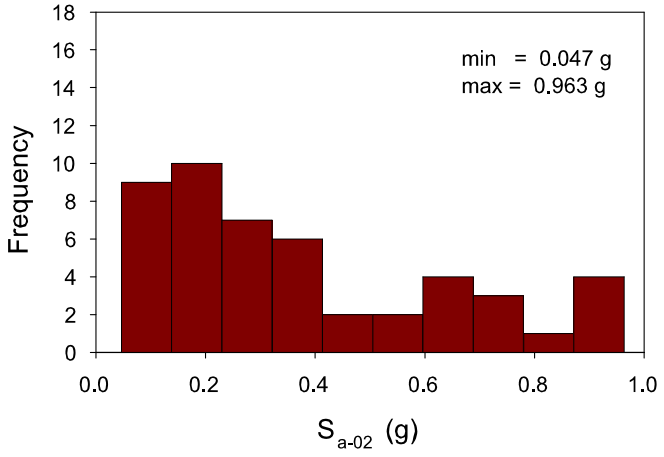

Figure 3-14: Histogram of S_a Values of Rix and Fernandez Ground Motion Suite at 0.2 Seconds.

Following the procedure outlined previously, each of these 48 ground motions was used to generate records with orthogonal components. Figure 3-15 illustrates the components, as simulated from the original ground motions, for three different magnitudes (5.5, 6.5, and 7.5). The difference in frequency content, as compared to the Wen and Wu suite, is obvious in this figure.

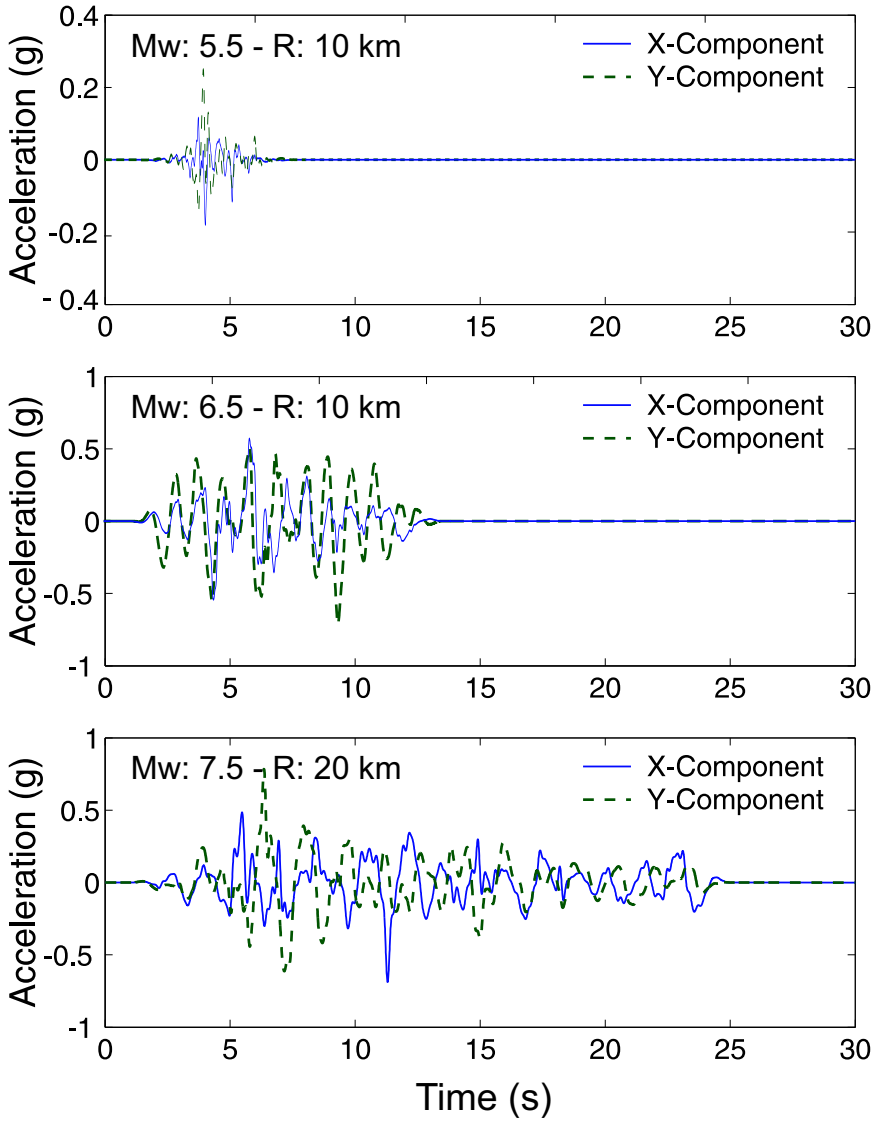

Figure 3-15: Orthogonal Components of Sample Ground Motions - Rix and Fernandez.

The frequency content of this ground motion suite is more clearly seen by looking at the mean response spectrum shown in Figure 3-16. There is an obvious shift to the longer period range, as compared with the Wen and Wu suite, with the main energy content in the 0.5 to 1 seconds range. Figure 3-17 compares the mean response spectra for the two ground motion suites.

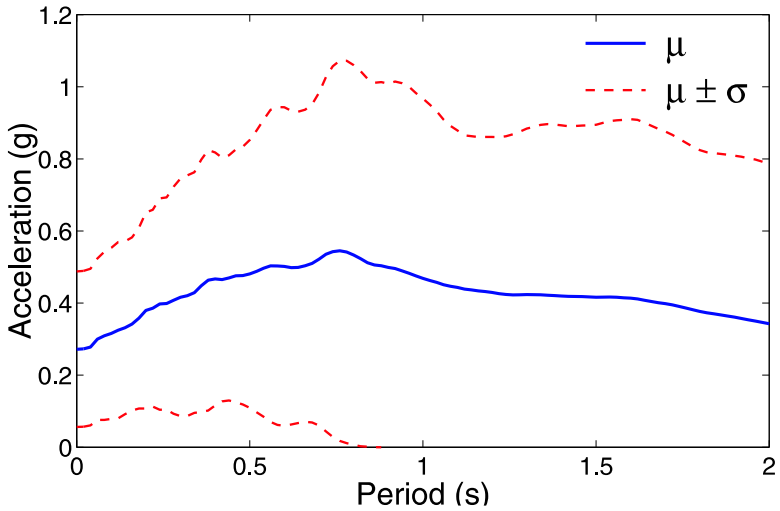

Figure 3-16: Mean and Mean ± One Standard Deviation of Response Spectra - Rix and Fernandez.

There are clear reasons for the perceived differences between the two suites of ground motions. The Wen and Wu ground motions are representative of three different cities (Memphis, St. Louis, Carbondale) with different soil profiles where as the Rix and Fernandez ground motions are developed for Memphis. Memphis is noted for deep soil column and St. Louis is located over a relatively thin soil layer. Figure 3-17 illustrates the effects of nonlinear soil behavior in the short period range and the soil column resonances in the long period range. A second reason for the difference between ground motions suites is the

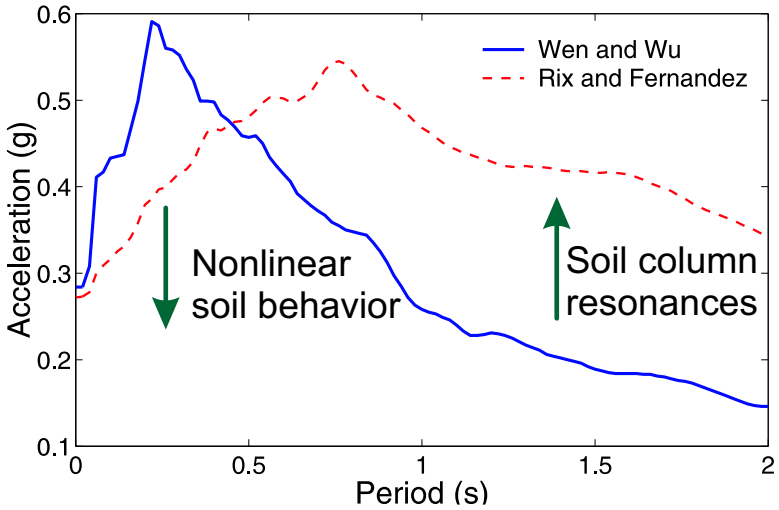

Figure 3-17: Mean Response Spectra for Wen and Rix Ground Motion Suites.

underlying source model used. Rix and Fernandez used the Frankel et al. (USGS, 1996) model while Wen and Wu used the Atkinson and Boore Atkinson and Boore (1995) model. A third difference is that the Rix and Fernandez ground motions are deterministic whereas the Wen and Wu ground motions are probabilistic.

3.4 Closure

In this chapter, the seismic hazard present in the Central and Southeastern United States is highlighted. It is seen that although seismic activity in the region is not as frequent as that in the Western US, there is serious cause for concern due to the geological make-up of the region.

Two suites of synthetic ground motions are identified to help quantify the nature of the seismic hazard in the region. One suite is constructed of probabilistic ground motions and the other suite is constructed of scenario seismic events. The final ground motions, which

are used throughout this study, were manipulated to produce two orthogonal components for each ground motion.

When comparing the two suites of time histories, it is clear that the frequency content and typical time durations are different. The suite based on the work of Wen and Wu (2001) tend to be strong in the short period range whereas the suite based on the work of Rix and Fernandez-Leon (2004) is strong in the long period range. As suspected, this difference will become evident in the demand and fragility calculations presented later in this document. This is also the likely reason that differences in bridge responses are more pronounced when spectral intensity measures, as opposed to PGA, are used to generate demand models (See Chapter 7).

CHAPTER IV

BRIDGE INVENTORY OF THE CENTRAL AND SOUTHEASTERN UNITED STATES

To carry on a study of the vulnerability or fragility of highway bridges in the Central and Southeastern United States, it is essential to have an understanding of the bridge inventory in the region. An in-depth study of the bridge inventory for the CSUS is presented in this chapter. This inventory study utilizes the National Bridge Inventory (NBI) database and specific bridge plans which were attained from the various state departments of transportation (DOTs).

There are 11 states considered in this study which are listed in Table 4-1. These states were selected for inclusion based on their relative seismic hazards. Figure 4-1 presents the 11 states overlaying the 2% in 50 year hazard map for the region. It is recognized that there could be a number of additional states included but the goal is to keep the number manageable while maintaining a representative cross-section of the region.

Table 4-1: States Considered in the Inventory Study.

States		
Alabama	Indiana	North Carolina
Arkansas	Kentucky	South Carolina
Georgia	Mississippi	Tennessee
Illinois	Missouri	

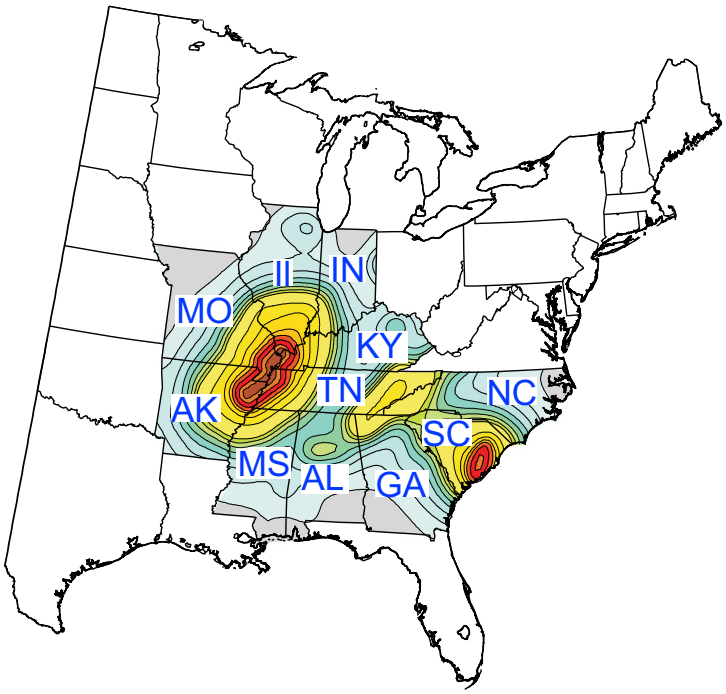

Figure 4-1: States Considered in the Inventory Study with Hazard Map.

The first task of this study is to identify typical bridge classes and select a small number of bridge classes which would represent a significant portion of the overall inventory. This is presented in the next section. The subsequent sections are devoted to exploring the characteristics of the selected bridge classes.

4.1 Highway Bridge Inventory Analysis

When assessing the vulnerability of bridges in a region it would be ideal to obtain construction plans for each bridge and generate their respective fragility curves. However, this is a very costly approach and is not feasible for a region of any size. Helped by the fact that many bridges in a particular region are similar, more general bridge classes can be defined to which every bridge will be assigned. The task then, is to generate fragility curves for the

typical bridge classes and not for individual bridges. This is the approach implemented in this study. The bridge classes are created and the individual bridges are grouped using the National Bridge Inventory (NBI) database as the basis.

In 1967, the Silver Bridge over the Ohio River collapsed and killed 46 people as the result of a fracture in a pin connection (Phares et al., 2000). This failure highlighted the need to regularly inspect our Nation's bridges. The direct result was the generation of the National Bridge Inspection Standards (NBIS) in 1971. These new standards required that every bridge on public roads be inspected at least every two years (FHWA, 1994). To help track and document these inspections, a framework was developed called the National Bridge Inventory (NBI) database. This database contains basic information about the bridge such as location, design type, material type, dimensions, conditions etc. and is to be maintained by the state in which it resides.

Although the information provided in the NBI database is not a complete description of each bridge it does provide sufficient information to allow for general classification. The bridges in this study are assigned to one of 11 classes based on their construction material, construction type and the number of spans. This information is contained in three of the 116 fields in the NBI. Table 4-2 and Table 4-3 show the possible construction materials and possible construction types as they are listed in the *Recording and Coding Guide for the Structure Inventory and Appraisal of the Nation's Bridges*, which is a guide to the NBI.

As mentioned previously, the bridges in the 11 states are assigned to one of 11 bridge classes. These classes are defined with the assumption that those bridges assigned to them would have similar responses to seismic excitation. It is also assumed that tunnels and culverts represent a significantly different type of system and are not considered as part

Table 4-2: Construction Materials Listed in NBI (FHWA, 1995a).

Description
Concrete
Concrete Continuous
Steel
Steel Continuous
Prestressed Concrete
Prestressed Concrete Continuous
Wood or Timber
Masonry
Aluminum, Wrought Iron, or Cast Iron
Other

Table 4-3: Construction Types Listed in NBI (FHWA, 1995a).

Description	
Slab	Suspension
Stringer/Multi-beam or Girder	Stayed Girder
Girder and Floorbeam System	Movable - Lift
Tee Beam	Movable - Bascule
Box Beam or Girders - Multiple	Movable - Swing
Box Beam or Girders - Single or Spread	Tunnel
Frame	Culvert
Orthotropic	Mixed Types
Truss - Deck	Segmental Box Girder
Truss - Thru	Channel Beam
Arch - Deck	Other
Arch - Thru	

Table 4-4: Bridge Classes and Their Proportions.

Name	Abbreviation	Number	Percentage
Multi-Span Continuous Concrete Girder	MSC Concrete	10,638	6.5%
Multi-Span Continuous Steel Girder	MSC Steel	21,625	13.2%
Multi-Span Continuous Slab	MSC Slab	5,955	3.6%
Multi-Span Continuous Concrete Box Girder	MSC Concrete-Box	916	0.6%
Multi-Span Simply Supported Concrete Girder	MSSS Concrete	30,923	18.9%
Multi-Span Simply Supported Steel Girder	MSSS Steel	18,477	11.3%
Multi-Span Simply Supported Slab	MSSS Slab	9,981	6.1%
Multi-Span Simply Supported Concrete Box Girder	MSSS Concrete-Box	4,909	3.0%
Single-Span Concrete Girder	SS Concrete	22,793	13.9%
Single-Span Steel Girder	SS Steel	18,281	11.2%
Other		18,945	11.7%
Total		163,433	100%

of this study. Table B-1 in Appendix B lists the defined bridge classes and the NBI data entries that belong to those classes. There are $163,443$ bridges in the target area and the proportion of these bridges that fall in each of the respective bridge classes are shown in Table 4-4.

Upon examination of the results presented in Table 4-4, it is seen that nine of the ten bridge classes make up 87.8% of the total number of bridges in the CSUS. The only bridge class listed in Table 4-4 that does not contribute significantly to the total number of bridges is the MSC Concrete-Box girder class. It represents less than 1% of the overall inventory and is therefore not included in the fragility study for the region. Overall, nine bridge classes, which are concisely presented in Table 4-5, are considered in later chapters. To facilitate discussion and comparison later on, it is also useful to note the equivalent HAZUS bridge classes (FEMA, 2003). These equivalent designations are also given in Table 4-5.

Table 4-5: Nine Bridge Classes Considered for Fragility Study.

Bridge Classes	HAZUS Designations
MSC Concrete	HWB10, HWB22
MSC Slab	HWB10, HWB22
MSC Steel	HWB15, HWB26
MSSS Concrete	HWB5, HWB17
MSSS Concrete-Box	HWB5, HWB17
MSSS Slab	HWB5, HWB17
MSSS Steel	HWB12, HWB24
SS Concrete	HWB3
SS Steel	HWB3

4.2 Bridge Class Statistics

With the nine bridge classes identified, it is now necessary to examine the bridge characteristics that are associated with each class. This is done once again by looking at the NBI and evaluating each bridge class independently. Although it is desirable to get complete descriptions of each bridge, the NBI does not contain that kind of detailed information. Therefore general inferences on the bridge classes can be made from the NBI but actual bridge plans are required to assign typical details to each class. From the data provided in the database, the following information is obtained and analyzed:

- Number of spans
- Maximum span length
- Deck width
- Vertical underclearance (Infer column height)
- Skew angle
- Year Built/Rebuilt

- Deck condition rating
- Superstructure condition rating
- Substructure condition rating

This information gives insight about the typical geometric configuration of each bridge class. The year a bridge was built gives an indication about the design as it pertains to seismic considerations. It was not until approximately 1990 that seismic design began to make its way into bridges being built in the non-California regions of the United States (FEMA, 2003). Also the condition ratings lend some insight into the deterioration these bridges have incurred over the years and give an indication of the appropriateness of modeling according to as-built plans.

For some of these items, it is sufficient to note their general tendencies such as the mean, median, standard deviation and data range. For other items it is necessary to explore their relative likelihoods to allow for future simulations. These items specifically are the number of spans, the span length, the deck width and the vertical underclearance. This information can be formulated and presented in a couple of different ways, one of which is through the estimation of the probability laws. These probability laws that describe these data using conventional statistical tools such as parameter estimation and distribution testing (Ang and Tang, 1975; Hayter, 2002). Although this can be useful, particularly with small data sets, it is not necessary in this case. With the data set sizes being on the order of thousands and also being representative of the entire population, a simpler and more exact approach can be taken to describe the distribution of the respective bridge parameters. This approach

is simply to create a cumulative distribution function (CDF) empirically from the data. It is a non-parametric representation of the data set's distribution.

4.2.1 Empirical Cumulative Distribution Functions

A cumulative distribution function, $F_X(\alpha)$, gives the probability that the value of a particular parameter will be less than or equal to some level α as given in Equation 4.1.

$$F_X(\alpha) = P[X \leq \alpha] \tag{4.1}$$

The empirical CDF is generated by first recognizing that each individual sample from a data set of size N has an equal probability of occurring which is $\frac{1}{N}$. The data set is then rank ordered where $x_1 \leq x_2 \leq x_3 \leq \cdots \leq x_N$. The value of the CDF of the i^{th} observation is then calculated by Equation 4.2.

$$F_X(x_i) = \frac{i}{N} \tag{4.2}$$

Although there are different ways of actually estimating the values of the empirical CDFs, (e.g. rank mean, rank median etc.), when the sample sizes become as large as they are in this study, there is only a negligible difference between the proposed estimators. Figure 4-2 shows an example of an empirical CDF as it would be generated from a data set.

4.2.2 Number of Spans

It is clear that the number of spans takes on discrete values in the form of integers. It is therefore appropriate to model the number of spans with a discrete distribution. Because of the nature of discrete distributions it is unnecessary to fit the data to a known distribution but

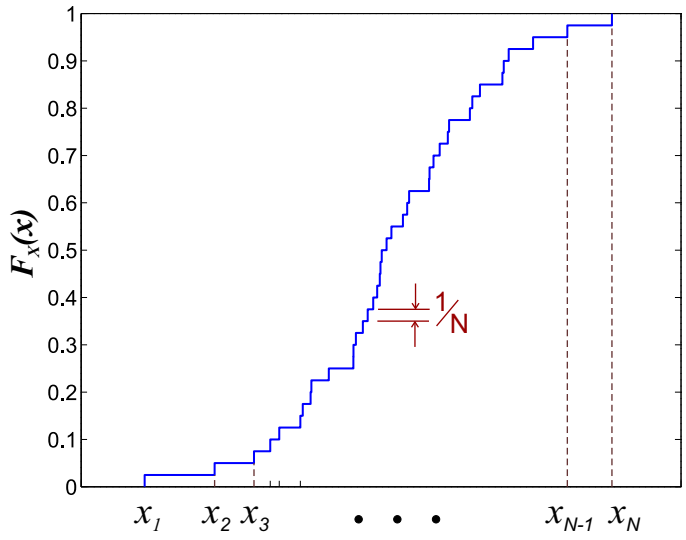

Figure 4-2: Sample of Empirical Cumulative Distribution Function (CDF).

Table 4-6: Span Number Statistics for Seven Multi-Span Bridge Classes.

Class	Mean	Std. Dev.	Median	Mode
MSC Concrete	3.83	2.01	3	3
MSC Slab	3.31	1.64	3	3
MSC Steel	3.72	2.53	3	3
MSSS Concrete	4.19	2.69	3	3
MSSS Concrete-Box	3.06	0.98	3	3
MSSS Slab	4.17	2.68	3	3
MSSS Steel	3.68	2.20	3	3

rather examine the frequency of the data at each span number. Therefore, in this study, the non-parametric probability mass function (PMF) for the number of spans in each bridge class was generated. This was accomplished by counting the number of bridges with a particular number of spans and dividing by the total number of bridges. Figures 4-3 and 4-4 show the PMFs for each of the seven multi-span bridge classes. Table 4-6 gives some of the statistics for this parameter for the same bridge classes.

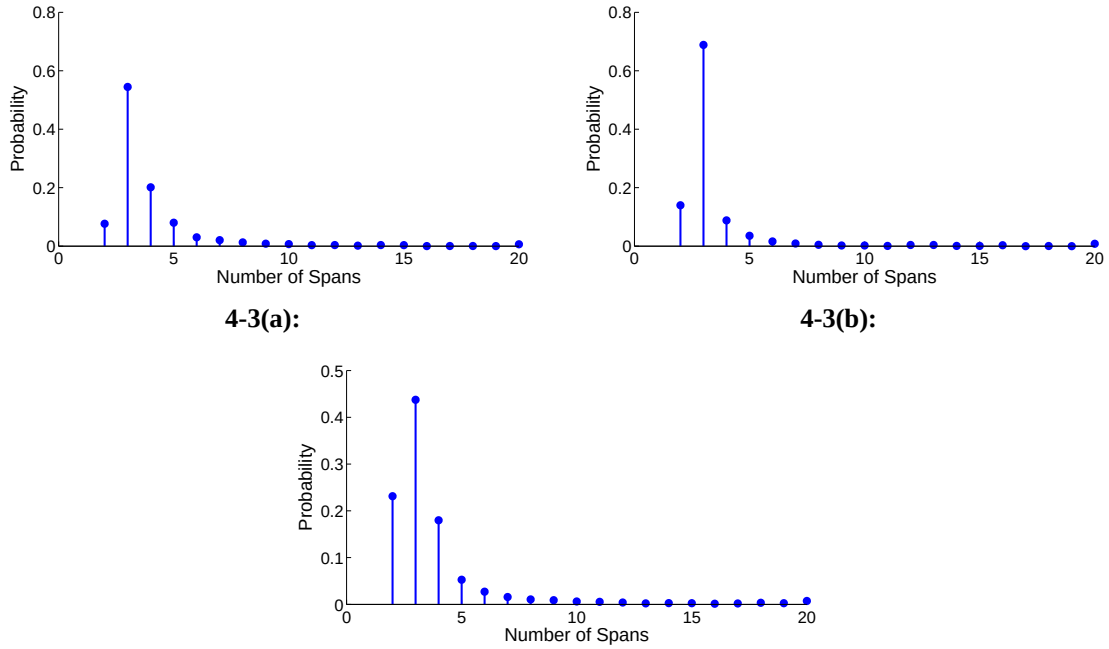

Figure 4-3: Non-Parametric PMFs for Multi-Span Continuous Bridge Types (a) Concrete (b) Slab (c) Steel.

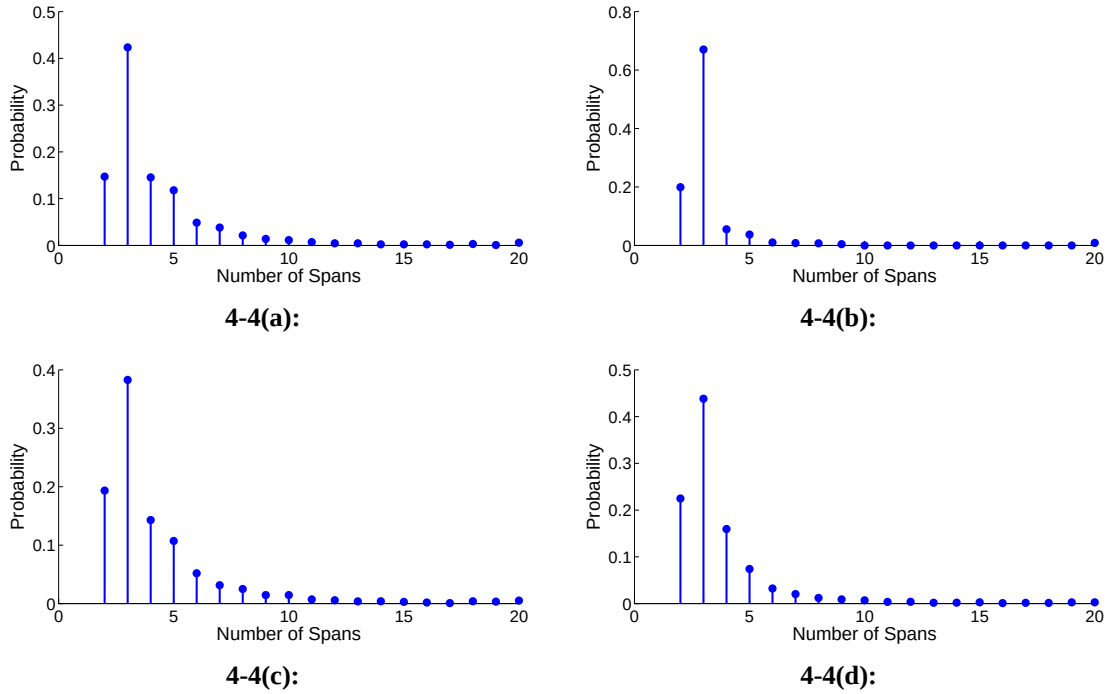

Figure 4-4: Non-Parametric PMFs for Multi-Span Simply Supported Bridge Types (a) Concrete (b) Concrete_Box (c) Slab (d) Steel.

There are a number of interesting points that should be highlighted with respect to the bridge span number statistics. Examination of PMFs for the seven multi-span bridges reveals that the large majority of these bridges have two to five spans. There is a noticeable difference in the level of dispersion between the continuous girder bridges and the simply supported girder bridges. One would expect that longer bridges (i.e. more spans) are more disposed to have simply supported girders and indeed the data supports this expectation. For the three continuous girder bridge classes, it is seen that over 90% of all their bridges are five spans or less. he simply supported girder bridge classes tend to have more of their bridges with a larger number of spans. However, they still have over 82% of all their bridges with five spans or less. It is noted that the Concrete-Box girder bridge is the one exception to this trend.

It is also important to note in Table 4-6, that the most likely number of spans for any bridge class is three. The median number of spans for all of the bridges classes is also three. Therefore, the analytical bridge models developed in this study all contain three spans except for the two single span bridge classes. It is much simpler and more straight forward to use a fixed number of spans for fragility curve generation. Furthermore, HAZUS provides a straight forward way for fragility curve adjustment depending on the number of spans (FEMA, 2003) making this a viable approach.

4.2.3 Maximum Span Length

The NBI does not list the length of every span in a bridge because of the logistics of doing so. Rather, it provides the length of the bridge's longest span in meters. Although this does not give a complete description of the span configuration of the bridge, it does give a sound

basis from which to make assumptions. In this study, it is assumed that the span length configuration is symmetric along the length of the bridge. For a two span bridge this would imply that both spans have a length equal to the maximum span length. For bridges with more than two spans it is assumed that all middle spans have lengths equal to the maximum while the two end spans, that tie into the abutments, have some typical fixed length. This study assumes that these end spans have a fixed length of 12.2 meters which was deduced from acquired bridge plans. For bridges with three spans or greater, it is typical that the end spans function as the approach spans whose lengths don't fluctuate much from bridge to bridge.

Some basic statistics (i.e. mean, median and standard deviation) for the maximum span length of each bridge class are presented in Table 4-7. These statistics are useful in giving an idea of central tendency and dispersion but they do not sufficiently describe the data for the purposes of this study. The empirical CDFs for the maximum span length of each bridge class is required, as they give a complete description of the data distribution and allow for the chosen simulation techniques. The plots of the CDFs are given in Figure 4-5.

There are a few trends in the maximum span lengths that are worth noting. As expected, bridge classes with continuous spans typically have longer span lengths. For example, in Table 4-7 it is seen that the average span length for the MSC Concrete bridge is 19.89 meters while its simply supported counter part, MSSS Concrete bridge has an average length of 12.43 meters. This trend is consistent through the steel and slab bridges as well.

When comparing the MSSS Concrete bridge with its steel and slab equivalents, it is noted that the steel girder bridges tend to have the longest span lengths with an average length of 15.45 meters. This is followed by the concrete and slab bridges having average

Table 4-7: Maximum Span Length Statistics for Nine Bridge Classes.

Class	Mean (m)	Std. Dev. (m)	Median (m)
MSC Concrete	19.89	7.24	19.20
MSC Slab	9.63	4.39	9.10
MSC Steel	26.38	15.25	24.35
MSSS Concrete	12.43	6.51	10.40
MSSS Concrete-Box	13.91	4.76	12.80
MSSS Slab	7.35	3.61	6.00
MSSS Steel	15.45	9.20	13.10
SS Concrete	15.07	7.42	13.40
SS Steel	17.87	11.67	13.70

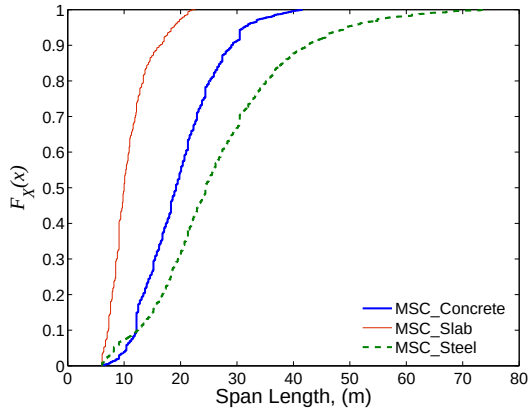

4-5(a):

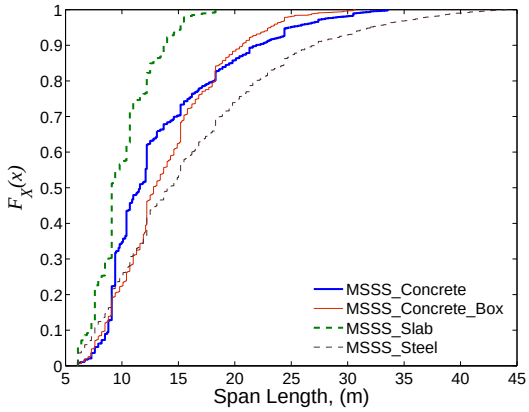

4-5(b):

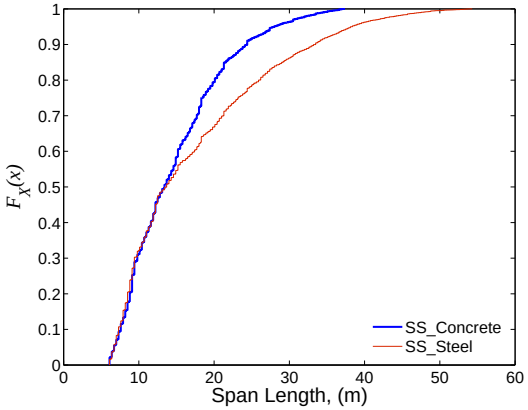

4-5(c):

Figure 4-5: Empirical Cumulative Distribution Functions for the Maximum Span Lengths of (a) Continuous Span Bridges (b) Simple Span Bridges (c) Single Span Bridges.

Table 4-8: Deck Width Statistics for Nine Bridge Classes.

Class	Mean (m)	Std. Dev. (m)	Median (m)
MSC Concrete	12.87	5.29	12.60
MSC Slab	10.73	4.33	9.80
MSC Steel	12.16	6.37	11.70
MSSS Concrete	10.14	4.01	9.10
MSSS Concrete-Box	8.69	2.05	8.20
MSSS Slab	9.14	2.66	8.40
MSSS Steel	9.61	5.02	8.20
SS Concrete	8.59	2.84	7.90
SS Steel	6.29	2.24	5.76

span lengths of 12.43 meters and 7.35 meters respectively. This trend is also consistent in the continuous span and single span bridge classes. These trends are also clearly evident in Figure 4-5.

4.2.4 Deck Width

Similar to the maximum span length, the deck width is measured in meters and is used for simulation purposes later in this study. The recorded deck width in the NBI is the out-to-out (parapet-to-parapet) width along the majority of the bridge length. Some bridges do flare as a result of an on-ramp or an off-ramp but these configurations are not a significant part of the inventory and are not considered as part of this study. Once again, the mean, median and standard deviation for each bridge class are calculated and presented in Table 4-8. The empirical CDFs calculated from the respective data sets for the bridge deck width are presented in Figure 4-6.

The deck widths of the continuous girder bridge classes range on average between 10.73 and 12.87 meters. However, examination of the empirical CDFs show that there is

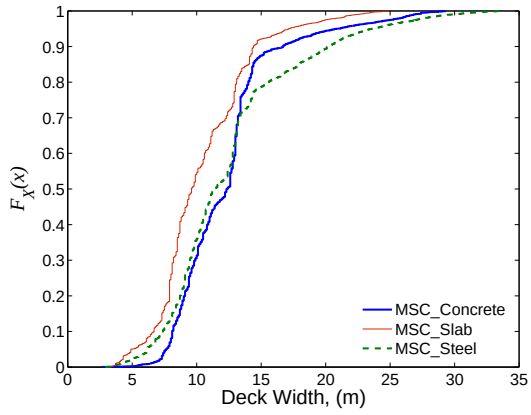

4-6(a):

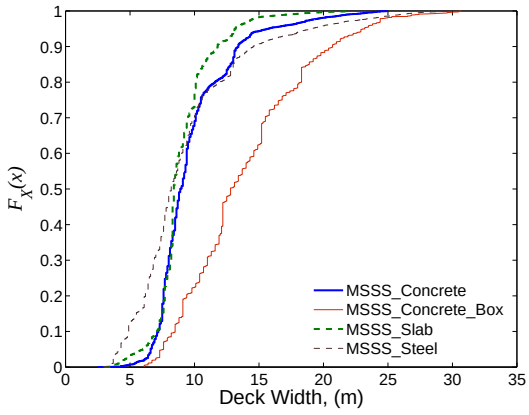

4-6(b):

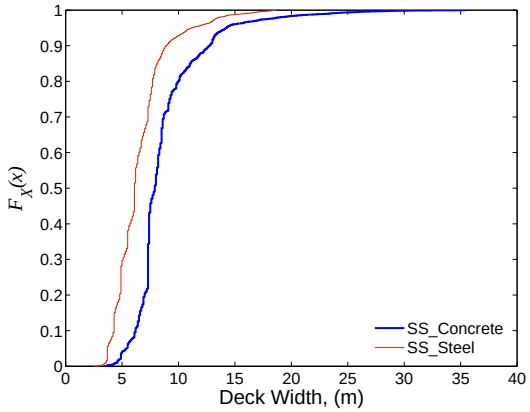

4-6(c):

Figure 4-6: Empirical Cumulative Distribution Functions for Deck Widths of (a) Continuous Span Bridges (b) Simple Span Bridges (c) Single Span Bridges.

relatively small difference in the overall distribution of deck widths between the different continuous girder bridges. These widths are slightly larger than the simply supported bridge classes, which range between 8.69 and 10.14 meters. It is interesting to note that the single span concrete and single span steel bridge classes have average widths of 8.59 and 6.29 meters respectively. These are considerably narrower than the multi-span bridges. This phenomenon may be due to the types of roads on which the single span bridges lie. These types of bridges would most likely be built on rural roads that require a short bridge to cross something such as a small stream bed.

4.2.5 Column Height

The seismic response of a bridge is sensitive to the height of the columns or bents. The NBI, unfortunately, does not explicitly record the height of bridge bents and/or columns. There is a data cell, however, that does record the underclearance of the bridge. This underclearance is measured from the underside of the bridge superstructure to the roadway or railway surface beneath the bridge (FHWA, 1995a). From this information an inference may be made as to the height of the columns or piers. It is assumed that the pier heights correspond directly with the underclearance and the column heights would be on average one meter less to account for depth of the bent beam and the height of the bearings.

A relatively low percentage of the bridges recorded in the NBI actually have an entry other than zero in the underclearance data cell. The coding guide allows for a zero to be entered if the feature below the bridge is not a roadway or railway. To be able to make a stronger inference on the column heights the data from all bridge classes are combined,

from which an empirical CDF can be estimated, among other statistics. The assumption that follows, is that all bridge classes have similar typical pier/column heights.

After combining the underclearance data from all the bridge classes, the empirical CDF was generated and plotted in Figure 4-7(a). Initial observation of this CDF shows that the distribution is not unimodal, as evidenced by the step in the CDF. This is more clearly seen by examination of the frequency diagram plotted in Figure 4-7(b) which shows that the data has two distinct modes.

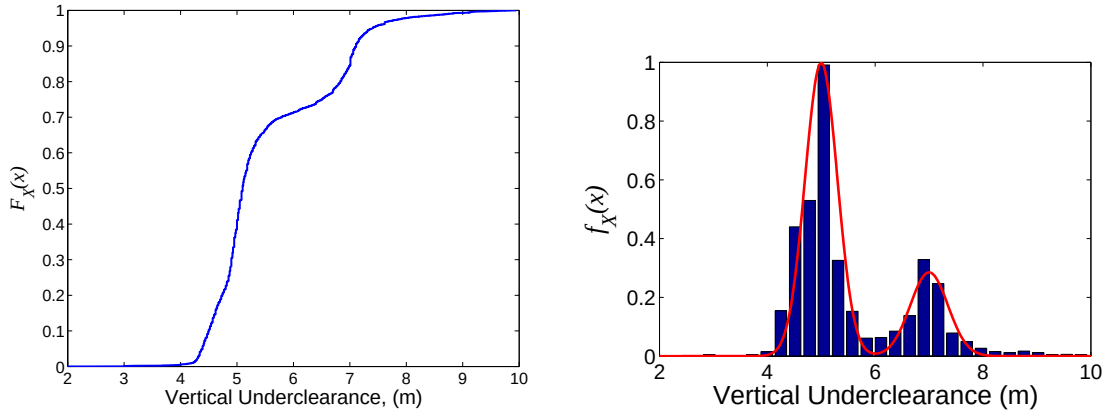

4-7(a): **4-7(b):**

Figure 4-7: Vertical Underclearance of Highway Bridges (a) Empirical CDF (b) Frequency Plot.

The approximate values for the first and second modes of the distribution are roughly 5.0 and 7.0 meters respectively. Other statistics such as the mean and standard deviation are less informative for a bimodal distribution than they are for unimodal distributions and are therefore not presented here. Although there is no clear explanation for the bimodal nature of this data, the modal values agree well with the acquired bridge plans. For the

deterministic models a value of 5.0 meters is assumed for all bridge classes that employ multi-column bents.

4.2.6 Bridge Skew Angle

Skew angle is another common bridge parameter of interest that is provided in the NBI. The skew, θ, is the angle measured between the center line of the bridge supports and the line perpendicular to the bridge center line. Figure 4-8 provides a schematic depicting the skew for clarity. When the skew angle gets large it can significantly alter the response of a bridge. It is easier, however, to make modeling assumptions when the skew angle is small. For this reason this parameter was investigated for each class of bridges.

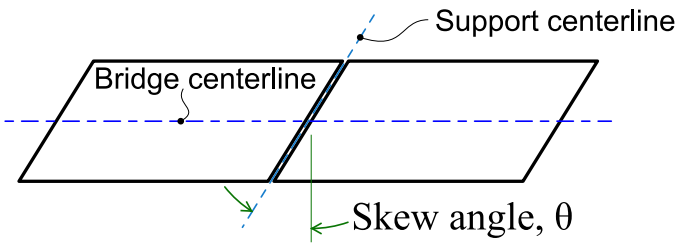

Figure 4-8: Schematic Depicting Bridge Skew Angle.

It is of interest to see the percentages of bridges, in a particular bridge class, within certain ranges. Table 4-9 lists the percentages of bridges in each class in four angle ranges. These ranges are $\theta = 0°$, $1° \leq \theta < 15°$, $15° \leq \theta < 30°$ and $\theta \geq 30°$. Also included in the table are a few sample statistics for each class such as mean, standard deviation and median.

Table 4-9: Skew Angle Statistics for Nine Bridge Classes.

Class	**Mean (Deg.)**	**Std. Dev. (Deg.)**	**Median (Deg.)**	0° **(%)**	1° – 15° **(%)**	15° – 30° **(%)**	< 30° **(%)**
MSC Concrete	13.11	15.74	6.00	47.0	18.1	21.0	13.9
MSC Slab	9.89	13.74	0.00	56.9	16.0	19.0	8.1
MSC Steel	13.19	16.14	5.00	47.1	17.0	19.9	16.0
MSSS Concrete	7.14	13.36	0.00	72.4	8.4	12.2	7.0
MSSS Concrete-Box	11.78	15.08	0.00	54.1	12.9	21.4	11.7
MSSS Slab	4.09	10.75	0.00	84.8	4.5	7.1	3.7
MSSS Steel	10.24	15.41	0.00	60.4	12.4	14.9	12.2
SS Concrete	7.67	13.57	0.00	70.6	8.8	13.2	7.4
SS Steel	4.21	11.00	0.00	83.8	5.2	6.5	4.5

It is interesting to note for the continuous girder bridges, that anywhere between 64.1% and 72.9% of the bridges have skew angles of 15 degrees or less with a large majority of those being zero degrees. When the MSSS and the SS bridges are considered it is seen that even a larger percentage of the bridges are 15 degrees or less. For these classes, this ranges between 67.0% and 89.3%. This implies that the majority of all the bridges considered in this study have a small skew angle. Because of this it is justified to ignore the skew angle in the fragility analysis of these bridge classes. In addition, HAZUS-MH provides a methodology to adjust fragility curves to account for skew if it is required (FEMA, 2003).

4.2.7 Assorted Statistics

There are a few other statistics which aren't explicitly required for simulation purposes but rather are used for validating assumptions. These statistics include the year of construction and the deck, superstructure and substructure ratings.

Table 4-10: Construction Year Statistics for Nine Bridge Classes.

Class	**Median (year)**	< 1990 **(%)**
MSC Concrete	1985	66.8
MSC Slab	1980	72.6
MSC Steel	1975	79.6
MSSS Concrete	1972	80.7
MSSS Concrete-Box	1982	76.9
MSSS Slab	1971	84.0
MSSS Steel	1965	90.8
SS Concrete	1979	74.7
SS Steel	1969	83.5

4.2.7.1 Construction/Reconstruction Year

As stated earlier, the construction year can give an indication as to whether seismic considerations were implemented rigorously in the design phase of the bridge. HAZUS-MH highlights that if a bridge in California was built prior to 1975, then it has a conventional and not a seismic design (FEMA, 2003). However, for non-California bridges the switch from conventional to seismic design procedures did not occur until 1990. Therefore, the year built is used to make decisions when generating analytical models. Table 4-10 presents the median year of construction and also the percentage of the inventory that was built prior to 1990.

The MSC Concrete bridge class appears to contain the newest bridges. It has a median construction year of 1985 with only 66.8% of its bridges being conventionally designed. Thus, it appears that it is one of the more popular bridge construction types in recent years. On the other extreme is the MSSS Steel bridge class with a median construction year of 1965 and having over 90% of its bridges being conventionally designed.

Some general observations are that the steel bridges appear to be a less favorable construction material than concrete in recent years. This trend can be seen when looking at the median as well as the percentage. In addition, it appears that the simply supported girder bridges were more favored in earlier years but as seismic concerns became greater their continuous girder counterparts became the preference. This is understandable due to the unseating problems that simply supported bridges have exhibited in the past. Continuous spans have also been more common because of the elimination of servicing required at the hinges.

Clearly, the majority of bridges under consideration were built prior to 1990. Therefore, this study assumes a non-seismic design when generating analytical models.

4.2.7.2 Condition Ratings

Every two years bridges in the inventory database are inspected and rated on their condition. The rating scale is from zero to nine with nine being excellent condition and zero being a failed condition. These ratings are given for the deck, superstructure and substructure of each bridge. This information is not explicitly used when modeling but rather gives an indication of the appropriateness of generating models from existing bridge plans. Table 4-11 gives the median rating values for each of the three components.

The median rating for most of the bridges and their components is seven, which is to be interpreted as being in good condition with a few minor problems. One exception is the MSSS Steel bridge class which has a six (satisfactory) rating for the deck and substructure. This is to be expected since this bridge class contains the oldest bridges. Most of the bridges

Table 4-11: Median Condition Ratings for Nine Bridge Classes.

Class	Deck	Superstructure	Substructure
MSC Concrete	7	7	7
MSC Slab	7	7	7
MSC Steel	7	7	7
MSSS Concrete	7	7	7
MSSS Concrete-Box	7	7	7
MSSS Slab	7	7	7
MSSS Steel	6	7	6
SS Concrete	8	8	8
SS Steel	8	7	7

will be modeled based on typical bridge plans. However, experimental results will be used to calibrate the steel girder bridge models to help account for some of this deterioration.

4.3 Closure

Nine bridge classes typical to the CSUS are identified. These nine bridges account for almost 90% of the over 160,000 highway bridges in the region. Statistics show that the majority of all of these bridges have three spans and are of a regular configuration (i.e little or no skew). Seismic design was not performed when most of these bridges were built, thus, indicating the lack of seismic details in most of these bridges.

The information from this inventory analysis is not only used to identify typical bridge classes but also to identify some of their basic structural and geometric characteristics. By the very nature of the inventory information obtained herein, the fragility curves which result from are most appropriate when considering suites of bridges across a region. If a specific bridge is of interest, the actual configuration and structural parameters of that bridge should be used to generate a bridge specific fragility curve.

CHAPTER V

THREE-DIMENSIONAL ANALYTICAL MODELS OF TYPICAL BRIDGES IN THE CENTRAL AND SOUTHEASTERN UNITED STATES

The fragility curve generation methodology presented and used in this study is an analytical approach and therefore requires analytical models of the subject bridges. These analytical models can be generated with varying degrees of fidelity and any number of simplifying assumptions. Analysis time increases as the fidelity of the model increases. Although there is typically more confidence in the the models with higher fidelity, simplifying assumptions are often required to make the processing times more feasible.

One common area of simplification comes in choosing the number of modeling dimensions, two (2-D) or three (3-D). A two dimensional model is much more desirable because a three dimensional model may be particularly complex. The question as to which two dimensions should be modeled (i.e. longitudinal or transverse) arises and is not easily answered. There have been a number of studies that indicate that the longitudinal direction controls the response of the bridge (Choi, 2002; Rashidi and Ala Saadeghvaziri, 1997; Shinozuka, 1998) while others maintain that the loading in the transverse direction controls the damage of the bridge (Ala Saadeghvaziri and Rashidi, 1998; Cheng et al., 1998). There are yet others who believe that a bridge must be modeled in three dimensions and have the

longitudinal and transverse responses combined in some fashion to adequately represent the system (ATC, 1991; Jernigan and Hwang, 2002; Yashinsky, 1999). In a probabilistic framework this last recommendation makes sense. It is highly probable that although the longitudinal direction controls in a deterministic setting, the transverse response still makes a significant contribution in a probabilistic setting. This is best understood in the framework of total probability. Equation 5.1 illustrates the law of total probability when calculating the probability of reaching some limit state, LS.

$$P[LS] = P[LS|long] \cdot P[long] + P[LS|trans] \cdot P[trans] \tag{5.1}$$

Although the probability is high of entering the limit state when the loading is in the longitudinal direction, the total probability can still be affected by a transverse loading. This type of effect cannot be measured in a deterministic analysis.

It is clear from the many different views on this issue that there is no definite methodology that should be used for the analytical modeling of bridges. It may also be irresponsible to assign one methodology to all different bridge types. Therefore, in this study, 3-D models will be generated for all nine of the subject bridge types presented in Chapter 4. With the 3-D models, it becomes possible to explore the nature of the 2-D responses in a probabilistic framework.

5.1 Typical Highway Bridge Construction

Highway bridges, such as the one shown in Figure 5-1, are usually constructed by using a number of typical bridge components. These components are classified into one of three main categories. The first such category is known as the superstructure which consists

of the girders, deck slab and parapet. These components are illustrated and labeled in Figure 5-2. The second category is known as the substructure which are the components which provided support to the superstructure. The substructure consists of abutments, bents (beams and columns), footings and foundations (piles). The third category of components are the bearings whose primary responsibility is to tie the superstructure to the substructure.

Figure 5-1: Picture of Example Highway Bridge.

The analytical bridge models generated in this study have a high degree of fidelity and therefore require a significant amount of detail in modeling the various bridge components. The models are created in the analysis software *O*penSees which was initiated and is maintained by the Pacific Earthquake Engineering Research (PEER) Center (McKenna and Feneves, 2005). Appendix C contains a comprehensive discussion of each relevant bridge component and its associated analytical model.

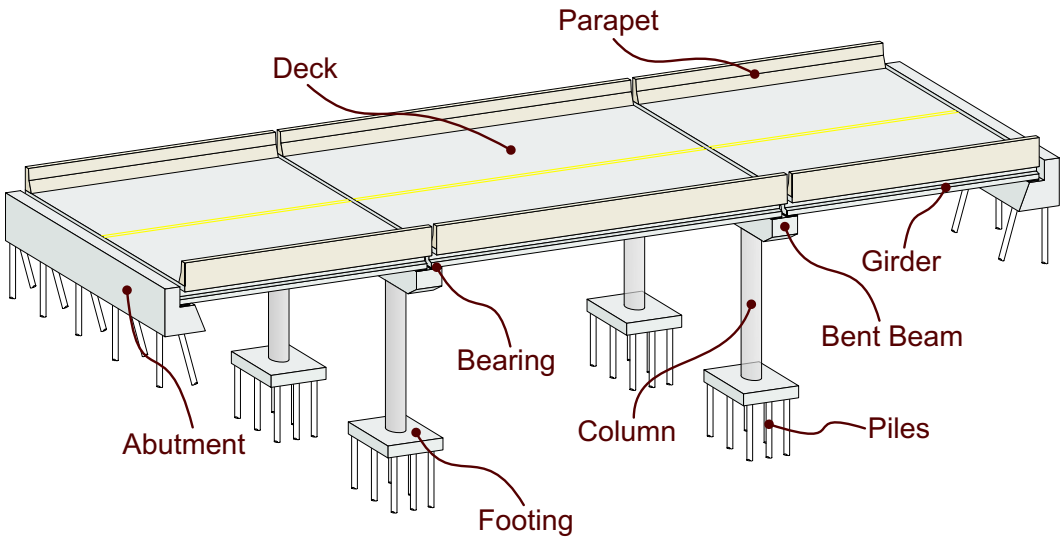

Figure 5-2: Illustration of Major Bridge Components.

5.2 Three Dimensional Analytical Models of Typical Bridges

In this section, analytical models of the nine considered bridge classes which are common to the CSUS are developed and presented. The intent here is to present the analytical model for a typical configuration for each bridge class and illustrate a typical seismic response for each class. Nonlinearities are considered in material and bridge component behavior. Five percent Rayleigh damping is used in these models. The damping coefficients are calculated such that five percent damping occurs in the first two modes as calculated by the eigenvalue analysis. Note five percent damping is used for the deterministic analyses presented in this chapter. In later chapters the damping ratio is assumed to be a random variable.

The seismic response is illustrated using a single ground motion from the suite of Rix ground motions (Rix and Fernandez-Leon, 2004). The selected ground motion has a magnitude 7.5, an epicentral distance of 20 km and a duration of 25.1 seconds. The ground

motion also has a peak ground acceleration (PGA) of 0.65 g and a response spectrum with five percent damping, as is presented in Figure 5-3. The time history analyses are conducted using a time step of 0.0025 seconds. However, these time steps may be reduced further when numerical convergence issues arise. It is also noted that the ground motions are applied at the pile caps and abutments where the soil-structure interaction is simply accounted for with a set of springs. This pattern holds for all time history analyses performed in this study.

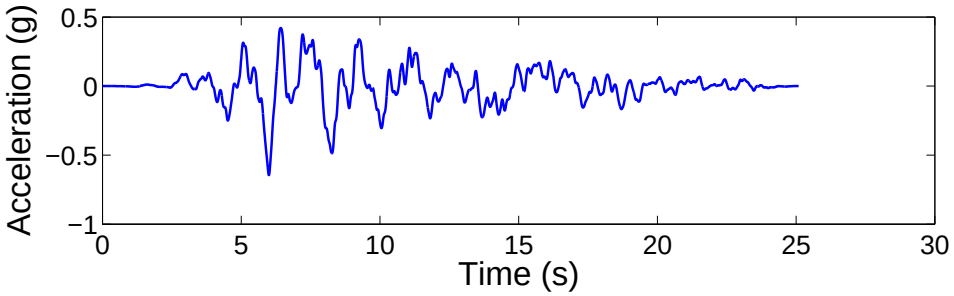

5-3(a):

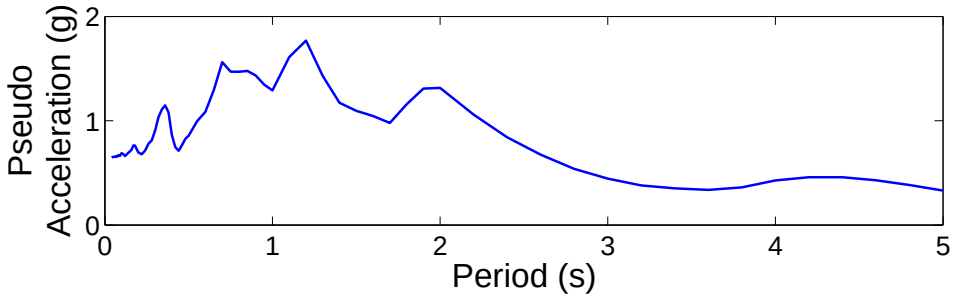

5-3(b):

Figure 5-3: Ground Motion Used for Illustration of Seismic Responses (a) Time History (b) Response Spectrum (5% Damping).

5.2.1 Multi-Span Simply Supported Concrete Girder Bridge

5.2.1.1 Layout

A typical configuration for a Multi-Span Simply Supported Concrete (MSSS Concrete) girder bridge is shown in Figure 5-4. This bridge has three spans which are 12.2, 24.4 and 12.2 m long respectively for a total length of 48.8 m. The width of each span is 15.01 m which is constructed of eight AASHTO type prestressed girders. The girders for the end spans are AASHTO Type I girders which bear on a pile type abutment at one end and a multi-column bent at the other end. The center span utilizes AASHTO Type III girders which are supported fully by two multi-column bents. The bearings for this bridge are elastomeric pads with two 25.4 mm ϕ steel dowels as seen in Figure C-25. For the type I girders the pads are 406 mm long by 152 mm wide and 25.4 mm thick while the type III girders use pads which are 559 mm long by 203 mm wide and still 25.4 mm thick. As mentioned previously, the only difference between the fixed type and the expansion type bearings is the size and shape of the holes for the steel dowels. The fixed bearings and expansion bearings alternate along the length of the bridge and are noted as triangles and circles respectively in Figure 5-4.

The multi-column bents for this bridge each consist of a 1066.8 mm wide by 1219.2 mm deep reinforced concrete bent beam held up by three 914 mm ϕ by 4600 mm tall circular reinforced concrete columns which in turn are tied to individual pile foundations. These columns are spaced horizontally at 5.0 m on center. The bent beam uses 15-#29 and 4-#16 reinforcing bars across the section while transverse steel is provided by #16 stirrups spaced on average of 305 mm as seen in Figure 5-5(b). The columns use 12- #29 bars to

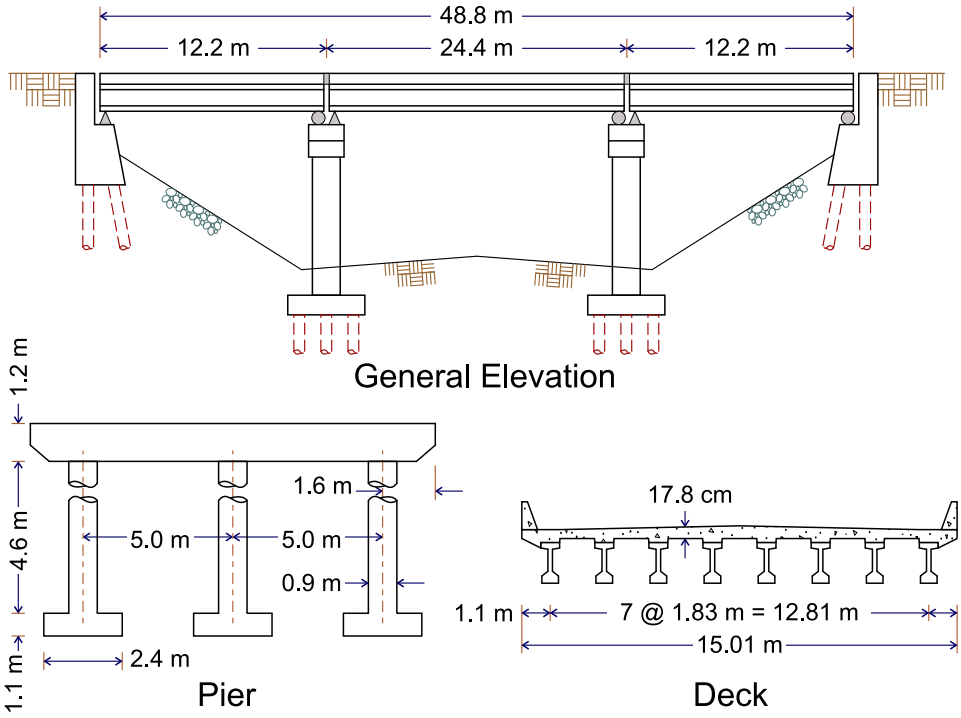

Figure 5-4: MSSS Concrete Girder Bridge Configuration.

provide longitudinal reinforcement which are contained by #13 transverse bars spaced at 305 mm which is shown in Figure 5-5(a). The design strength for the concrete is assumed to be 20.7 MPa while the reinforcing steel has a yield strength of 414 MPa. The specifics of these column details come from an investigation of existing bridge plans and also from the work done by Hwang et al. (2000).

The layout for the pile foundations used for this bridge type are illustrated in Figure C-51(b). The pile caps are 2438 mm square and 1092 mm thick reinforced concrete footings with the reinforcement being placed on the bottom side. Eight piles are used in this layout and are embedded into the bottom of the footing approximately 305 mm with no positive connection provided between the two. The pile cap is connected with the columns using

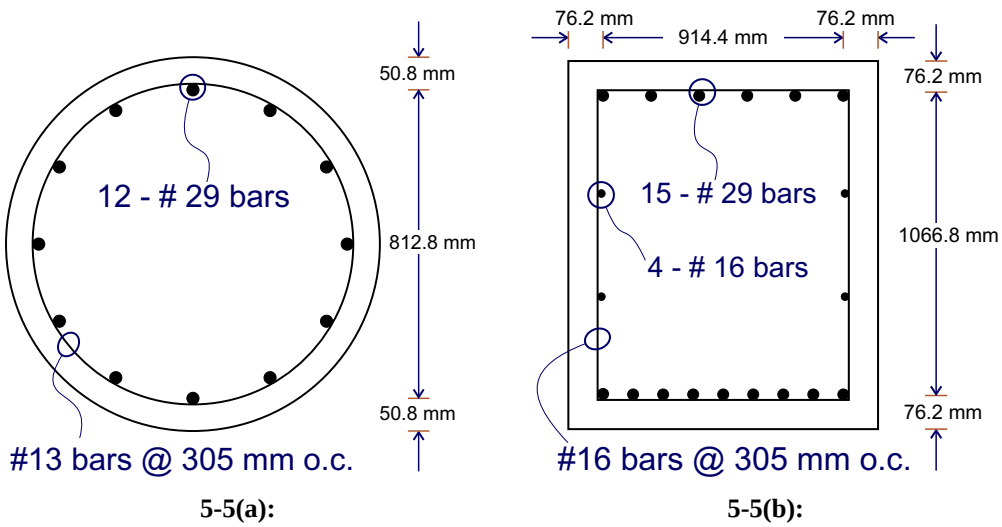

Figure 5-5: Concrete Member Reinforcing Layout (a) Bent Beam (b) Columns.

914 mm long lap splices at the bases of the columns. It is this lap splice which has proven to be problematic and a source of failure under seismic loadings.

The abutments used for this bridge are the pile-bent girder seat type abutments which were introduced in Section C.4. Using existing bridge plans for guidance, it is assumed that the abutments for this bridge type utilize a 2.4 m tall back wall in conjunction with ten driven piles.

5.2.1.2 Seismic Response

An eigenvalue analysis of this bridge using *O*penSees reveals that its fundamental period is approximately 0.62 seconds with the predominant motion being in the longitudinal direction. This is a very dominant mode in that it activates ~ 84 percent of its mass in this direction. The mode shape for this period is presented in Figure 5-6 and thus confirms the longitudinal nature of the mode. The second mode is a transverse mode which is decoupled from the first mode with a period of 0.46 seconds, activating ~ 78 percent of the

bridge's mass. For a more detailed presentation of the modal data for all bridge types, refer to Appendix D.

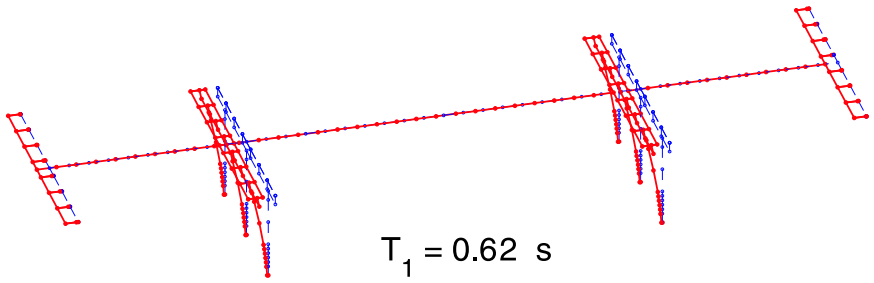

Figure 5-6: Fundamental Mode of MSSS Concrete Girder Bridge.

As mentioned previously, this bridge was subjected the the 0.65 g earthquake presented in Figure 5-3 to illustrate the nature of its response to seismic loading. The loading was applied to the bridge in the longitudinal direction and also applied in the transverse direction to allow for comparison of the different loading directions. Only the responses of a few of the bridge components are presented in this section due to the large number of components and responses in each bridge.

Figure 5-7 presents the displacement time histories for each of the three decks under the different loading scenarios. Under the longitudinal loading, the simple supported nature of the individual spans is highlighted in that the spans are permitted to move out of phase with each other. This results in an overall displacement of approximately 100 mm. This also results in column drifts of approximately 0.015 mm/mm. Under the transverse loading scenario the two end spans of the bridge displaced more-or-less equally but the center span with its larger mass experienced displacements as large as 180 mm. This loading however,

produced column drifts on the order of 0.005 mm/mm thus indicating that most of the displacement was due to deformation in the bearings.

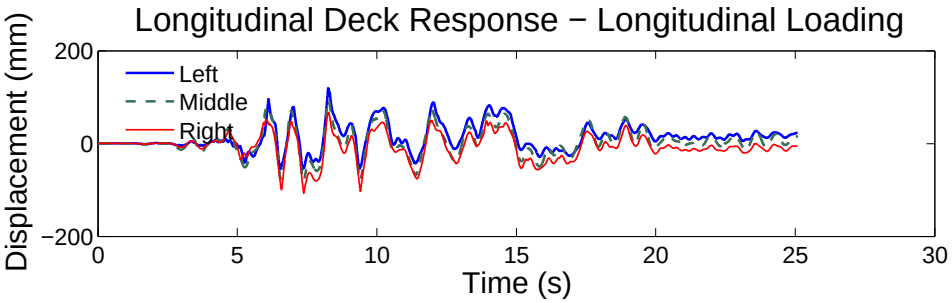

5-7(a):

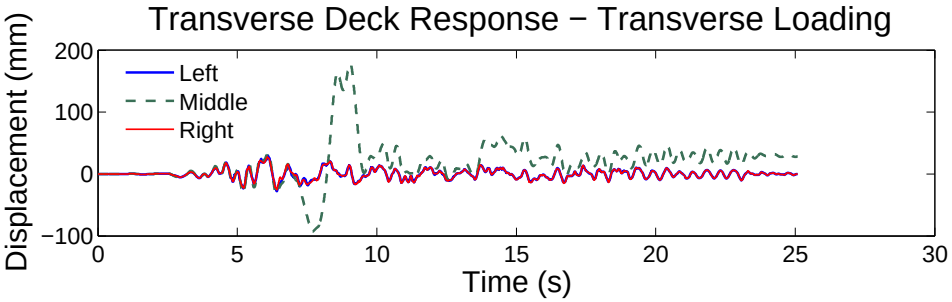

5-7(b):

Figure 5-7: Deck Displacement Time Histories for MSSS Concrete Girder Bridge Under (a) Longitudinal Loading (b) Transverse Loading.

In addition to column drift, the responses of the columns are also monitored and presented in terms of a moment-curvature relationship. Figure 5-8 shows this response for the columns in the right most bent, as seen in Figure 5-4. The maximum moment seen in the columns under longitudinal loading is on the order of 1600 kN-m resulting in a curvature of about 0.01 m^{-1}. Another way of looking at the deformation or curvature of the columns is through a curvature ductility demand ratio, μ_c, which is given in Equation 5.2.

$$\mu_c = \frac{\kappa_{max}}{\kappa_{yield}} \tag{5.2}$$

Where κ_{yield} is the curvature in the column which causes first yield of the outer most reinforcing bar and κ_{max} is the maximum curvature demanded of the column throughout the loading. Under longitudinal loading, the ductility demand is around 2.8 while transverse loading produces a demand ductility which is less than one indicating that the column remains elastic. The same trend is observed for the other column line. It is clear from these results that the longitudinal direction tends to be the most critical direction as far as column response is concerned.

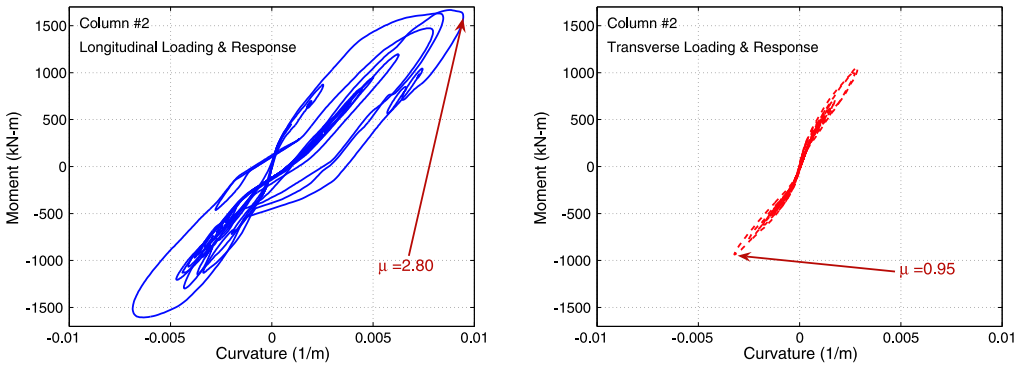

5-8(a): **5-8(b):**

Figure 5-8: Columns of the MSSS Concrete Girder Bridge Under (a) Longitudinal Loading (b) Transverse Loading

Another set of components which are of interest are the fixed and expansion bearings. Their responses are given in terms of a force-displacement hysteresis from which maximum deformations can be attained. Only the responses of the fixed bearings are presented here in Figure 5-9 because the response of the expansion bearings were not much different. This

similarity in responses of the two bearing types illustrates the relatively small impact that the steel retaining dowels have on the overall response of the bridge. It is easily seen, in Figure 5-9, the point where these steel dowels engage. Fixed bearings numbered 1, 2 and 3 correspond with the bearings under the left, middle and right spans respectively. The maximum response under longitudinal loading occurred in fixed bearing #1 which resulted in a maximum deformation of approximately 120 mm. However, the peak response in the bearings occurred in bearing #2 under the transverse load with a maximum deformation of 170 mm. In this case there is no clear loading direction which is more critical than the other, thereby strengthening the argument for needing 3-D models.

The relatively flexible nature of these bearings does allow for a certain degree of decoupling of the superstructure from the substructure, but these types of bearings are also susceptible to larger deformations. These larger deformations could result in the bearings walking out from under the girders or could also lead to an unseating of the girders. Although the figures are not presented here, there is evidence shown by the impact elements that there was pounding between the individual decks and also the end spans with the abutments. This pounding can help to limit the bearing deformation in one direction but can also cause on increase in demand on other components, such as the abutments.

As introduced in Section C.4, the abutments respond in passive action (soil) and active action (piles) in the longitudinal direction. However, the abutment response is only characterized by the piles in the transverse direction. For this bridge type, the passive response of the abutments in the longitudinal direction appears to dominate as seen in Figure 5-10. In passive action the response became nonlinear resulting in a deformation which exceeded 25 mm. The pile action of the abutments never did exceed the linear range with maximum

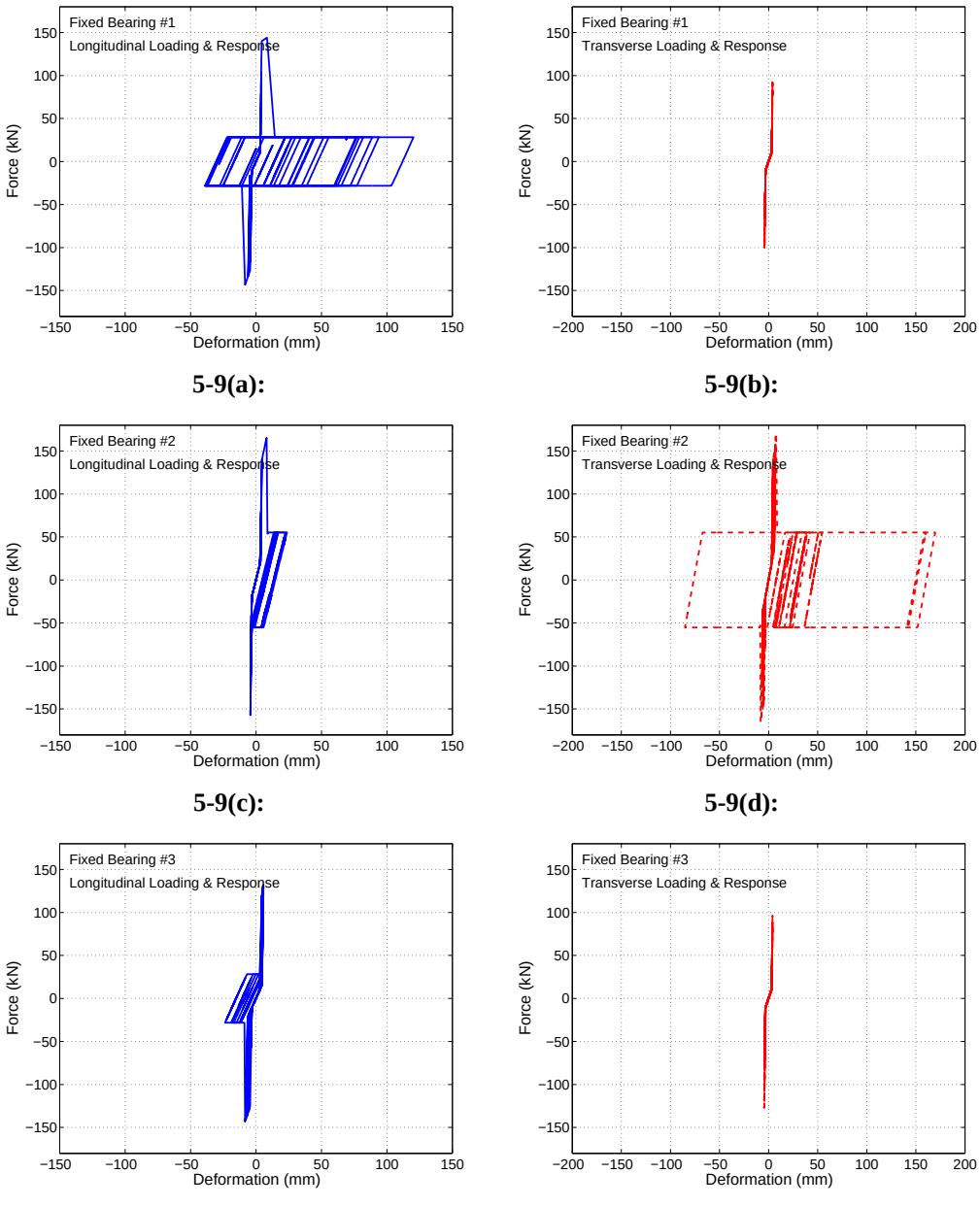

Figure 5-9: Fixed Bearings of the MSSS Concrete Girder Bridge Under (a) #1 - Longitudinal Loading (b) #1 - Transverse Loading (c) #2 - Longitudinal Loading (d) #2 - Transverse Loading (e) #3 - Longitudinal Loading (f) #3 - Transverse Loading

deformations not much greater than 5 mm. This behavior is not alarming in that pounding between the decks and abutments would tend to engage passive action while doing little to engage active action. Since transverse loading doesn't produce much in the way of pounding, very little force gets transferred to the abutments.

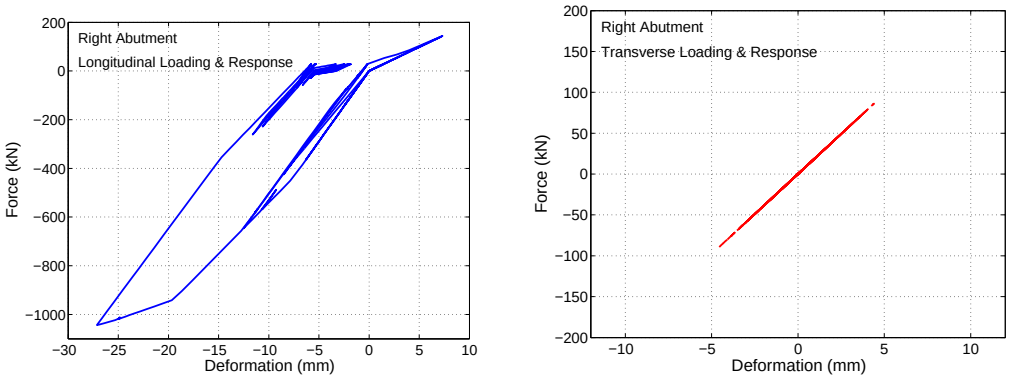

5-10(a): **5-10(b):**

Figure 5-10: Right Abutment of the MSSS Concrete Girder Bridge Under (a) Longitudinal Loading (b) Transverse Loading

5.2.2 Multi-Span Continuous Concrete Girder Bridge

5.2.2.1 Layout

The multi-span continuous concrete girder bridge is very similar to the MSSS Concrete girder bridge. The layouts and configurations, as seen in Figures 5-4 and 5-11, are identical except for one detail. The spans are made continuous by casting a concrete parapet between the deck and girders as is illustrated in the detail of 5-11. This is generally done to reduce maintenance as well as to reduce the dead load moment. This modification also helps when

it comes to seismic loading in that it reduces the number of gaps at which pounding may occur.

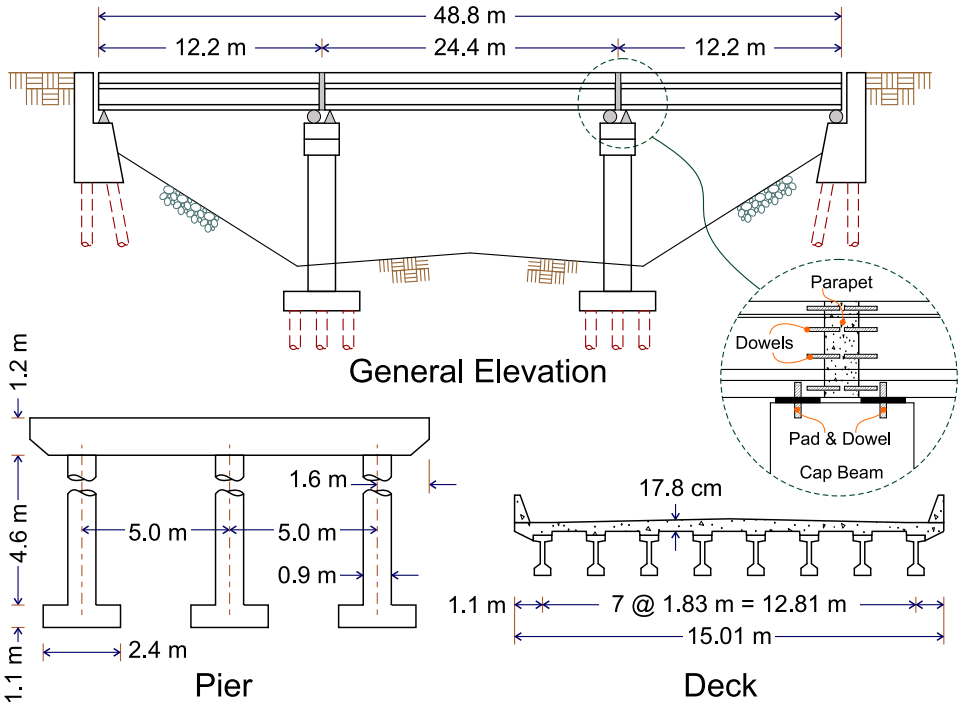

Figure 5-11: MSC Concrete Girder Bridge Configuration.

5.2.2.2 Seismic Response

With the addition of the parapet to the concrete girder bridge, the period shifts from 0.62 seconds to 0.54 seconds. This of course indicates that the structure became more stiff because of the parapet. This first mode, whose mode shape is presented in Figure 5-12, activates ~93 percent of its mass in the longitudinal direction. The second mode is a transverse mode with a period of 0.42 seconds activating ~92 percent of its mass (see Table D-2).

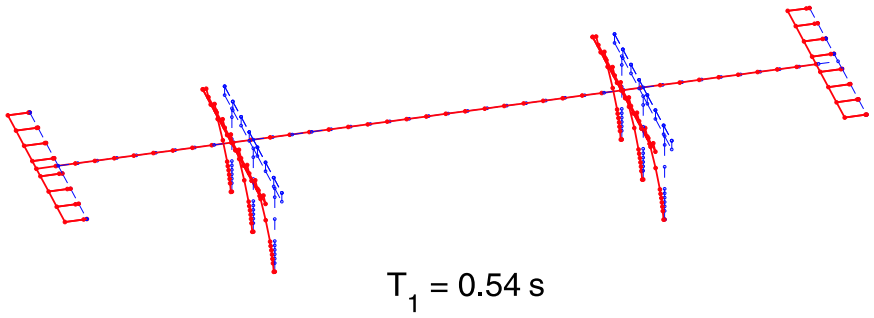

Figure 5-12: Fundamental Mode of MSC Concrete Girder Bridge.

The overall displacement time history of the decks is not much different for this bridge than for its simply supported counter part. However, it is observed that the decks and the columns seem to move more-or-less together. This results in relatively low deformation in the bearings over the bents but increases the demand in both the columns and the bearings located at the abutments. Figure 5-13, which is the column response for the right most column line, shows that the ductility demand on the columns increased to approximately $\mu_c = 3.65$ and $\mu_c = 2.36$ for longitudinal and transverse loading respectively. Since the overall displacements of the deck did not change much and the deformation did not occur in the bearings over the bents, it stands to reason that the deformation must occur in the columns as is seen.

As previously mentioned, the bearings over the bents experienced relatively little deformation under both loading conditions. These deformations are on the order of 5 mm. This is not what was observed for the bearings over the abutments, however, where large deformations on the order of 120 mm for longitudinal loading and 50 mm for transverse loading are responsible for pounding at the abutments. This pounding at the abutments is

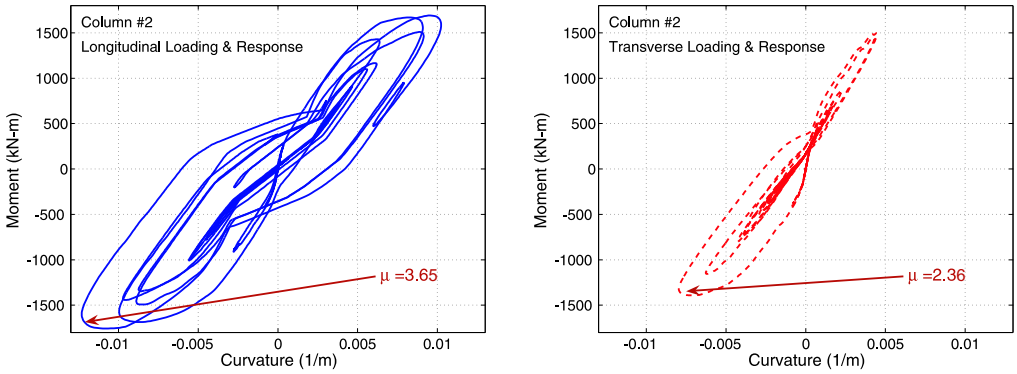

5-13(a): **5-13(b):**

Figure 5-13: Columns of the MSC Concrete Girder Bridge Under (a) Longitudinal Loading (b) Transverse Loading

responsible for passive responses similar to those observed in Figure 5-10, with a maximum deformation of 38 mm.

5.2.3 Multi-Span Simply Supported Concrete Box-Girder Bridge

5.2.3.1 Layout

Another bridge which is closely related to the previously discussed bridge types is the multi-span simply supported concrete box girder bridge (MSSS Concrete-Box). A typical configuration for this bridge type is given in Figure 5-14 which highlights some the slight differences which are present. The substructure, including the abutments, bents and foundations, is the same as before with the differences coming in the superstructure. The three spans have a length of 12.2 m, 18.2 m and 12.2 m and are built using multiple precast box girders which are post-tensioned together in the transverse direction. The change in span lengths and in the structural configuration of the decks result in a change of the mass of the system which in turn changes the response of the bridge.

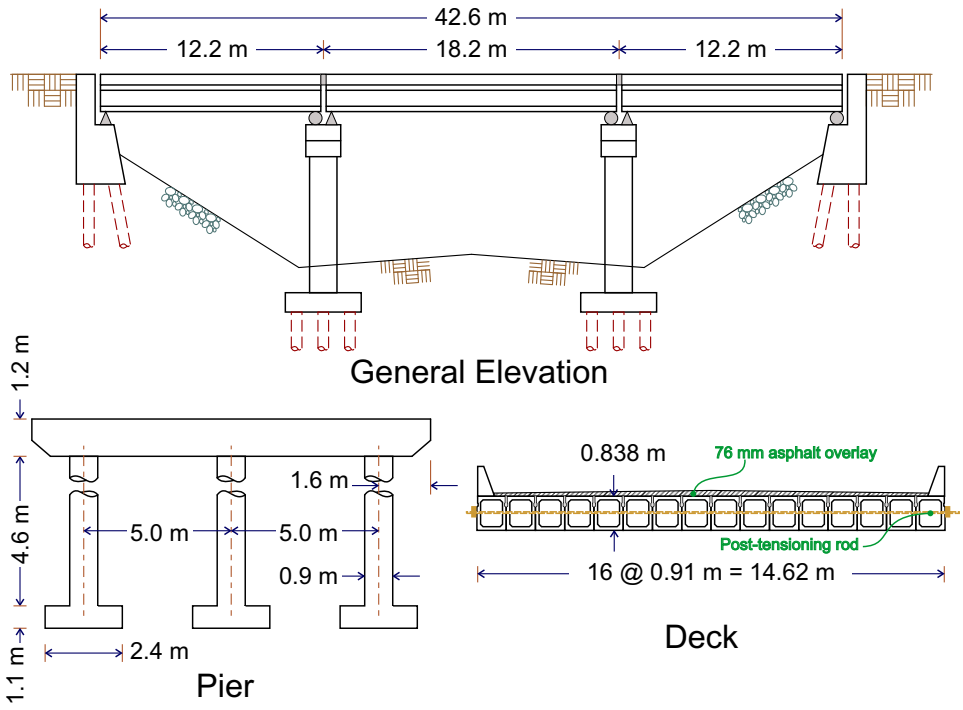

Figure 5-14: MSSS Concrete-Box Girder Bridge Configuration.

The bearing system for this bridge type is slightly different than those for the prestressed concrete girders. These bearings are still made of elastomeric rubber but are much larger and thinner. The bearings run the full width of each box girder segment, which is generally 914 mm wide, and provide a bearing length somewhere between 305 mm and 457 mm depending on the span length. The thickness of the pad is generally 6.4 mm thick for spans less than 14.6 m and 12.7 mm thick for those spans greater than 14.6 m. As seen in Equation C.1, the stiffness of the bearing is a function of its cross-sectional area and its thickness. Because of their larger areas and smaller thicknesses, the stiffness of these bearings is greater than for those used with the AASHTO-type girders. Two steel retention

dowels are used in each end of the box girders. A schematic of this bearing configuration is given in Figure 5-15.

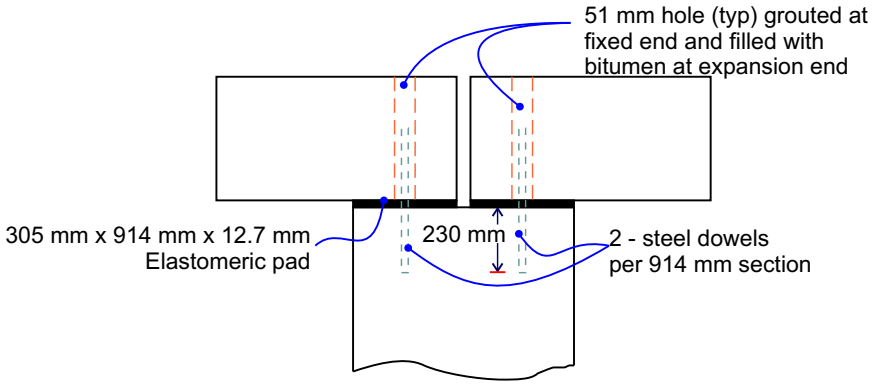

Figure 5-15: Typical Elastomeric Bearing Used for Concrete-Box Girder and Slab Bridges.

5.2.3.2 Seismic Response

The aforementioned shift in the mass and stiffness of this bridge system causes there to be a noticeable change in the fundamental period of the bridge which is 0.31 seconds. This is approximately half the period calculated for the MSSS Concrete bridge but it still is a longitudinal mode activating over 93 percent of the mass (Figure 5-16). The second horizontal mode for this bridge is transverse with a period of roughly 0.14 seconds.

The response of the decks looks very much the same as that displayed in Figure 5-7 for the MSSS Concrete bridge, however, the maximum displacement is around 50 mm instead of 100 mm in the longitudinal direction and 30 mm in the transverse direction. This reduced response is seen throughout most of the other bridge components. The response for the far

right concrete column line is presented in Figure 5-17 which shows that both longitudinal and transverse loading caused a curvature ductility of less than $\mu_c = 1.0$.

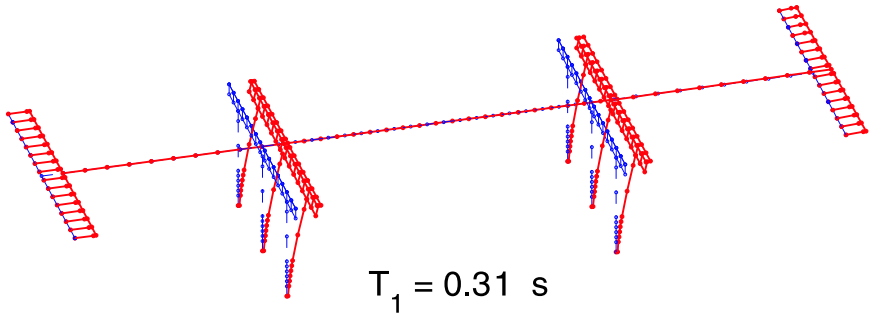

Figure 5-16: Fundamental Mode of MSSS Concrete-Box Girder Bridge.

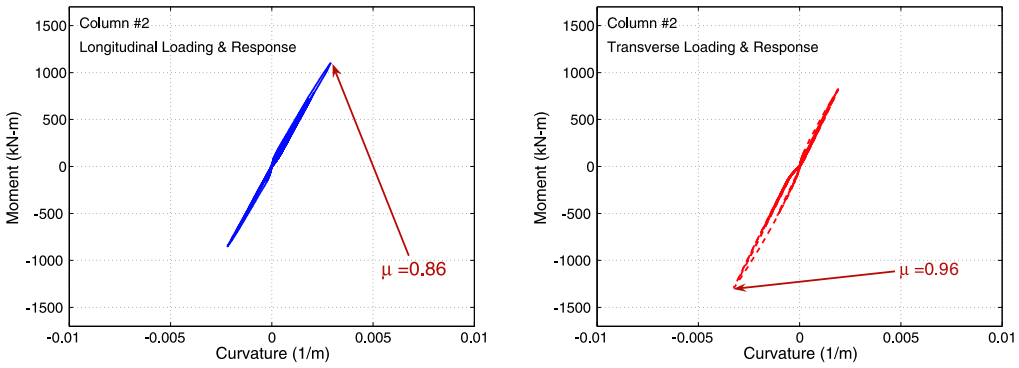

5-17(a): **5-17(b):**

Figure 5-17: Columns of the MSSS Concrete-Box Girder Bridge Under (a) Longitudinal Loading (b) Transverse Loading

The same trend is observed in the response of the bearings, both fixed and expansion types. Under longitudinal loading, the maximum deformations in the bearings are 17 mm

and 6 mm for the expansion and fixed bearings respectively. These deformations are even smaller under transverse loading where all deformations come in under 3 mm.

It is clear from examination of the column and bearing responses that they may not be the most vulnerable components in this bridge type. This becomes more apparent as the responses of the abutments are evaluated. Figure 5-18 shows the response of the right most abutment, as both the right and the left abutment responses are nearly identical. It is observed that this bridge type tends to activate the piles in the abutment, which results in active deformations exceeding 50 mm. Although this loading causes the piles to enter a highly nonlinear range, while in the passive action it never leaves the linear range. This is a completely different behavior than that observed in the concrete girder bridges where most of the abutment response was in passive action. This significant change is not difficult to understand as we consider once again the increased stiffness of the bearing system. Previously the bearings were fairly flexible and allowed for relatively large displacements to occur between the decks and the abutments. These large deformations resulted in pounding on the abutment and hence a significant demand in passive action. On the other hand the relative displacement between the deck and abutments for this bridge type is quite small thereby eliminating any pounding effects. This causes all loads from the decks to be transferred to the abutments via the bearings themselves. This load transfer is indiscriminate as to which way it loads the abutments. Since the stiffness of the abutments is lower in active action (pulling away from the back-fill), larger deformations are observed in this direction.

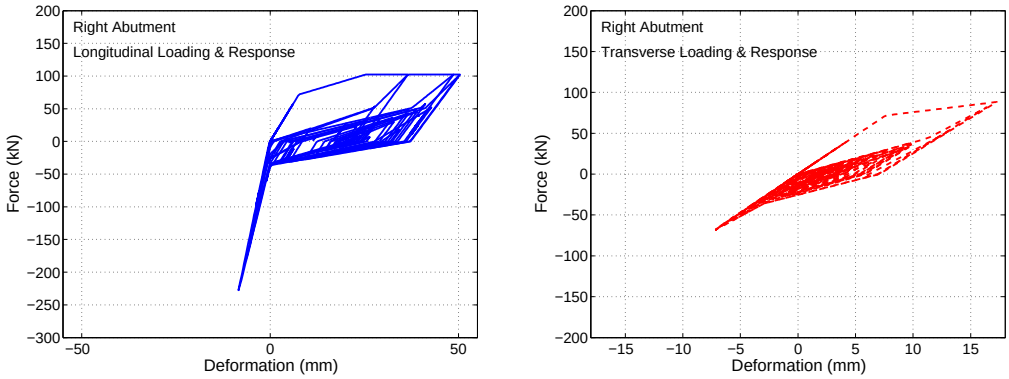

5-18(a): **5-18(b):**

Figure 5-18: Abutments of the MSSS Concrete-Box Girder Bridge Under (a) Longitudinal Loading (b) Transverse Loading

5.2.4 Multi-Span Slab Bridges

5.2.4.1 Layout

Two bridge classes which are very closely related to the box girder bridges are the multi-span simply supported (MSSS Slab) and the multi-span continuous slab (MSC Slab) bridges. Their superstructure or decks are often constructed in the same manner using 914 mm wide precast prestressed concrete sections which also use the same bearing system as given in Figure 5-15. Cast in place reinforced concrete can also used, but the bearing system is still generally the same .

The slab bridge construction is generally used for bridges requiring shorter span lengths which also results in a smaller substructure system. The configuration for the slab bridges, both simply supported and continuous, is shown in Figure 5-19. All three of the spans are equal in length measuring 9.15 m resulting in an overall bridge length of 27.45 m. These spans are made continuous either by casting a concrete parapet between the segments or

my making a continuous pour for cast in place concrete. The deck comes in at a width of 10.1 m and a depth of 0.41 m.

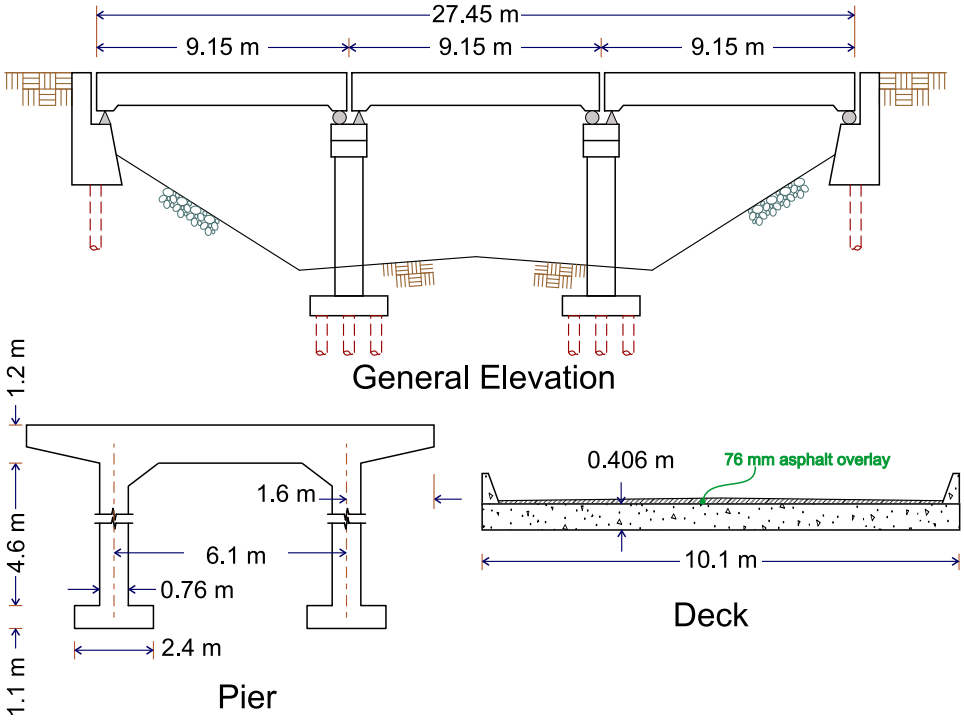

Figure 5-19: MSSS Slab Bridge Configuration.

The main difference between the box girder and the slab bridges comes in the substructure. With shorter spans and subsequently smaller loads, the substructure for the slab bridges tend to be smaller. Figure 5-19 provides a sketch of the two column bent used for this bridge type. It was very common when many of these bridges were built to use standardized bridge plans to minimize design work. The configuration of this bent was taken from one such set of plans used by the state of Tennessee. Column and bent cap sizes, abutments and footing designs were not changed when the span length changed.

The bent consists of two 762 mm square reinforced columns which are spaced at 6.1 m on center (see Figure 5-20(a)). They are 4.6 m tall using 8-#25 bars as longitudinal reinforcement and transverse reinforcement being provided by #6 bars spaced at 305 mm center to center. It is interesting to note that the column design including reinforcement schedule, as indicated on the plans, is used for columns which range in height from two meters to 15 meters.

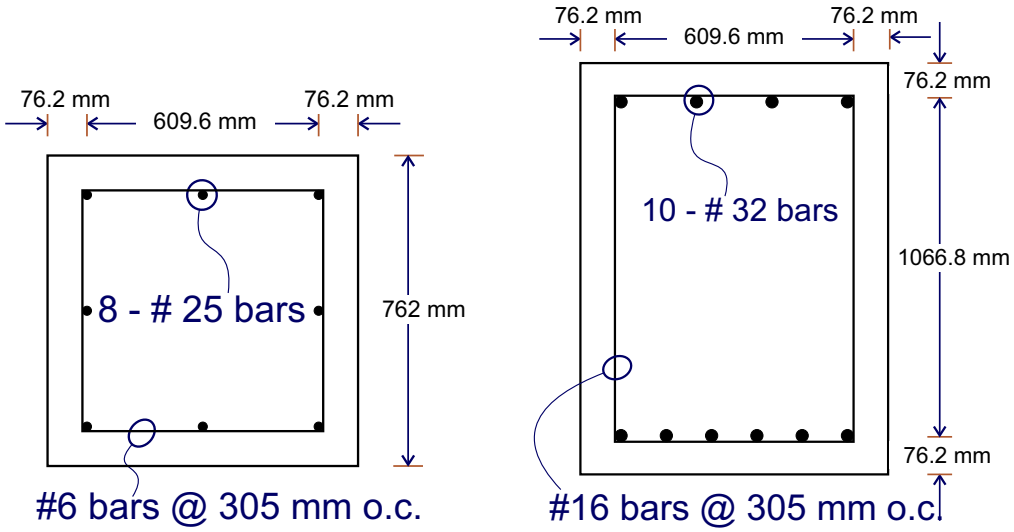

Figure 5-20: Reinforced Concrete Member Reinforcing Layout for Slab Type Bridges (a) Bent Beam (b) Columns.

The size and reinforcement schedule for the bent beam is given in Figure 5-20(b). Like the columns the bent beam design which comes in at 762 mm wide by 1,219 mm deep, does not change as the span length changes. This design uses 10 - #32 longitudinal reinforcing bars and #16 bars for the stirrups.

The abutments and foundations still use pile type construction. The abutments use single piles spaced at approximately 2,133 mm on center for a total of six piles per abutment. The column foundations use six piles per footing which is 1.58 m wide by 2.34 m long and 1.1 m thick. This footing layout is seen in Figure C-51(a).

5.2.4.2 Seismic Response

With the short and relatively stiff nature of both the simply supported and continuous bridge types, their fundamental periods are quite short. The MSSS Slab has a fundamental period of 0.28 seconds while its continuous counter part comes in at 0.25 seconds. These bridge types are different from the ones previously discussed in that their fundamental modes are transverse which activate in excess of 93 percent of the mass. The first mode shape for the simply supported bridge is given in Figure 5-21. The first mode for the continuous slab bridge is very similar and hence is not presented here.

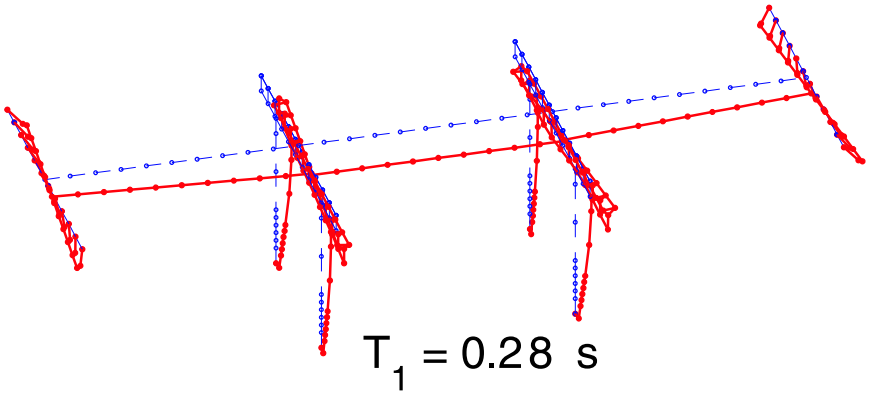

Figure 5-21: Fundamental Mode of MSSS Slab Bridge.

The general responses for both bridge types are very similar. The deck displacements for the MSSS Slab bridge, as seen in Figure 5-22, peak at approximately 10 mm and 35 mm for the longitudinal and transverse loads respectively. The continuous bridge sees maximum displacements around 10 mm and 20 mm for the same respective loading conditions.

The columns see very low levels of demand under the given loading scenarios. These demand ductilities range from $\mu_c = 0.22$ for longitudinal loading to $\mu_c = 0.53$ for transverse loading of the MSSS bridge. The MSC bridge saw slightly larger ductility demands which ranged from $\mu_c = 0.19$ under longitudinal loading to $\mu_c = 0.85$ under transverse loading. These responses may be a strong indication that the transverse direction controls the response of slab type bridges.

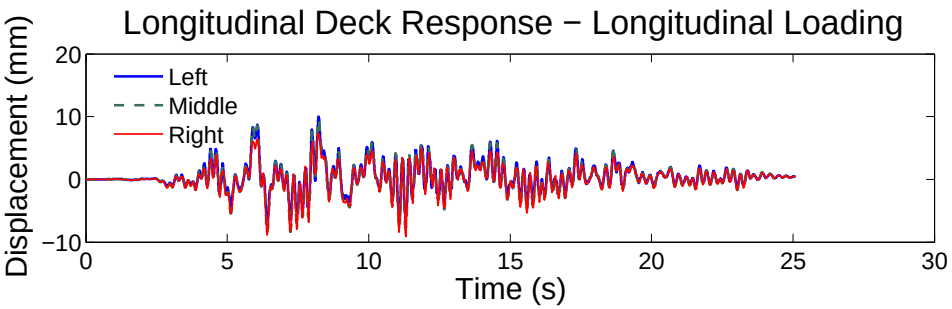

5-22(a):

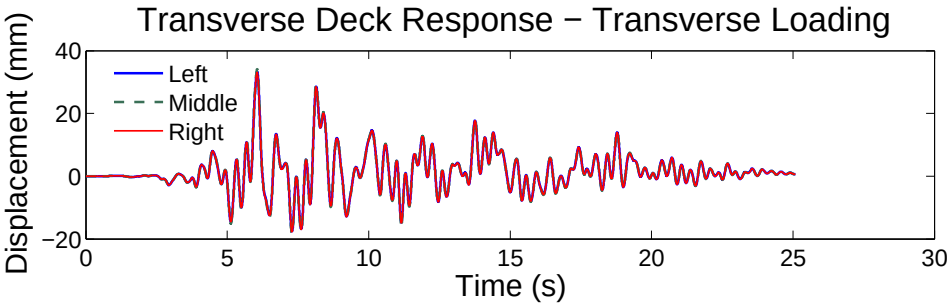

5-22(b):

Figure 5-22: Deck Displacement Time Histories for MSSS Slab Bridge Under (a) Longitudinal Loading (b) Transverse Loading.

As before, the bearings exhibit very minimal response with maximum deformations not exceeding 5 mm for both loading directions. This is a consistent phenomenon between the fixed and expansion type bearings which is a result of the steel dowels not being engaged at such small deformations.

Abutments for these bridge types tend operate mostly in the active action which is seen in Figure 5-23. This is similar to the MSSS Concrete-Box girder bridge, which is not surprising considering the slab bridges utilize the same bearing type and configuration, which was the cause of this phenomenon. Maximum abutment deformations are around 10 mm for both bridges under longitudinal loading but they increase to just over 20 mm under transverse loading.

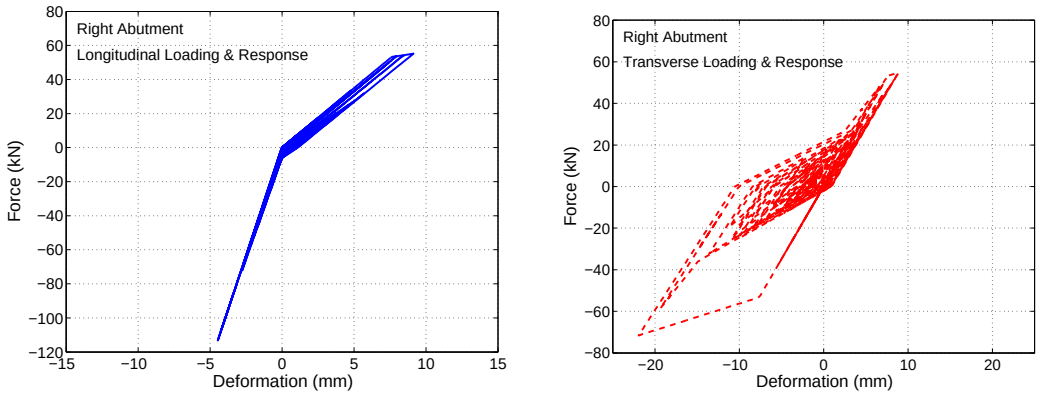

5-23(a): **5-23(b):**

Figure 5-23: Abutments of the MSSS Slab Girder Bridge Under (a) Longitudinal Loading (b) Transverse Loading

5.2.5 Multi-Span Simply Supported Steel Girder Bridge

5.2.5.1 Layout

The basic geometric configuration for the multi-span simply supported steel girder bridge is the same as for the concrete girder bridge. As illustrated in Figure 5-24, the three spans have lengths of 12.2, 24.4 and 12.2 m long which results in a 48.8 m bridge length. The deck width is 15 m wide and uses eight steel plate girders with a concrete composite deck on top. This superstructure is lighter than those built from concrete.

The gaps which are present between adjacent decks measure on average to be 25.4 mm while the gaps between abutment back walls and the decks measure 38.1 mm. As seen previously, the size of these gaps play a significant role in the degree of pounding that occurs in the bridge during a seismic event.

The substructure for this bridge is identical to that of the MSSS Concrete bridge. The only other difference is in the bearing system used to tie the superstructure to the substructure. Section C.2 discusses common types of steel bearings used for steel girder bridges which were classified as either high-type or low-type and either fixed or expansion types. The bridge model in this section assumes that the high-type bearings, which are illustrated in Figure C-2, are implemented. These high-type bearings are typically used for longer spans and therefore deemed appropriate for this model. The bearings are placed in the bridge such that each span has fixed bearings at one end and expansion bearings at the other as shown with the triangles and circles, respectively in Figure 5-24.

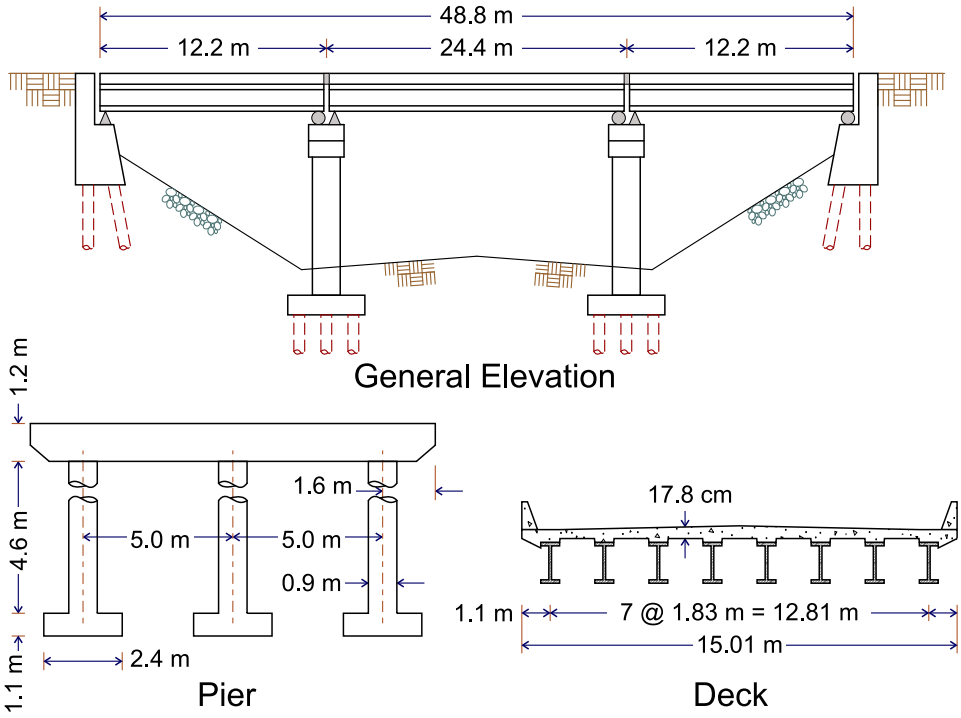

Figure 5-24: MSSS Steel Bridge Configuration.

5.2.5.2 Seismic Response

The first mode, which is characterized by longitudinal motion, has a period of 0.30 seconds. The mode activates mass equal to ~84 percent in this direction. The second mode, which is predominantly transverse, has a shorter period of 0.25 seconds and an activated mass of ~90 percent. A plot of the fundamental mode shape is given in Figure 5-25.

Close observation of the plot of the fundamental mode shape will highlight one of the distinguishing characteristics of this bridge, which is the stiffness differential that exists between the left-most span and the other two spans. The left-most bearing on the left span is a fixed-type bearing which ties into the abutment and does not allow much movement in the deck. The other two spans are tied into the relatively flexible columns and the far

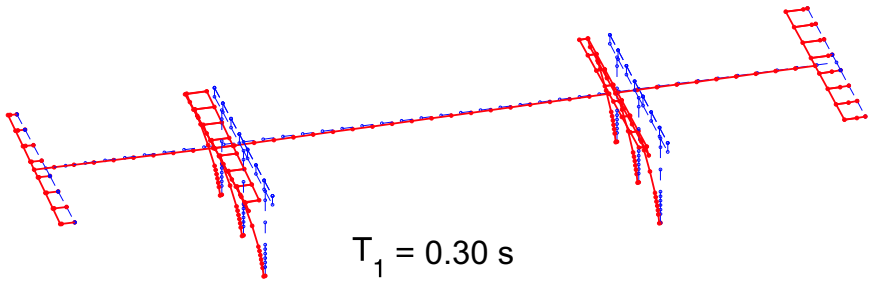

Figure 5-25: Fundamental Mode of MSSS Steel Girder Bridge.

right abutment with an expansion bearing and are therefore inclined to displace more. This behavior is also clearly illustrated in Figure 5-26(a) which shows the displacement time histories of the three deck sections. It is observed that the right two spans move more-or-less together but the response of the left span is quite a bit smaller and considerably different.

The curvature ductility demand on the concrete columns is slightly less than those in the concrete girder bridges. The maximum demand placed on the columns is a ductility level of approximately $\mu_c = 2.0$, as is seen in Figure 5-27. Once again the transverse loading of the bridge caused ductility demands not much greater than $\mu_c = 1.0$.

Past studies have shown that the steel bearings used in this study are a vulnerable component of this bridge type (Choi, 2002). For this reason it is informative to observe the responses of all of the bearings for this bridge when it is subjected to longitudinal loading. Figure 5-28 shows the responses of the high-type bearings, both fixed and expansion. Figure 5-28(a) demonstrates the composite behavior that exists in the high-type steel bearings. The internal hysteresis loop, which captures the frictional component of the bearing response, is narrower for this bearing than for the one attached to the middle span, as seen

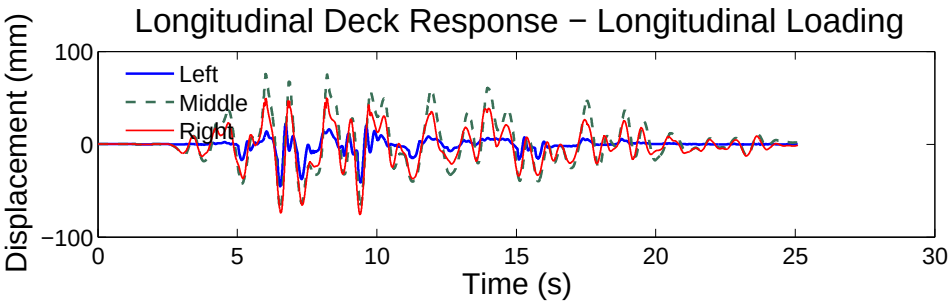

5-26(a):

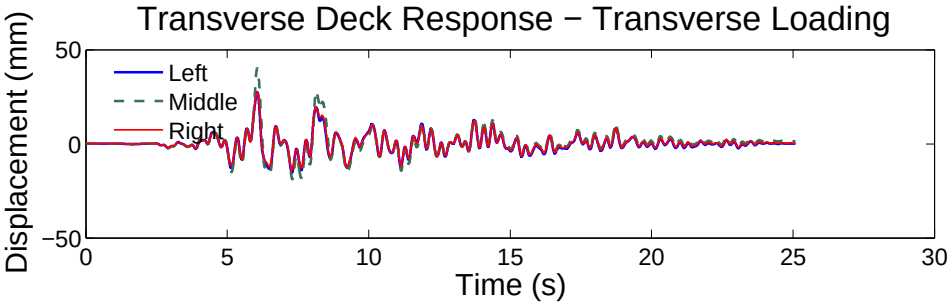

5-26(b):

Figure 5-26: Deck Displacement Time Histories for MSSS Steel Girder Bridge Under (a) Longitudinal Loading (b) Transverse Loading.

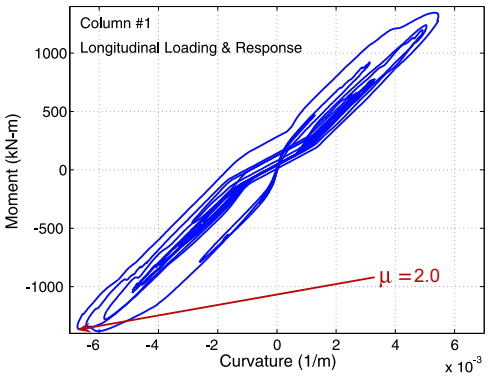

5-27(a):

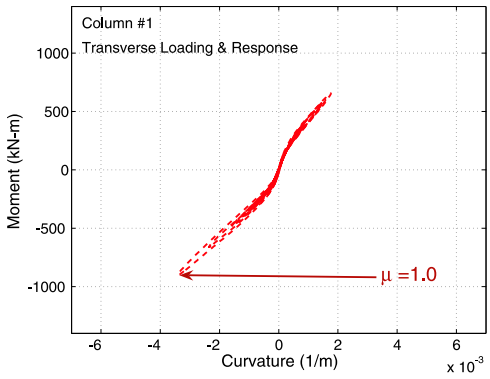

5-27(b):

Figure 5-27: Columns of Left Bent of the MSSS Steel Girder Bridge Under (a) Longitudinal Loading (b) Transverse Loading

in Figure 5-28(c). This is because the frictional response component of each bearing is a function of the normal force which is applied to it. Therefore, the shorter end spans have a smaller mass producing smaller reactions and hence generate smaller hysteresis loops.

As previously mentioned, the far left span appears to respond somewhat independent of the rest of the structure. This tends to place large demands on the bearings associated with this span as presented in Figures 5-28(a) and 5-28(b). The fixed bearing sees a deformation demand of up to 40 mm and the rocker bearing sees movement approaching 80 mm. This type of movement in these bearing types generally result is some type of fracture or toppling of the bearing. It should be pointed out that because the bearings behave the way they do, not much demand is placed on the abutments, which remain practically linear.

5.2.6 Multi-Span Continuous Steel Girder Bridge

A description of the geometric configuration of the continuous span version of steel girder bridges is given in Figure 5-29. As indicated by the description the steel girders are continuous over the top of the bents. This is done to achieve longer spans than can be done with simply supported girders. Therefore, the typical bridge configuration used in this study has three spans which all have the same length of 30.3 m giving an overall length of 90.9 m to the bridge. The deck width for this bridge is also 15 m and constructed with eight steel plate girders. Sometimes the steel girders are haunched over each of the internal supports to provide more capacity for vertical loads. Other than a small change in mass, this does not change the seismic behavior much. For this reason and also to simplify the generation of the analytical model, girders without haunches are used.

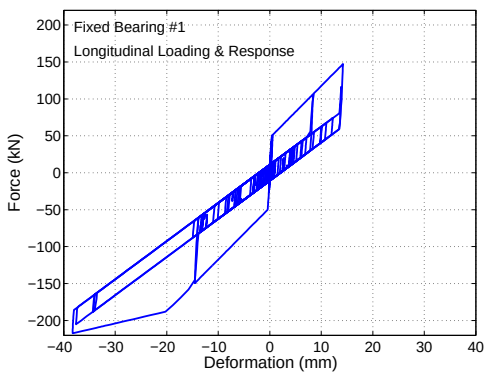

5-28(a):

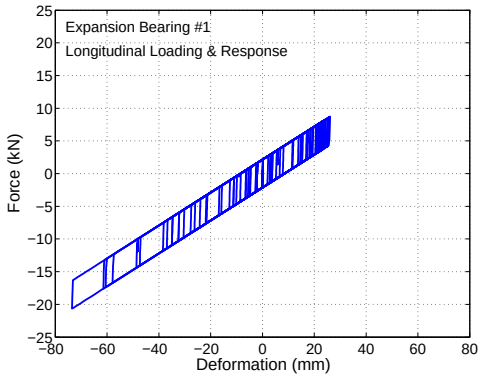

5-28(b):

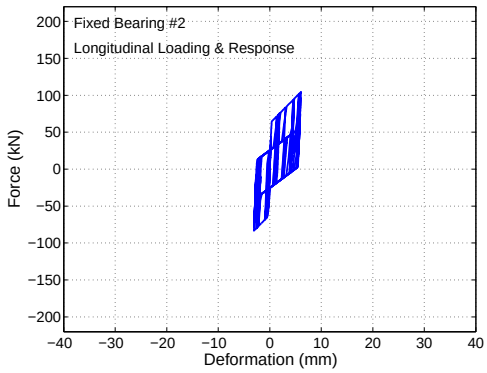

5-28(c):

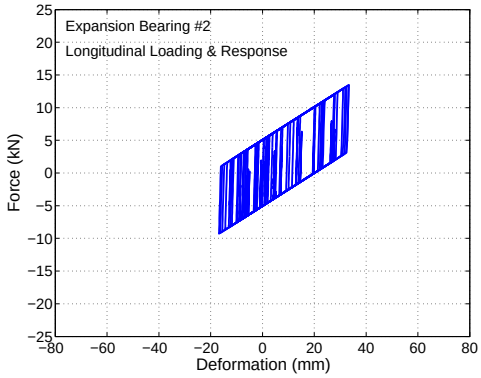

5-28(d):

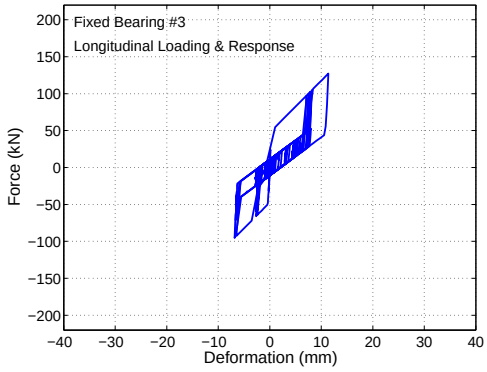

5-28(e):

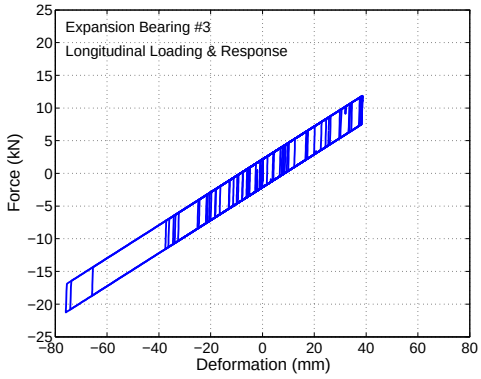

5-28(f):

Figure 5-28: Bearing Responses of the MSSS Steel Girder Bridge Under Longitudinal Loading (a) Left - Fixed (b) Left - Rocker (c) Middle - Fixed (d) Middle - Rocker (e) Right - Fixed (f) Right - Rocker.

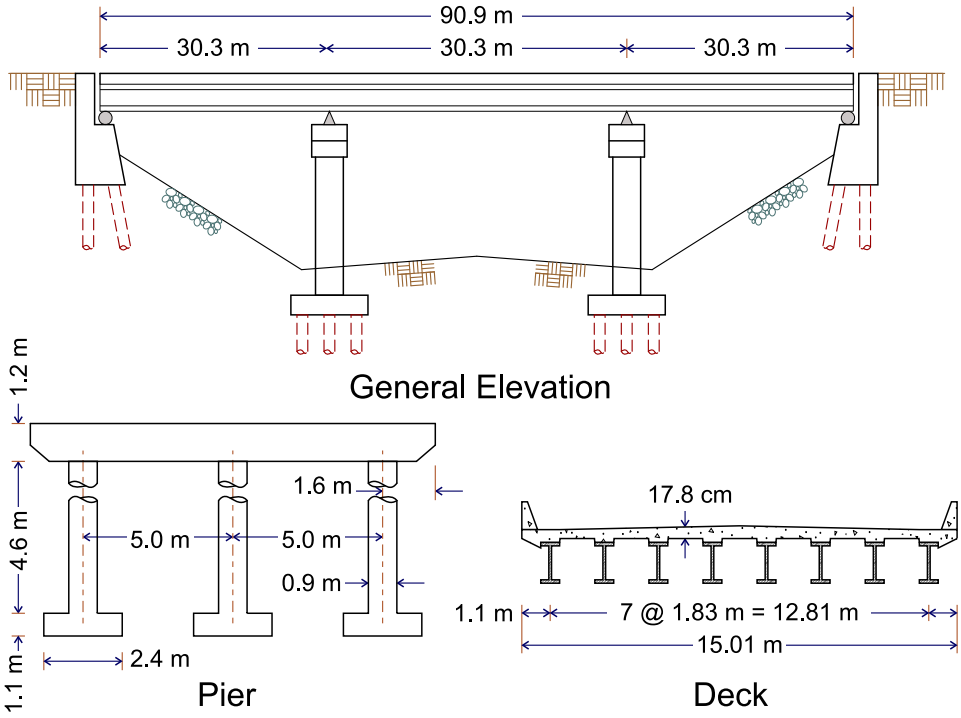

Figure 5-29: MSC Steel Bridge Configuration.

Although the multi-column bent and abutment assemblies are identical to the simply supported version of this bridge, the bearing layout is noticeably different. This bridge still uses the high-type bearings, using a single row of fixed-types over each of the bents and a row of rocker bearings at each of the abutments. This layout can be seen in Figure 5-29.

5.2.6.1 Seismic Response

The longer span lengths and the reduced number of bearings in the continuous span steel bridge cause it to have a longer period than the simply supported version. The first mode, which is a longitudinal mode with a period of 0.44 seconds, is shown in Figure 5-30. This same mode activates 96 percent of the mass in this direction, where the second mode, which is has a period of 0.31 seconds, activates 95 percent of its mass.

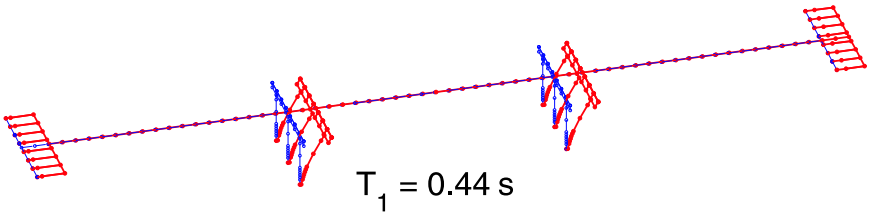

Figure 5-30: Fundamental Mode of MSC Steel Girder Bridge.

The displacement time history of the deck segments in both the longitudinal and transverse directions are seen in Figure 5-31. As expected, the deck segments move together for both loading scenarios with maximum displacements exceeding 150 mm in the longitudinal direction and around 100 mm in the transverse direction. Due to the large mass and the relatively small bearing stiffnesses at the abutments, this bridge experiences the largest deck displacements of all bridge types. It is also noticed that the motion of the decks tend to be of a long period nature.

The large displacements under which the decks are subjected are not without their consequences. The curvature ductility demand on the columns as the bridge is subjected to longitudinal loading is quite large. Figure 5-32(a) shows this demand to be around $\mu_c = 6.28$. Poorly detailed columns, which have lap splices at the base of the columns and low levels of confinement steel, are severely damaged under this level of demand. Transverse loading places a much smaller, yet significant demand of $\mu_c = 2.18$, as shown in Figure 5-32(b).

The longitudinal loading of the MSC Steel bridge does not cause much displacement demand on the fixed bearings, which are located over the bents. Figure 5-33(a) shows this demand to be much less than 5 mm. The response of the expansion or rocker bearings,

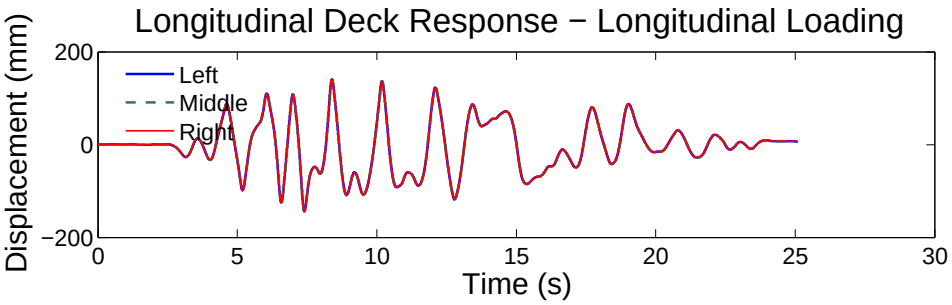

5-31(a):

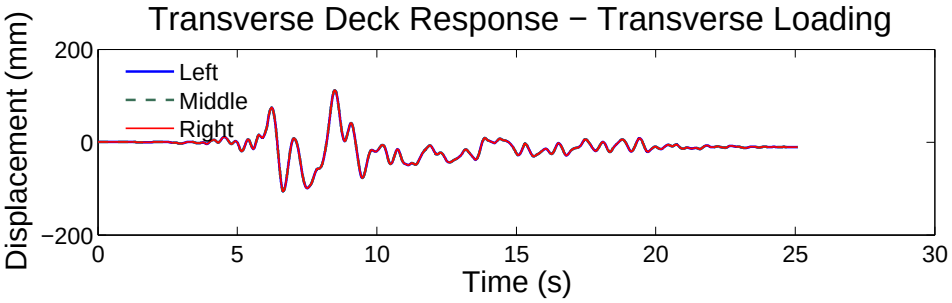

5-31(b):

Figure 5-31: Deck Displacement Time Histories for MSC Steel Girder Bridge Under (a) Longitudinal Loading (b) Transverse Loading.

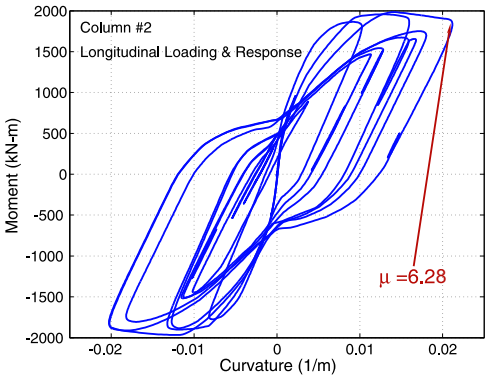

5-32(a):

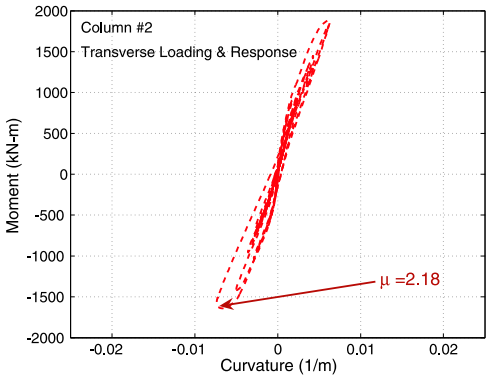

5-32(b):

Figure 5-32: Columns of Right Bent of the MSC Steel Girder Bridge Under (a) Longitudinal Loading (b) Transverse Loading

which are located at the abutments experience a much larger demand. The maximum deformation in the rocker bearings, as seen in Figure 5-34(a), exceeds 160 mm. Deformations as large as these pose a serious threat, as toppling of the bearing is imminent.

The bearings, both fixed and expansion, experience large demands under a transverse loading scenario. The hysteresis loop shown in Figure 5-33(b) depict deformations exceeding 60 mm and forces greater than 300 kN at each fixed bearing. The response of the expansion bearing, as seen in Figure 5-34(b), shows that the loads are large enough to fail the keeper plates and still achieve deformations up to 120 mm.

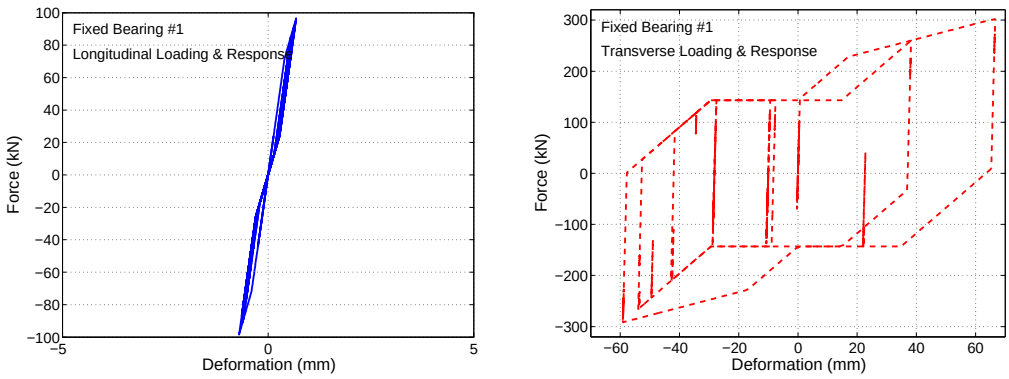

5-33(a): **5-33(b):**

Figure 5-33: Fixed Bearing at Left Bent of the MSC Steel Girder Bridge Under (a) Longitudinal Loading (b) Transverse Loading.

The large longitudinal displacements of the deck and deformations in the expansion bearings also cause significant pounding to occur at the abutments. As is the case when pounding occurs, the abutments are loaded in passive action, which in this case results in deformations of approximately 65 mm as seen in Figure 5-34(a). When deformations reach

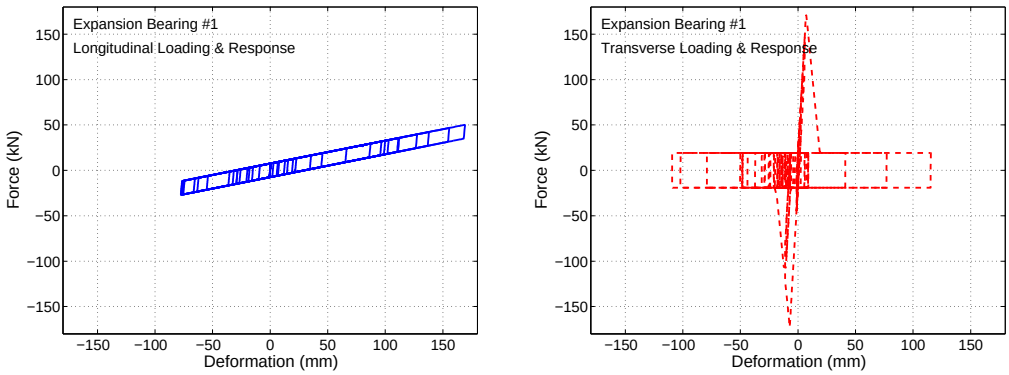

5-34(a): **5-34(b):**

Figure 5-34: Expansion Bearing at Left Abutment of the MSC Steel Girder Bridge Under (a) Longitudinal Loading (b) Transverse Loading.

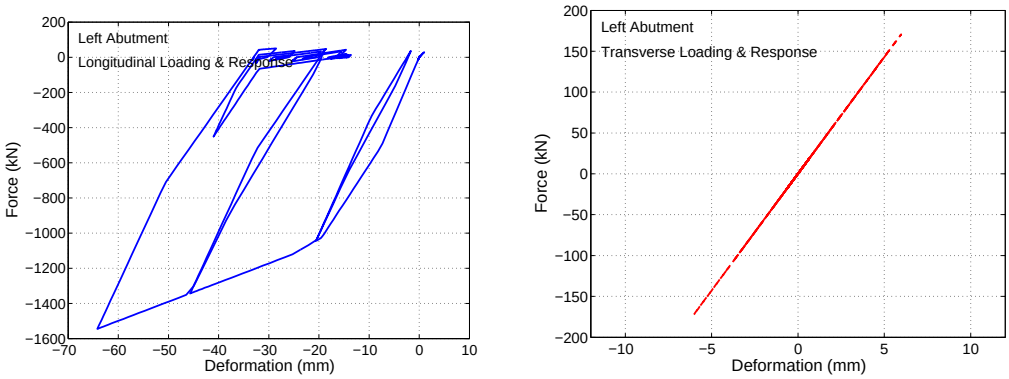

5-35(a): **5-35(b):**

Figure 5-35: Left Abutment of the MSC Steel Girder Bridge Under (a) Longitudinal Loading (b) Transverse Loading.

levels this high they cause high pressures upon the back wall of the abutment, which not only fails the soil, but causes failure in the back wall itself.

Due to the fuse type nature of the expansion bearings in the transverse direction, not much load is transferred to the abutments under transverse loading. Figure 5-34(b) shows loads per 1.9 m width of abutment do not exceed 200 kN or 8 mm of deformation. This is in contrast with the ~1,500 kN load caused by the longitudinal loading.

5.2.7 Single-Span Concrete Girder Bridge

5.2.7.1 Layout

A typical single span bridge with concrete girders is shown in Figure 5-36. Construction of this bridge is very similar to that of the the MSSS Concrete bridge other than it has no intermediate supports. These single span bridges tend to be used in situations where a short span is required or where an intermediate support is not feasible. The span length for this bridge is 18.3 m while its width is 9.0 m, utilizing five concrete girders. These girders are AASHTO type II and have a 16.5 cm thick concrete deck placed on top to create a composite action.

Where this bridge uses the AASHTO type girders, the bearing types are the same as in Figure C-25. The 25.4 mm thick elastomeric pads used with these girder are 457 mm by 203 mm. These are still used in conjunction with steel restraining dowels, where the only difference between a fixed and an expansion bearing is the size of the slot in which the dowels insert.

The abutments used with this bridge type tend to be much taller so as to eliminate wasted space due to sloping abutment fill. The abutment design assigned to the bridge

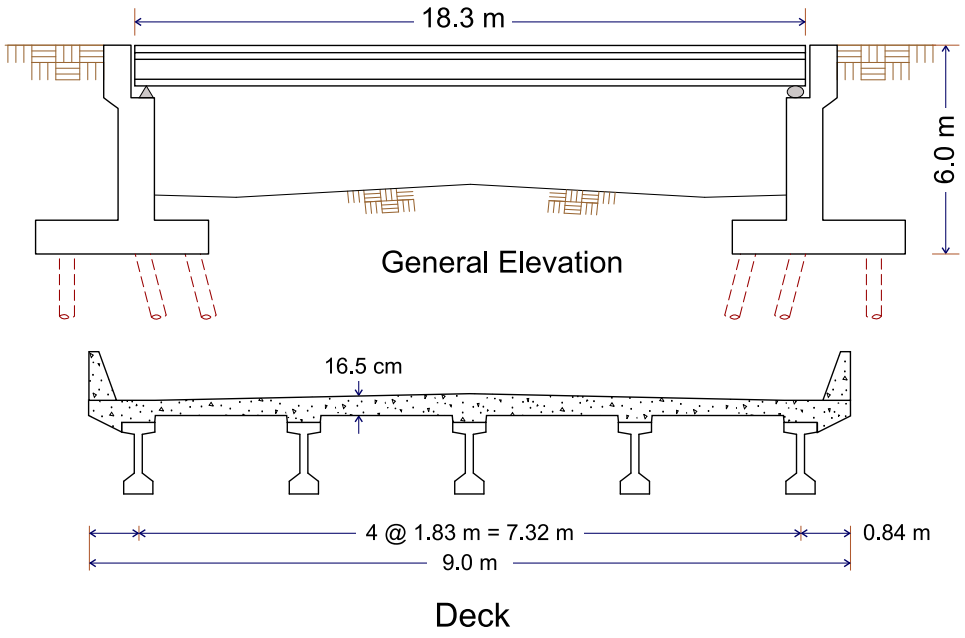

Figure 5-36: SS Concrete Bridge Configuration.

in this study uses a back wall height of 6.0 m. Because of their tall nature they typically employ many more piles below the footing than their multi-span bridge counterparts do in an effort to provide additional resistance. The total number of piles used for this un-skewed bridge with five girders is 15.

5.2.7.2 Seismic Response

The first mode of this bridge is a transverse mode with a period of 0.32 seconds and an activated mass of 100 percent (see Figure 5-37). The second mode is a longitudinal mode with a period of 0.32 seconds and an activated mass of 100 percent. This is indicative of the highly simplistic behavior that a single span bridge is prone to exhibit.

The deck response to longitudinal loading, as shown in Figure 5-38(a), shows a maximum displacement of approximately 30 mm. It is interesting to note that there appears

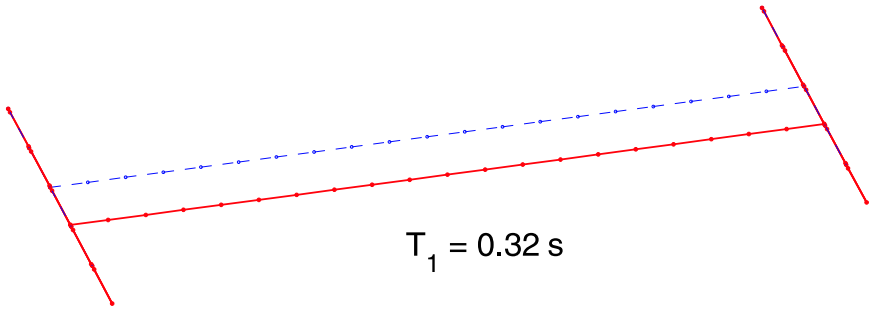

Figure 5-37: Fundamental Mode of SS Concrete Girder Bridge.

to be a permanent residual displacement of approximately 15 mm after the excitation has subsided. The bridge response to transverse loading (Figure 5-38(b)), however, does not result in the same degree of deformation and hence displays no residual displacement.

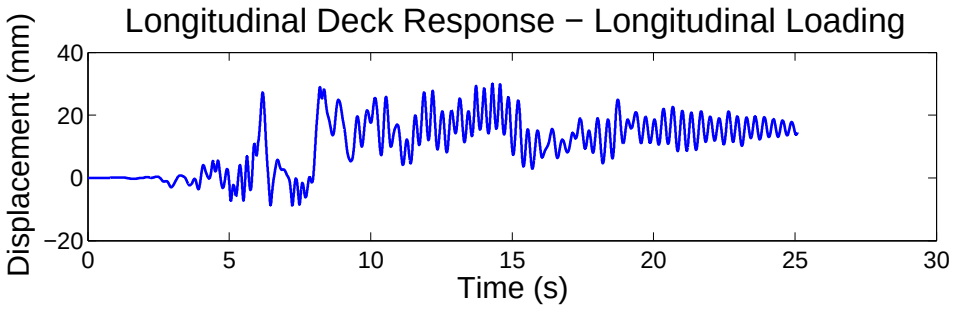

5-38(a):

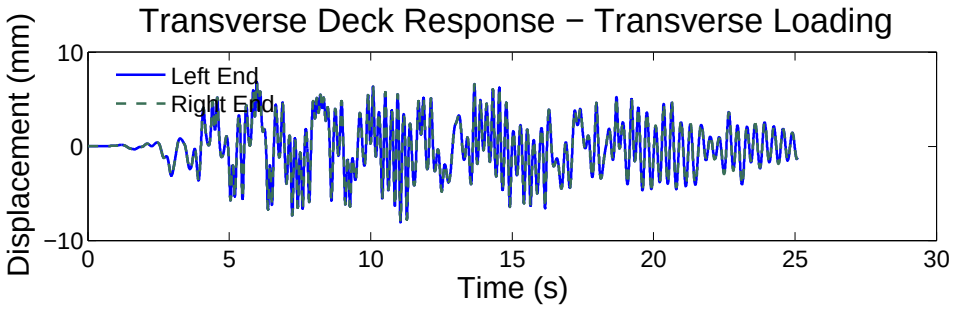

5-38(b):

Figure 5-38: Deck Displacement Time History for SS Concrete Girder Bridge Under (a) Longitudinal Loading (b) Transverse Loading.

The bearings at each end of the bridge experienced failure of the steel dowels when loaded in the longitudinal direction, as seen in Figure 5-39. This resulted in deformations in the bearings that are around 30 mm, which does not appear to be too excessive. The response in the transverse direction is even smaller. The maximum deformation just exceeds 5 mm which manages to load up the dowels but not fail them.

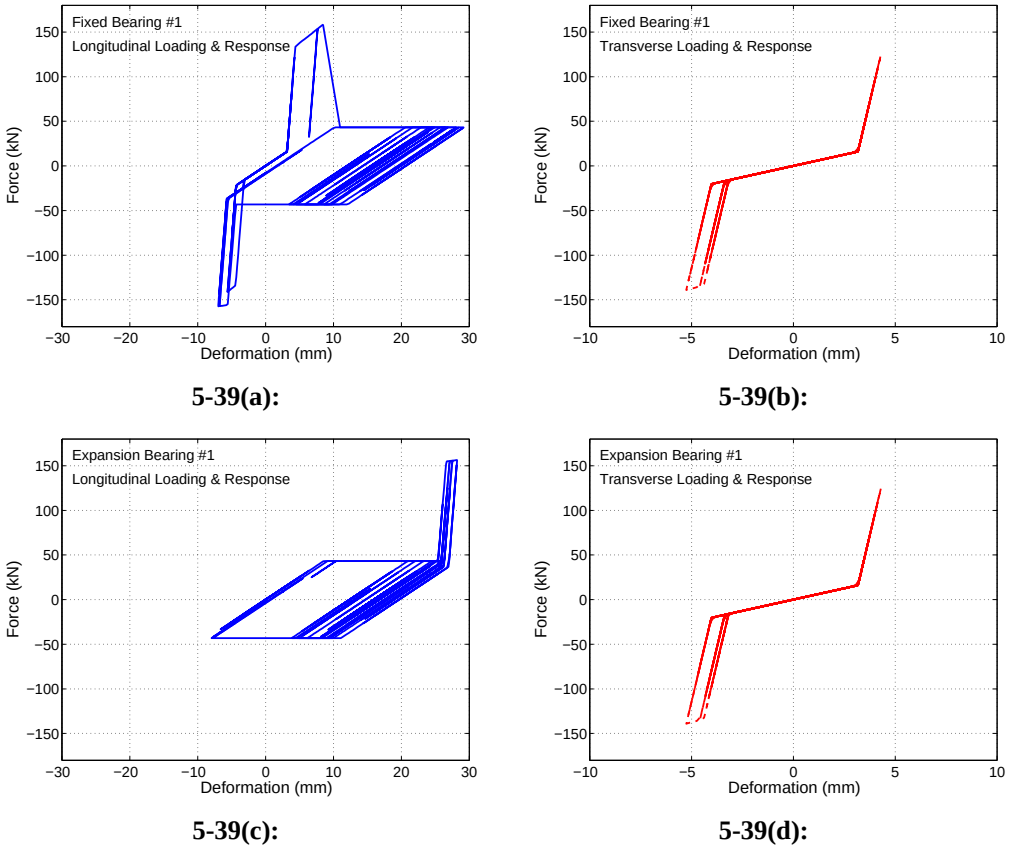

Figure 5-39: Bearing Responses of the SS Concrete Girder Bridge for (a) Fixed - Longitudinal Loading (b) Fixed - Transverse Loading (c) Expansion - Longitudinal Loading (d) Expansion - Transverse Loading.

As seen before, the flexibility of the bearings tend to isolate the deck from the abutments. Since the gaps between the deck and abutments are large at approximately 76 mm,

there is no pounding that occurs. When no pounding occurs the demand placed on the abutments is relatively small. This seismic load never caused the abutments to leave their linear range in either passive or active action.

5.2.8 Single-Span Steel Girder Bridge

5.2.8.1 Layout

The geometric layout for the single-span steel girder bridge is identical to the SS Concrete girder bridge as presented in the previous section. As can be noticed from inspection of Figure 5-40, the difference comes in the type of girder system used. The concrete girders are replaced by steel girders and the elastomeric bearings are exchanged for low-type steel bearings.

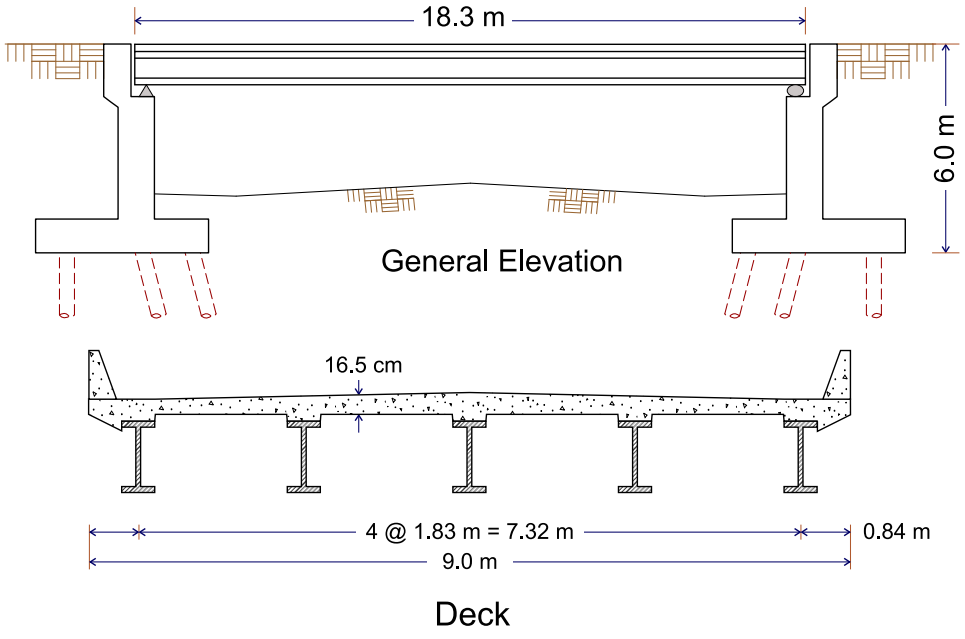

Figure 5-40: SS Steel Bridge Configuration.

As mentioned before, single span bridges tend to have shorter spans and are hence more likely to have been built using the low-type steel bearings, which are presented in Figure C-3. These bearings are much more stiff than their high-type counter parts due mainly to their configuration and mode of operation.

5.2.8.2 Seismic Response

The very light superstructure and the very stiff bearings cause the SS Steel bridge to have the shortest fundamental period of all bridge types at 0.17 seconds. In fact, the first mode happens to be a vertical mode which activates 81 percent of its mass, the shape of which is given in Figure 5-41. The second mode, which has a period of 0.10 seconds, is a transverse mode activating 99 percent of its mass.

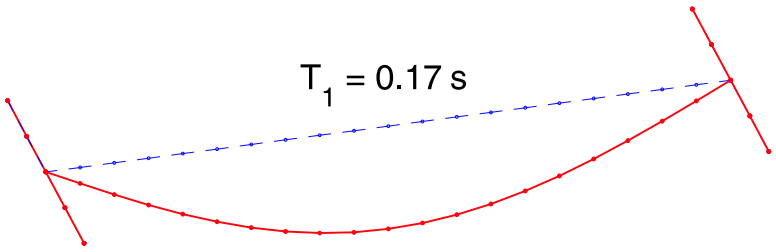

Figure 5-41: Fundamental Mode of SS Steel Girder Bridge.

Due to the short periods of the horizontal modes of this bridge, the responses of its components under seismic loading are really quite small. Figure 5-42 shows the displacements under which the deck goes. The displacements in both the longitudinal and transverse directions are not much greater than 5 mm. As expected, when the deck response is this

small, no pounding is expected and hence the abutment response is small, with deformations much less than 5 mm.

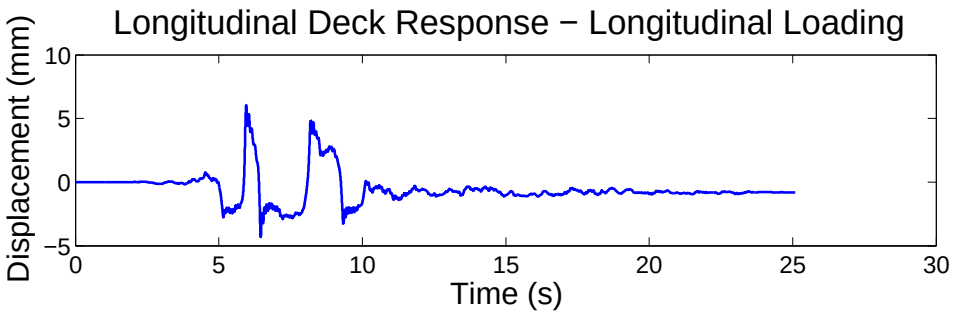

5-42(a):

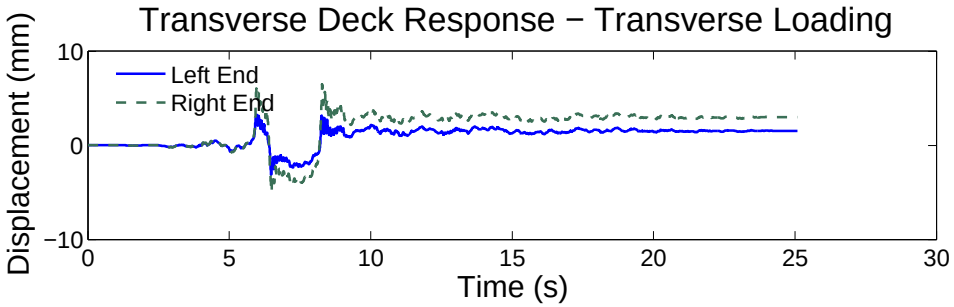

5-42(b):

Figure 5-42: Deck Displacement Time History for SS Steel Girder Bridge Under (a) Longitudinal Loading (b) Transverse Loading.

The bearings are the only components in the bridge that exhibit any degree of nonlinear behavior, as seen in Figures 5-43 and 5-44. The nonlinearity of these component responses comes from the addition of frictional forces to the forces on the anchor bolts. In spite of the nonlinear response, the maximum deformations are right around 5 mm. Thus, the bearings are not considered to have been damaged under this scenario.

The SS Steel girder bridge has previously been determined to not be very vulnerable to seismic events (Choi, 2002). The results from the analysis presented in this section would tend to support this conclusion.

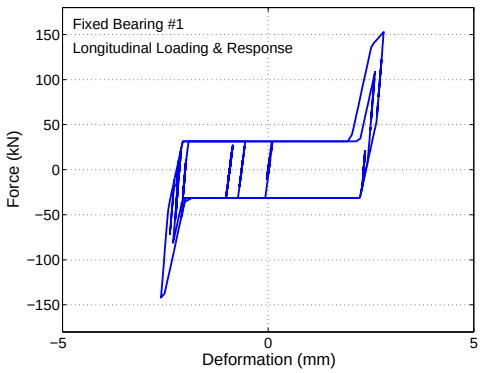

5-43(a):

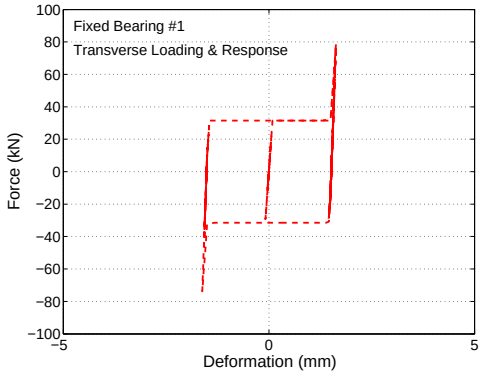

5-43(b):

Figure 5-43: Fixed Bearing of the SS Steel Girder Bridge Under (a) Longitudinal Loading (b) Transverse Loading.

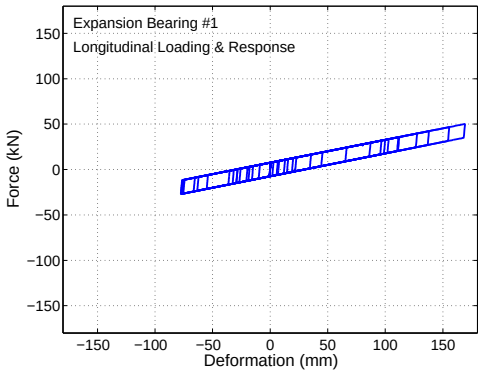

5-44(a):

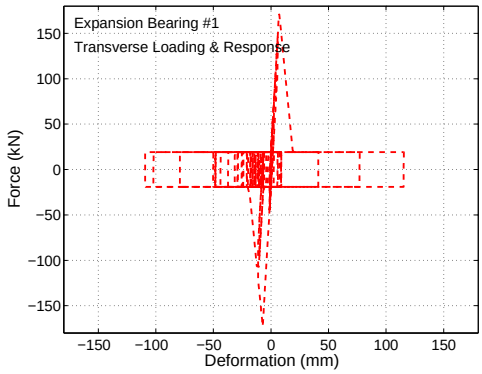

5-44(b):

Figure 5-44: Expansion Bearing of the SS Steel Girder Bridge Under (a) Longitudinal Loading (b) Transverse Loading.

5.3 Closure

In this chapter, 3-D analytical bridge models are presented for the nine bridge classes presented in Chapter 4. The analytical models are created in *O*penSees using component models developed with a high degree of rigor in Appendix C. Because of the lack of instrumented bridges subjected to earthquakes, there is little opportunity to validate these bridge models. However, experimental data for the various bridge components does allow for development of appropriate component models.

Using a single synthetic ground motion specific to Memphis, TN, each bridge model was loaded in its two orthogonal axes. This loading scenario is intended, not to facilitate the drawing of conclusions, but rather give some sense for the relative response of the various bridge types and also to use as a sanity check. Table 5-1 gives a simplified break down of the vulnerable components of each bridge. An X indicates that the associated component response implies vulnerability. From the deterministic analyses conducted in this chapter, it appears as if the columns and the transverse behavior of the abutments are the most vulnerable components across all bridge types. The longitudinal responses of the bearings, both steel and elastomeric, also exibit vulnerabilities which are cause for concern.

The multi-span simply supported bridges tend to place significant deformation demands on their bearings. This is especially true for the steel girder bridge which utilizes steel type bearings. Pounding of adjacent decks is believed to be partially responsible for this phenomenon. This is not so critical for the inherently smaller bridge types such as the MSSS Slab and Concrete-Box girder bridges where pounding does not occur so readily.

When the superstructures are made continuous, as in the MSC bridges, the demand appears to shift partially from the bearings to the columns and abutments. Pounding is restricted to the abutments thus placing larger demands on them in the passive action. The MSC Steel girder bridge clearly shows this phenomenon.

The single span bridges appear to be the least vulnerable of all the bridge types. This lack of vulnerability is due to the low inertial loads to which these bridge types are subjected. The small inertial loads are attributed to these bridges being relatively short (see Chapter 4). A more in-depth investigation of the seismic response of each bridge type is carried out in the subsequent chapters of this document.

The responses discussed in this chapter are for a set of bridges which use typical values for their analytical modeling parameters. It is likely that the general trend of these responses change as the parameter values change. In the next chapter, an investigation into the sensitivity each bridge response has to a number of different modeling parameters, is performed. This allows for a more complete exploration of the bridge component vulnerabilities.

Table 5-1: Summary of Vulnerable Components for Nine Bridge Classes - Deterministic Analyses.

	Vulnerable Bridge Components							
Bridge Type	**Col**	**[a]Fxd-Long**	**[a]Fxd-Tran**	**[b]Exp-Long**	**[b]Exp-Tran**	**[c]Ab-Pass**	**[c]Ab-Act**	**[c]Ab-Tran**
MSC Concrete	X	X		X				X
MSC Slab	X						X	X
MSC Steel	X	X	X	X	X	X		X
MSSS Concrete	X	X		X			X	X
MSSS Concrete-Box	X						X	X
MSSS Slab	X						X	X
MSSS Steel	X	X	X	X	X			
SS Concrete								
SS Steel				X	X			

[a]Fixed Bearings

[b]Expansion Bearings

[c]Abutments

CHAPTER VI

SCREENING OF BRIDGE STRUCTURAL PARAMETERS

6.1 Introduction

There are many parameters that go into defining the analytical bridge models which are developed as part of this study. These parameters may be geometric in nature, such as span length and column height or they may help define material or component behavior such as concrete strength and bearing stiffness. Experience and common sense suggest, that the values these parameters assume in real life will vary from structure to structure and may also vary over time. A logical question that follows is whether or not this variation has any significant impact upon the response of the structure. Answering this question for each parameter will dictate whether its inherent variation must be explicitly considered or if it may be neglected.

A number of methods are available to assist in the identification of significant parameters or factors. These methods are generally called screening or sensitivity studies. One of the more traditional and intuitive of these methods is an approach called "one-factor-at-a-time" (Wu and Hamada, 2000). In this method all but one of the factors are held at a constant value. At this time, one factor is investigated by itself, changing its value and observing the apparent impact it has upon the model. This is then done for each factor of

interest. This is an iterative and consequently inefficient approach to the problem. Another drawback of this method is its inability to estimate some factor interactions.

An extension of the "one-factor-at-a-time" approach used is to explicitly examine the derivatives of selected response quantities. The derivatives of these response quantities, such as drift, deformation, forces etc., are functions of the various parameters in the model and define the slopes of the response functions. The gradient of these response functions are a measure of the sensitivity that the response has to each parameter (Haukaas, 2003). Although a powerful and informative approach, this method requires that sensitivity equations for the various parameters of interest be implemented into a finite element code. Work on implementation of these equations in the *O*penSees framework has begun but currently lacks the comprehensive library required for this study.

A method which is increasing in popularity is to screen the parameters using a "design of experiments" (DOE) approach. This is a statistical approach which investigates the significance of each factor while reducing the computational effort as compared to "one-factor-at-a-time." This approach is the variable screening method adopted in this study. The following sections include a more detailed description of it's setup and analysis and also a presentation of the inferences made for each bridge type.

6.2 Screening Experiments

As previously mentioned, the screening of parameters for their relative significance is performed in this study using a DOE approach. A conventional full factorial experiment is a comprehensive study of all possible combinations of the parameters' values. In a two-level design, each parameter is considered at two values, both upper and lower, traditionally

Table 6-1: Sample Full Factorial Experimental Design.

Run	Parameters		
No.	**A**	**B**	**C**
1	-	-	-
2	-	-	+
3	-	+	+
4	-	+	-
5	+	-	-
6	+	-	+
7	+	+	+
8	+	+	-

noted as (+) and (-) respectively. For each combination of parameter levels, the experiment, or in this case the bridge, is analyzed and the responses of interest are monitored. Setups such as these require the running of 2^k experiments, where k is the number of parameters being considered. Table 6-1 illustrates this concept using three parameters A, B and C.

Looking at all possible combinations of factor levels for each model allows an exploration of the effects of each factor. It also allows the interaction effects that may or may not exist between parameters. Although this is an ideal and most desired setup, one can see that this becomes very computationally expensive when a large number of parameters must be considered. For example, an experiment with 14 parameters, as is the case in this study, will require $2^{14} \rightarrow 16,384$ analyses. It is clear, that even if this were a reasonable number of analyses to run for one bridge, it is not feasible when this must be done for nine different bridge types.

Although the full factorial approach is highly informative, it is neither feasible or necessary for the purposes of this study. When one is willing to sacrifice some information, particularly high-order interaction effects, then the experimental setup may be reduced by

a fraction 2^{-p}, requiring the total number of runs to be 2^{k-p}. Explicitly, the value of p is the fractional reduction in the number of experiments required. This value of p is determined by the experimenter, balancing the economics of the experiment with the information that is desired.

One direct consequence of taking only a fraction of the full factorial design is that some of the higher order effects become confounded or aliased with some of the lower order effects. The term effects, as used here, is a measure of the change in model response due to a change in a parameter or combination of parameters from their lower levels to their upper levels. The actual calculation of these effects will be discussed later but suffice it to say that in a fractional factorial experiment one may not be able to attribute an observed effect uniquely to a single parameter. Rather it may be due to some interaction of parameters.

Although aliasing may appear to be a problem, there exist a few principles which help to deal with it. The first such principle is the hierarchical ordering principle, which states that the lower order effects are more likely to be important than the higher order effects. The second principle states that the number of relatively important effects in a factorial experiment is small. Finally, the third principle states, that in order for the interaction between two parameters to be significant, at least one of the two parameters must also be significant (Wu and Hamada, 2000). Therefore, if the fractional factorial design is such that the main effects are only aliased with interactions of order three or higher then the results that are attained are most likely due to the main effects of the single parameter.

What follows next is the concept of parameter screening using fractional factorial design. Many times an experiment has too many parameters to be able to reasonably consider their interaction effects in addition to their main effects. For this reason the concept of

screening designs was developed. A screening experiment is built around the three previously mentioned principles and assumes that given a large number of parameters, considering the main effects only, is acceptable in determining significance. Once the number of parameters is reduced to a manageable number then second and higher order effects may be treated explicitly. Therefore, the main task becomes creating a fractional factorial design which produces main effects which are clear from aliasing with two-factor interactions. The following subsections will introduce the screening design used in this study and discuss the analysis and interpretation of the results.

6.2.1 Blocking

As mentioned previously, there are many parameters that define the analytical model of any particular bridge. The parameters that define the geometry of the bridge tend to be troublesome in that they often significantly alter the nature of the bridge. For instance, the number of spans is one such parameter. It becomes difficult to say that a two span bridge is nominally identical to a six span bridge and therefore is not a part of the same homogeneous population. The same situation applies to other geometric parameters such as span length, deck width and column height. Therefore, it may not be appropriate to consider these parameters in the same way as one would consider the material parameters.

The concept of blocking within the screening experiment is one way of dealing with the heterogeneity caused by these geometric parameters. Blocking is a way to take similar populations, often with hard to change parameters, and place them into one group. The differences between the blocks may then be examined. The general guideline for blocking is that the units within a block should be more homogeneous than units between blocks (Wu

and Hamada, 2000). It is proposed in this study that the geometry be treated by creating eight typical bridge samples for each bridge class. This can be accomplished by sampling on the geometry information presented in Chapter 4 using a Latin-Hypercube technique (Ayyub and Lai, 1989; Iman and Conover, 1980). These eight bridge samples can then be assigned to different blocks for treatment within the screening experiment. Thus, the significance of geometry is considered on more of a macro scale rather than at the parameter level. The actual samples of the bridge classes are presented with the discussion of each bridge. These same samples are be used throughout the remainder of the study.

6.2.2 Screening Design

The fractional factorial screening design implemented in this study is chosen such that all main effects are clear from aliasing with all two-factor interactions. When a maximum of 15 parameters is considered, a design with 32 runs is required to accomplish this (Wu and Hamada, 2000). This means that the design would be classified as a 2^{k-p} design where $k - p = 5$. The 32 runs are then separated in to eight blocks to allow for the geometry, as previously discussed. The statistical software package JMP, which is put out by the SAS Institute, is used to generate these designs (SAS, 2004). Table 6-2 gives an illustration of the design used for the SS Steel girder bridge, which considers nine parameters.

The design is taken one step further as there is some concern as to the effect of ground motion intensity on the screening results. For this reason, two additional replicates of the screening design are generated resulting in a total of 96 runs for each bridge class. Each set of 32 runs is subjected to one ground motion and thus three ground motions are used. The three ground motions are selected from the suite of synthetic ground motions provided

Table 6-2: Screening Design for SS Steel Bridge (2^{9-4}) using JMP (SAS, 2004).

Run	Block	Parameter No.								
No.	No.	1	2	3	4	5	6	7	8	9
1	4	-	-	-	-	-	-	-	-	-
2	5	-	-	-	-	+	+	+	+	+
3	1	-	-	-	+	-	+	+	+	+
4	8	-	-	-	+	+	-	-	-	-
5	7	-	-	+	-	-	+	+	-	-
6	2	-	-	+	-	+	-	-	+	+
7	6	-	-	+	+	-	-	-	+	+
8	3	-	-	+	+	+	+	+	-	-
9	3	-	+	-	-	-	+	-	+	-
10	6	-	+	-	-	+	-	+	-	+
11	2	-	+	-	+	-	-	+	-	+
12	7	-	+	-	+	+	+	-	+	-
13	8	-	+	+	-	-	-	+	+	-
14	1	-	+	+	-	+	+	-	-	+
15	5	-	+	+	+	-	+	-	-	+
16	4	-	+	+	+	+	-	+	+	-
17	8	+	-	-	-	-	+	-	-	+
18	1	+	-	-	-	+	-	+	+	-
19	5	+	-	-	+	-	-	+	+	-
20	4	+	-	-	+	+	+	-	-	+
21	3	+	-	+	-	-	-	+	-	+
22	6	+	-	+	-	+	+	-	+	-
23	2	+	-	+	+	-	+	-	+	-
24	7	+	-	+	+	+	-	+	-	+
25	7	+	+	-	-	-	-	-	+	+
26	2	+	+	-	-	+	+	+	-	-
27	6	+	+	-	+	-	+	+	-	-
28	3	+	+	-	+	+	-	-	+	+
29	4	+	+	+	-	-	+	+	+	+
30	5	+	+	+	-	+	-	-	-	-
31	1	+	+	+	+	-	-	-	-	-
32	8	+	+	+	+	+	+	+	+	+

by Rix and Fernandez-Leon (2004), with magnitudes of 5.5, 6.5 and 7.5 and epicentral distances of 10 km, 10 km and 20 km respectively. They have peak ground accelerations of 0.217 g, 0.484 g and 0.646 g and durations of 8.06, 13.45 and 25.09 seconds.

After generating the screening design, a time history analysis of each bridge realization is performed and various responses of interest are recorded. The analysis of the data to determine the significant factors is performed using an analysis of variance (ANOVA).

6.2.3 Analysis of Variance

In an ANOVA, each parameter is investigated to see its effect upon the variance of the measured response. Those parameters that don't affect the variance of y much are designated as insignificant. This task is formalized through the creation of an ANOVA table in which a hypothesis test is performed on each parameter. The null hypothesis, H_o, states that the given parameter is insignificant, while the alternative hypothesis, H_A, states otherwise (Hayter, 2002). Appendix E gives a description of how to calculate the ANOVA table for a fractional factorial design with blocking where only main effects are considered.

6.3 Parameter Screening for Typical Bridges

As pointed out previously, a screening experiment for each of the nine bridge types is conducted using a 32 run three-replicate blocked design. Each set of 32 runs is executed using one of three earthquake ground motion records. Responses of the various vulnerable bridge components are recorded and are used for screening various structural parameters. Table 6-3 presents a list of the responses and their abbreviations. The parameters are screened looking at both main effects plots and also the analysis of variance.

Table 6-3: Monitored Component Responses for Screening Experiments of All Bridge Types.

Abbreviation	Description
Ductility*	Curvature ductility of concrete columns
Fxd-tran	Deformation of fixed bearings in transverse direction
Fxd-long	Deformation of fixed bearings in longitudinal direction
Exp-tran	Deformation of expansion bearings in transverse direction
Exp-long	Deformation of expansion bearings in longitudinal direction
Ab-pass	Deformation of abutments in longitudinal passive action
Ab-act	Deformation of abutments in longitudinal active action
Ab-tran	Deformation of abutments in transverse direction

*Only applicable to multi-span bridges.

6.3.1 Multi-Span Simply Supported Concrete Girder Bridge

To accommodate the blocking design of the screening experiments, eight bridge samples are generated sampling upon the geometric distribution properties presented in Chapter 4. Table 6-4 lists the bridge samples that are created for the MSSS Concrete girder bridge. It should be noted that all bridges in this study are developed as three span bridges. As seen in Chapter 4, the most commonly occurring number of spans is three. In addition, the risk assessment framework used by HAZUS-MH utilizes fragility functions which are discretized by the number of spans a bridge possesses (FEMA, 2003). Hence, the assumption made in this study will allow for a more direct implementation into HAZUS-MH.

The bridge samples, or in other words realizations, have span lengths that range from 7.6 m to 27.4 m. The deck width ranges from 6.6 m to 18.6 m and the column heights are from 3.34 m to 6.06 m.

There are 15 parameters which are considered for the screening experiment of this bridge type. The majority of these parameters help to describe the material properties and

Table 6-4: Geometric Bridge Samples of MSSS Concrete Girder Bridge.

Bridge No.	Spans	Span Length (m)	Deck Width (m)	Column Height (m)
1	3	7.60	8.20	4.43
2	3	9.10	7.50	3.34
3	3	10.70	12.60	3.74
4	3	20.10	8.60	4.00
5	3	13.40	10.40	4.23
6	3	9.40	9.20	6.01
7	3	12.20	18.60	6.06
8	3	27.40	6.60	3.88

component behaviors for this bridge. There are a few other parameters which also help to define the geometry and loading of the bridge. Table 6-5 lists the considered parameters and their lower and upper values which are used.

The upper and lower levels are selected such that they encompass the most reasonable values for each parameter. The ranges for concrete strength, steel strength, dowel gap, abutment gap, deck gap and damping ratio give specific values for the levels because they are consistent throughout the bridge. The levels for all remaining parameters are expressed in terms of a percentage of their deterministic values. These deterministic values are calculated and used in accordance with the models given and implemented in Appendix C.

A separate analysis of variance is conducted for each of the eight responses outlined in Table 6-3. The significance level used for the analyses in this study is 0.05 because it is a very common and well accepted level. This is to say that if the p-value from the ANOVA table is less than 0.05 then the parameter is assumed to contribute significantly to the variance of the response. It should therefore be treated as a random variable and not as a deterministic value. Due to the length and number of ANOVA tables required for each

Table 6-5: Parameters Considered in the Screening of MSSS Concrete, MSSS Concrete Box and MSSS Slab Bridges.

Parameter No.	Description	Abbreviation	Lower Level	Upper Level	Units
1	Concrete strength	Conc Str	26.4	40.6	MPa
2	Steel strength	Steel Str	438	555	MPa
3	Coefficient of friction for elastomeric pads	Pad Frict	50	150	%
4	Initial stiffness of elastomeric pads	Pad Stiff	50	150	%
5	Dowel strength	Dowel Str	80	120	%
6	Gap at dowels for expansion bearing only	Dowel Gap	0	50.8	mm
7	Initial stiffness of passive abutment	Ab-Pas Stf	50	150	%
8	Initial Stiffness of active abutment	Ab-Act Stf	50	150	%
9	Rotational stiffness of foundations	Fnd-Rot Stf	50	150	%
10	Translational stiffness of foundations	Fnd-Hor Stf	50	150	%
11	Mass	Mass	90	110	%
12	Damping ratio	Damp Ratio	0.02	0.08	ratio
13	Gap between abutments and decks	Abut Gap	36	40	mm
14	Gap between decks	Deck Gap	20	31	mm
15	Loading direction (Long or Trans)	Load Dir	L	T	

bridge, a presentation of the entire table is not feasible. For this reason, just the p-values pertaining to each parameter and its associated response is presented. Table 6-6 presents the p-values calculated for the MSSS Concrete bridge where those less than 0.05 are in bold face.

The ANOVA table is shown here to facilitate a comparison and discussion of screening results. An observation of Table 6-6 reveals that given a significance level of 0.05, there are nine of the 15 parameters which are significant for at least one of the measured responses listed in Table 6-7. For instance, steel strength is a significant parameter as far as the curvature ductility demand is concerned. Foundation rotational stiffness, damping ratio and load direction also add significantly to the variance of the curvature ductility demand.

Load direction appears to be the most consistently significant parameter, since it is significant in every monitored response, with very low p-values. This comes as no surprise when one recognizes that the response quantities which are being monitored are also direction dependent.

Table 6-6: Calculated p-values for MSSS Concrete Bridge.

Parameter	P-Value							
	Ductility	**Fxd-Tran**	**Fxd-Long**	**Exp-Tran**	**Exp-Long**	**Ab-Pass**	**Ab-Act**	**Ab-Tran**
Conc Str	0.850	0.915	0.242	0.243	0.316	0.536	0.509	0.324
Steel Str	**0.043**	0.881	0.491	0.220	0.567	0.310	0.287	0.367
Pad Frict	0.674	0.214	**0.040**	0.379	**0.035**	0.212	0.642	0.660
Pad Stiff	0.154	0.111	0.336	0.094	0.285	0.069	0.464	0.424
Dowel Str	0.528	0.938	0.230	0.139	0.194	0.100	0.983	0.142
Dowel Gap	0.460	0.898	0.506	0.232	0.318	0.197	**0.011**	0.567
Ab-Pas Stf	0.427	0.867	0.422	0.256	0.240	**0.003**	0.705	0.674
Ab-Act Stf	0.441	0.233	**0.015**	0.390	0.062	0.864	**0.000**	**0.000**
Fnd-Rot Stf	**0.002**	0.207	0.637	0.399	0.460	0.731	0.707	0.573
Fnd-hor Stf	0.225	0.100	0.216	0.070	0.276	**0.022**	0.224	0.306
Mass	0.294	0.077	0.088	0.071	0.242	0.952	0.764	0.870
Damp Ratio	**0.008**	0.966	0.777	0.120	0.372	0.098	0.588	0.253
Abut Gap	0.941	0.931	0.857	0.125	0.655	0.719	0.067	0.372
Hinge Gap	0.217	0.984	0.186	0.147	0.107	0.772	0.513	0.857
Load Dir	**0.000**	**0.038**	**0.000**	**0.019**	**0.000**	**0.000**	**0.000**	**0.000**
Blocks	**0.000**	0.156	**0.009**	**0.028**	**0.001**	**0.001**	0.344	0.430

Bold faced numbers are less than 0.05 and considered a sign of significance.

Table 6-7: Significant Parameters for MSSS Concrete Bridge.

Significant Parameters		
Steel Str	Pad Frict	Dowel Gap
Ab-Pas Stf	Ab-Act Stf	Fnd-Rot Stf
Fnd-Hor Stf	Damp Ratio	Load Dir

Finding that the blocks are important was also expected. As mentioned previously, the blocks contain the effects of both gross geometry and also seismic intensity. One would anticipate that a 5.5 magnitude earthquake on a bridge with a span length of 30 m would induce a different response than a 7.5 magnitude earthquake would on a 10 m long span bridge. The real surprise comes in that blocks are only significant in four of the eight responses.

6.3.2 Multi-Span Simply Supported Concrete Box Girder Bridge

The MSSS Concrete and the MSSS Concrete Box girder bridges are very similar in make-up, in that they have the same substructure and similar superstructures. The girder systems and bearing types are similar by both using elastomeric pads. The typical values for the geometric parameters are different and result in the eight geometric bridge samples presented in Table 6-8. The span lengths range from 7.3 m to 20.7 m while the deck width is between 7.1 and 16.2 m. The column heights range between 3.5 and 6.4 m.

Because of the similarity of the bridge components between this bridge type and the MSSS Concrete bridge type, the modeling parameters considered are the same. The 15 modeling parameters considered for this bridge are presented in Table 6-5. The upper and lower ranges for the values of each parameter do not change from the Concrete bridge because the materials and nature of the components are the same.

Table 6-8: Geometric Bridge Samples of MSSS Concrete Box Girder Bridge.

Bridge No.	Spans	Span Length (m)	Deck Width (m)	Column Height (m)
1	3	7.30	8.40	4.12
2	3	12.20	7.10	4.06
3	3	15.50	7.30	3.65
4	3	8.80	9.10	5.40
5	3	18.30	16.20	3.52
6	3	14.90	10.20	3.93
7	3	20.70	7.40	6.44
8	3	11.60	7.70	5.91

Using the same screening design and also the same three ground motions, time-history analyses are conducted for the eight bridges presented in Table 6-8. An ANOVA is performed for the eight component responses, as previously outlined in Table 6-3. The p-values resulting from each of the hypothesis tests are presented in Table 6-30 at the end of the chapter.

Because of the size and thickness of the elastomeric bearings in this bridge type, it tends to be considerably stiffer than its concrete counterpart. This causes there to be a shift in some of the parameters which are seen as significant in the modeling of this bridge type. Table 6-9 lists the eight parameters which are significant for one or more of the monitored responses. As seen previously, the loading direction plays the most significant role in the response of the bridge. In fact, the only response where this parameter is not seen as significant is the column ductilities, because this is the only response which is not load direction specific.

Other significant parameters include the bearing model parameters which are pad friction, pad stiffness and dowel strength. As mentioned, the pads in this bridge type tend to

Table 6-9: Significant Parameters for MSSS Concrete Box Girder Bridge.

Significant Parameters		
Pad Frict	Pad Stiff	Dowel Str
Ab-Act Stf	Mass	Damp Ratio
Hinge Gap	Load Dir	

be more stiff than those in the MSSS Concrete girder bridge. What these results show is that this difference in stiffness is indeed an appropriate variation to capture and thus lends strength to the argument that the MSSS Concrete and MSSS Concrete Box girder bridges should be separate bridge classes. The remaining parameters, which are deemed significant, include the mass, damping ratio, active abutment stiffness and the gaps at hinges. At a minimum, these are the parameters which must be treated probabilistically in future studies.

6.3.3 Multi-Span Simply Supported Slab Bridge

The multi-span simply supported slab bridge is quite similar to the concrete box girder bridge. The substructure is different, as shown in Chapter 5, yet the superstructure is very much the same. Probably the largest difference between the two bridges is the typical length of the bridge spans. The eight sample bridges generated from the empirical CDFs of the bridge geometry data are given in Table 6-10. As already pointed out, the span lengths for this bridge, which range between 6.7 and 14.0 m, are much shorter than for the concrete-box girder bridge. Deck widths are also narrower ranging between 5.8 and 15.4 m. The column heights have a minimum of 3.4 m and a maximum of 6.1 m.

The ANOVA for each of the modeling parameters and each of the component responses result in the p-values given in Table 6-31 at the end of the chapter. The parameters which

Table 6-10: Geometric Bridge Samples of MSSS Slab Bridge.

Bridge No.	Spans	Span Length (m)	Deck Width (m)	Column Height (m)
1	3	10.70	10.00	4.86
2	3	7.60	8.70	3.39
3	3	12.80	10.10	5.70
4	3	9.10	14.50	4.33
5	3	6.70	5.80	4.09
6	3	14.00	8.40	3.77
7	3	10.40	8.20	3.93
8	3	9.10	7.70	6.11

have p-values less than 0.05, for at least one structural response quantity, are listed in Table 6-11. Once again, loading direction appears to be the most significant of all the parameters. Gaps at the abutments also appear to play a significant role in the response of four of the bridge components, thus, indicating the presence of pounding in the bridge. When pounding at the abutments occurs, one should also see an increase in the passive demand placed on the abutments. This may be the reason that the passive stiffness of the abutment in this model is determined to be significant.

It is also interesting to note that the mass of the bridge does not appear to be a significant parameter in this model. One likely cause of this phenomenon is that the typical mass of the bridge in comparison to the stiffness of the bearings is relatively small. Therefore, a ten percent shift in the mass may not change the overall modal properties or response of the bridge by much.

Table 6-11: Significant Parameters for MSSS Slab Bridge.

Significant Parameters		
Conc Str	Pad Frict	Pad Stiff
Ab-Pas Stf	Ab-Act Stf	Damp Ratio
Abut Gap	Load Dir	

Table 6-12: Geometric Bridge Samples of MSC Concrete Girder Bridge.

Bridge No.	Spans	Span Length (m)	Deck Width (m)	Column Height (m)
1	3	39.60	21.20	4.00
2	3	22.60	12.80	3.93
3	3	18.90	10.80	6.29
4	3	21.00	8.00	3.19
5	3	26.20	13.10	4.20
6	3	10.40	14.10	3.64
7	3	14.50	8.70	4.46
8	3	15.20	9.80	5.93

6.3.4 Multi-Span Continuous Concrete Girder Bridge

A presentation of the continuous span concrete girder and concrete slab bridges is given next. As seen before, one common motive for building continuous type bridges is to facilitate the building of longer bridge spans. It is seen in Chapter 4 that this indeed holds true with the bridges in the CSUS. The range of spans lengths for the MSC Concrete girder bridge, as give in Table 6-12, is between 10.4 and 39.6 m. The deck widths also have a much larger range than do the simply supported bridges, where the minimum width is 8.0 m and the maximum width is 21.2 m. These deck widths are likely due to the particular applications of this bridge type, particularly in high loading environments. Similar to the other bridge types, the column heights vary between 3.2 m and 6.3 m tall.

The continuous nature of the MSC Concrete girder and MSC Slab bridges eliminates the hinge gap which is present in their simply supported counter parts. As shown in Table 6-13, this cuts the number of parameters down from 15 to 14. All other parameters and value ranges are identical to the MSSS types of bridges except for the abutment gaps. It is customary in continuous span bridges to provide larger gaps than normally would appear in the simply supported bridges. This is because all thermal expansion and contraction along the entire length of the bridge must be accommodated at the abutment gaps. As a result, the lower and upper levels for the abutment gap are 37 mm and 116 mm respectively (Choi, 2002).

The ANOVA of the component responses of this bridge type (see Table 6-32 at end of chapter) show that the significance of the active stiffness of the abutments is second only to loading direction. This is measured in terms of the number of responses for which it is significant. Some of the load to the abutments is transferred through the friction component of the bearings while the remaining part of the load is transferred through the retention dowels. This is probably the reason for the abutment stiffness being significant to the bearing responses, where there is clearly an interaction occurring. Other significant modeling parameters, presented concisely in Table 6-14, include dowel strength, damping ratio and abutment gap size.

6.3.5 Multi-Span Continuous Slab Bridge

Table 6-15 gives the eight bridge samples, used in both the screening study and subsequent fragility analysis, for the MSC Slab bridge. As pointed out for the concrete girder bridges,

Table 6-13: Parameters Considered in the Screening of MSC Concrete and MSC Slab Bridges.

Parameter No.	Description	Abbreviation	Lower Level	Upper Level	Units
1	Concrete strength	Conc Str	26.4	40.6	MPa
2	Steel strength	Steel Str	438	555	MPa
3	Coefficient of friction for elastomeric pads	Pad Frict	50	150	%
4	Initial stiffness of elastomeric pads	Pad Stiff	50	150	%
5	Dowel strength	Dowel Str	80	120	%
6	Gap at dowels for expansion bearing only	Dowel Gap	0	50.8	mm
7	Initial stiffness of passive abutment	Ab-Pas Stf	50	150	%
8	Initial Stiffness of active abutment	Ab-Act Stf	50	150	%
9	Rotational stiffness of foundations	Fnd-Rot Stf	50	150	%
10	Translational stiffness of foundations	Fnd-Hor Stf	50	150	%
11	Mass	Mass	90	110	%
12	Damping ratio	Damp Ratio	0.02	0.08	ratio
13	Gap between abutments and decks	Abut Gap	37	116	mm
14	Loading direction (Long or Trans)	Load Dir	L	T	

Table 6-14: Significant Parameters for MSC Concrete Girder Bridge.

Significant Parameters		
Dowel Str	Ab-Act Stf	Damp Ratio
Abut Gap	Load Dir	

Table 6-15: Geometric Bridge Samples of MSC Slab Bridge.

Bridge No.	Spans	Span Length (m)	Deck Width (m)	Column Height (m)
1	3	15.30	8.80	4.08
2	3	13.90	13.00	3.85
3	3	6.70	15.10	4.26
4	3	8.90	7.20	5.98
5	3	7.60	10.60	6.34
6	3	9.10	11.10	5.40
7	3	10.60	8.00	3.90
8	3	12.10	6.90	2.47

this bridge class typically has longer span lengths than does its simply supported counterpart. The bridge samples have span lengths which range from 6.7 m to 15.3 m long. The deck width is similar, with values between 6.9 m and 15.1 m. It is clear that the possibility of short wide spans is very real. One would expect this to have a large influence on the responses of the bridges. Column heights vary from 2.5 to 6.3 m tall.

Looking at the same 14 modeling parameters as given in Table 6-13, an ANOVA is conducted, resulting in the p-values presented in Table 6-33 at end of chapter. Of the significant parameters listed in Table 6-16, the active stiffness of the abutment appears to be the most significant parameter. This is not only seen by the fact it is significant for all component responses, but also by the fact that most of the p-values ~ 0.00. Loading direction is also highly significant, affecting all parameters significantly except for the column ductility. Five other parameters also are considered significant in one or more component responses. This includes three bearing model parameters, which are significant in the bearing responses.

Table 6-16: Significant Parameters for MSC Slab Bridge.

Significant Parameters		
Pad Frict	Pad Stiff	Dowel Str
Ab-Act Stf	Fnd-hor Stf	Damp Ratio
	Load Dir	

Table 6-17: Geometric Bridge Samples of MSSS Steel Girder Bridge.

Bridge No.	Spans	Span Length (m)	Deck Width (m)	Column Height (m)
1	3	18.30	8.70	5.10
2	3	20.40	8.00	3.62
3	3	15.50	4.90	5.95
4	3	13.70	10.50	4.02
5	3	25.60	29.70	3.54
6	3	7.30	5.50	3.90
7	3	8.80	7.40	4.26
8	3	10.40	12.80	6.62

6.3.6 Multi-Span Simply Supported Steel Girder Bridge

The eight bridge samples, derived from the inventory information in Chapter 4 and used throughout this study for the MSSS Steel girder bridge class, are given in Table 6-17. The span lengths range from very short at 7.3 m long to relatively long at 25.6 m. The deck widths vary from 4.9 m up to 29.7 m. Although 29.7 m is the widest bridge sample, the next closest one is 12.8 m wide. This will help to draw out the influences that deck width exerts on the response of these bridge types. The column heights are between 3.5 m and 6.0 m.

Some of the modeling parameters which are used in the concrete type bridges are also used in the steel bridge types (e.g. concrete strength, steel strength, abutment stiffnesses and foundation stiffnesses). The difference between the two general types of bridges lie in the

modeling parameters of the bearings. As discussed in Chapter C, these steel-type bridges typically use steel bearings. Each bearing type, both fixed and expansion, is governed by a coefficient of friction. The initial stiffness of the fixed bearings is also considered giving a total of 14 parameters.

The abutment and hinge gaps vary more for the steel bridges than they do for the concrete bridges. This is due to the difference between the coefficients of thermal expansion for the two materials, steel and concrete. For this screening study, the gap between the decks and abutments is between 28 mm and 48 mm. The gaps between just the decks are between 18 mm and 33 mm.

The p-values, for the hypothesis tests associated with the ANOVA for the component responses of this steel bridge type, are given in Table 6-34 at end of chapter. It is interesting to note that of the 14 parameters which were screened for this bridge type, only two were not found to be significant for at least one of the component responses. The two parameters not found significant are concrete strength and friction of the expansion bearings. The remainder of the parameters are labeled as significant and listed in Table 6-19.

Damping ratio and loading direction appear to be the most significant of the modeling parameters yet the fixed bearing stiffness also plays a significant role. In this bridge type, it is also informative to note that the abutment modeling parameters are significant for mostly the abutment responses and the bearing modeling parameters are mostly significant for the response of the bearings. This could be indicative of a lessened degree of component interaction, as compared with previously discussed bridge types.

Table 6-18: Parameters Considered in the Screening of MSSS Steel Girder Bridge.

Parameter No.	Description	Abbreviation	Lower Level	Upper Level	Units
1	Concrete strength	Conc Str	26.4	40.6	MPa
2	Steel strength	Steel Str	438	555	MPa
3	Coefficient of friction for steel expansion bearing	Exp Frict	50	150	%
4	Coefficient of friction for steel fixed bearing	Fxd Frict	50	150	%
5	Initial stiffness of steel fixed bearing	Fxd Stiff	80	120	%
6	Initial stiffness of passive abutment	Ab-Pas Stf	50	150	%
7	Initial Stiffness of active abutment	Ab-Act Stf	50	150	%
8	Rotational stiffness of foundations	Fnd-Rot Stf	50	150	%
9	Translational stiffness of foundations	Fnd-Hor Stf	50	150	%
10	Mass	Mass	90	110	%
11	Damping ratio	Damp Ratio	0.02	0.08	ratio
12	Gap between abutments and decks	Abut Gap	28	48	mm
13	Gap between adjacent decks	Hinge Gap	18	33	mm
14	Loading direction (Long or Trans)	Load Dir	L	T	

Table 6-19: Significant Parameters for MSSS Steel Girder Bridge.

Significant Parameters		
Steel Str	Fxd Frict	Fxd Stiff
Ab-Pas Stf	Ab-Act Stf	Fnd-Rot Stf
Fnd-Hor Stf	Mass	Damp Ratio
Abut Gap	Hinge Gap	Load Dir

Table 6-20: Geometric Bridge Samples of MSC Steel Girder Bridge.

Bridge No.	Spans	Span Length (m)	Deck Width (m)	Column Height (m)
1	3	13.40	13.00	3.72
2	3	39.00	12.90	3.49
3	3	25.10	10.20	3.93
4	3	29.90	14.50	5.42
5	3	18.20	20.10	4.20
6	3	19.80	5.50	5.76
7	3	22.30	10.30	4.08
8	3	40.80	7.90	6.74

6.3.7 Multi-Span Continuous Steel Girder Bridge

The bridge samples for the MSC Steel girder bridge are given in Table 6-20 which show the span lengths to range between 13.4 m and 40.8 m. These span lengths are considerably longer than those used in the MSSS Steel girder bridge. Once again this is due to continuous girders being capable of longer spans. The deck widths vary from 5.5 m to 20.1 m while the column heights range from 3.5 m to 6.7 m.

The modeling parameters for the MSC Steel girder bridge, given in Table 6-21, are the same as those for the MSSS Steel girder bridge except for the elimination of the hinge gaps, giving a total of 13 screened parameters. The sizes of the abutment gaps are also different, with an average opening of 76 mm wide for this bridge type. Appropriate lower and upper levels for the value of this parameter are 37 mm and 116 mm respectively.

The p-values, as calculated in ANOVA, for the MSC Steel girder bridge components are given in Table 6-35 at end of chapter. Unlike its simply supported counter part, this bridge type does not see so many significant parameters. Of the seven significant parameters listed in Table 6-22, it appears that loading direction and abutment gap size are the most

Table 6-21: Parameters Considered in the Screening of MSC Steel Girder Bridge.

Parameter No.	Description	Abbreviation	Lower Level	Upper Level	Units
1	Concrete strength	Conc Str	26.4	40.6	MPa
2	Steel strength	Steel Str	438	555	MPa
3	Coefficient of friction for steel expansion bearing	Exp Frict	50	150	%
4	Coefficient of friction for steel fixed bearing	Fxd Frict	50	150	%
5	Initial stiffness of steel fixed bearing	Fxd Stiff	80	120	%
6	Initial stiffness of passive abutment	Ab-Pas Stf	50	150	%
7	Initial Stiffness of active abutment	Ab-Act Stf	50	150	%
8	Rotational stiffness of foundations	Fnd-Rot Stf	50	150	%
9	Translational stiffness of foundations	Fnd-Hor Stf	50	150	%
10	Mass	Mass	90	110	%
11	Damping ratio	Damp Ratio	0.02	0.08	ratio
12	Gap between abutments and decks	Abut Gap	37	116	mm
13	Loading direction (Long or Trans)	Load Dir	L	T	

Table 6-22: Significant Parameters for MSC Steel Girder Bridge.

Significant Parameters		
Fxd Frict	Fxd Stiff	Ab-Act Stf
Mass	Damp Ratio	Abut Gap
	Load Dir	

Table 6-23: Geometric Bridge Samples of SS Concrete Girder Bridge.

Bridge No.	Span Length (m)	Deck Width (m)
1	20.40	9.50
2	7.90	7.70
3	10.40	6.20
4	18.00	7.30
5	8.40	9.00
6	15.50	13.20
7	12.20	8.40
8	23.20	6.90

important. Significance of the abutment gaps once again is indicative of pounding in the bridge model. This pounding at the abutments can cause an increased demand on the steel bearings, thus explaining the significance that abutment gaps have in determining bearing responses.

6.3.8 Single Span Concrete Girder Bridge

Eight statistical samples of the SS Concrete girder bridge are presented in Table 6-23. The span lengths of these bridge samples range between 7.9 m and 23.2 m, but the majority of the samples are in the 10 - 18 m range. The variation in the deck widths is much less extreme with a range of 6.2 m to 13.2 m. What this indicates is that the large majority of single span concrete girder bridges are composed of just two lanes.

Table 6-24: Parameters Considered in the Screening of SS Concrete Girder Bridge.

Parameter No.	Description	Abbreviation	Lower Level	Upper Level	Units
1	Coefficient of friction for elastomeric pads	Pad Frict	50	150	%
2	Initial stiffness of elastomeric pads	Pad Stiff	50	150	%
3	Dowel strength	Dowel Str	80	120	%
4	Gap at dowels for expansion bearing only	Dowel Gap	0	50.8	mm
5	Initial stiffness of passive abutment	Ab-Pas Stf	50	150	%
6	Initial Stiffness of active abutment	Ab-Act Stf	50	150	%
7	Mass	Mass	90	110	%
8	Damping ratio	Damp Ratio	0.02	0.08	ratio
9	Gap between abutments and decks	Abut Gap	97	107	mm
10	Loading direction (Long or Trans)	Load Dir	L	T	

Eliminating columns and foundations from the concrete type bridges reduces the total number of parameters to be considered down to 10, as seen in Table 6-24. It should be pointed out that the parameter levels for this bridge type are the same as those for both the MSSS Concrete and MSC Concrete bridges. The only difference is found at the abutment gaps. With an average gap size of 101 mm, the lower and upper levels are assigned as 97 mm and 107 mm respectively.

Table 6-36, at the end of the chapter, presents the p-values from the ANOVA of SS Concrete girder bridge component responses. The significant parameters for this bridge type are subsequently listed in Table 6-25. The active responses of the abutments appear to be influenced by the largest number of parameters, which is five. These include dowel gap, active stiffness, damping ratio, abutment gap and loading direction. The transverse

Table 6-25: Significant Parameters for SS Concrete Girder Bridge.

Significant Parameters		
Pad Frict	Dowel Str	Dowel Gap
Ab-Pas Stf	Ab-Act Stf	Damp Ratio
Abut Gap	Load Dir	

Table 6-26: Geometric Bridge Samples of SS Steel Girder Bridge.

Bridge No.	Span Length (m)	Deck Width (m)
1	9.40	6.30
2	20.80	11.90
3	14.90	8.20
4	7.90	5.50
5	39.90	3.70
6	24.40	6.10
7	12.50	4.90
8	6.60	7.40

response of both the fixed and expansion bearings have more-or-less the same sensitivities. This is to be expected in that the models of both bearing types are identical in the transverse direction. This finding lends strength to the capabilities of the screening tool used in this study.

6.3.9 Single Span Steel Girder Bridge

The bridge samples used in this study for the single span steel girder bridges are given in Table 6-26. The span lengths for this bridge type, which range from 6.6 m to 39.9 m, are consistently longer that those for the single span concrete bridges. This phenomenon highlights the superior strength to weight ratio of steel girders as compared to concrete girders. The deck widths for this bridge type are relatively narrow ranging from 3.7 m to 11.9 m indicating the substantial presence of one and two lane bridges.

Table 6-27: Parameters Considered in the Screening of SS Steel Girder Bridge.

Parameter No.	Description	Abbreviation	Lower Level	Upper Level	Units
1	Coefficient of friction for steel expansion bearing	Exp Frict	50	150	%
2	Coefficient of friction for steel fixed bearing	Fxd Frict	50	150	%
3	Initial stiffness of steel fixed bearing	Fxd Stiff	80	120	%
4	Initial stiffness of passive abutment	Ab-Pas Stf	50	150	%
5	Initial Stiffness of active abutment	Ab-Act Stf	50	150	%
6	Mass	Mass	90	110	%
7	Damping ratio	Damp Ratio	0.02	0.08	ratio
8	Gap between abutments and decks	Abut Gap	97	106	mm
9	Loading direction (Long or Trans)	Load Dir	L	T	

Table 6-27 lists the parameters and their associated levels as used for this bridge type in this study. Overall, nine parameters are considered, which also coincide with those listed for the MSC Steel bridge in Table 6-21. Parameters one through eight have levels identical to the previous bridges, most of which are relative in nature. The abutment gap has a lower level of 97 mm and and upper level of 106 mm.

Using the p-values calculated from the ANOVA of the SS Steel bridge component responses and given in Table 6-37 at the end of chapter, five parameters are deemed significant. A list of these parameters is given in Table 6-28. The friction of both the expansion and fixed bearings appear to be significant. This may be a direct result of the type of bearing which is used in this type of bridge. The steel bearings are the low-type, giving them a much larger stiffness than their high-type counterparts. Thus, a more significant portion of

Table 6-28: Significant Parameters for SS Steel Girder Bridge.

Significant Parameters		
Exp Frict	Fxd Frict	Ab-Pas Stf
Ab-Act Stf	Load Dir	

the movement in these bearings results from sliding and thus explains the significance of friction.

6.4 Closure

The purpose of this chapter is to explore the impact that various modeling parameters have upon the responses of the bridge types being considered in this study. Results from these screening studies are useful in identifying modeling parameters which should be treated in a probabilistic manner as opposed to a deterministic approach. This also helps to give a more clear understanding of the parameters which require the most rigor during analytical model development. A design-of-experiments screening study, which is a statistical approach, is used to explore the variation in eight specific component responses as a result of change in various modeling parameter values.

The results of this study may be more straight forward if only one bridge response was to be monitored, such as the ductility demand on the concrete columns. However, the parameters which are significant for each bridge tend to vary from component to component. Table 6-29 lists the three most significant modeling parameters for each bridge type. The parameters are listed in order of significance, where ranking is determined from the number of response measures for which it is significant. Since the blocking and loading direction are significant for almost all bridge components, these are dropped from the table

to allow for presentation of the next three significant parameters. As seen in Table 6-29, each bridge has different significant modeling parameters. However, the active abutment stiffness, bearing friction and bearing stiffness appears to be the most prevalent of the significant parameters across all bridge types.

As previously alluded to, it is very feasible that almost all modeling parameters for a given bridge are deemed significant, as is the case with the MSSS Steel girder bridge. When one acknowledges that nine bridge classes are considered, each with eight responses, there is no surprise that each modeling parameter is significant in at least one instance. This, therefore, requires probability distributions to be defined for all of these parameters. Consequently, for the probabilistic seismic demand simulations conducted in Chapter 7, all parameters are treated as random variables even though the need may not always be present.

Although the specific findings from this chapter are not used explicitly in this study, they do make some important contributions to the earthquake engineering community. Analytical bridge models are often used to assist in developing design procedures, retrofit strategies and in making other seismic mitigation decisions. The results of this study help to clarify the significance and thus the emphasis that should be placed on some of the bridge modeling parameters. In general, as seen in Table 6-29, the abutment models and the bearing models appear to be the most significant parameters (excluding geometric parameters) in determining the seismic response of a bridge. Therefore, additional experimental studies may be warranted to facilitate the development more accurate models of these components.

Table 6-29: Summary of Most Significant Modeling Parameters for Each Bridge Class.

Bridge Description	Parameter 1	Parameter 2	Parameter 3
MSC Concrete	Act - Abut Stiff	Abutment Gap	Dowel Strength
MSC Slab	Act - Abut Stiff	Brg Pad Friction	Dowel Strength
MSC Steel	Abutment Gap	Act - Abut Stiff	Fxd Brg Stiff
MSSS Concrete	Act - Abut Stiff	Brg Pad Friction	Fnd Rot Stiff
MSSS Concrete-Box	Act - Abut Stiff	Dowel Strength	Brg Pad Stiff
MSSS Slab	Act - Abut Stiff	Brg Pad Friction	Abutment Gap
MSSS Steel	Damping Ratio	Fxd Brg Stiff	Act - Abut Stiff
SS Concrete	Pass - Abut Stiff	Brg Pad Friction	Act - Abut Stiff
SS Steel	Exp Brg Friction	Act - Abut Stiff	Fxd Brg Friction

Table 6-30: Calculated p-values for MSSS Concrete Box Bridge.

Parameter	P-Value							
	Ductility	**Fxd-Tran**	**Fxd-Long**	**Exp-Tran**	**Exp-Long**	**Ab-Pass**	**Ab-Act**	**Ab-Tran**
Conc Str	0.123	0.381	0.855	0.787	0.859	0.241	0.167	0.115
Steel Str	0.971	0.695	0.413	0.843	0.406	0.419	0.916	0.467
Pad Frict	0.819	**0.035**	0.942	**0.005**	0.844	0.372	0.817	0.448
Pad Stiff	0.692	0.157	**0.000**	0.713	**0.000**	0.350	0.878	0.686
Dowel Str	0.542	**0.006**	**0.000**	0.207	**0.000**	0.308	0.221	0.059
Dowel Gap	0.227	0.113	0.623	0.697	0.715	0.389	0.248	0.532
Ab-Pas Stf	0.115	0.409	0.383	0.702	0.660	0.090	0.268	0.883
Ab-Act Stf	**0.002**	0.378	0.393	0.855	0.406	0.120	**0.009**	**0.000**
Fnd-Rot Stf	0.069	0.521	0.942	0.316	0.859	0.426	0.952	0.789
Fnd-hor Stf	0.469	0.913	0.870	0.573	0.743	0.263	0.336	0.964
Mass	0.159	0.192	**0.001**	0.120	**0.001**	0.254	0.805	0.254
Damp Ratio	0.215	0.143	**0.000**	0.265	**0.000**	0.588	0.752	0.417
Abut Gap	0.290	0.463	0.548	0.063	0.495	0.361	0.375	0.439
Hinge Gap	0.987	0.890	**0.000**	0.753	**0.000**	0.256	0.450	0.852
Load Dir	0.372	**0.000**	**0.000**	**0.000**	**0.000**	**0.030**	**0.001**	**0.000**
Blocks	**0.001**	**0.008**	**0.000**	**0.007**	**0.000**	0.394	0.367	0.539

Bold faced numbers are less than 0.05 and considered a sign of significance.

Table 6-31: Calculated p-values for MSSS Slab Bridge.

Parameter	P-Value							
	Ductility	**Fxd-Tran**	**Fxd-Long**	**Exp-Tran**	**Exp-Long**	**Ab-Pass**	**Ab-Act**	**Ab-Tran**
Conc Str	0.558	**0.017**	0.346	0.267	0.284	0.638	0.324	0.873
Steel Str	0.959	0.292	0.767	0.880	0.708	0.479	0.262	0.540
Pad Frict	0.210	**0.003**	0.066	**0.002**	**0.046**	0.925	**0.038**	0.601
Pad Stiff	0.143	0.216	**0.000**	0.307	**0.000**	0.759	0.777	0.799
Dowel Str	0.782	0.310	0.318	0.327	0.355	0.307	0.627	0.640
Dowel Gap	0.133	0.626	0.486	0.056	0.650	0.671	0.711	0.061
Ab-Pas Stf	0.363	0.258	0.214	0.963	0.092	**0.000**	0.919	0.636
Ab-Act Stf	**0.000**	0.395	**0.012**	0.588	**0.016**	0.101	0.101	**0.001**
Fnd-Rot Stf	0.102	0.137	0.346	0.434	0.503	0.102	0.656	0.970
Fnd-hor Stf	0.933	0.788	0.274	0.410	0.239	0.499	0.596	0.922
Mass	0.889	0.154	0.640	0.441	0.686	0.156	0.483	0.393
Damp Ratio	0.178	0.916	**0.001**	0.500	**0.000**	0.971	0.781	0.344
Abut Gap	**0.006**	0.930	**0.000**	0.744	**0.000**	0.361	0.236	**0.030**
Hinge Gap	0.407	0.944	0.088	0.835	0.143	0.380	0.250	0.494
Load Dir	**0.000**	0.779	**0.000**	0.157	**0.000**	**0.000**	**0.001**	**0.000**
Blocks	**0.000**	**0.001**	**0.000**	**0.001**	**0.000**	**0.000**	0.078	0.427

Bold faced numbers are less than 0.05 and considered a sign of significance.

Table 6-32: Calculated p-values for MSC Concrete Bridge.

Parameter	P-Value							
	Ductility	**Fxd-Tran**	**Fxd-Long**	**Exp-Tran**	**Exp-Long**	**Ab-Pass**	**Ab-Act**	**Ab-Tran**
Conc Str	0.636	0.942	0.411	0.898	0.423	0.602	0.325	0.198
Steel Str	0.408	0.891	0.948	0.977	0.963	0.316	0.904	0.888
Pad Frict	0.160	0.157	0.084	0.256	0.081	0.736	0.601	0.118
Pad Stiff	0.109	0.566	0.469	0.737	0.485	0.193	0.847	0.284
Dowel Str	**0.037**	0.765	0.127	0.779	0.131	0.425	0.459	0.804
Dowel Gap	0.429	0.821	0.543	0.978	0.560	0.396	0.822	0.293
Ab-Pas Stf	0.344	0.821	0.864	0.896	0.847	0.097	0.890	0.541
Ab-Act Stf	0.544	0.388	**0.049**	0.442	**0.046**	0.503	**0.000**	**0.001**
Fnd-Rot Stf	0.467	0.843	0.278	0.760	0.286	0.066	0.404	0.360
Fnd-hor Stf	0.807	0.325	0.326	0.398	0.337	0.102	0.301	0.187
Mass	0.144	0.332	0.948	0.526	0.934	0.948	0.922	0.799
Damp Ratio	**0.002**	0.594	0.053	0.686	0.051	0.104	0.707	0.117
Abut Gap	0.108	**0.001**	0.197	**0.003**	0.203	**0.002**	0.387	0.359
Load Dir	**0.001**	**0.000**	**0.016**	**0.000**	**0.015**	**0.000**	**0.000**	**0.000**
Blocks	**0.000**	**0.001**	0.265	**0.001**	0.268	**0.001**	0.888	0.640

Bold faced numbers are less than 0.05 and considered a sign of significance.

Table 6-33: Calculated p-values for MSC Slab Bridge.

Parameter	P-Value							
	Ductility	**Fxd-Tran**	**Fxd-Long**	**Exp-Tran**	**Exp-Long**	**Ab-Pass**	**Ab-Act**	**Ab-Tran**
Conc Str	0.795	0.792	0.159	0.475	0.158	0.617	0.539	0.492
Steel Str	0.090	0.429	0.614	0.557	0.612	0.814	0.599	0.848
Pad Frict	0.549	**0.018**	**0.006**	**0.032**	**0.006**	0.659	**0.048**	0.408
Pad Stiff	0.819	0.635	**0.001**	0.922	**0.001**	0.788	0.966	0.720
Dowel Str	0.425	0.120	**0.040**	0.100	**0.039**	0.284	0.192	**0.044**
Dowel Gap	0.251	0.669	0.598	0.284	0.595	0.912	0.619	0.787
Ab-Pas Stf	0.258	0.639	0.721	0.570	0.730	**0.005**	0.300	0.764
Ab-Act Stf	**0.000**	**0.040**	**0.000**	**0.044**	**0.000**	**0.003**	**0.014**	**0.002**
Fnd-Rot Stf	0.623	0.335	0.932	0.323	0.929	0.735	0.483	0.220
Fnd-hor Stf	0.760	0.323	**0.005**	0.139	**0.005**	0.141	0.284	0.236
Mass	0.563	0.996	0.357	0.828	0.359	0.420	0.965	0.892
Damp Ratio	**0.019**	0.089	0.148	0.141	0.147	0.296	0.076	0.401
Abut Gap	0.334	0.791	0.883	0.809	0.880	0.288	0.786	0.234
Load Dir	0.272	**0.001**	**0.000**	**0.001**	**0.000**	**0.000**	**0.000**	**0.000**
Blocks	**0.018**	0.379	**0.014**	0.306	**0.014**	0.105	0.413	0.374

Bold faced numbers are less than 0.05 and considered a sign of significance.

Table 6-34: Calculated p-values for MSSS Steel Girder Bridge.

Parameter	P-Value							
	Ductility	**Fxd-Tran**	**Fxd-Long**	**Exp-Tran**	**Exp-Long**	**Ab-Pass**	**Ab-Act**	**Ab-Tran**
Conc Str	0.367	0.319	0.719	0.580	0.564	0.960	0.233	0.559
Steel Str	**0.013**	0.671	0.768	0.828	0.602	0.483	0.654	0.827
Exp Frict	0.729	0.436	0.769	0.918	0.194	0.648	0.066	0.469
Fxd Frict	**0.000**	0.568	**0.000**	0.372	**0.019**	0.623	0.565	0.492
Fxd Stiff	**0.006**	**0.039**	**0.000**	0.142	**0.001**	0.545	0.346	0.267
Ab-Pas Stf	0.720	0.180	0.889	0.478	0.949	**0.015**	0.906	0.516
Ab-Act Stf	0.948	0.325	0.917	0.887	0.659	**0.048**	**0.000**	**0.000**
Fnd-Rot Stf	0.328	0.105	0.598	**0.034**	0.803	**0.018**	0.451	0.565
Fnd-hor Stf	0.630	0.219	0.681	0.380	0.772	0.194	**0.024**	0.483
Mass	0.652	**0.002**	0.146	**0.010**	0.302	0.126	**0.010**	0.246
Damp Ratio	**0.001**	**0.001**	**0.000**	**0.005**	**0.000**	**0.000**	0.348	0.130
Abut Gap	0.664	0.266	**0.045**	0.183	**0.003**	0.308	0.392	0.751
Hinge Gap	0.788	0.538	**0.009**	0.894	**0.000**	0.058	0.720	0.110
Load Dir	**0.000**	**0.000**	**0.000**	**0.000**	**0.000**	**0.000**	**0.001**	**0.000**
Blocks	**0.000**	**0.000**	**0.000**	**0.000**	**0.000**	**0.000**	**0.007**	0.574

Bold faced numbers are less than 0.05 and considered a sign of significance.

Table 6-35: Calculated p-values for MSC Steel Girder Bridge.

Parameter	P-Value							
	Ductility	**Fxd-Tran**	**Fxd-Long**	**Exp-Tran**	**Exp-Long**	**Ab-Pass**	**Ab-Act**	**Ab-Tran**
Conc Str	0.591	0.856	0.269	0.853	0.251	0.728	0.603	0.139
Steel Str	0.590	0.710	0.774	0.836	0.083	0.932	0.122	0.234
Exp Frict	0.825	0.722	0.766	0.995	0.490	0.953	0.077	0.154
Fxd Frict	0.158	**0.004**	**0.004**	0.587	0.796	0.874	0.660	0.534
Fxd Stiff	**0.008**	**0.013**	0.682	0.073	0.075	**0.015**	0.122	0.202
Ab-Pas Stf	0.633	0.732	0.787	0.650	0.822	0.262	0.346	0.450
Ab-Act Stf	0.600	0.763	0.264	0.998	**0.009**	0.953	**0.000**	**0.022**
Fnd-Rot Stf	0.136	0.680	0.247	0.854	0.814	0.960	0.631	0.514
Fnd-hor Stf	0.500	0.790	0.526	0.762	0.926	0.566	0.395	0.271
Mass	0.375	**0.024**	0.380	0.906	0.453	0.850	0.483	0.133
Damp Ratio	0.665	**0.003**	**0.029**	0.217	0.313	0.264	0.766	0.662
Abut Gap	**0.000**	**0.001**	**0.028**	**0.001**	0.239	0.070	0.153	0.130
Load Dir	**0.003**	**0.001**	**0.001**	**0.000**	**0.003**	**0.000**	**0.000**	**0.006**
Blocks	**0.001**	**0.000**	**0.004**	**0.000**	0.555	**0.001**	0.182	0.463

Bold faced numbers are less than 0.05 and considered a sign of significance.

Table 6-36: Calculated p-values for SS Concrete Bridge.

Parameter	P-Value						
	Fxd-Tran	**Fxd-Long**	**Exp-Tran**	**Exp-Long**	**Ab-Pass**	**Ab-Act**	**Ab-Tran**
Pad Frict	**0.044**	0.492	**0.044**	0.408	0.100	0.389	0.565
Pad Stiff	0.089	0.188	0.058	0.122	0.380	0.376	0.077
Dowel Str	**0.039**	0.198	**0.048**	0.130	0.694	0.784	0.447
Dowel Gap	0.068	0.398	0.105	0.308	0.076	**0.000**	0.185
Ab-Pas Stf	**0.003**	0.183	**0.002**	0.118	**0.001**	0.156	**0.018**
Ab-Act Stf	0.971	0.256	0.713	0.186	0.338	**0.000**	**0.000**
Mass	0.448	0.421	0.421	0.330	0.508	0.803	0.213
Damp Ratio	0.766	0.405	0.600	0.313	0.875	**0.004**	0.777
Abut Gap	0.511	0.241	0.649	0.172	0.578	**0.026**	0.335
Load Dir	**0.000**	0.073	**0.000**	**0.039**	**0.000**	**0.000**	**0.000**
Blocks	**0.007**	0.461	**0.001**	0.412	**0.010**	**0.007**	0.430

Bold faced numbers are less than 0.05 and considered a sign of significance.

Table 6-37: Calculated p-values for SS Steel Girder Bridge.

Parameter	P-Value						
	Fxd-Tran	**Fxd-Long**	**Exp-Tran**	**Exp-Long**	**Ab-Pass**	**Ab-Act**	**Ab-Tran**
Exp Frict	**0.008**	**0.040**	**0.001**	**0.000**	**0.007**	0.797	**0.023**
Fxd Frict	**0.000**	**0.000**	**0.024**	0.744	0.108	0.397	0.948
Fxd Stiff	0.282	0.951	0.656	0.722	0.838	0.947	0.416
Ab-Pas Stf	0.287	0.942	0.825	0.898	**0.004**	0.562	0.270
Ab-Act Stf	0.464	0.990	0.061	0.570	**0.000**	**0.000**	**0.001**
Mass	0.983	0.961	0.646	0.565	0.090	0.397	0.218
Damp Ratio	0.622	0.942	0.534	0.892	0.788	0.867	0.341
Abut Gap	0.085	0.558	0.130	0.962	0.691	0.570	0.837
Load Dir	**0.000**	**0.000**	**0.000**	**0.000**	**0.000**	**0.000**	**0.000**
Blocks	**0.000**	0.266	**0.000**	**0.000**	0.089	**0.004**	0.064

Bold faced numbers are less than 0.05 and considered a sign of significance.

CHAPTER VII

PROBABILISTIC SEISMIC DEMAND ANALYSES

7.1 Introduction

In the framework of the risk and loss assessment of highway networks, as presented in Chapter 2, quantifying the seismic demand placed on bridges is an essential component. This is best illustrated by looking at the overall formulation of seismic loss estimation as it exists in a probabilistic setting. This loss estimation is described most concisely through Equation 7.1 (Ellingwood and Wen, 2005).

$$P[Loss] = \sum_{s} \sum_{LS} \sum_{d} P[Loss|D = d] \cdot P[D = d|LS] \cdot P[LS|IM = s] \cdot P[IM = s] \quad (7.1)$$

where IM is an appropriate intensity measure which is chosen to represent the seismic hazard (e.g. peak ground acceleration, spectral acceleration) and s is the realization of that intensity measure. The term LS is some specified structural limit state, sometimes called engineering demand parameter (EDP), which is a measure of the structural response (e.g. deformation, ductility). The terms D and d are the damage state and the realization of the damage state, respectively. These are often given in qualitative terms which give some indication of functionality level (e.g. slight, moderate, extensive, complete). And finally, $Loss$ is some metric, appropriately defined, to capture the overall impact of the seismic hazard (e.g. Life loss, monetary losses). Although other forms of the loss equation are

given (Porter, 2003), they all accomplish essentially the same thing which is to convolve hazards, damage and functionality into some description of loss.

The quantification of seismic demand is represented in Equation 7.1 by the conditional probability, $P[LS|IM = s]$. This conditional probability, explicitly stated, is the probability of meeting or exceeding a specified level of damage, LS, given a ground motion which has a certain level of intensity, s. This conditional probability is often assumed to follow a two parameter lognormal probability distribution (Cornell et al., 2002; Song and Ellingwood, 1999). In addition to this probability law representing well the seismic demand, it also tends to simplify the mathematics required to manipulate it.

7.1.1 Probabilistic Seismic Demand Models

When using analytical procedures, particularly nonlinear time history analyses, the seismic demand is described through probabilistic seismic demand models (PSDMs) which are given in terms of an appropriate intensity measure. In addition to the lognormal assumption, it has been suggested by Cornell et al. (2002) that the estimate of the median demand ($\hat{EDP}$) can be represented by a power model as given in Equation 7.2.

$$\hat{EDP} = aIM^b \tag{7.2}$$

where IM is the seismic intensity measure of choice and both a and b are regression coefficients. After estimating the dispersion ($\beta_{EDP|IM}$), which is conditional upon the intensity measure, the PSDM can be written as in Equation 7.3.

$$P[EDP \geq d|IM] = 1 - \Phi\left(\frac{\ln(d) - \ln\left(aIM^b\right)}{\beta_{EDP|IM}}\right) \tag{7.3}$$

The generation of PSDMs in this study follows the procedure as outlined in Figure 2-8 of Chapter 2. As a recap, the basic procedure is as follows:

1. Assemble a suite of N ground motions which are applicable to the area of interest. This suite should represent a broad range of values for the chosen intensity measure.

2. Generate N statistical samples of the subject structure. These samples should be generated by sampling on various modeling parameters which may be deemed significant (e.g. damping ratio, material strength). Thus, N statistically significant yet nominally identical bridge samples are made.

3. Perform a full nonlinear time history analysis for each ground motion-bridge pair. Key responses should be monitored throughout the analysis.

4. For each analysis, peak responses are recorded and plotted versus the value of the intensity measure for that ground motion. A regression of this data is then used to estimate a, b and $\beta_{EDP|IM}$.

The actual regression used to estimate the parameters a and b from Equation 7.2 is more easily facilitated in a transformed space. The transformation is simply performed by taking the natural logarithm of both sides of Equation 7.2 which results in the linear form of Equation 7.4.

$$\ln(EDP) = \ln(a) + b \cdot \ln(IM) \tag{7.4}$$

Figure 7-1 illustrates the nature of the regression in the transformed space. As mentioned previously, the variation about the median in the transformed space is assumed to

be lognormal. Therefore, in the transformed space, this variation should be normal as is indicated in Figure 7-1. Furthermore, the variation measured about the mean ($\ln(\hat{EDP})$) which is noted as σ in Figure 7-1, is an estimate of the conditional lognormal standard deviation (dispersion) $\beta_{EDP|IM}$. It should be noted, that some researchers have investigated the use of a bilinear regression in the transformed space as opposed to the linear form given in Equation 7.4. Their conclusion, however, was that given the range over which this relation is assumed to be valid, the benefit from a bilinear model was marginal and did not justify the added complexity (Mackie and Stojadinovic, 2003).

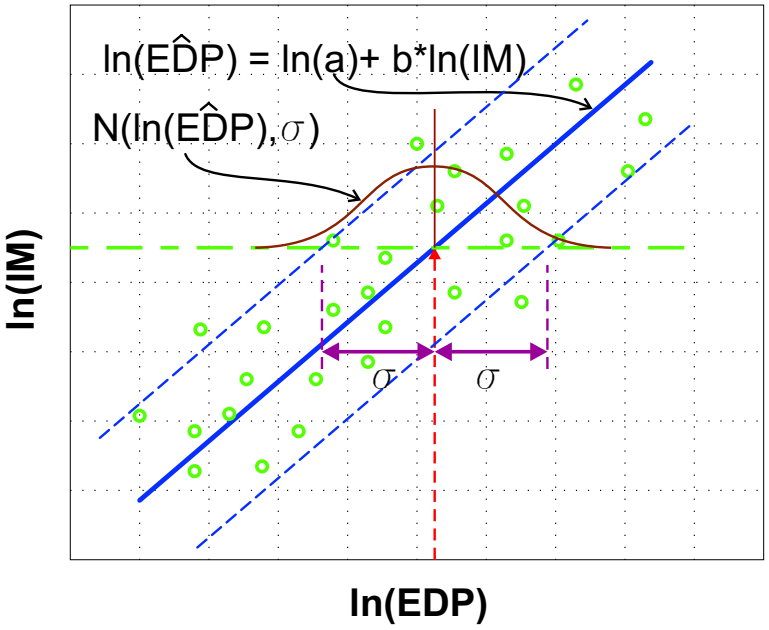

Figure 7-1: Illustration of PSDM in Transformed State.

7.1.2 Selection of Appropriate Intensity Measure

A question that often arises when attempting to predict structural demand as a function of intensity measure, is which intensity measure should be used? The Applied Technology Council, in their work on bridges, chose to use the Modified Mercalli Intensity Scale as the descriptive intensity measure (ATC, 1985). This information was later modified such that it was expressed using one of two intensity measures for use in FEMA's loss assessment program HAZUS (FEMA, 1997). The specific intensity measures used were peak ground acceleration (PGA) and permanent ground deformation (PGD). The latest version of HAZUS has switched to the use of spectral acceleration at a period of one second ($S_a\ 1s$) and PGD.

It is clear that there may not be a single intensity measure which is appropriate for all cases. In an attempt to address this issue Mackie and Stojadinovic (2003) identified 23 intensity measures that could be used for PSDMs of highway bridges. They pointed out that for a parameter to be optimal it should be efficient. Efficiency is measured by the standard deviation of the logarithm of the demand model, which is the amount of variability in the demand parameter for a given intensity measure. In their study, Mackie and Stojadinovic (2003) found that those intensity parameters which are spectral quantities, based on the fundamental period of the bridge, tend to be the most efficient (e.g spectral acceleration, S_a, spectral displacement, S_d).

There is a recognition, however, that it is often impractical to use a structurally based intensity measure for portfolios of bridges or buildings. This is believed to be the motivation for HAZUS-MH using the spectral acceleration at one second ($S_a\ 1s$) as the chosen

intensity measure. There has also been a recognition that efficiency may be improved if more than one intensity measure is used (Baker and Cornell, 2005b). In the current study, four different intensity measures are considered, which are shown in Table 7-1. An explicit consideration of the efficiency of each of these intensity measures is given later in this chapter.

The geometric mean of the periods is calculated as $T_{gm} = \sqrt{T_{long_1} \cdot T_{tran_1}}$, where T_{long_1} and T_{tran_1} are the fundamental periods in the longitudinal and transverse directions respectively. This follows the recommendations of Baker and Cornell (2005c). Because the ground motions, used in this analysis, are given in two orthogonal components, the acceleration values used, are computed as the geometric mean of the acceleration of each component at the period of interest ($S_a = \sqrt{S_{ax} \cdot S_{ay}}$).

Table 7-1: Intensity Measures Considered in This Study.

Intensity Measure	Description
PGA	Peak ground acceleration
S_{a-02s}	Spectral acceleration at 0.2 sec
S_{a-1s}	Spectral acceleration at 1.0 sec
S_{a-gm}	Spectral acceleration at geometric mean of the fundamental periods of both longitudinal and transverse directions (T_{gm})

7.1.3 Bridge Component Probabilistic Seismic Demand Models

Traditionally, when analytical fragility curves have been developed for highway bridges, one primary bridge component has been considered to be indicative of the overall fragility of the bridge. The bridge component of choice for fragility definition has primarily been the

bridge columns (Hwang et al., 2000; Karim and Yamazaki, 2001; Mackie and Stojadinovic, 2001; Nateghi and Shahsavar, 2004). Although this may be an appropriate assumption for certain bridge types, it has been shown that, for bridges typical to the CSUS, additional bridge components should be considered.

In a study of bridges typical to the CSUS, Nielson and DesRoches (2004) illustrated that there are significant differences between bridge column fragilities and bridge system fragilities. They found that the error of this assumption could be as large as 100 percent. A recognition of this error resulted in Choi et al. (2004) considering bearings, in addition to the columns, for their bridge fragility assessments. Following this pattern, the work in this study considers several of the seismically vulnerable bridge components, namely the columns, fixed bearings, expansion bearings and abutments. Therefore, the probabilistic seismic demands must be estimated for each of these bridge components which is further discussed in the next section.

7.2 Probabilistic Seismic Demand Models for 3-D Systems

The probabilistic seismic demand models (PSDMs) for bridge components are essential for generating fragility curves for the individual components. The component fragility curves are useful in identifying the most vulnerable components and in making retrofit decisions. However, system (bridge) fragility curves are essential for use in seismic risk assessment platforms. If component fragility curves are already available then the system wide fragility curves can be developed directly from them.

7.2.1 Joint PSDMs

For the methodology used in this study to generate system fragility curves, it is essential to first obtain a system wide probabilistic seismic demand model. This is accomplished by combining the component PSDMs into a system PSDM that takes the form of a joint probability distribution. Recognizing that each of the PSDMs for the bridge components are assumed to be lognormally distributed, the assemblage of the bridge wide JPSDM is a straight forward process.

Consider that $\underline{X} = (X_1, \ldots, X_n)$ is a random vector representing the demands placed on n bridge components whose marginal distributions are lognormally distributed. Using the transformation $Y_i = \ln(X_i)$, the random vector $\underline{Y} = (Y_1, \ldots, Y_n)$ is then normally distributed. If a joint probability distribution is jointly normal then the only pieces of information needed to fully describe it are the vector of means $\underline{\mu_y}$ and the covariance matrix Σ_y. Therefore, the JPSDMs used in this study are developed in this transformed space.

The covariance matrix Σ_y can be derived directly from the individual x_i values. Performing the recommended change of variables, $y_i = \ln(x_i)$, helps to simplify the procedure. The correlation coefficients are calculated by comparing y_i values instead of the x_i values. Thus, the correlation matrices which are presented herein, are really the correlation between $\ln(x_i)$ and $\ln(x_j)$ and not between x_i and x_j. $\hat{\mu}_y$ is estimated directly by $\overline{y} = \frac{1}{n}\sum_{i=1}^{n} \ln(x_i)$ and $\hat{\sigma_y}^2$ is estimated by $s^2 = \frac{1}{n-1}\sum_{i=1}^{n}(\ln(x_i) - \overline{\ln(x)})^2$. Now all required operations on the joint probability density function can be done with a jointly normal PDF. One needs to take care however, that actual realizations of the JPDF are transformed back to the original coordinate system, $x_i = \exp(y_i)$.

7.2.2 Correlation Dependency on Intensity Level

In this study, 48 different ground motions with differing intensity measures are used for identification of each PSDM. Therefore, the correlation coefficients between responses are calculated across a broad range of intensity measures. One concern however, is the the correlation between responses may change as the intensity of the earthquake changes. An investigation of this requires that a suite of ground motions be selected and scaled to a specific intensity and the correlation between the responses be calculated. This should be repeated for various intensity levels from which correlation trends may be monitored.

A simple investigation of this correlation dependency is carried out for the MSSS Steel girder bridge. A suite of 30 synthetic ground motions is applied to the subject bridge with the bridge component responses being monitored. The ground motions are scaled to specific spectral accelerations {0.2, 0.4, 0.6, 0.8, 1.0, 1.5, 2.0 g} at the fundamental period of the bridge. This results in 30 component responses at each level of spectral acceleration. For illustration purposes, three component responses and their correlations are monitored – fixed bearings (fx), expansion bearings (ex) and columns (col). Figure 7-2 shows the correlations between these three components and how they change with respect to intensity level. The correlation between the expansion bearing and column responses, ρ_{ex-col}, is quite high with values over 0.97 across the entire range of acceleration values, resulting in very little fluctuation. The other two correlation coefficients, ρ_{fx-col} and ρ_{fx-ex}, vary a little more across the acceleration values, showing a general convex-up trend. The trend does not appear to be significant and could partially be attributed to sampling error. Therefore, in this study, constant correlation coefficients across the entire range of intensity levels are

assumed. This assumption significantly reduces the amount of work involved and is not believed to be a major source of error.

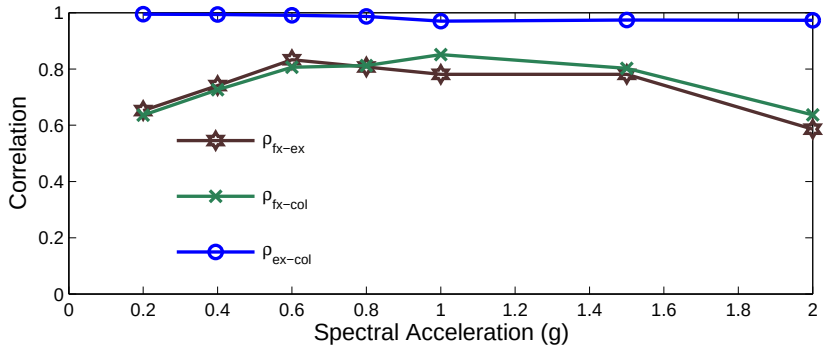

Figure 7-2: Correlation Dependency on Spectral Acceleration.

7.3 Uncertainty in Modeling Parameters

Uncertainty in the seismic demand placed on highway bridges can be classified into two main categories, specifically aleatoric and epistemic. Aleatoric uncertainty is associated with inherent randomness in the system or process and therefore can only be managed and not reduced. Epistemic uncertainty, which is associated with a lack of knowledge, ignorance or course modeling, can generally be reduced with the acquisition of additional information and understanding (Ellingwood and Wen, 2005). It is not always easy to separate out the different sources of uncertainty in a given problem. Traditionally, randomness in seismic ground motions is considered to be aleatoric in nature, however when dealing with synthetic ground motions, the uncertainty built into these ground motions can not only be attributed to seismological mechanisms but also path and site characteristics. More

knowledge pertaining to attenuation relationships and soil effects can reduce some of this uncertainty, thereby alluding to its epistemic nature.

In this study, both the epistemic and aleatoric uncertainties in the seismic loading are considered compositely. This is accomplished through the use of the synthetic ground motion suites presented in Chapter 3. Uncertainty modeling in the structural modeling parameters, discussed in Chapter 6, are addressed specifically in this section.

7.3.1 Material Uncertainties

7.3.1.1 Steel

Concrete and reinforcing steel are a typical materials in the existing bridge structures. They are used in many locations, including the abutments, foundations, decks and bents. In this study, uncertainties in the concrete and reinforcing steel used in the bents are considered explicitly, despite the results in Chapter 6 showing the bridges are not particularly sensitive to them. This is done because they are not difficult to incorporate and they do significantly affect a few of the responses. In a study by Ellingwood and Hwang (1985), they found that the strength of steel for grade 413 (60) reinforcing bars tends to follow a right skewed distribution for which a lognormal distribution is chosen. They found that bars of size 10 to 36 – common sizes in existing bridges – have a mean strength of 463 MPa and a coefficient of variation (COV) of 0.08. Following these findings a two parameter lognormal distribution with parameter values $\lambda = 6.13$ and $\zeta = 0.08$ is used to model the distribution of steel in this study.

7.3.1.2 Concrete

The cast-in-place concrete used in these bridge types typically has a design strength, f_c', of 20.7 MPa at 28 days. Following the assumptions in the study by Choi (2002) the strength of the aged concrete is normally distributed with a mean strength, μ, of 33.8 MPa and a standard deviation, σ, of 4.3 MPa.

7.3.2 Bridge Bearing Uncertainties

As shown in Chapter 6, there are a number of different bearing parameters which affect the responses of the various bridges. These parameters include bearing stiffness, coefficient of friction, dowel strength (concrete bridges only) and dowel gap (concrete bridges only). The following gives a description of the uncertainty models used for these parameters.

7.3.2.1 Steel Bearing Stiffness

There is not adequate information available pertaining to the variability in the stiffnesses of the steel bearings. However, it is recognized that there are any number of different steel type bearings such as high-type fixed or bolster-type. When sufficient information on probability distributions is not available, it is acceptable to assume a uniform distribution with reasonable upper and lower limits to roughly account for uncertainty. Thus, an approximation of the uncertainty in the steel bearing stiffnesses is achieved through the assumption that they are uniformly distributed between 50% and 150% of the published stiffness values provided by Mander et al. (1996).

7.3.2.2 Elastomeric Bearing Stiffness

As previously presented in Equation C.1, the stiffness of elastomeric bearings is a function of the rubber's shear modulus, *G*. As is the case with the steel bearings, information is not readily available pertaining to the variation of the shear modulus for the elastomeric bearings. Therefore, the assumption of uniform distribution is once again used. The AASHTO LRFD Design Specifications indicates that the shear modulus of this bearing material ranges between 0.66 MPa and 2.07 MPa (AASHTO, 1998). Thus these are the uniform distribution parameter values used for this material.

7.3.2.3 Coefficient of Friction for Bearings

One of the key parameters for defining the analytical models for both steel and elastomeric bearings is the coefficient of friction (COF) between the bearings and the concrete bent beam. Using the work by Mander et al. (1996), Dutta (1999) proposed that the COF for the steel bearings could be modeled as lognormal random variables where the median values are given by Mander's models and the lognormal standard deviation, ζ, can be conservatively assumed at 0.5. Furthermore, he proposed that the COF for elastomeric pads also follows a lognormal distribution where the median value is calculated as in Equation C.2 and the lognormal standard deviation is 0.1. A concise presentation of these probability models is presented in Table 7-2.

7.3.2.4 Dowel Strength and Gap

It is reasonable to assume that the overall dowel strength is directly related to the steel strength. Therefore it is assumed that like the steel strength, the dowel strength also follows a lognormal distribution with the same coefficient of variation (COV) of 0.08. Since

Table 7-2: Probability Distributions for Bearing Coefficients of Friction.

Coefficient of Friction – Probability Models				
Bearing Type	**Model Type**	**Median**	λ	ζ
Fixed steel high-type – longitudinal	lognormal	0.21	-1.56	0.5
Fixed steel high-type – transverse	lognormal	0.37	-0.99	0.5
Rocker steel high-type – longitudinal	lognormal	0.04	-3.22	0.5
Rocker steel high-type – transverse	lognormal	0.1	-2.30	0.5
Fixed steel low-type – longitudinal	lognormal	0.2	-1.61	0.5
Fixed steel low-type – transverse	lognormal	0.35	-1.05	0.5
Sliding steel low-type – longitudinal	lognormal	0.37	-0.99	0.5
Sliding steel low-type – transverse	lognormal	0.37	-0.99	0.5
Elastomeric	lognormal	equation C.2	$ln(median)$	0.1

the median strength for each dowel, as previously presented, is given as 58 kN then the lognormal parameter, λ, for a composite of two dowels is equal to 4.75.

The gap between the dowel and the slotted girder is assumed to be uniformly distributed. The parameter values are based on the typical length of the slots which are placed in the bottom of the concrete girders and are calculated to be 0 mm and 50.8 mm.

7.3.3 Uncertainty in Abutment and Foundation Stiffnesses

7.3.3.1 Passive Stiffness of Abutments

Caltrans proposed that the likely range of the passive stiffness of bridge abutments is between 11.5 kN/mm/m and 28.8 kN/mm/m (Caltrans, 1999). It is therefore, assumed as part of this study that the abutment stiffness follows a uniform distribution with these bounds.

7.3.3.2 Active Stiffness of Abutments

As presented in Chapter 6, the active action of the abutments is defined by the stiffness of the piles from which they are built. The assumed stiffness of piles in this study follows the

recommendation of Caltrans giving an initial stiffness of 7 kN/mm/pile. A reasonable assumption which incorporates uncertainty into the value is to assume a uniform distribution with bounds which are 50% and 150% of this recommended value. Thus, the uniformly distributed pile stiffness has bounds of 3.5 kN/mm/pile and 10.5 kN/mm/pile.

7.3.3.3 Translational Foundation Stiffness

The translational stiffness of the column foundations is linearly related to the lateral stiffness of the piles. Therefore, following the uniform distribution assumption given for the piles, the bounds on foundation stiffness for the non-slab multi-span bridges are given as 28 kN/mm and 84 kN/mm. These bounds are different for the slab type bridges because their foundations use fewer piles, thus being 21 kN/mm and 63 kN/mm.

7.3.3.4 Rotational Foundation Stiffness

The rotational stiffness of the foundations is calculated directly from the vertical stiffness of the individual piles. The assumption, as proposed by Choi (2002) and used in this study, is that the expected value for the vertical stiffness of each pile is 175 kN/mm. Once again the distribution is assumed to be uniform with bounds being 50% and 150% of the suggested value. This gives each individual pile a vertical stiffness range of 87.5 kN/mm and 262.5 kN/mm.

7.3.4 Uncertainty in Assorted Modeling Parameters

7.3.4.1 Mass

The variation in the mass of the bridge is assumed to come solely from incidental sources. This is to say, that mass changes due to factors such as span length and column height are treated explicitly elsewhere and are not included here. The sources of variation in the mass

comes from sources such as variable slab thickness, re-pavement procedures and material densities. Therefore it is assumed that the variation in the mass can be accounted for with a uniform distribution which has bounds of 90% and 110% of the mass of the standard bridges. Specific values for the mass bounds are not presented here since mass is different for each bridge type.

7.3.4.2 Damping Ratio

The uncertainty in the damping ratio is modeled using a normal distribution. In a study performed by Fang et al. (1999) on tall buildings, they found that the damping in the structures followed closely a normal distribution, which assumption is extended to this study. The parameters for this distribution are calculated considering the typical range of damping ratios for bridges – 0.02 to 0.07 (Bavirisetty et al., 2000) – represents the 2^{nd} percentile and the 98^{th} percentile. This gives a mean damping ratio of 0.045 and a standard deviation of 0.0125.

7.3.4.3 Internal Hinge Gaps

Following the study by Choi (2002), the internal hinges of the multi-span simply supported bridges are assumed to be normally distributed. The mean values are taken as the gap size of the typical as-built bridges, which is 25.4 mm. The standard deviation is calculated by considering the effects of thermal expansion, giving a value of 4.32 mm for the steel bridges and 3.30 mm for the concrete, box and slab bridges.

7.3.4.4 Abutment - Deck Gaps

As with the internal gaps, the deck-abut gaps are assumed to be normally distributed. Taken from Choi's study (Choi, 2002), the mean and standard deviation for the multi-span simply supported steel bridges is 38.1 mm and 5.84 mm respectively. The MSSS concrete, box and slab bridges have the same mean value of 38.1 mm but have a standard deviation of 1.09 mm. The continuous steel bridges have a mean gap of 76.2 mm with a standard deviation of 24.1 mm while the concrete and slab bridges have a smaller gaps with a mean of 38.1 mm and a standard deviation of 4.32 mm. The mean gap size for the single span bridges is 101.6 mm where the steel bridge has a standard deviation of 4.19 mm and the concrete bridge has a standard deviation of 3.05 mm.

7.3.4.5 Loading Direction

The direction from which the main component of an earthquake strikes a bridge is believed to be significant in determining the response of that bridge. It is recognized that this is a major source of uncertainty in the bridge response. One may legitimately argue, for a bridge in a particular location with a prescribed orientation, that there would be a definite bias in the incident angle of the seismic load. In this study, suites of bridges in many different locations and with many different orientations are being considered. Therefore, for any given suite there is no bias on a particular loading direction. For this reason, it is assumed in this study that the loading direction is a random variable, α, and is uniformly distributed from 0 to 2π radians as measured from the longitudinal axis (refer to Figure 7-3). The range was selected from 0 - 2π because the bridges are only symmetric about the

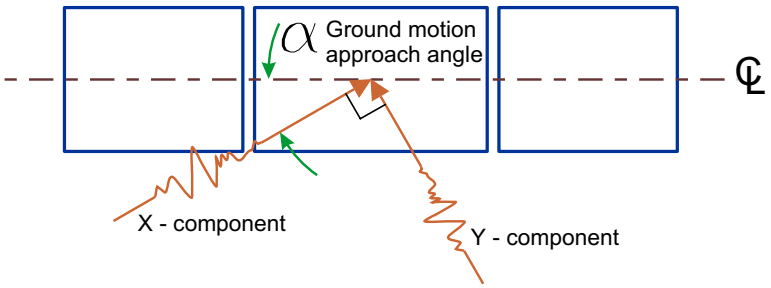

Figure 7-3: Angle of Seismic Loading.

longitudinal axis. The actual impact of this uncertainty is explicitly addressed in Chapter 8.

7.4 PSDMs for Highway Bridges

Probabilistic seismic demand models are generated using the two different suites of 48 ground motions discussed in Chapter 3. The seismic demand model equations are presented in tabular form for the transformed state space. The correlation matrix is also given in tabular format for the transformed state space. As mentioned previously, dealing in the transformed state space simplifies the manipulation of the JPDF.

Because of the very nature of the model formats, specific discussion of the seismic demand models is difficult. Comparisons between bridge types and ground motions suites are best performed using fragility curves. Therefore, in the following sections, the models are presented without an associated discussion.

7.4.1 Multi-Span Continuous Concrete Girder Bridge

As previously stated, 48 bridge models for the MSC Concrete bridge are subjected to two suites of ground motions. These samples of bridge models are representative of the inventory for this particular bridge type. Furthermore, these bridge models are identical for both suites of ground motions. This allows for the comparison of ground motion suites without the added error due to the sampling of structural parameters.

7.4.1.1 Rix and Fernandez-Leon Ground Motions

Table 7-3: PSDMs for MSC Concrete Bridge Components (Rix).

	PGA			S_a **(T = Geometric Mean)**		
Response	**PSDM**	R^2	$\beta_{D\|PGA}$	**PSDM**	R^2	$\beta_{D\|Sa}$
$\ln(\mu_\phi)$	$1.157 * \ln(PGA) + 1.039$	0.76	0.57	$1.173 * \ln(S_a) + 0.240$	0.83	0.48
$\ln(fx_L)$	$1.076 * \ln(PGA) + 4.677$	0.67	0.67	$1.076 * \ln(S_a) + 3.877$	0.69	0.65
$\ln(fx_T)$	$0.577 * \ln(PGA) + 2.703$	0.35	0.69	$0.641 * \ln(S_a) + 2.370$	0.45	0.63
$\ln(ex_L)$	$0.945 * \ln(PGA) + 4.612$	0.76	0.47	$0.924 * \ln(S_a) + 3.879$	0.74	0.50
$\ln(ex_T)$	$0.572 * \ln(PGA) + 2.689$	0.35	0.67	$0.635 * \ln(S_a) + 2.358$	0.46	0.61
$\ln(ab_P)$	$1.230 * \ln(PGA) + 3.622$	0.69	0.73	$1.190 * \ln(S_a) + 2.662$	0.66	0.77
$\ln(ab_A)$	$0.437 * \ln(PGA) + 2.599$	0.21	0.71	$0.440 * \ln(S_a) + 2.295$	0.23	0.71
$\ln(ab_T)$	$0.873 * \ln(PGA) + 2.789$	0.61	0.61	$0.880 * \ln(S_a) + 2.180$	0.65	0.58
	S_a **(T = 0.2 sec)**			S_a **(T = 1.0 sec)**		
Response	**PSDM**	R^2	$\beta_{D\|Sa}$	**PSDM**	R^2	$\beta_{D\|Sa}$
$\ln(\mu_\phi)$	$1.142 * \ln(S_a) + 0.329$	0.72	0.58	$0.780 * \ln(S_a) + 0.001$	0.68	0.66
$\ln(fx_L)$	$1.073 * \ln(S_a) + 4.025$	0.57	0.77	$0.683 * \ln(S_a) + 3.613$	0.52	0.81
$\ln(fx_T)$	$0.642 * \ln(S_a) + 2.454$	0.38	0.67	$0.361 * \ln(S_a) + 2.143$	0.27	0.73
$\ln(ex_L)$	$0.927 * \ln(S_a) + 3.983$	0.59	0.63	$0.635 * \ln(S_a) + 3.726$	0.64	0.59
$\ln(ex_T)$	$0.637 * \ln(S_a) + 2.443$	0.39	0.65	$0.358 * \ln(S_a) + 2.134$	0.27	0.71
$\ln(ab_P)$	$1.246 * \ln(S_a) + 2.900$	0.60	0.83	$0.851 * \ln(S_a) + 2.547$	0.64	0.78
$\ln(ab_A)$	$0.422 * \ln(S_a) + 2.337$	0.17	0.73	$0.325 * \ln(S_a) + 2.248$	0.22	0.71
$\ln(ab_T)$	$0.884 * \ln(S_a) + 2.309$	0.54	0.66	$0.582 * \ln(S_a) + 1.996$	0.53	0.67

Table 7-4: Correlation Matrix for MSC Concrete Bridge Component Responses (Rix).

	$\ln(\mu_\phi)$	$\ln(fx_L)$	$\ln(fx_T)$	$\ln(ex_L)$	$\ln(ex_T)$	$\ln(ab_P)$	$\ln(ab_A)$	$\ln(ab_T)$
$\ln(\mu_\phi)$	1.000	0.933	0.718	0.946	0.722	0.899	0.591	0.761
$\ln(fx_L)$	0.933	1.000	0.671	0.969	0.676	0.864	0.613	0.738
$\ln(fx_T)$	0.718	0.671	1.000	0.703	0.999	0.706	0.219	0.469
$\ln(ex_L)$	0.946	0.969	0.703	1.000	0.705	0.910	0.653	0.717
$\ln(ex_T)$	0.722	0.676	0.999	0.705	1.000	0.711	0.224	0.474
$\ln(ab_P)$	0.899	0.864	0.706	0.910	0.711	1.000	0.573	0.639
$\ln(ab_A)$	0.591	0.613	0.219	0.653	0.224	0.573	1.000	0.761
$\ln(ab_T)$	0.761	0.738	0.469	0.717	0.474	0.639	0.761	1.000

7.4.1.2 *Wen and Wu Ground Motions*

Table 7-5: PSDMs for MSC Concrete Bridge Components (Wen).

	PGA			S_a **(T = Geometric Mean)**		
Response	**PSDM**	R^2	$\beta_{D\|PGA}$	**PSDM**	R^2	$\beta_{D\|Sa}$
$\ln(\mu_\phi)$	$1.324 * \ln(PGA) + 1.162$	0.62	0.70	$0.782 * \ln(S_a) + 0.470$	0.76	0.57
$\ln(fx_L)$	$1.281 * \ln(PGA) + 4.750$	0.71	0.56	$0.676 * \ln(S_a) + 3.962$	0.72	0.55
$\ln(fx_T)$	$0.828 * \ln(PGA) + 3.186$	0.34	0.77	$0.436 * \ln(S_a) + 2.699$	0.34	0.77
$\ln(ex_L)$	$1.077 * \ln(PGA) + 4.478$	0.64	0.56	$0.621 * \ln(S_a) + 3.949$	0.76	0.45
$\ln(ex_T)$	$0.815 * \ln(PGA) + 3.125$	0.36	0.73	$0.417 * \ln(S_a) + 2.576$	0.41	0.63
$\ln(ab_P)$	$1.065 * \ln(PGA) + 2.829$	0.42	0.86	$0.617 * \ln(S_a) + 2.271$	0.57	0.69
$\ln(ab_A)$	$0.637 * \ln(PGA) + 2.766$	0.31	0.65	$0.458 * \ln(S_a) + 2.577$	0.46	0.65
$\ln(ab_T)$	$0.984 * \ln(PGA) + 3.040$	0.48	0.70	$0.571 * \ln(S_a) + 2.511$	0.48	0.76
	S_a **(T = 0.2 sec)**			S_a **(T = 1.0 sec)**		
Response	**PSDM**	R^2	$\beta_{D\|Sa}$	**PSDM**	R^2	$\beta_{D\|Sa}$
$\ln(\mu_\phi)$	$1.181 * \ln(S_a) + 0.274$	0.90	0.37	$0.697 * \ln(S_a) + 1.027$	0.80	0.53
$\ln(fx_L)$	$0.986 * \ln(S_a) + 3.721$	0.86	0.38	$0.600 * \ln(S_a) + 4.406$	0.81	0.45
$\ln(fx_T)$	$0.790 * \ln(S_a) + 2.734$	0.59	0.61	$0.388 * \ln(S_a) + 2.988$	0.39	0.74
$\ln(ex_L)$	$0.863 * \ln(S_a) + 3.677$	0.84	0.35	$0.549 * \ln(S_a) + 4.371$	0.85	0.36
$\ln(ex_T)$	$0.763 * \ln(S_a) + 2.664$	0.60	0.57	$0.400 * \ln(S_a) + 2.984$	0.45	0.67
$\ln(ab_P)$	$0.811 * \ln(S_a) + 1.971$	0.53	0.72	$0.550 * \ln(S_a) + 2.725$	0.58	0.73
$\ln(ab_A)$	$0.589 * \ln(S_a) + 2.382$	0.48	0.56	$0.333 * \ln(S_a) + 2.705$	0.42	0.59
$\ln(ab_T)$	$0.921 * \ln(S_a) + 2.425$	0.67	0.61	$0.484 * \ln(S_a) + 2.860$	0.58	0.63

Table 7-6: Correlation Matrix for MSC Concrete Bridge Component Responses (Wen).

	$\ln(\mu_\phi)$	$\ln(fx_L)$	$\ln(fx_T)$	$\ln(ex_L)$	$\ln(ex_T)$	$\ln(ab_P)$	$\ln(ab_A)$	$\ln(ab_T)$
$\ln(\mu_\phi)$	1.000	0.938	0.752	0.954	0.767	0.822	0.713	0.775
$\ln(fx_L)$	0.938	1.000	0.751	0.981	0.760	0.806	0.685	0.757
$\ln(fx_T)$	0.752	0.751	1.000	0.733	0.981	0.650	0.305	0.451
$\ln(ex_L)$	0.954	0.981	0.733	1.000	0.755	0.864	0.696	0.734
$\ln(ex_T)$	0.767	0.760	0.981	0.755	1.000	0.669	0.312	0.456
$\ln(ab_P)$	0.822	0.806	0.650	0.864	0.669	1.000	0.583	0.556
$\ln(ab_A)$	0.713	0.685	0.305	0.696	0.312	0.583	1.000	0.883
$\ln(ab_T)$	0.775	0.757	0.451	0.734	0.456	0.556	0.883	1.000

7.4.2 Multi-Span Simply Supported Concrete Girder Bridge

7.4.2.1 Rix and Fernandez-Leon Ground Motions

Table 7-7: PSDMs for MSSS Concrete Bridge Components (Rix).

	PGA			**S_a (T = Geometric Mean)**		
Response	**PSDM**	R^2	$\beta_{D\|PGA}$	**PSDM**	R^2	$\beta_{D\|Sa}$
$\ln(\mu_\phi)$	$1.080 * \ln(PGA) + 0.999$	0.82	0.45	$1.145 * \ln(S_a) + 0.338$	0.84	0.43
$\ln(fx_L)$	$1.055 * \ln(PGA) + 4.047$	0.66	0.66	$1.157 * \ln(S_a) + 3.498$	0.67	0.69
$\ln(fx_T)$	$0.295 * \ln(PGA) + 1.900$	0.55	0.23	$0.326 * \ln(S_a) + 1.732$	0.66	0.20
$\ln(ex_L)$	$1.009 * \ln(PGA) + 4.682$	0.76	0.50	$1.025 * \ln(S_a) + 3.990$	0.77	0.49
$\ln(ex_T)$	$0.498 * \ln(PGA) + 2.385$	0.39	0.55	$0.503 * \ln(S_a) + 2.047$	0.38	0.55
$\ln(ab_P)$	$1.174 * \ln(PGA) + 2.899$	0.79	0.53	$1.170 * \ln(S_a) + 2.077$	0.76	0.57
$\ln(ab_A)$	$0.891 * \ln(PGA) + 3.031$	0.68	0.53	$0.903 * \ln(S_a) + 2.371$	0.75	0.45
$\ln(ab_T)$	$1.022 * \ln(PGA) + 2.465$	0.73	0.54	$1.069 * \ln(S_a) + 1.798$	0.79	0.48
	S_a (T = 0.2 sec)			**S_a (T = 1.0 sec)**		
Response	**PSDM**	R^2	$\beta_{D\|Sa}$	**PSDM**	R^2	$\beta_{D\|Sa}$
$\ln(\mu_\phi)$	$1.108 * \ln(S_a) + 0.452$	0.70	0.60	$0.788 * \ln(S_a) + 0.140$	0.79	0.49
$\ln(fx_L)$	$1.098 * \ln(S_a) + 3.544$	0.56	0.79	$0.753 * \ln(S_a) + 3.197$	0.60	0.76
$\ln(fx_T)$	$0.307 * \ln(S_a) + 1.749$	0.52	0.23	$0.195 * \ln(S_a) + 1.625$	0.50	0.24
$\ln(ex_L)$	$1.014 * \ln(S_a) + 4.119$	0.67	0.59	$0.727 * \ln(S_a) + 3.840$	0.77	0.49
$\ln(ex_T)$	$0.511 * \ln(S_a) + 2.124$	0.34	0.57	$0.324 * \ln(S_a) + 1.919$	0.33	0.57
$\ln(ab_P)$	$1.148 * \ln(S_a) + 2.205$	0.66	0.68	$0.811 * \ln(S_a) + 1.877$	0.73	0.60
$\ln(ab_A)$	$0.853 * \ln(S_a) + 2.474$	0.55	0.63	$0.631 * \ln(S_a) + 2.306$	0.59	0.65
$\ln(ab_T)$	$1.091 * \ln(S_a) + 1.976$	0.73	0.55	$0.673 * \ln(S_a) + 1.527$	0.62	0.64

Table 7-8: Correlation Matrix for MSSS Concrete Bridge Component Responses (Rix).

	$\ln(\mu_\phi)$	$\ln(fx_L)$	$\ln(fx_T)$	$\ln(ex_L)$	$\ln(ex_T)$	$\ln(ab_P)$	$\ln(ab_A)$	$\ln(ab_T)$
$\ln(\mu_\phi)$	1.000	0.859	0.631	0.967	0.657	0.946	0.842	0.865
$\ln(fx_L)$	0.859	1.000	0.678	0.855	0.713	0.875	0.648	0.753
$\ln(fx_T)$	0.631	0.678	1.000	0.643	0.978	0.690	0.438	0.630
$\ln(ex_L)$	0.967	0.855	0.643	1.000	0.676	0.926	0.806	0.827
$\ln(ex_T)$	0.657	0.713	0.978	0.676	1.000	0.721	0.416	0.632
$\ln(ab_P)$	0.946	0.875	0.690	0.926	0.721	1.000	0.813	0.858
$\ln(ab_A)$	0.842	0.648	0.438	0.806	0.416	0.813	1.000	0.816
$\ln(ab_T)$	0.865	0.753	0.630	0.827	0.632	0.858	0.816	1.000

7.4.2.2 Wen and Wu Ground Motions

Table 7-9: PSDMs for MSSS Concrete Bridge Components (Wen).

	PGA			**S_a (T = Geometric Mean)**		
Response	**PSDM**	R^2	$\beta_{D\|PGA}$	**PSDM**	R^2	$\beta_{D\|Sa}$
$\ln(\mu_\phi)$	$1.062 * \ln(PGA) + 0.599$	0.56	0.65	$0.665 * \ln(S_a) + 0.154$	0.73	0.51
$\ln(fx_L)$	$1.225 * \ln(PGA) + 4.150$	0.57	0.73	$0.722 * \ln(S_a) + 3.566$	0.63	0.70
$\ln(fx_T)$	$0.847 * \ln(PGA) + 3.217$	0.33	0.82	$0.451 * \ln(S_a) + 2.686$	0.33	0.82
$\ln(ex_L)$	$1.024 * \ln(PGA) + 4.367$	0.64	0.53	$0.617 * \ln(S_a) + 3.914$	0.80	0.40
$\ln(ex_T)$	$0.916 * \ln(PGA) + 3.440$	0.32	0.92	$0.514 * \ln(S_a) + 2.914$	0.35	0.90
$\ln(ab_P)$	$0.974 * \ln(PGA) + 2.386$	0.45	0.73	$0.570 * \ln(S_a) + 1.837$	0.60	0.59
$\ln(ab_A)$	$0.821 * \ln(PGA) + 2.756$	0.41	0.66	$0.490 * \ln(S_a) + 2.339$	0.51	0.61
$\ln(ab_T)$	$0.812 * \ln(PGA) + 2.291$	0.51	0.55	$0.529 * \ln(S_a) + 1.881$	0.56	0.59
	S_a (T = 0.2 sec)			**S_a (T = 1.0 sec)**		
Response	**PSDM**	R^2	$\beta_{D\|Sa}$	**PSDM**	R^2	$\beta_{D\|Sa}$
$\ln(\mu_\phi)$	$0.995 * \ln(S_a) + 0.030$	0.90	0.31	$0.545 * \ln(S_a) + 0.523$	0.73	0.51
$\ln(fx_L)$	$1.037 * \ln(S_a) + 3.384$	0.72	0.61	$0.654 * \ln(S_a) + 4.184$	0.74	0.59
$\ln(fx_T)$	$0.738 * \ln(S_a) + 2.680$	0.47	0.73	$0.391 * \ln(S_a) + 3.001$	0.36	0.80
$\ln(ex_L)$	$0.879 * \ln(S_a) + 3.705$	0.91	0.26	$0.511 * \ln(S_a) + 4.245$	0.80	0.40
$\ln(ex_T)$	$0.860 * \ln(S_a) + 2.928$	0.52	0.77	$0.453 * \ln(S_a) + 3.293$	0.40	0.86
$\ln(ab_P)$	$0.857 * \ln(S_a) + 1.735$	0.75	0.47	$0.524 * \ln(S_a) + 2.352$	0.68	0.56
$\ln(ab_A)$	$0.710 * \ln(S_a) + 2.193$	0.66	0.48	$0.425 * \ln(S_a) + 2.676$	0.57	0.57
$\ln(ab_T)$	$0.789 * \ln(S_a) + 1.805$	0.75	0.43	$0.434 * \ln(S_a) + 2.175$	0.57	0.59

Table 7-10: Correlation Matrix for MSSS Concrete Bridge Component Responses (Wen).

	$\ln(\mu_\phi)$	$\ln(fx_L)$	$\ln(fx_T)$	$\ln(ex_L)$	$\ln(ex_T)$	$\ln(ab_P)$	$\ln(ab_A)$	$\ln(ab_T)$
$\ln(\mu_\phi)$	1.000	0.879	0.707	0.947	0.745	0.918	0.805	0.878
$\ln(fx_L)$	0.879	1.000	0.760	0.895	0.811	0.852	0.622	0.673
$\ln(fx_T)$	0.707	0.760	1.000	0.676	0.954	0.696	0.533	0.628
$\ln(ex_L)$	0.947	0.895	0.676	1.000	0.707	0.912	0.802	0.805
$\ln(ex_T)$	0.745	0.811	0.954	0.707	1.000	0.723	0.585	0.664
$\ln(ab_P)$	0.918	0.852	0.696	0.912	0.723	1.000	0.773	0.793
$\ln(ab_A)$	0.805	0.622	0.533	0.802	0.585	0.773	1.000	0.895
$\ln(ab_T)$	0.878	0.673	0.628	0.805	0.664	0.793	0.895	1.000

7.4.3 Multi-Span Simply Supported Concrete Box-Girder Bridge

7.4.3.1 Rix and Fernandez-Leon Ground Motions

Table 7-11: PSDMs for MSSS Concrete-Box Bridge Components (Rix).

	PGA			S_a **(T = Geometric Mean)**		
Response	**PSDM**	R^2	$\beta_{D\|PGA}$	**PSDM**	R^2	$\beta_{D\|Sa}$
$\ln(\mu_\phi)$	$1.001 * \ln(PGA) + 0.398$	0.70	0.57	$1.179 * \ln(S_a) + 0.086$	0.86	0.40
$\ln(fx_L)$	$0.899 * \ln(PGA) + 2.058$	0.76	0.44	$1.054 * \ln(S_a) + 1.795$	0.77	0.46
$\ln(fx_T)$	$1.018 * \ln(PGA) + 1.450$	0.65	0.66	$1.153 * \ln(S_a) + 1.047$	0.72	0.58
$\ln(ex_L)$	$1.159 * \ln(PGA) + 2.760$	0.71	0.65	$1.304 * \ln(S_a) + 2.290$	0.78	0.57
$\ln(ex_T)$	$1.017 * \ln(PGA) + 1.451$	0.65	0.66	$1.165 * \ln(S_a) + 1.098$	0.76	0.55
$\ln(ab_P)$	$0.866 * \ln(PGA) + 2.539$	0.77	0.41	$0.970 * \ln(S_a) + 2.184$	0.85	0.34
$\ln(ab_A)$	$0.992 * \ln(PGA) + 3.485$	0.75	0.50	$1.181 * \ln(S_a) + 3.195$	0.85	0.41
$\ln(ab_T)$	$0.848 * \ln(PGA) + 2.529$	0.67	0.52	$0.993 * \ln(S_a) + 2.210$	0.82	0.38
	S_a **(T = 0.2 sec)**			S_a **(T = 1.0 sec)**		
Response	**PSDM**	R^2	$\beta_{D\|Sa}$	**PSDM**	R^2	$\beta_{D\|Sa}$
$\ln(\mu_\phi)$	$1.141 * \ln(S_a) + 0.036$	0.80	0.47	$0.659 * \ln(S_a) + -0.521$	0.60	0.67
$\ln(fx_L)$	$1.001 * \ln(S_a) + 1.720$	0.72	0.51	$0.588 * \ln(S_a) + 1.219$	0.65	0.54
$\ln(fx_T)$	$1.093 * \ln(S_a) + 0.971$	0.65	0.65	$0.676 * \ln(S_a) + 0.523$	0.56	0.73
$\ln(ex_L)$	$1.250 * \ln(S_a) + 2.220$	0.72	0.64	$0.752 * \ln(S_a) + 1.679$	0.58	0.78
$\ln(ex_T)$	$1.092 * \ln(S_a) + 0.971$	0.65	0.65	$0.674 * \ln(S_a) + 0.524$	0.56	0.74
$\ln(ab_P)$	$0.995 * \ln(S_a) + 2.192$	0.85	0.33	$0.569 * \ln(S_a) + 1.742$	0.65	0.51
$\ln(ab_A)$	$1.187 * \ln(S_a) + 3.227$	0.83	0.44	$0.659 * \ln(S_a) + 2.612$	0.59	0.67
$\ln(ab_T)$	$0.967 * \ln(S_a) + 2.199$	0.76	0.44	$0.539 * \ln(S_a) + 1.724$	0.53	0.62

Table 7-12: Correlations for MSSS Concrete-Box Bridge Component Responses (Rix).

	$\ln(\mu_\phi)$	$\ln(fx_L)$	$\ln(fx_T)$	$\ln(ex_L)$	$\ln(ex_T)$	$\ln(ab_P)$	$\ln(ab_A)$	$\ln(ab_T)$
$\ln(\mu_\phi)$	1.000	0.913	0.950	0.895	0.950	0.885	0.890	0.932
$\ln(fx_L)$	0.913	1.000	0.899	0.943	0.897	0.873	0.923	0.861
$\ln(fx_T)$	0.950	0.899	1.000	0.900	0.999	0.830	0.861	0.866
$\ln(ex_L)$	0.895	0.943	0.900	1.000	0.901	0.856	0.944	0.840
$\ln(ex_T)$	0.950	0.897	0.999	0.901	1.000	0.832	0.860	0.863
$\ln(ab_P)$	0.885	0.873	0.830	0.856	0.832	1.000	0.943	0.880
$\ln(ab_A)$	0.890	0.923	0.861	0.944	0.860	0.943	1.000	0.898
$\ln(ab_T)$	0.932	0.861	0.866	0.840	0.863	0.880	0.898	1.000

7.4.3.2 *Wen and Wu Ground Motions*

Table 7-13: PSDMs for MSSS Concrete-Box Bridge Components (Wen).

	PGA			S_a **(T = Geometric Mean)**		
Response	**PSDM**	R^2	$\beta_{D\|PGA}$	**PSDM**	R^2	$\beta_{D\|Sa}$
$\ln(\mu_\phi)$	$0.899 * \ln(PGA) + 0.382$	0.61	0.49	$0.633 * \ln(S_a) + -0.285$	0.70	0.41
$\ln(fx_L)$	$0.694 * \ln(PGA) + 2.106$	0.47	0.50	$0.461 * \ln(S_a) + 1.536$	0.42	0.53
$\ln(fx_T)$	$0.692 * \ln(PGA) + 1.083$	0.34	0.66	$0.439 * \ln(S_a) + 0.489$	0.28	0.68
$\ln(ex_L)$	$1.113 * \ln(PGA) + 3.047$	0.58	0.65	$0.787 * \ln(S_a) + 2.226$	0.57	0.67
$\ln(ex_T)$	$0.666 * \ln(PGA) + 1.078$	0.36	0.61	$0.424 * \ln(S_a) + 0.512$	0.30	0.64
$\ln(ab_P)$	$0.672 * \ln(PGA) + 2.474$	0.62	0.36	$0.443 * \ln(S_a) + 1.894$	0.55	0.39
$\ln(ab_A)$	$1.062 * \ln(PGA) + 3.952$	0.68	0.50	$0.731 * \ln(S_a) + 3.109$	0.63	0.54
$\ln(ab_T)$	$0.933 * \ln(PGA) + 2.823$	0.62	0.49	$0.600 * \ln(S_a) + 2.064$	0.60	0.48
	S_a **(T = 0.2 sec)**			S_a **(T = 1.0 sec)**		
Response	**PSDM**	R^2	$\beta_{D\|Sa}$	**PSDM**	R^2	$\beta_{D\|Sa}$
$\ln(\mu_\phi)$	$0.683 * \ln(S_a) + -0.279$	0.75	0.37	$0.378 * \ln(S_a) + 0.075$	0.63	0.45
$\ln(fx_L)$	$0.536 * \ln(S_a) + 1.585$	0.53	0.47	$0.284 * \ln(S_a) + 1.822$	0.41	0.53
$\ln(fx_T)$	$0.535 * \ln(S_a) + 0.563$	0.39	0.63	$0.290 * \ln(S_a) + 0.818$	0.31	0.67
$\ln(ex_L)$	$0.895 * \ln(S_a) + 2.288$	0.68	0.57	$0.473 * \ln(S_a) + 2.680$	0.52	0.71
$\ln(ex_T)$	$0.528 * \ln(S_a) + 0.557$	0.38	0.63	$0.286 * \ln(S_a) + 0.810$	0.31	0.67
$\ln(ab_P)$	$0.477 * \ln(S_a) + 1.899$	0.60	0.37	$0.258 * \ln(S_a) + 2.149$	0.51	0.39
$\ln(ab_A)$	$0.816 * \ln(S_a) + 3.149$	0.73	0.46	$0.432 * \ln(S_a) + 3.510$	0.56	0.59
$\ln(ab_T)$	$0.646 * \ln(S_a) + 2.068$	0.64	0.46	$0.349 * \ln(S_a) + 2.347$	0.58	0.46

Table 7-14: Correlations for MSSS Concrete-Box Bridge Component Responses (Wen).

	$\ln(\mu_\phi)$	$\ln(fx_L)$	$\ln(fx_T)$	$\ln(ex_L)$	$\ln(ex_T)$	$\ln(ab_P)$	$\ln(ab_A)$	$\ln(ab_T)$
$\ln(\mu_\phi)$	1.000	0.846	0.838	0.874	0.842	0.835	0.883	0.853
$\ln(fx_L)$	0.846	1.000	0.824	0.930	0.823	0.821	0.869	0.735
$\ln(fx_T)$	0.838	0.824	1.000	0.806	0.998	0.606	0.698	0.669
$\ln(ex_L)$	0.874	0.930	0.806	1.000	0.799	0.838	0.929	0.764
$\ln(ex_T)$	0.842	0.823	0.998	0.799	1.000	0.606	0.697	0.678
$\ln(ab_P)$	0.835	0.821	0.606	0.838	0.606	1.000	0.927	0.766
$\ln(ab_A)$	0.883	0.869	0.698	0.929	0.697	0.927	1.000	0.833
$\ln(ab_T)$	0.853	0.735	0.669	0.764	0.678	0.766	0.833	1.000

7.4.4 Multi-Span Continuous Slab Bridge

7.4.4.1 Rix and Fernandez-Leon Ground Motions

Table 7-15: PSDMs for MSC Slab Bridge Components (Rix).

	PGA			S_a **(T = Geometric Mean)**		
Response	**PSDM**	R^2	$\beta_{D\|PGA}$	**PSDM**	R^2	$\beta_{D\|Sa}$
$\ln(\mu_\phi)$	$1.087 * \ln(PGA) + 0.153$	0.73	0.58	$1.250 * \ln(S_a) + -0.260$	0.73	0.63
$\ln(fx_L)$	$0.845 * \ln(PGA) + 1.892$	0.49	0.76	$1.023 * \ln(S_a) + 1.652$	0.56	0.76
$\ln(fx_T)$	$0.773 * \ln(PGA) + 0.958$	0.51	0.67	$0.888 * \ln(S_a) + 0.590$	0.63	0.57
$\ln(ex_L)$	$1.017 * \ln(PGA) + 2.295$	0.58	0.76	$1.119 * \ln(S_a) + 1.803$	0.63	0.71
$\ln(ex_T)$	$0.774 * \ln(PGA) + 0.960$	0.51	0.67	$0.889 * \ln(S_a) + 0.592$	0.63	0.57
$\ln(ab_P)$	$0.793 * \ln(PGA) + 2.491$	0.64	0.52	$0.913 * \ln(S_a) + 2.149$	0.79	0.39
$\ln(ab_A)$	$0.953 * \ln(PGA) + 3.220$	0.61	0.66	$1.084 * \ln(S_a) + 2.792$	0.73	0.55
$\ln(ab_T)$	$1.102 * \ln(PGA) + 3.743$	0.79	0.49	$1.248 * \ln(S_a) + 3.294$	0.79	0.53
	S_a **(T = 0.2 sec)**			S_a **(T = 1.0 sec)**		
Response	**PSDM**	R^2	$\beta_{D\|Sa}$	**PSDM**	R^2	$\beta_{D\|Sa}$
$\ln(\mu_\phi)$	$1.207 * \ln(S_a) + -0.262$	0.65	0.72	$0.685 * \ln(S_a) + -0.899$	0.57	0.72
$\ln(fx_L)$	$1.003 * \ln(S_a) + 1.671$	0.51	0.80	$0.565 * \ln(S_a) + 1.177$	0.37	0.91
$\ln(fx_T)$	$0.840 * \ln(S_a) + 0.605$	0.52	0.66	$0.493 * \ln(S_a) + 0.226$	0.48	0.61
$\ln(ex_L)$	$1.099 * \ln(S_a) + 1.826$	0.58	0.76	$0.622 * \ln(S_a) + 1.288$	0.43	0.89
$\ln(ex_T)$	$0.841 * \ln(S_a) + 0.607$	0.52	0.66	$0.494 * \ln(S_a) + 0.228$	0.49	0.61
$\ln(ab_P)$	$0.899 * \ln(S_a) + 2.170$	0.73	0.45	$0.485 * \ln(S_a) + 1.706$	0.47	0.63
$\ln(ab_A)$	$1.072 * \ln(S_a) + 2.823$	0.69	0.59	$0.591 * \ln(S_a) + 2.287$	0.46	0.78
$\ln(ab_T)$	$1.155 * \ln(S_a) + 3.184$	0.76	0.52	$0.727 * \ln(S_a) + 2.725$	0.68	0.60

Table 7-16: Correlation Matrix for MSC Slab Bridge Component Responses (Rix).

	$\ln(\mu_\phi)$	$\ln(fx_L)$	$\ln(fx_T)$	$\ln(ex_L)$	$\ln(ex_T)$	$\ln(ab_P)$	$\ln(ab_A)$	$\ln(ab_T)$
$\ln(\mu_\phi)$	1.000	0.799	0.748	0.794	0.748	0.870	0.862	0.955
$\ln(fx_L)$	0.799	1.000	0.824	0.925	0.823	0.864	0.935	0.774
$\ln(fx_T)$	0.748	0.824	1.000	0.793	1.000	0.722	0.738	0.765
$\ln(ex_L)$	0.794	0.925	0.793	1.000	0.793	0.875	0.943	0.796
$\ln(ex_T)$	0.748	0.823	1.000	0.793	1.000	0.722	0.737	0.765
$\ln(ab_P)$	0.870	0.864	0.722	0.875	0.722	1.000	0.966	0.840
$\ln(ab_A)$	0.862	0.935	0.738	0.943	0.737	0.966	1.000	0.846
$\ln(ab_T)$	0.955	0.774	0.765	0.796	0.765	0.840	0.846	1.000

7.4.4.2 *Wen and Wu Ground Motions*

Table 7-17: PSDMs for MSC Slab Bridge Components (Wen).

	PGA			S_a **(T = Geometric Mean)**		
Response	**PSDM**	R^2	$\beta_{D\|PGA}$	**PSDM**	R^2	$\beta_{D\|Sa}$
$\ln(\mu_\phi)$	$1.386 * \ln(PGA) + 1.009$	0.60	0.78	$1.056 * \ln(S_a) + 0.053$	0.72	0.67
$\ln(fx_L)$	$1.445 * \ln(PGA) + 3.487$	0.61	0.79	$0.989 * \ln(S_a) + 2.397$	0.62	0.78
$\ln(fx_T)$	$0.717 * \ln(PGA) + 1.043$	0.45	0.54	$0.477 * \ln(S_a) + 0.421$	0.45	0.54
$\ln(ex_L)$	$1.638 * \ln(PGA) + 3.970$	0.63	0.85	$1.140 * \ln(S_a) + 2.753$	0.66	0.83
$\ln(ex_T)$	$0.716 * \ln(PGA) + 1.042$	0.45	0.54	$0.476 * \ln(S_a) + 0.421$	0.45	0.54
$\ln(ab_P)$	$0.882 * \ln(PGA) + 2.972$	0.55	0.54	$0.618 * \ln(S_a) + 2.358$	0.59	0.52
$\ln(ab_A)$	$1.487 * \ln(PGA) + 4.635$	0.67	0.71	$1.022 * \ln(S_a) + 3.525$	0.70	0.68
$\ln(ab_T)$	$1.154 * \ln(PGA) + 4.120$	0.63	0.60	$0.838 * \ln(S_a) + 3.313$	0.73	0.52
	S_a **(T = 0.2 sec)**			S_a **(T = 1.0 sec)**		
Response	**PSDM**	R^2	$\beta_{D\|Sa}$	**PSDM**	R^2	$\beta_{D\|Sa}$
$\ln(\mu_\phi)$	$1.163 * \ln(S_a) + 0.019$	0.76	0.61	$0.631 * \ln(S_a) + 0.577$	0.61	0.78
$\ln(fx_L)$	$1.087 * \ln(S_a) + 2.363$	0.66	0.74	$0.634 * \ln(S_a) + 2.961$	0.60	0.81
$\ln(fx_T)$	$0.537 * \ln(S_a) + 0.453$	0.47	0.54	$0.303 * \ln(S_a) + 0.743$	0.41	0.57
$\ln(ex_L)$	$1.279 * \ln(S_a) + 2.743$	0.73	0.73	$0.700 * \ln(S_a) + 3.322$	0.59	0.91
$\ln(ex_T)$	$0.536 * \ln(S_a) + 0.453$	0.47	0.54	$0.302 * \ln(S_a) + 0.743$	0.40	0.57
$\ln(ab_P)$	$0.694 * \ln(S_a) + 2.353$	0.66	0.47	$0.400 * \ln(S_a) + 2.723$	0.59	0.52
$\ln(ab_A)$	$1.129 * \ln(S_a) + 3.496$	0.75	0.61	$0.638 * \ln(S_a) + 4.066$	0.65	0.73
$\ln(ab_T)$	$0.932 * \ln(S_a) + 3.290$	0.79	0.45	$0.544 * \ln(S_a) + 3.860$	0.73	0.51

Table 7-18: Correlation Matrix for MSC Slab Bridge Component Responses (Wen).

	$\ln(\mu_\phi)$	$\ln(fx_L)$	$\ln(fx_T)$	$\ln(ex_L)$	$\ln(ex_T)$	$\ln(ab_P)$	$\ln(ab_A)$	$\ln(ab_T)$
$\ln(\mu_\phi)$	1.000	0.908	0.795	0.912	0.794	0.875	0.937	0.944
$\ln(fx_L)$	0.908	1.000	0.803	0.917	0.802	0.878	0.955	0.890
$\ln(fx_T)$	0.795	0.803	1.000	0.836	1.000	0.742	0.779	0.820
$\ln(ex_L)$	0.912	0.917	0.836	1.000	0.836	0.897	0.969	0.900
$\ln(ex_T)$	0.794	0.802	1.000	0.836	1.000	0.742	0.778	0.819
$\ln(ab_P)$	0.875	0.878	0.742	0.897	0.742	1.000	0.949	0.879
$\ln(ab_A)$	0.937	0.955	0.779	0.969	0.778	0.949	1.000	0.923
$\ln(ab_T)$	0.944	0.890	0.820	0.900	0.819	0.879	0.923	1.000

7.4.5 Multi-Span Simply Supported Slab Bridge

7.4.5.1 Rix and Fernandez-Leon Ground Motions

Table 7-19: PSDMs for MSSS Slab Bridge Components (Rix).

	PGA			**S_a (T = Geometric Mean)**		
Response	**PSDM**	R^2	$\beta_{D\|PGA}$	**PSDM**	R^2	$\beta_{D\|Sa}$
$\ln(\mu_\phi)$	$1.098 * \ln(PGA) + 0.683$	0.72	0.59	$1.170 * \ln(S_a) + 0.112$	0.76	0.55
$\ln(fx_L)$	$0.744 * \ln(PGA) + 1.864$	0.53	0.61	$0.941 * \ln(S_a) + 1.706$	0.67	0.56
$\ln(fx_T)$	$0.760 * \ln(PGA) + 0.767$	0.62	0.53	$0.763 * \ln(S_a) + 0.289$	0.64	0.48
$\ln(ex_L)$	$0.962 * \ln(PGA) + 2.464$	0.52	0.81	$1.111 * \ln(S_a) + 2.077$	0.63	0.71
$\ln(ex_T)$	$0.763 * \ln(PGA) + 0.766$	0.61	0.53	$0.772 * \ln(S_a) + 0.295$	0.63	0.49
$\ln(ab_P)$	$0.716 * \ln(PGA) + 2.345$	0.68	0.43	$0.820 * \ln(S_a) + 2.047$	0.81	0.34
$\ln(ab_A)$	$0.837 * \ln(PGA) + 3.293$	0.68	0.51	$0.981 * \ln(S_a) + 2.937$	0.81	0.40
$\ln(ab_T)$	$1.197 * \ln(PGA) + 3.866$	0.69	0.71	$1.221 * \ln(S_a) + 3.140$	0.73	0.62
	S_a (T = 0.2 sec)			**S_a (T = 1.0 sec)**		
Response	**PSDM**	R^2	$\beta_{D\|Sa}$	**PSDM**	R^2	$\beta_{D\|Sa}$
$\ln(\mu_\phi)$	$1.163 * \ln(S_a) + 0.134$	0.72	0.59	$0.769 * \ln(S_a) + -0.187$	0.64	0.71
$\ln(fx_L)$	$0.934 * \ln(S_a) + 1.722$	0.63	0.58	$0.513 * \ln(S_a) + 1.255$	0.41	0.76
$\ln(fx_T)$	$0.742 * \ln(S_a) + 0.282$	0.58	0.52	$0.467 * \ln(S_a) + 0.022$	0.45	0.63
$\ln(ex_L)$	$1.045 * \ln(S_a) + 1.985$	0.59	0.71	$0.616 * \ln(S_a) + 1.558$	0.42	0.90
$\ln(ex_T)$	$0.754 * \ln(S_a) + 0.293$	0.58	0.52	$0.474 * \ln(S_a) + 0.025$	0.46	0.63
$\ln(ab_P)$	$0.816 * \ln(S_a) + 2.066$	0.77	0.37	$0.420 * \ln(S_a) + 1.676$	0.56	0.46
$\ln(ab_A)$	$0.979 * \ln(S_a) + 2.961$	0.78	0.43	$0.577 * \ln(S_a) + 2.603$	0.55	0.65
$\ln(ab_T)$	$1.192 * \ln(S_a) + 3.135$	0.67	0.68	$0.796 * \ln(S_a) + 2.776$	0.60	0.81

Table 7-20: Correlation Matrix MSSS Slab Bridge Component Responses (Rix).

	$\ln(\mu_\phi)$	$\ln(fx_L)$	$\ln(fx_T)$	$\ln(ex_L)$	$\ln(ex_T)$	$\ln(ab_P)$	$\ln(ab_A)$	$\ln(ab_T)$
$\ln(\mu_\phi)$	1.000	0.887	0.924	0.867	0.924	0.882	0.901	0.931
$\ln(fx_L)$	0.887	1.000	0.921	0.941	0.925	0.914	0.956	0.803
$\ln(fx_T)$	0.924	0.921	1.000	0.886	0.998	0.875	0.881	0.812
$\ln(ex_L)$	0.867	0.941	0.886	1.000	0.893	0.891	0.951	0.759
$\ln(ex_T)$	0.924	0.925	0.998	0.893	1.000	0.878	0.883	0.805
$\ln(ab_P)$	0.882	0.914	0.875	0.891	0.878	1.000	0.955	0.815
$\ln(ab_A)$	0.901	0.956	0.881	0.951	0.883	0.955	1.000	0.833
$\ln(ab_T)$	0.931	0.803	0.812	0.759	0.805	0.815	0.833	1.000

7.4.5.2 Wen and Wu Ground Motions

Table 7-21: PSDMs for MSSS Slab Bridge Components (Wen).

	PGA			S_a **(T = Geometric Mean)**		
Response	**PSDM**	R^2	$\beta_{D\|PGA}$	**PSDM**	R^2	$\beta_{D\|Sa}$
$\ln(\mu_\phi)$	$1.268 * \ln(PGA) + 0.931$	0.70	0.56	$0.935 * \ln(S_a) + 0.026$	0.80	0.46
$\ln(fx_L)$	$1.102 * \ln(PGA) + 2.693$	0.69	0.50	$0.680 * \ln(S_a) + 1.808$	0.52	0.68
$\ln(fx_T)$	$1.129 * \ln(PGA) + 1.319$	0.73	0.47	$0.686 * \ln(S_a) + 0.423$	0.62	0.56
$\ln(ex_L)$	$1.602 * \ln(PGA) + 3.736$	0.72	0.68	$1.089 * \ln(S_a) + 2.562$	0.68	0.74
$\ln(ex_T)$	$1.105 * \ln(PGA) + 1.262$	0.71	0.48	$0.678 * \ln(S_a) + 0.395$	0.61	0.56
$\ln(ab_P)$	$0.741 * \ln(PGA) + 2.623$	0.61	0.40	$0.390 * \ln(S_a) + 1.972$	0.46	0.43
$\ln(ab_A)$	$1.051 * \ln(PGA) + 4.018$	0.60	0.58	$0.673 * \ln(S_a) + 3.238$	0.50	0.70
$\ln(ab_T)$	$0.967 * \ln(PGA) + 3.258$	0.56	0.58	$0.687 * \ln(S_a) + 2.600$	0.65	0.52
	S_a **(T = 0.2 sec)**			S_a **(T = 1.0 sec)**		
Response	**PSDM**	R^2	$\beta_{D\|Sa}$	**PSDM**	R^2	$\beta_{D\|Sa}$
$\ln(\mu_\phi)$	$0.949 * \ln(S_a) + -0.120$	0.84	0.38	$0.545 * \ln(S_a) + 0.418$	0.76	0.47
$\ln(fx_L)$	$0.714 * \ln(S_a) + 1.644$	0.64	0.49	$0.376 * \ln(S_a) + 1.941$	0.49	0.58
$\ln(fx_T)$	$0.841 * \ln(S_a) + 0.464$	0.76	0.45	$0.481 * \ln(S_a) + 0.908$	0.69	0.51
$\ln(ex_L)$	$1.253 * \ln(S_a) + 2.631$	0.78	0.61	$0.627 * \ln(S_a) + 3.037$	0.56	0.86
$\ln(ex_T)$	$0.834 * \ln(S_a) + 0.439$	0.75	0.45	$0.472 * \ln(S_a) + 0.863$	0.67	0.51
$\ln(ab_P)$	$0.491 * \ln(S_a) + 2.005$	0.60	0.37	$0.298 * \ln(S_a) + 2.302$	0.51	0.45
$\ln(ab_A)$	$0.828 * \ln(S_a) + 3.281$	0.67	0.53	$0.408 * \ln(S_a) + 3.518$	0.47	0.66
$\ln(ab_T)$	$0.810 * \ln(S_a) + 2.602$	0.75	0.44	$0.475 * \ln(S_a) + 3.090$	0.70	0.47

Table 7-22: Correlation Matrix for MSSS Slab Bridge Component Responses (Wen).

	$\ln(\mu_\phi)$	$\ln(fx_L)$	$\ln(fx_T)$	$\ln(ex_L)$	$\ln(ex_T)$	$\ln(ab_P)$	$\ln(ab_A)$	$\ln(ab_T)$
$\ln(\mu_\phi)$	1.000	0.868	0.926	0.908	0.926	0.835	0.865	0.886
$\ln(fx_L)$	0.868	1.000	0.882	0.931	0.874	0.898	0.949	0.753
$\ln(fx_T)$	0.926	0.882	1.000	0.915	0.997	0.813	0.828	0.782
$\ln(ex_L)$	0.908	0.931	0.915	1.000	0.906	0.872	0.940	0.778
$\ln(ex_T)$	0.926	0.874	0.997	0.906	1.000	0.802	0.812	0.780
$\ln(ab_P)$	0.835	0.898	0.813	0.872	0.802	1.000	0.927	0.815
$\ln(ab_A)$	0.865	0.949	0.828	0.940	0.812	0.927	1.000	0.795
$\ln(ab_T)$	0.886	0.753	0.782	0.778	0.780	0.815	0.795	1.000

7.4.6 Multi-Span Continuous Steel Girder Bridge

7.4.6.1 Rix and Fernandez-Leon Ground Motions

Table 7-23: PSDMs for MSC Steel Bridge Components (Rix).

	PGA			S_a **(T = Geometric Mean)**		
Response	**PSDM**	R^2	$\beta_{D\|PGA}$	**PSDM**	R^2	$\beta_{D\|Sa}$
$\ln(\mu_\phi)$	$1.754 * \ln(PGA) + 2.962$	0.86	0.63	$1.620 * \ln(S_a) + 1.596$	0.78	0.78
$\ln(fx_L)$	$1.400 * \ln(PGA) + 2.022$	0.61	0.98	$1.343 * \ln(S_a) + 0.989$	0.60	1.00
$\ln(fx_T)$	$1.502 * \ln(PGA) + 2.401$	0.58	1.12	$1.725 * \ln(S_a) + 1.635$	0.76	0.87
$\ln(ex_L)$	$1.396 * \ln(PGA) + 6.116$	0.85	0.51	$1.210 * \ln(S_a) + 4.938$	0.68	0.75
$\ln(ex_T)$	$1.804 * \ln(PGA) + 4.367$	0.70	1.03	$1.875 * \ln(S_a) + 3.204$	0.81	0.82
$\ln(ab_P)$	$2.524 * \ln(PGA) + 4.784$	0.62	1.73	$2.174 * \ln(S_a) + 2.640$	0.49	2.01
$\ln(ab_A)$	$0.696 * \ln(PGA) + 0.680$	0.46	0.66	$0.562 * \ln(S_a) + 0.086$	0.38	0.64
$\ln(ab_T)$	$0.939 * \ln(PGA) + 2.583$	0.71	0.53	$0.964 * \ln(S_a) + 1.979$	0.78	0.46
	S_a **(T = 0.2 sec)**			S_a **(T = 1.0 sec)**		
Response	**PSDM**	R^2	$\beta_{D\|Sa}$	**PSDM**	R^2	$\beta_{D\|Sa}$
$\ln(\mu_\phi)$	$1.761 * \ln(S_a) + 1.981$	0.75	0.82	$1.250 * \ln(S_a) + 1.481$	0.85	0.64
$\ln(fx_L)$	$1.449 * \ln(S_a) + 1.295$	0.57	1.03	$1.025 * \ln(S_a) + 0.879$	0.64	0.94
$\ln(fx_T)$	$1.589 * \ln(S_a) + 1.671$	0.56	1.15	$0.986 * \ln(S_a) + 1.013$	0.49	1.23
$\ln(ex_L)$	$1.405 * \ln(S_a) + 5.339$	0.75	0.66	$1.029 * \ln(S_a) + 4.984$	0.91	0.40
$\ln(ex_T)$	$1.899 * \ln(S_a) + 3.469$	0.68	1.06	$1.203 * \ln(S_a) + 2.726$	0.62	1.17
$\ln(ab_P)$	$2.577 * \ln(S_a) + 3.426$	0.56	1.86	$1.901 * \ln(S_a) + 2.793$	0.69	1.57
$\ln(ab_A)$	$0.769 * \ln(S_a) + 0.335$	0.48	0.64	$0.632 * \ln(S_a) + 0.202$	0.72	0.48
$\ln(ab_T)$	$1.036 * \ln(S_a) + 2.170$	0.75	0.50	$0.663 * \ln(S_a) + 1.771$	0.68	0.56

Table 7-24: Correlation Matrix for MSC Steel Bridge Component Responses (Rix).

	$\ln(\mu_\phi)$	$\ln(fx_L)$	$\ln(fx_T)$	$\ln(ex_L)$	$\ln(ex_T)$	$\ln(ab_P)$	$\ln(ab_A)$	$\ln(ab_T)$
$\ln(\mu_\phi)$	1.000	0.813	0.811	0.957	0.870	0.862	0.772	0.829
$\ln(fx_L)$	0.813	1.000	0.710	0.805	0.683	0.669	0.609	0.649
$\ln(fx_T)$	0.811	0.710	1.000	0.726	0.900	0.730	0.677	0.841
$\ln(ex_L)$	0.957	0.805	0.726	1.000	0.804	0.856	0.767	0.793
$\ln(ex_T)$	0.870	0.683	0.900	0.804	1.000	0.757	0.652	0.844
$\ln(ab_P)$	0.862	0.669	0.730	0.856	0.757	1.000	0.784	0.737
$\ln(ab_A)$	0.772	0.609	0.677	0.767	0.652	0.784	1.000	0.805
$\ln(ab_T)$	0.829	0.649	0.841	0.793	0.844	0.737	0.805	1.000

7.4.6.2 *Wen and Wu Ground Motions*

Table 7-25: PSDMs for MSC Steel Bridge Components (Wen).

	PGA			S_a **(T = Geometric Mean)**		
Response	**PSDM**	R^2	$\beta_{D\|PGA}$	**PSDM**	R^2	$\beta_{D\|Sa}$
$\ln(\mu_\phi)$	$1.932 * \ln(PGA) + 2.246$	0.73	0.81	$1.053 * \ln(S_a) + 0.842$	0.76	0.76
$\ln(fx_L)$	$1.888 * \ln(PGA) + 2.308$	0.60	1.06	$0.956 * \ln(S_a) + 0.771$	0.55	1.11
$\ln(fx_T)$	$1.802 * \ln(PGA) + 2.730$	0.53	1.16	$0.828 * \ln(S_a) + 1.060$	0.46	1.17
$\ln(ex_L)$	$1.599 * \ln(PGA) + 5.510$	0.68	0.75	$0.937 * \ln(S_a) + 4.457$	0.81	0.58
$\ln(ex_T)$	$1.738 * \ln(PGA) + 3.720$	0.61	0.95	$0.973 * \ln(S_a) + 2.587$	0.58	1.08
$\ln(ab_P)$	$2.356 * \ln(PGA) + 3.112$	0.47	1.73	$1.366 * \ln(S_a) + 1.578$	0.52	1.68
$\ln(ab_A)$	$0.608 * \ln(PGA) + 0.165$	0.27	0.69	$0.301 * \ln(S_a) + -0.341$	0.24	0.70
$\ln(ab_T)$	$0.873 * \ln(PGA) + 2.376$	0.52	0.57	$0.429 * \ln(S_a) + 1.646$	0.44	0.61
	S_a **(T = 0.2 sec)**			S_a **(T = 1.0 sec)**		
Response	**PSDM**	R^2	$\beta_{D\|Sa}$	**PSDM**	R^2	$\beta_{D\|Sa}$
$\ln(\mu_\phi)$	$1.500 * \ln(S_a) + 0.819$	0.87	0.55	$0.939 * \ln(S_a) + 1.938$	0.87	0.57
$\ln(fx_L)$	$1.424 * \ln(S_a) + 0.852$	0.65	0.99	$0.915 * \ln(S_a) + 1.947$	0.73	0.87
$\ln(fx_T)$	$1.231 * \ln(S_a) + 1.068$	0.63	0.88	$0.806 * \ln(S_a) + 2.127$	0.63	0.96
$\ln(ex_L)$	$1.324 * \ln(S_a) + 4.458$	0.86	0.51	$0.820 * \ln(S_a) + 5.386$	0.89	0.44
$\ln(ex_T)$	$1.426 * \ln(S_a) + 2.642$	0.65	0.98	$0.873 * \ln(S_a) + 3.615$	0.67	0.96
$\ln(ab_P)$	$1.950 * \ln(S_a) + 1.599$	0.56	1.61	$1.252 * \ln(S_a) + 3.097$	0.63	1.48
$\ln(ab_A)$	$0.509 * \ln(S_a) + -0.248$	0.36	0.64	$0.403 * \ln(S_a) + 0.329$	0.58	0.52
$\ln(ab_T)$	$0.691 * \ln(S_a) + 1.740$	0.62	0.50	$0.423 * \ln(S_a) + 2.209$	0.64	0.49

Table 7-26: Correlation Matrix for MSC Steel Bridge Component Responses (Wen).

	$\ln(\mu_\phi)$	$\ln(fx_L)$	$\ln(fx_T)$	$\ln(ex_L)$	$\ln(ex_T)$	$\ln(ab_P)$	$\ln(ab_A)$	$\ln(ab_T)$
$\ln(\mu_\phi)$	1.000	0.864	0.835	0.962	0.843	0.858	0.708	0.834
$\ln(fx_L)$	0.864	1.000	0.828	0.832	0.697	0.743	0.648	0.683
$\ln(fx_T)$	0.835	0.828	1.000	0.779	0.765	0.745	0.669	0.830
$\ln(ex_L)$	0.962	0.832	0.779	1.000	0.837	0.852	0.695	0.771
$\ln(ex_T)$	0.843	0.697	0.765	0.837	1.000	0.706	0.493	0.656
$\ln(ab_P)$	0.858	0.743	0.745	0.852	0.706	1.000	0.704	0.741
$\ln(ab_A)$	0.708	0.648	0.669	0.695	0.493	0.704	1.000	0.765
$\ln(ab_T)$	0.834	0.683	0.830	0.771	0.656	0.741	0.765	1.000

7.4.7 Multi-Span Simply Supported Steel Girder Bridge

7.4.7.1 Rix and Fernandez-Leon Ground Motions

Table 7-27: PSDMs for MSSS Steel Bridge Components (Rix).

	PGA			S_a **(T = Geometric Mean)**		
Response	**PSDM**	R^2	$\beta_{D\|PGA}$	**PSDM**	R^2	$\beta_{D\|Sa}$
$\ln(\mu_\phi)$	$1.444 * \ln(PGA) + 1.654$	0.86	0.51	$1.402 * \ln(S_a) + 0.760$	0.75	0.69
$\ln(fx_L)$	$2.298 * \ln(PGA) + 4.722$	0.80	1.02	$2.416 * \ln(S_a) + 3.528$	0.81	0.98
$\ln(fx_T)$	$1.929 * \ln(PGA) + 3.354$	0.79	0.90	$2.213 * \ln(S_a) + 2.579$	0.84	0.83
$\ln(ex_L)$	$1.329 * \ln(PGA) + 5.388$	0.84	0.51	$1.300 * \ln(S_a) + 4.576$	0.74	0.65
$\ln(ex_T)$	$1.463 * \ln(PGA) + 2.589$	0.81	0.62	$1.590 * \ln(S_a) + 1.873$	0.86	0.54
$\ln(ab_P)$	$1.374 * \ln(PGA) + 2.935$	0.72	0.76	$1.365 * \ln(S_a) + 2.122$	0.65	0.84
$\ln(ab_A)$	$0.809 * \ln(PGA) + 2.278$	0.70	0.45	$0.848 * \ln(S_a) + 1.845$	0.74	0.42
$\ln(ab_T)$	$0.985 * \ln(PGA) + 2.027$	0.79	0.45	$1.078 * \ln(S_a) + 1.538$	0.81	0.44
	S_a **(T = 0.2 sec)**			S_a **(T = 1.0 sec)**		
Response	**PSDM**	R^2	$\beta_{D\|Sa}$	**PSDM**	R^2	$\beta_{D\|Sa}$
$\ln(\mu_\phi)$	$1.448 * \ln(S_a) + 0.844$	0.76	0.67	$1.027 * \ln(S_a) + 0.433$	0.85	0.52
$\ln(fx_L)$	$2.444 * \ln(S_a) + 3.610$	0.79	1.04	$1.598 * \ln(S_a) + 2.728$	0.76	1.12
$\ln(fx_T)$	$2.178 * \ln(S_a) + 2.511$	0.82	0.85	$1.281 * \ln(S_a) + 1.591$	0.68	1.09
$\ln(ex_L)$	$1.344 * \ln(S_a) + 4.656$	0.75	0.64	$0.949 * \ln(S_a) + 4.267$	0.84	0.52
$\ln(ex_T)$	$1.589 * \ln(S_a) + 1.906$	0.82	0.61	$0.984 * \ln(S_a) + 1.281$	0.72	0.76
$\ln(ab_P)$	$1.397 * \ln(S_a) + 2.188$	0.64	0.85	$0.945 * \ln(S_a) + 1.728$	0.66	0.83
$\ln(ab_A)$	$0.857 * \ln(S_a) + 1.871$	0.72	0.43	$0.542 * \ln(S_a) + 1.542$	0.62	0.50
$\ln(ab_T)$	$1.072 * \ln(S_a) + 1.550$	0.76	0.49	$0.655 * \ln(S_a) + 1.137$	0.69	0.55

Table 7-28: Correlation Matrix for MSSS Steel Bridge Component Responses (Rix).

	$\ln(\mu_\phi)$	$\ln(fx_L)$	$\ln(fx_T)$	$\ln(ex_L)$	$\ln(ex_T)$	$\ln(ab_P)$	$\ln(ab_A)$	$\ln(ab_T)$
$\ln(\mu_\phi)$	1.000	0.899	0.810	0.966	0.838	0.864	0.832	0.825
$\ln(fx_L)$	0.899	1.000	0.896	0.917	0.901	0.935	0.881	0.934
$\ln(fx_T)$	0.810	0.896	1.000	0.811	0.944	0.815	0.804	0.901
$\ln(ex_L)$	0.966	0.917	0.811	1.000	0.843	0.877	0.804	0.852
$\ln(ex_T)$	0.838	0.901	0.944	0.843	1.000	0.812	0.805	0.912
$\ln(ab_P)$	0.864	0.935	0.815	0.877	0.812	1.000	0.914	0.905
$\ln(ab_A)$	0.832	0.881	0.804	0.804	0.805	0.914	1.000	0.909
$\ln(ab_T)$	0.825	0.934	0.901	0.852	0.912	0.905	0.909	1.000

7.4.7.2 Wen and Wu Ground Motions

Table 7-29: PSDMs for MSSS Steel Bridge Components (Wen).

	PGA			S_a **(T = Geometric Mean)**		
Response	**PSDM**	R^2	$\beta_{D\|PGA}$	**PSDM**	R^2	$\beta_{D\|Sa}$
$\ln(\mu_\phi)$	$1.431 * \ln(PGA) + 1.140$	0.83	0.44	$0.875 * \ln(S_a) + -0.118$	0.80	0.46
$\ln(fx_L)$	$2.057 * \ln(PGA) + 4.115$	0.73	0.85	$1.321 * \ln(S_a) + 2.554$	0.74	0.84
$\ln(fx_T)$	$2.219 * \ln(PGA) + 3.792$	0.68	1.04	$1.520 * \ln(S_a) + 2.105$	0.77	0.88
$\ln(ex_L)$	$1.272 * \ln(PGA) + 4.810$	0.71	0.55	$0.908 * \ln(S_a) + 3.848$	0.88	0.36
$\ln(ex_T)$	$1.326 * \ln(PGA) + 2.476$	0.69	0.61	$0.711 * \ln(S_a) + 1.239$	0.55	0.68
$\ln(ab_P)$	$1.169 * \ln(PGA) + 2.313$	0.59	0.66	$0.757 * \ln(S_a) + 1.375$	0.60	0.65
$\ln(ab_A)$	$0.772 * \ln(PGA) + 2.311$	0.57	0.45	$0.457 * \ln(S_a) + 1.634$	0.49	0.49
$\ln(ab_T)$	$0.779 * \ln(PGA) + 1.604$	0.55	0.47	$0.502 * \ln(S_a) + 0.977$	0.54	0.48
	S_a **(T = 0.2 sec)**			S_a **(T = 1.0 sec)**		
Response	**PSDM**	R^2	$\beta_{D\|Sa}$	**PSDM**	R^2	$\beta_{D\|Sa}$
$\ln(\mu_\phi)$	$1.067 * \ln(S_a) + 0.008$	0.86	0.40	$0.628 * \ln(S_a) + 0.662$	0.81	0.47
$\ln(fx_L)$	$1.540 * \ln(S_a) + 2.571$	0.76	0.80	$0.932 * \ln(S_a) + 3.634$	0.78	0.78
$\ln(fx_T)$	$1.826 * \ln(S_a) + 2.361$	0.82	0.79	$1.006 * \ln(S_a) + 3.160$	0.72	0.97
$\ln(ex_L)$	$1.023 * \ln(S_a) + 3.837$	0.92	0.29	$0.612 * \ln(S_a) + 4.509$	0.85	0.39
$\ln(ex_T)$	$0.881 * \ln(S_a) + 1.327$	0.66	0.59	$0.532 * \ln(S_a) + 1.866$	0.58	0.70
$\ln(ab_P)$	$0.894 * \ln(S_a) + 1.425$	0.66	0.60	$0.529 * \ln(S_a) + 1.981$	0.63	0.63
$\ln(ab_A)$	$0.546 * \ln(S_a) + 1.674$	0.54	0.46	$0.321 * \ln(S_a) + 2.003$	0.52	0.48
$\ln(ab_T)$	$0.594 * \ln(S_a) + 1.010$	0.61	0.44	$0.357 * \ln(S_a) + 1.395$	0.60	0.44

Table 7-30: Correlation Matrix for MSSS Steel Bridge Component Responses (Wen).

	$\ln(\mu_\phi)$	$\ln(fx_L)$	$\ln(fx_T)$	$\ln(ex_L)$	$\ln(ex_T)$	$\ln(ab_P)$	$\ln(ab_A)$	$\ln(ab_T)$
$\ln(\mu_\phi)$	1.000	0.914	0.905	0.950	0.863	0.861	0.775	0.790
$\ln(fx_L)$	0.914	1.000	0.859	0.924	0.867	0.891	0.802	0.809
$\ln(fx_T)$	0.905	0.859	1.000	0.867	0.883	0.833	0.757	0.795
$\ln(ex_L)$	0.950	0.924	0.867	1.000	0.809	0.876	0.780	0.806
$\ln(ex_T)$	0.863	0.867	0.883	0.809	1.000	0.820	0.781	0.836
$\ln(ab_P)$	0.861	0.891	0.833	0.876	0.820	1.000	0.897	0.867
$\ln(ab_A)$	0.775	0.802	0.757	0.780	0.781	0.897	1.000	0.928
$\ln(ab_T)$	0.790	0.809	0.795	0.806	0.836	0.867	0.928	1.000

7.4.8 Single-Span Concrete Girder Bridge

7.4.8.1 Rix and Fernandez-Leon Ground Motions

Table 7-31: PSDMs for SS Concrete Bridge Components (Rix).

	PGA			**S_a (T = Geometric Mean)**		
Response	**PSDM**	R^2	$\beta_{D\|PGA}$	**PSDM**	R^2	$\beta_{D\|Sa}$
$\ln(fx_L)$	$0.465 * \ln(PGA) + 2.253$	0.34	0.57	$0.589 * \ln(S_a) + 2.104$	0.52	0.48
$\ln(fx_T)$	$0.271 * \ln(PGA) + 1.714$	0.53	0.23	$0.314 * \ln(S_a) + 1.591$	0.67	0.19
$\ln(ex_L)$	$0.542 * \ln(PGA) + 2.511$	0.43	0.55	$0.673 * \ln(S_a) + 2.322$	0.62	0.45
$\ln(ex_T)$	$0.256 * \ln(PGA) + 1.673$	0.54	0.21	$0.296 * \ln(S_a) + 1.559$	0.67	0.18
$\ln(ab_P)$	$0.897 * \ln(PGA) + 1.024$	0.55	0.72	$1.101 * \ln(S_a) + 0.740$	0.66	0.68
$\ln(ab_A)$	$0.939 * \ln(PGA) + 1.554$	0.54	0.76	$1.083 * \ln(S_a) + 1.110$	0.70	0.61
$\ln(ab_T)$	$0.853 * \ln(PGA) + 1.514$	0.63	0.58	$1.039 * \ln(S_a) + 1.093$	0.79	0.47
	S_a (T = 0.2 sec)			**S_a (T = 1.0 sec)**		
Response	**PSDM**	R^2	$\beta_{D\|Sa}$	**PSDM**	R^2	$\beta_{D\|Sa}$
$\ln(fx_L)$	$0.525 * \ln(S_a) + 2.027$	0.47	0.45	$0.299 * \ln(S_a) + 1.814$	0.28	0.59
$\ln(fx_T)$	$0.315 * \ln(S_a) + 1.615$	0.62	0.20	$0.163 * \ln(S_a) + 1.441$	0.37	0.26
$\ln(ex_L)$	$0.619 * \ln(S_a) + 2.311$	0.47	0.53	$0.340 * \ln(S_a) + 1.988$	0.33	0.60
$\ln(ex_T)$	$0.295 * \ln(S_a) + 1.579$	0.61	0.19	$0.154 * \ln(S_a) + 1.413$	0.39	0.24
$\ln(ab_P)$	$1.124 * \ln(S_a) + 0.864$	0.62	0.72	$0.544 * \ln(S_a) + 0.131$	0.39	0.83
$\ln(ab_A)$	$1.059 * \ln(S_a) + 1.175$	0.60	0.71	$0.588 * \ln(S_a) + 0.650$	0.41	0.86
$\ln(ab_T)$	$0.981 * \ln(S_a) + 1.150$	0.64	0.61	$0.519 * \ln(S_a) + 0.687$	0.47	0.70

Table 7-32: Correlation Matrix for SS Concrete Bridge Component Responses (Rix).

	$\ln(fx_L)$	$\ln(fx_T)$	$\ln(ex_L)$	$\ln(ex_T)$	$\ln(ab_P)$	$\ln(ab_A)$	$\ln(ab_T)$
$\ln(fx_L)$	1.000	0.727	0.991	0.782	0.840	0.753	0.677
$\ln(fx_T)$	0.727	1.000	0.738	0.923	0.654	0.652	0.718
$\ln(ex_L)$	0.991	0.738	1.000	0.783	0.887	0.820	0.726
$\ln(ex_T)$	0.782	0.923	0.783	1.000	0.669	0.609	0.654
$\ln(ab_P)$	0.840	0.654	0.887	0.669	1.000	0.911	0.792
$\ln(ab_A)$	0.753	0.652	0.820	0.609	0.911	1.000	0.848
$\ln(ab_T)$	0.677	0.718	0.726	0.654	0.792	0.848	1.000

7.4.8.2 *Wen and Wu Ground Motions*

Table 7-33: PSDMs for SS Concrete Bridge Components (Wen).

	PGA			**S_a (T = Geometric Mean)**		
Response	**PSDM**	R^2	$\beta_{D\|PGA}$	**PSDM**	R^2	$\beta_{D\|Sa}$
$\ln(fx_L)$	$1.105 * \ln(PGA) + 3.827$	0.45	0.83	$0.622 * \ln(S_a) + 2.991$	0.40	0.86
$\ln(fx_T)$	$0.501 * \ln(PGA) + 2.462$	0.24	0.60	$0.167 * \ln(S_a) + 1.901$	0.08	0.66
$\ln(ex_L)$	$1.043 * \ln(PGA) + 3.870$	0.46	0.77	$0.614 * \ln(S_a) + 3.121$	0.45	0.78
$\ln(ex_T)$	$0.792 * \ln(PGA) + 3.059$	0.31	0.79	$0.429 * \ln(S_a) + 2.485$	0.22	0.92
$\ln(ab_P)$	$0.566 * \ln(PGA) + 1.105$	0.34	0.53	$0.288 * \ln(S_a) + 0.667$	0.35	0.45
$\ln(ab_A)$	$0.647 * \ln(PGA) + 1.653$	0.38	0.56	$0.396 * \ln(S_a) + 1.202$	0.41	0.55
$\ln(ab_T)$	$0.937 * \ln(PGA) + 1.977$	0.47	0.68	$0.436 * \ln(S_a) + 1.091$	0.28	0.79
	S_a (T = 0.2 sec)			**S_a (T = 1.0 sec)**		
Response	**PSDM**	R^2	$\beta_{D\|Sa}$	**PSDM**	R^2	$\beta_{D\|Sa}$
$\ln(fx_L)$	$0.872 * \ln(S_a) + 3.017$	0.54	0.76	$0.471 * \ln(S_a) + 3.430$	0.43	0.85
$\ln(fx_T)$	$0.347 * \ln(S_a) + 2.039$	0.22	0.60	$0.195 * \ln(S_a) + 2.219$	0.19	0.61
$\ln(ex_L)$	$0.846 * \ln(S_a) + 3.130$	0.58	0.68	$0.461 * \ln(S_a) + 3.541$	0.46	0.77
$\ln(ex_T)$	$0.650 * \ln(S_a) + 2.555$	0.34	0.85	$0.350 * \ln(S_a) + 2.858$	0.27	0.89
$\ln(ab_P)$	$0.389 * \ln(S_a) + 0.653$	0.42	0.42	$0.272 * \ln(S_a) + 0.969$	0.40	0.51
$\ln(ab_A)$	$0.570 * \ln(S_a) + 1.189$	0.50	0.54	$0.319 * \ln(S_a) + 1.487$	0.41	0.58
$\ln(ab_T)$	$0.689 * \ln(S_a) + 1.195$	0.48	0.68	$0.396 * \ln(S_a) + 1.587$	0.43	0.71

Table 7-34: Correlation Matrix for SS Concrete Bridge Component Responses (Wen).

	$\ln(fx_L)$	$\ln(fx_T)$	$\ln(ex_L)$	$\ln(ex_T)$	$\ln(ab_P)$	$\ln(ab_A)$	$\ln(ab_T)$
$\ln(fx_L)$	1.000	0.688	0.993	0.843	0.592	0.611	0.566
$\ln(fx_T)$	0.688	1.000	0.672	0.588	0.383	0.431	0.474
$\ln(ex_L)$	0.993	0.672	1.000	0.833	0.653	0.670	0.608
$\ln(ex_T)$	0.843	0.588	0.833	1.000	0.512	0.513	0.548
$\ln(ab_P)$	0.592	0.383	0.653	0.512	1.000	0.954	0.829
$\ln(ab_A)$	0.611	0.431	0.670	0.513	0.954	1.000	0.835
$\ln(ab_T)$	0.566	0.474	0.608	0.548	0.829	0.835	1.000

7.4.9 Single-Span Steel Girder Bridge

7.4.9.1 Rix and Fernandez-Leon Ground Motions

Table 7-35: PSDMs for SS Steel Bridge Components (Rix).

	PGA			S_a **(T = Geometric Mean)**		
Response	**PSDM**	R^2	$\beta_{D\|PGA}$	**PSDM**	R^2	$\beta_{D\|Sa}$
$\ln(fx_L)$	$2.115 * \ln(PGA) + 2.236$	0.69	1.24	$2.280 * \ln(S_a) + 1.676$	0.78	1.05
$\ln(fx_T)$	$1.737 * \ln(PGA) + 0.854$	0.60	1.24	$1.934 * \ln(S_a) + 0.485$	0.73	1.03
$\ln(ex_L)$	$2.191 * \ln(PGA) + 2.987$	0.78	1.01	$2.280 * \ln(S_a) + 2.310$	0.84	0.85
$\ln(ex_T)$	$1.683 * \ln(PGA) + 1.774$	0.59	1.24	$1.844 * \ln(S_a) + 1.372$	0.68	1.08
$\ln(ab_P)$	$1.313 * \ln(PGA) + 1.146$	0.63	0.87	$1.404 * \ln(S_a) + 0.793$	0.72	0.76
$\ln(ab_A)$	$1.259 * \ln(PGA) + 1.338$	0.62	0.83	$1.303 * \ln(S_a) + 0.983$	0.68	0.77
$\ln(ab_T)$	$1.099 * \ln(PGA) + 1.148$	0.52	0.93	$1.242 * \ln(S_a) + 0.941$	0.65	0.80
	S_a **(T = 0.2 sec)**			S_a **(T = 1.0 sec)**		
Response	**PSDM**	R^2	$\beta_{D\|Sa}$	**PSDM**	R^2	$\beta_{D\|Sa}$
$\ln(fx_L)$	$2.220 * \ln(S_a) + 1.172$	0.66	1.30	$1.366 * \ln(S_a) + 0.256$	0.56	1.47
$\ln(fx_T)$	$1.862 * \ln(S_a) + 0.031$	0.60	1.24	$1.115 * \ln(S_a) + -0.782$	0.48	1.41
$\ln(ex_L)$	$2.249 * \ln(S_a) + 1.828$	0.72	1.14	$1.360 * \ln(S_a) + 0.937$	0.61	1.32
$\ln(ex_T)$	$1.758 * \ln(S_a) + 0.917$	0.56	1.28	$1.001 * \ln(S_a) + 0.079$	0.41	1.49
$\ln(ab_P)$	$1.234 * \ln(S_a) + 0.363$	0.50	1.01	$0.765 * \ln(S_a) + -0.081$	0.47	1.01
$\ln(ab_A)$	$1.198 * \ln(S_a) + 0.594$	0.52	0.93	$0.749 * \ln(S_a) + 0.179$	0.49	0.94
$\ln(ab_T)$	$1.150 * \ln(S_a) + 0.592$	0.50	0.95	$0.654 * \ln(S_a) + 0.043$	0.36	1.07

Table 7-36: Correlation Matrix for SS Steel Bridge Component Responses (Rix).

	$\ln(fx_L)$	$\ln(fx_T)$	$\ln(ex_L)$	$\ln(ex_T)$	$\ln(ab_P)$	$\ln(ab_A)$	$\ln(ab_T)$
$\ln(fx_L)$	1.000	0.869	0.952	0.884	0.902	0.877	0.837
$\ln(fx_T)$	0.869	1.000	0.843	0.924	0.799	0.738	0.812
$\ln(ex_L)$	0.952	0.843	1.000	0.851	0.918	0.936	0.853
$\ln(ex_T)$	0.884	0.924	0.851	1.000	0.817	0.759	0.861
$\ln(ab_P)$	0.902	0.799	0.918	0.817	1.000	0.946	0.936
$\ln(ab_A)$	0.877	0.738	0.936	0.759	0.946	1.000	0.890
$\ln(ab_T)$	0.837	0.812	0.853	0.861	0.936	0.890	1.000

7.4.9.2 Wen and Wu Ground Motions

Table 7-37: PSDMs for SS Steel Bridge Components (Wen).

	PGA			S_a **(T = Geometric Mean)**		
Response	**PSDM**	R^2	$\beta_{D\|PGA}$	**PSDM**	R^2	$\beta_{D\|Sa}$
$\ln(fx_L)$	$2.088 * \ln(PGA) + 2.496$	0.59	1.17	$1.108 * \ln(S_a) + 0.362$	0.25	1.58
$\ln(fx_T)$	$1.523 * \ln(PGA) + 1.048$	0.30	1.58	$0.948 * \ln(S_a) + -0.416$	0.17	1.72
$\ln(ex_L)$	$1.941 * \ln(PGA) + 2.819$	0.62	1.04	$1.201 * \ln(S_a) + 0.946$	0.34	1.37
$\ln(ex_T)$	$1.997 * \ln(PGA) + 2.732$	0.55	1.22	$1.104 * \ln(S_a) + 0.670$	0.24	1.59
$\ln(ab_P)$	$1.213 * \ln(PGA) + 1.057$	0.44	0.94	$0.568 * \ln(S_a) + -0.300$	0.14	1.16
$\ln(ab_A)$	$1.395 * \ln(PGA) + 1.742$	0.53	0.89	$0.610 * \ln(S_a) + 0.192$	0.15	1.19
$\ln(ab_T)$	$0.947 * \ln(PGA) + 1.064$	0.27	1.06	$0.411 * \ln(S_a) + -0.030$	0.07	1.19
	S_a **(T = 0.2 sec)**			S_a **(T = 1.0 sec)**		
Response	**PSDM**	R^2	$\beta_{D\|Sa}$	**PSDM**	R^2	$\beta_{D\|Sa}$
$\ln(fx_L)$	$1.204 * \ln(S_a) + 0.549$	0.39	1.43	$0.759 * \ln(S_a) + 1.432$	0.42	1.39
$\ln(fx_T)$	$0.916 * \ln(S_a) + -0.382$	0.21	1.68	$0.635 * \ln(S_a) + 0.459$	0.27	1.61
$\ln(ex_L)$	$1.244 * \ln(S_a) + 1.081$	0.48	1.21	$0.783 * \ln(S_a) + 1.991$	0.52	1.17
$\ln(ex_T)$	$1.299 * \ln(S_a) + 0.964$	0.45	1.36	$0.805 * \ln(S_a) + 1.877$	0.46	1.34
$\ln(ab_P)$	$0.749 * \ln(S_a) + -0.061$	0.32	1.03	$0.501 * \ln(S_a) + 0.571$	0.39	0.98
$\ln(ab_A)$	$0.815 * \ln(S_a) + 0.462$	0.35	1.04	$0.551 * \ln(S_a) + 1.169$	0.44	0.97
$\ln(ab_T)$	$0.644 * \ln(S_a) + 0.256$	0.24	1.08	$0.466 * \ln(S_a) + 0.902$	0.34	1.01

Table 7-38: Correlation Matrix for SS Steel Bridge Component Responses (Wen).

	$\ln(fx_L)$	$\ln(fx_T)$	$\ln(ex_L)$	$\ln(ex_T)$	$\ln(ab_P)$	$\ln(ab_A)$	$\ln(ab_T)$
$\ln(fx_L)$	1.000	0.759	0.932	0.857	0.785	0.820	0.764
$\ln(fx_T)$	0.759	1.000	0.786	0.771	0.809	0.817	0.840
$\ln(ex_L)$	0.932	0.786	1.000	0.857	0.849	0.873	0.771
$\ln(ex_T)$	0.857	0.771	0.857	1.000	0.861	0.865	0.861
$\ln(ab_P)$	0.785	0.809	0.849	0.861	1.000	0.949	0.892
$\ln(ab_A)$	0.820	0.817	0.873	0.865	0.949	1.000	0.882
$\ln(ab_T)$	0.764	0.840	0.771	0.861	0.892	0.882	1.000

7.5 Discussion of Ground Motion Intensity Measures

As stated previously, probabilistic seismic demand models are generally expressed in terms of one or more intensity measures (e.g. PGA, S_a). The quality of each model is largely dependent on the efficiency of the intensity measure(s) selected. This is to say, that the intensity measure (IM) that results in the smallest dispersion around the estimated median is said to be the most efficient IM.

Efficiency is not the only requirement for the selection of an appropriate IM. Mackie and Stojadinovic (2003) state that other considerations include practicality and sufficiency. Practicality refers to whether or not the IM has any direct correlation to known engineering measurements. This phenomenon is illustrated in Figure 7-4. Sufficiency applies to cases where an engineering demand measurement and a particular IM have no conditional dependence on ground motion characteristics such as magnitude and distance.

Another consideration is that the chosen IM should be readily applicable to an entire portfolio of bridges. This is best illustrated by considering the source of bridge information, which is often only the National Bridge Inventory (NBI) database (FHWA, 2002) as is the case with HAZUS-MH (FEMA, 2003). This database only gives basic geometry and construction information and therefore is not conducive to deriving structurally based intensity measures such as the spectral acceleration at the fundamental period (S_{a-f}).

Finally, the chosen intensity measure should have hazard computability (Giovenale et al., 2004). The ultimate use of the PSDMs is to convolve them with the hazard in a region of interest to quantify the seismic threat the bridges face. This convolution requires

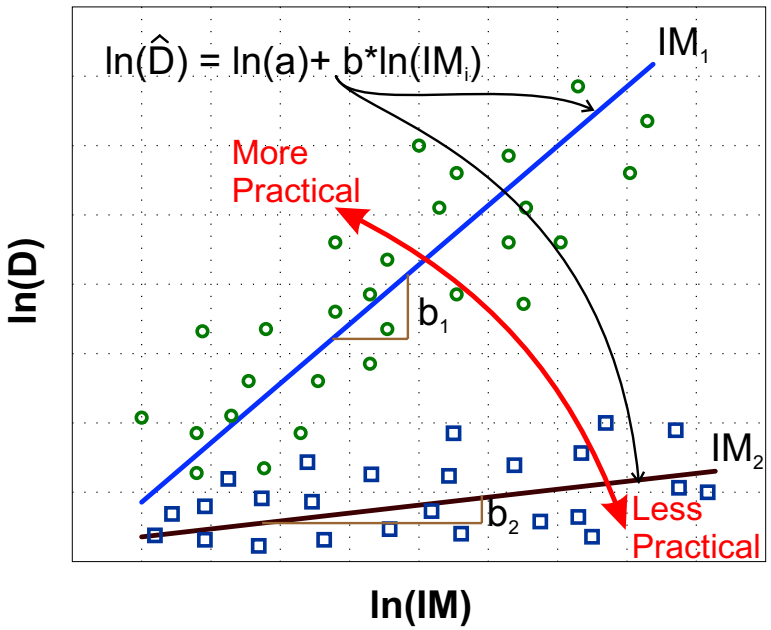

Figure 7-4: Illustration of Practicality of an IM.

the probabilistic seismic hazard for the selected region to be calculated in terms of the selected IM. Hazard maps and hazard curves are readily available in terms of PGA and for spectral accelerations at a discrete number of values. Thus implying that even if a more efficient IM is defined, the computability of the hazard in terms of that IM, may make it a less desirable choice (Giovenale et al., 2004).

7.5.1 Practicality and Efficiency

The appropriateness of the four intensity measures examined in this study (see Table 7-1) is evaluated in the framework of practicality and efficiency. With practicality being measured as correlation and efficiency being measured as dispersion, a term to measure their composite effect is beneficial. A new term, ζ, is proposed to more effectively measure

this composite contribution. The derivation of ζ, which is a modified measure of dispersion, is best seen in the context of Equation 7.3 which can be rewritten as follows.

$$
\begin{aligned}
P[EDP \geq d|IM] &= 1 - \Phi\left(\frac{\ln(d) - \ln\left(aIM^b\right)}{\beta_{EDP|IM}}\right) \\
&= \Phi\left(\frac{-\ln(d) + \ln\left(aIM^b\right)}{\beta_{EDP|IM}}\right) \\
&= \Phi\left(\frac{b\ln(IM) - (\ln(d) - \ln(a))}{\beta_{EDP|IM}}\right) \\
&= \Phi\left(\frac{\ln(IM) - \frac{\ln(d)-\ln(a)}{b}}{\frac{\beta_{EDP|IM}}{b}}\right) \\
&= \Phi\left(\frac{\ln(IM) - \lambda}{\zeta}\right) \qquad (7.5)
\end{aligned}
$$

where $\lambda = \frac{\ln(d)-\ln(a)}{b}$ and is the natural log of the median IM value for a specified level of demand, d. Also, the dispersion component is given as $\zeta = \frac{\beta_{EDP|IM}}{b}$. The term ζ, is thus a function of the efficiency measure $\beta_{EDP|IM}$ and a practicality measure b. Consequently, the appropriateness of intensity measures in this study is directly evaluated using ζ where smaller values are indicative of increased appropriateness.

7.5.2 Intensity Measure Case Studies

For evaluation of the appropriateness of the intensity measures given in Table 7-1, two bridge types are selected. The multi-span continuous concrete girder bridge and the multi-span simply supported steel girder bridge are the two classes selected for this evaluation. The motivation for their selection is that they represent classes of bridges whose fundamental periods are significantly different. The period ranges for the MSC Concrete and MSSS Steel bridges are 0.35 - 0.78 seconds and 0.17 - 0.32 seconds respectively.

For the sake of brevity, only three of the component responses are discussed because it is believed they sufficiently represent the trends in the other component responses. Specifically, the responses are the curvature ductility of the columns (μ_ϕ), longitudinal deformation of the fixed bearings (fx_L) and the active deformation of the abutments (ab_A). The term ζ for these responses are examined for both ground motion suites.

7.5.2.1 Multi-Span Continuous Concrete Bridge

The ζ values for the MSC Concrete bridge using four different intensity measures are presented in Tables 7-39 and 7-40 for the Rix and Wen ground motion suites respectively. Using the Rix ground motions, the modified dispersions are smallest when the S_{a-gm} intensity measure is used. The values that correspond with the three responses are 0.41, 0.60 and 1.61. However, these values do not change much when PGA is used giving respective values of 0.49, 0.62 and 1.62. This shows that there is not much difference in the appropriateness of these two intensity measures. It should be pointed out, though, that S_{a-1} is the worst of the intensity measures.

Table 7-39: ζ Values for MSC Concrete Girder Bridge (Rix).

	PGA			S_{a-gm}		
	b	$\beta_{D\|IM}$	ζ	b	$\beta_{D\|IM}$	ζ
μ_ϕ	1.157	0.57	0.49	1.173	0.48	0.41
fx_L	1.076	0.67	0.62	1.076	0.65	0.60
ab_A	0.437	0.71	1.62	0.440	0.71	1.61
	S_{a-02}			S_{a-1}		
	b	$\beta_{D\|IM}$	ζ	b	$\beta_{D\|IM}$	ζ
μ_ϕ	1.142	0.58	0.51	0.780	0.66	0.85
fx_L	1.073	0.77	0.72	0.683	0.81	1.19
ab_A	0.422	0.73	1.73	0.325	0.71	2.18

Table 7-40: ζ Values for MSC Concrete Girder Bridge (Wen).

	PGA			S_{a-gm}		
	b	$\beta_{D\|IM}$	ζ	b	$\beta_{D\|IM}$	ζ
μ_ϕ	1.324	0.70	0.53	0.782	0.57	0.73
fx_L	1.281	0.56	0.44	0.676	0.55	0.81
ab_A	0.637	0.65	1.02	0.458	0.65	1.42
	S_{a-02}			S_{a-1}		
	b	$\beta_{D\|IM}$	ζ	b	$\beta_{D\|IM}$	ζ
μ_ϕ	1.181	0.37	0.31	0.697	0.53	0.76
fx_L	0.986	0.38	0.39	0.600	0.45	0.75
ab_A	0.589	0.56	0.95	0.333	0.59	1.77

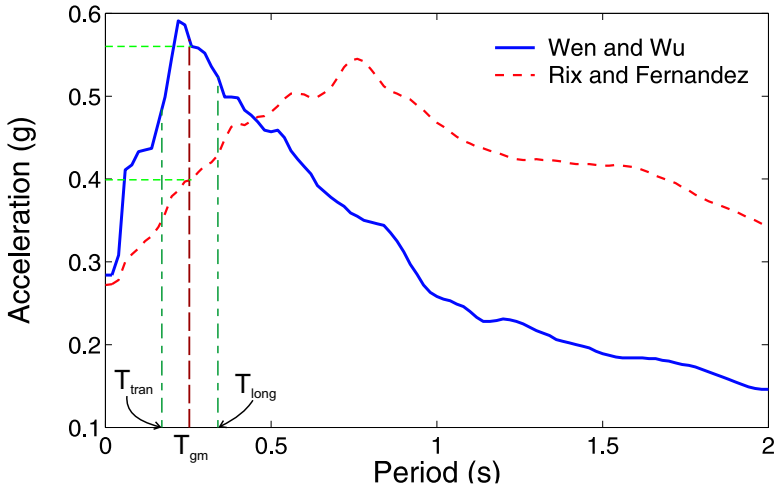

Figure 7-5: Frequency Content Differences in Ground Motion Suites.

When one considers the Wen suite of ground motions the appropriate intensity measure is determined to be S_{a-02} with ζ values of 0.31, 0.39 and 0.95 (see Table 7-40). The second most appropriate intensity measure, as determined using the metric ζ, is PGA, with respective values of 0.53, 0.44, and 1.02. Once again the worst intensity measure is determined to be S_{a-1}. The difference that occurs between the two ground motion suites is likely due to the frequency content of the suites as they compare with the periods of the bridge suites. For instance, using Figure 7-5 as a reference, a bridge whose response is dominated by the longitudinal mode would be similar for both ground motion suites. However, the spectral acceleration assessed at T_{gm} would be quite different. This phenomenon will likely reduce the efficiency of the S_{a-gm} in some cases as seen when comparing Tables 7-39 and 7-40.

7.5.2.2 Multi-Span Simply Supported Steel Bridge

Tables 7-41 and 7-42 show the ζ values for the MSSS Steel girder bridge subjected to the Rix and Wen ground motion suites respectively. For the Rix ground motion suite there is

not an intensity measure which is clearly more practical and efficient when compared to the others. As shown in Table 7-41, for the component responses μ_ϕ and ab_A PGA appears to be the most practical and efficient with ζ values of 0.32 and 0.23 respectively. However, S_{a-gm} is the most appropriate intensity measure when fx_L is considered.

Table 7-41: ζ Values for MSSS Steel Girder Bridge (Rix).

	PGA			S_{a-gm}		
	b	$\beta_{D\|IM}$	ζ	b	$\beta_{D\|IM}$	ζ
μ_ϕ	1.444	0.51	0.35	1.402	0.69	0.49
fx_L	2.298	1.02	0.44	2.416	0.98	0.41
ab_A	1.929	0.45	0.23	0.848	0.42	0.50
	S_{a-02}			S_{a-1}		
	b	$\beta_{D\|IM}$	ζ	b	$\beta_{D\|IM}$	ζ
μ_ϕ	1.448	0.67	0.46	1.027	0.52	0.51
fx_L	2.444	1.04	0.43	1.598	1.12	0.70
ab_A	0.857	0.43	0.50	0.542	0.50	0.92

Table 7-42: ζ Values for MSSS Steel Girder Bridge (Wen).

	PGA			S_{a-gm}		
	b	$\beta_{D\|IM}$	ζ	b	$\beta_{D\|IM}$	ζ
μ_ϕ	1.431	0.44	0.31	0.875	0.46	0.53
fx_L	2.057	0.85	0.41	1.321	0.84	0.64
ab_A	0.772	0.45	0.58	0.457	0.49	1.07
	S_{a-02}			S_{a-1}		
	b	$\beta_{D\|IM}$	ζ	b	$\beta_{D\|IM}$	ζ
μ_ϕ	1.067	0.40	0.37	0.628	0.47	0.75
fx_L	1.540	0.80	0.52	0.932	0.78	0.84
ab_A	0.546	0.46	0.84	0.321	0.48	1.50

For the Wen suite of ground motions, PGA appears to be the most appropriate intensity measure with ζ values of 0.31, 0.41 and 0.58. However, it can be seen that S_{a-02} is a close second with respective values of 0.37, 0.52 and 0.84. Once again S_{a-1} appears to be the least appropriate intensity measure giving ζ values of 0.75, 0.84 and 1.50.

Considering the information presented in this section, PGA appears to be the most practical and efficient of the four intensity measures investigated. Although it is not always the most efficient of parameters, it has an advantage of being independent of structural parameters and thus more suitable for use in representing suites of bridges. S_{a-02} is also independent of the specific structure and is also a reasonable intensity measure to use. One interesting outcome of this study is the discovery that S_{a-1} is consistently the least efficient and practical of the four IMs. This is a particularly significant finding considering that HAZUS-MH uses this specific intensity measure (FEMA, 2003).

7.6 Closure

Probabilistic seismic demand models for the components of nine bridge classes typical to the Central and Southeastern United States are generated using two distinct ground motion suites. The PSDMs are derived in terms of four specific intensity measures and are presented in the form of joint probability distributions. This form of the PSDM is essential to accomplishing the generation of "system" or fragility curves as it facilitates random sampling variables with stochastic dependence. A cursory review of the generated PSDMs gives an indication that the ground motion suite does play a significant role in the estimated demand.

Another point addressed in this chapter is the selection of an appropriate intensity measure. Contrary to common belief, peak ground acceleration, as opposed to spectral quantities, was found to be the most efficient and practical intensity measure for generation of PSDMs for the bridge types contained in this study. One possible reason for this finding is that more than one component is being considered and not all of them are particularly well behaved. Peak ground acceleration appears to be less sensitive to this fluctuation in behavior. It should be noted that the choice of PGA as the intensity measure is not completely out of line. Other researchers who have shown that PGA is the most appropriate intensity measure are still using it in their studies (Kim and Shinozuka, 2004).

CHAPTER VIII

SEISMIC FRAGILITY ANALYSIS OF HIGHWAY BRIDGES

8.1 Introduction

Seismic loss estimation requires information ranging from the seismic hazard to the conditional societal and economic impacts. This was illustrated previously in Equation 7.1. One very significant and vital part of this loss equation is known as the fragility function, $P[LS|IM]$. This fragility function is a probabilistic tool used to estimate the damage likely to occur during a seismic event. It is given explicitly as the probability of meeting or exceeding some limit state (LS) for a specific intensity of seismic excitation (IM).

These seismic fragility curves are a convolution of two separate probability statements. One such probability statement was given in Chapter 7 as the probabilistic seismic demand model presented in Equation 7.3 where EDP is the selected engineering demand parameter (e.g. column ductility, bearing deformation) and IM is the intensity measure used to quantify the seismic hazard (e.g. PGA). More generally, this statement is referred to as the seismic demand (D).

The other probability statement is given as the probability of meeting or exceeding some limit state (LS) conditioned on some specific level of demand (EDP) $P[LS|EDP]$. The limit states of the structure are chosen such that they have some relation to the operation

or functionality of the structure and are also referred to as structural capacities (C). Thus, the fragility statement is the probability of the seismic demand reaching or exceeding the structural capacity at a given intensity level as shown in Equation 8.1.

$$\text{Fragility} = P[D \geq C|IM] = P[C - D \leq 0.0|IM] \tag{8.1}$$

When both the seismic demand and the structural capacity follow lognormal distributions, the fragility equation takes the form given in Equation 2.3 and presented again in Equation 8.2.

$$P[C - D \leq 0.0|IM] = \Phi\left(\frac{\ln(S_d/S_c)}{\sqrt{\beta_{D|IM}^2 + \beta_c^2}}\right) \tag{8.2}$$

where $\beta_{D|IM}$ and β_C are the lognormal standard deviations (dispersions) of the demand and capacity, respectively, $\Phi(\cdot)$ is the standard normal cumulative distribution function, S_c is the median value for the limit state and S_d is the median for the seismic demand which is a function of the intensity measure IM.

In this chapter the seismic fragility curves for all nine bridge classes are developed. They utilize the seismic demand models developed in Chapter 7 for each of the various bridge components. The limit states, which are used, are presented in the following section. This chapter concludes by looking at the effects of ground motion suite selection and analytical modeling dimension (2-D vs. 3-D). Finally, a comparison is made of these fragility curves with past earthquake damage and the bridge fragility curves in HAZUS.

8.2 Limit States

Determining the limit states for the various components of each bridge is not a trivial task. The limit states, as used in Equation 8.2, requires that they be defined in terms of some metric used by the *EDP*, such as ductility or deformation. At the same time, they must also have some qualitative or functional interpretation which gives a sense of the type of impact this limit state carries.

The qualitative limit states used throughout this study are the same limit states defined and used in the FEMA loss assessment package HAZUS-MH (FEMA, 2003). The decision to use these limit states is an obvious one in that it will provide for the portability of the fragility functions developed in this study to HAZUS. The qualitative description of the four damage states: Slight, Moderate, Extensive and Complete are given in Table 8-1.

Table 8-1: HAZUS' Qualitative Limit States (FEMA, 2003).

Limit State	**Description**
Slight	Minor cracking and spalling to the abutment, cracks in shear keys at abutments, minor spalling and cracks at hinges, minor spalling at the column (damage requires no more than cosmetic repair) or minor cracking to the deck.
Moderate	Any column experiencing moderate (shear cracks) cracking and spalling (column structurally still sound), moderate movement of the abutment (<2"), extensive cracking and spalling of shear keys, any connection having cracked shear keys or bent bolts, keeper bar failure without unseating, rocker bearing failure or moderate settlement of the approach.
Extensive	any column degrading without collapse – shear failure – (column structurally unsafe), significant residual movement at connections, or major settlement approach, vertical offset of the abutment, differential settlement at connections, shear key failure at abutments.
Complete	any column collapsing and connection losing all bearing support, which may lead to imminent deck collapse, tilting of substructure due to foundation failure.

Associated with each of these limit states is a timeline for the restoration of the bridge functionality. Figure 8-1 shows the restoration timeline for each limit state, which is based on the opinion of four experts (ATC, 1985; FEMA, 2003). Thus, it is clear that each limit state carries with it a definition of bridge functionality over time.

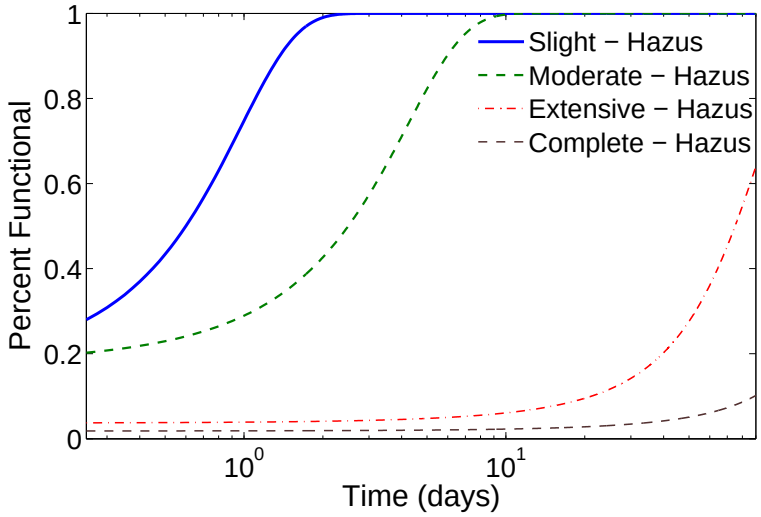

Figure 8-1: HAZUS – Bridge Functionality Restoration Curves (FEMA, 2003).

With the definition of qualitative limit states, the next task is to assign a quantitative measure to each of the limit states for each of the bridge components. The challenge lies in being able to define the limit states such that they are functionally equal. For example, the question may arise: "What ductility level in the columns will affect the functionality of the bridge to the same degree as a chosen deformation in the fixed bearings?" There are two main approaches to accomplishing this task, namely the prescriptive/physics based approach and the descriptive approach.

8.2.1 Prescriptive Approach

The prescriptive approach is an approach where an analyst prescribes the functional level of the bridge based on the physics of the system. An example of such a prescription may be that the analyst prescribes the bridge to be shut for one day to allow for inspection if the column reinforcement yields. Thus, one may use the constitutive model for each component to prescribe the various limit states. It is imperative that these prescriptions be set at levels that would be noticeable to a bridge inspector.

Based on experimental results and interpretation of bridge component behavior some prescriptive limit states are set for this study. These median values for these limit states are given in Table 8-2 and discussed in the following subsections.

Table 8-2: Median Values for Prescriptive Limit States.

Component	**Slight**	**Moderate**	**Extensive**	**Complete**
Concrete Column (μ_ϕ)	1.0	1.58	3.22	6.84
High-Steel Bearing Fixed-Long (mm)	6	20	40	255
High-Steel Bearing Fixed-Tran (mm)	6	20	40	255
High-Steel Bearing Rocker-Long (mm)	50	100	150	255
High-Steel Bearing Rocker-Tran (mm)	6	20	40	255
Low-Steel Bearing Fixed-Long (mm)	6	20	40	255
Low-Steel Bearing Fixed-Tran (mm)	6	20	40	255
Low-Steel Bearing Sliding-Long (mm)	50	100	150	255
Low-Steel Bearing Sliding-Tran (mm)	6	20	40	255
Elastomeric Bearing Fixed-Long (mm)	30	100	150	255
Elastomeric Bearing Fixed-Tran (mm)	30	100	150	255
Elastomeric Bearing Expan-Long (mm)	30	100	150	255
Elastomeric Bearing Expan-Tran (mm)	30	100	150	255
Abutment-Active (mm)	4	8	25	50
Abutment-Tran (mm)	4	8	25	50

8.2.1.1 Steel Bearings

The median values for the limit states of the high-type steel bearings in the longitudinal direction are set to be 6 mm, 20 mm, 40 mm and 255 mm for the slight, moderate, extensive and complete damage states respectively. It was observed in the work by Mander et al. (1996), that a longitudinal deformation of 6 mm in the fixed steel bearings resulted in the appearance of cracks in the concrete pier. This is believed to be a noticeable level of damage and may result in a more detailed evaluation. At a deformation of 20 mm, prying of the bearings and severe deformation in the anchor bolts was observed. Complete fracture of the bolts is assumed to occur at 40 mm which will permit either toppling or sliding of the bearings (see Figure C-6). A deformation or sliding of 255 mm is believed to exceed the typical seat width given for the bearings and therefore would result in complete collapse of the span.

The transverse behaviors of both the fixed and rocker type bearings are similar to that of the high-type fixed bearing in the longitudinal direction. Therefore, the same deformation limit states are assumed to apply for these cases. The low-type bearings are also subjected to the same types of limitations as their high-type counterparts and are therefore assigned the same limit states.

8.2.1.2 Elastomeric Bearings

The behavior of the elastomeric bearings is one which is controlled by sliding. Unrestricted sliding can only occur once a fracture of the steel retention dowels occurs. One would be tempted to defined the fracture of the steel dowels as a slight damage state but this is not a practical definition. It is difficult, if not impossible, for a bridge inspector to recognize this

fracture or to differentiate between the fixed and expansion bearings. For this reason, the limit states for the fixed and expansion elastomeric bearings, in both the longitudinal and transverse directions, are assumed to be the same.

A deformation of 30 mm is assumed to be the median deformation for slight damage. This degree of deformation would be noticeable yet would likely not cause much in the way of closure. A deformation of 100 mm may require that the deck be realigned and also implies possible dowel fracture. Thus, this is assumed as the moderate damage state. At a deformation of 150 mm dowel fracture is assured and would likely require some degree of repair (girder retention) in addition to deck realignment, resulting in an extensive damage state. Finally, the elastomeric bearings have the same unseating problem as do the steel bearings and thus warrant a deformation for the complete damage limit state to be 255 mm.

8.2.1.3 Columns

There are a number of different metrics which are available for defining the limit states of the reinforced concrete columns. These metrics include drift, displacement ductility (μ_Δ) and curvature ductility (μ_ϕ). As mentioned previously, the metric chosen for this study is curvature ductility which is defined in Equation 5.2 as the maximum realized curvature divided by the yield curvature or curvature at yield of the outer most steel reinforcing bar.

The detailing for the typical reinforced concrete column in the Central and Southeastern United States (CSUS) results in columns which have poorly confined longitudinal steel and also have lap splices located in the plastic hinge zones. Hwang et al. (2000) proposed limit states, in terms of displacement ductilities, of 1.0, 1.2, 1.76 and 4.76 which correspond to yield, cracking, spalling and reinforcement buckling, respectively. It is pointed out in the

Seismic Retrofitting Manual for Highway Bridges (FHWA, 1995b) that, for poorly confined columns, longitudinal steel will buckle at a displacement ductility of 3.0 and is thus the value chosen for use in this study.

The limit states defined are given in terms of displacement ductilities and must be translated into equivalent curvature ductilities. This conversion between ductility levels is provided by FHWA (1995b) in Equation 8.3

$$\mu_\phi = 1 + \frac{\mu_\Delta - 1}{3\frac{l_p}{l}\left(1 - 0.5\frac{l_p}{l}\right)} \tag{8.3}$$

Where l is the length of the column and l_p is the length of the plastic hinge calculated by Equation 8.4.

$$l_p = (0.08)l + 9d_b \tag{8.4}$$

Where d_b is the diameter of the longitudinal reinforcement.

Using the mean column height, as determined from the inventory analysis in Chapter 4, and d_b of 25.4 mm, the new curvature ductility limit states are calculated. The limit states are calculated to be 1.0, 1.58, 3.22 and 6.84 for the slight, moderate, extensive and complete damage states respectively.

8.2.1.4 Abutments

Following the recommendations of Choi (2002), the limit states for the abutment in active action are assumed to occur at 4 mm, 8 mm, 25 mm and 50 mm. These values correspond to the point of half of first yield, first yield, ultimate deformation and twice ultimate deformation respectively. These values are better understood by examining Figure C-37.

8.2.2 Uncertainty in Prescriptive Approach

In this study, the capacities or limit states of the various bridge components are assumed to follow a lognormal distribution. In Table 8-2 the median values used for each of the respective distributions are given. There is also uncertainty associated with each median which must be defined. This uncertainty is given in the form of a lognormal standard deviation or dispersion ($\beta_{prescriptive}$).

When enough information is not available for the assessment of the dispersion for each limit state, it is still beneficial to account for some degree of uncertainty. The assignment of this uncertainty can be assumed in a subjective manner. Estimates of the coefficient of variation (COV) are made for the four different limit states. The COV is assumed to be smaller for the slight and moderate limit states than for the extensive and complete damage states. In this study, the COV for the two lower limit states (COV_{slight}, $COV_{moderate}$) and the two higher limit states ($COV_{extensive}$, $COV_{complete}$) are assumed to be 0.25 and 0.5 respectively. The dispersion for a lognormal distribution is calculated by Equation 8.5. The prescriptive dispersions ($\beta_{prescriptive}$) are calculated to be 0.25 for the two lower limit states and 0.46 for the higher limit states.

$$\beta = \sqrt{\ln(1 + COV^2)} \tag{8.5}$$

8.2.3 Descriptive Approach

Another approach to estimating the limit states for various bridge components is to take a descriptive approach. This is to describe the limits that bridge inspectors/officials would

place on a bridge if they observed various levels of damage. This may be a more subjective approach but arguably may better represent what really happens following an earthquake.

A survey was designed and conducted by Padgett and DesRoches (2005) where bridge inspectors and officials were asked to describe the functionality timeline of a bridge for different levels of component damage. This survey was designed to elicit information pertaining to the relationship between bridge component damage and bridge functionality as a function of time. Some of the results from this survey are used in this study to help define appropriate limit states.

The survey respondents were asked to assign a functionality level (0%, 50% and 100%) for a bridge over discrete times (0 days, 1 day, 3 days, 7 days and 30 days) given certain observable conditions of the bridge components. For example, for the case where the bridge columns have observed cracking, the respondents indicated the functional level of the bridge. To facilitate the distillation of the responses, limit states in terms of bridge restoration were defined. Attempting to approximate the same restoration functions adopted by HAZUS-MH (see Figure 8-1), the limit states for the survey data were defined as they are presented in Figure 8-2.

Following these limit states, the responses of 28 bridge inspectors/officials from the CSUS are summarized for five different bridge conditions. Tables 8-3 through 8-7 show estimates of the percentiles of the cumulative distribution functions for the four limit states.

8.2.3.1 Mapping of Survey Results

The mapping of these results into response quantities measured by the analytical bridge model is required. In addition, for cases where ranges are specified, it becomes necessary

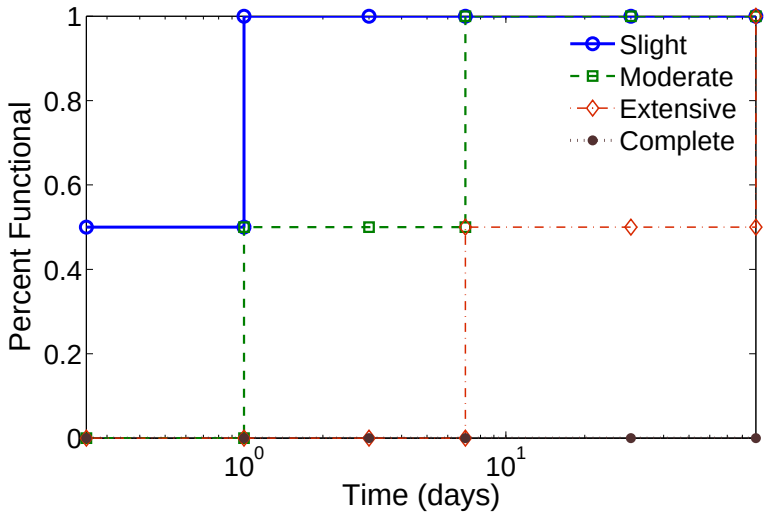

Figure 8-2: Survey - Bridge Functionality Restoration Curves.

Table 8-3: Survey Results for Longitudinal Offset at Expansion Joints (Padgett and DesRoches, 2005).

	P[Limit State |Δ]			
Damage (Δ), mm	**Slight**	**Moderate**	**Extensive**	**Complete**
$\Delta \leq 25.4$	0.179	0.000	0.000	0.000
$25.4 < \Delta \leq 152.4$	0.893	0.250	0.143	0.143
$\Delta > 152.4$	1.000	0.750	0.643	0.536

Table 8-4: Survey Results for Transverse Offset at Expansion Joints (Padgett and DesRoches, 2005).

	P[Limit State |Δ]			
Damage (Δ), mm	**Slight**	**Moderate**	**Extensive**	**Complete**
$\Delta \leq 25.4$	0.321	0.036	0.000	0.000
$25.4 < \Delta \leq 152.4$	0.750	0.429	0.214	0.107
$\Delta > 152.4$	0.929	0.714	0.536	0.464

Table 8-5: Survey Results for Settlement at Bridge Approach (Padgett and DesRoches, 2005).

	P[Limit State |Δ]			
Damage (Δ), mm	**Slight**	**Moderate**	**Extensive**	**Complete**
$\Delta \leq 25.4$	0.286	0.036	0.036	0.036
$25.4 < \Delta \leq 152.4$	0.889	0.148	0.000	0.000
$\Delta > 152.4$	1.000	0.464	0.214	0.071

Table 8-6: Survey Results for Column Conditions (Padgett and DesRoches, 2005).

	Ductility	**P[Limit State |μ_{phi}]**			
Damage	μ_{phi}	**Slight**	**Moderate**	**Extensive**	**Complete**
Cracking	1.58	0.519	0.185	0.148	0.148
Spalling	3.22	0.929	0.607	0.286	0.250
Reinforcement Buckling	6.84	0.964	0.929	0.786	0.750

Table 8-7: Survey Results for Abutment Conditions (Padgett and DesRoches, 2005).

	P[Limit State | Condition]			
Damage	**Slight**	**Moderate**	**Extensive**	**Complete**
Cracking	0.536	0.071	0.036	0.000
Spalling/Rotation	0.821	0.393	0.250	0.107

to assign a representative value. For the case where $\Delta \leq 25.4$ mm, the representative value is chosen to be 12.7 mm. For the other two ranges the values of 76.2 mm and 152.4 mm are chosen respectively.

The longitudinal offset at the expansion joints is assumed to be equivalent to the longitudinal deformation of the steel rocker bearings, steel sliding bearing and the elastomeric bearings (both fixed and expansion). The transverse offset at the expansion joint is assumed to be equivalent to the transverse deformation of the elastomeric bearings. Because of the physical nature of the steel fixed bearings there is no appropriate mapping provided by the survey results.

The mapping at the abutments is a little more difficult. In this study, the assumption is made that the settlement at the approach can be related to the active deformation of the abutment. Seed and Whitman (1970) showed that under dynamic loads, the soils behind retaining structures, such as abutments, will fail on a plane of approximately 35 degrees from horizontal. Using this finding, the vertical settlement of the soils is related to the

horizontal active displacement of of the abutment. The resulting values are presented in Table 8-8.

Table 8-8: Longitudinal Active Abutment Deformations Correlated to Approach Settlement.

Approach Settlement (mm)	Active Deformation (mm)
12.7	18.1
76.2	108.0
152.4	218.0

The mapping of the passive action of the abutments to a longitudinal displacement is facilitated by the work performed by Maroney et al. (1994). In their study, they found that for every 25.4 mm of passive displacement of the top of the abutment, it also rotates 0.008 radians. It is assumed that an inspector would not be able to see a rotation in the abutment until it reaches 0.03 radians. This then corresponds to a longitudinal deformation of 146 mm which is set to be equal to moderate damage (see Table 8-7). The onset of cracking is assumed to occur at the second yield point, as seen in Figure C-35, which is equivalent to 37 mm. This is then set to be equivalent to the slight damage state. The data from the respondents indicates their belief that it is unlikely to achieve an extensive or complete damage state due to abutment deformation (see Table 8-7). Therefore, only the two lower limit states are used with an assumed dispersion of 0.46.

Column ductilities are assigned to each of the descriptive damage states listed in the survey. This study used the mapping presented in Table 8-6.

8.2.4 Bayesian Update of Limit States

As seen, there are two sources of information pertaining to the bridge component limit states, physics based and survey based. Therefore, it is desired that the both sets of information be used in setting the limit states for this study. A Bayesian approach is an appropriate way of handling this task.

Bayesian theory allows one to update an assumed probability distribution whenever additional information is acquired. The underlying concept is shown by Bayes' Theorem which is given in Equation 8.6.

$$P[B_i|A] = \frac{P[A|B_i]P[B_i]}{\sum_{j=1}^{n} P[A|B_i]P[B_i]} \tag{8.6}$$

where A is the new information obtained and B_i is the updated information. A more thorough presentation of the Bayesian approach, as it is implemented in this study, is given in the work by Mosleh and Apostolakis (1986). In essence, they presented a way to get updated probability distributions (limit state distributions) when one is provided with percentile values from a group of experts. For the sake of brevity, a brief description of the exact process/formulae used in this study is given in Appendix F. What results from their methodology is a new distribution which incorporates the information from the physics based approach with the information from the survey results. As an example, Figure 8-3 shows the results of this procedure for the columns under a moderate damage state.

Following this procedure, the limit states for the columns, expansion bearings, elastomeric bearings and abutments are modified. The median (S_c) and dispersion (β_c) values for the limit states used in this study are presented in Table 8-9.

Table 8-9: Bayesian Updated Limit States for Bridge Components.

	Slight		Moderate		Extensive		Complete	
Component	**med**	**disp**	**med**	**disp**	**med**	**disp**	**med**	**disp**
Concrete Column (μ_ϕ)	1.29	0.59	2.10	0.51	3.52	0.64	5.24	0.65
High-Steel Bearing Fixed-Long (mm)	6.0	0.25	20.0	0.25	40.0	0.47	186.6	0.65
High-Steel Bearing Fixed-Tran (mm)	6.0	0.25	20.0	0.25	40.0	0.47	186.6	0.65
High-Steel Bearing Rocker-Long (mm)	37.4	0.60	104.2	0.55	136.1	0.59	186.6	0.65
High-Steel Bearing Rocker-Tran (mm)	6.0	0.25	20.0	0.25	40.0	0.47	186.6	0.65
Low-Steel Bearing Fixed-Long (mm)	6.0	0.25	20.0	0.25	40.0	0.47	186.6	0.65
Low-Steel Bearing Fixed-Tran (mm)	6.0	0.25	20.0	0.25	40.0	0.47	186.6	0.65
Low-Steel Bearing Sliding-Long (mm)	37.4	0.60	104.2	0.55	136.1	0.59	186.6	0.65
Low-Steel Bearing Sliding-Tran (mm)	6.0	0.25	20.0	0.25	40.0	0.47	186.6	0.65
Elastomeric Bearing Fixed-Long (mm)	28.9	0.60	104.2	0.55	136.1	0.59	186.6	0.65
Elastomeric Bearing Fixed-Tran (mm)	28.8	0.79	90.9	0.68	142.2	0.73	195.0	0.66
Elastomeric Bearing Expan-Long (mm)	28.9	0.60	104.2	0.55	136.1	0.59	186.6	0.65
Elastomeric Bearing Expan-Tran (mm)	28.8	0.79	90.9	0.68	142.2	0.73	195.0	0.66
Abutment-Passive (mm)	37.0	0.46	146.0	0.46	N/A	N/A	N/A	N/A
Abutment-Active (mm)	9.8	0.70	37.9	0.90	77.2	0.85	N/A	N/A
Abutment-Tran (mm)	9.8	0.70	37.9	0.90	77.2	0.85	N/A	N/A

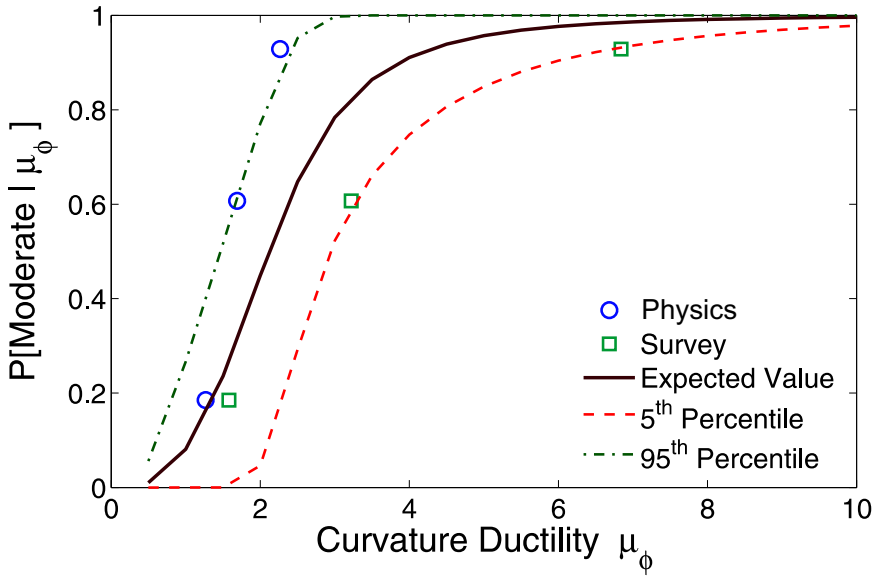

Figure 8-3: Bayesian Updating of Distribution of Moderate Damage State for Columns.

8.3 Bridge Component Fragility Curves

With the probabilistic seismic demand models developed in Chapter 7 and the limit state models developed in the previous section, it is now necessary and possible to generate the fragilities for each of the bridge components. This is done in closed form using Equation 8.2, where S_d is the median of the demand and S_c is the median of the chosen limit state. Following a similar equation manipulation as was done in Equation 7.5, Equation 8.2 can be rewritten as Equation 8.7 for use as component fragilities.

$$P[LS|IM] = \Phi\left(\frac{\ln(IM) - \ln(IM_m)}{\beta_{comp}}\right) \tag{8.7}$$

where $IM_m = \exp\left(\frac{\ln(S_c)-\ln(a)}{b}\right)$ and is defined as the median value of the intensity measure for the chosen limit state (LS) {slight, moderate, extensive, complete}, a and b are the

regression coefficients of the PSDMs and the dispersion component is given as $\beta_{comp} = \frac{\sqrt{\beta_{D|IM}^2 + \beta_c^2}}{b}$.

The component fragility curves for all nine bridge types are generated and presented in tabular form in Appendix G. Based on the findings of Chapter 7, the fragility curves are generated for the case where PGA is the intensity measure. Although they have no practical application for a region wide analysis, the fragility curves which utilize the spectral acceleration at the geometric mean of the bridge's first two periods (S_{a-gm}), are also presented for completeness. This is to provide some basis for comparison and further motivation for the selection of PGA as the appropriate intensity measure.

The component fragility curves do provide information about the components which are most susceptible to ground shaking. For example, Figure 8-4 shows the fragility curves for five components of the MSSS Steel girder bridge subjected to the Rix and Fernandez ground motions. The fragility curves are provided for two limit states (slight, extensive) to illustrate the component screening. As seen, the steel expansion and fixed bearings appear to be the most vulnerable components of this bridge type at the slight damage state. The columns are the next most vulnerable component followed by the transverse response of the bearings. The abutments are not shown in the figure to facilitate clarity but examination of Table G-29 shows the abutments to be the least vulnerable components. This trend also holds for the extensive damage state as seen in Figure 8-4(a).

8.4 Bridge Fragility Curves for As-Built Bridges

As mentioned in Chapter 7, component fragility curves are useful only to the extent that they help to highlight the weak links in an overall bridge system. They can also be helpful in

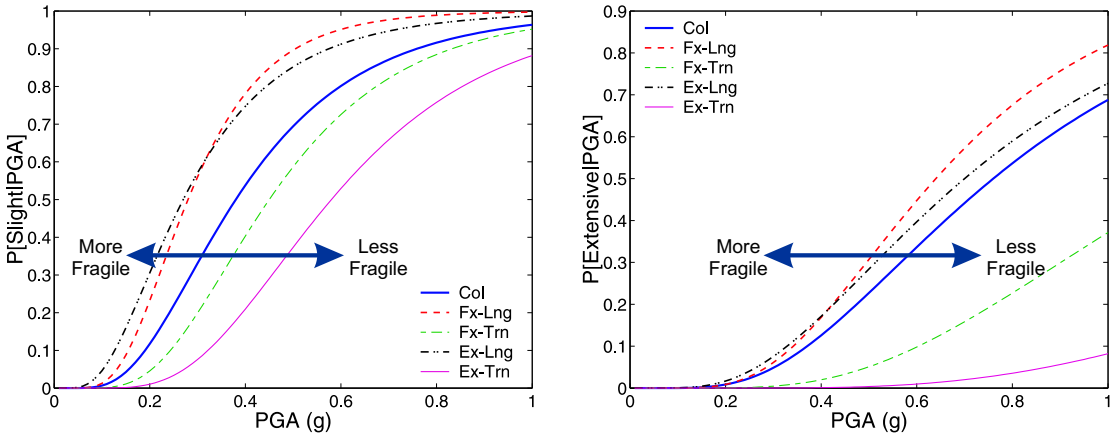

8-4(a): **8-4(b):**

Figure 8-4: Fragility Curves for Select Components of the MSSS Steel Girder Bridge Using Rix Ground Motions (a) Slight Damage (b) Extensive Damage.

choosing appropriate retrofit strategies. It is necessary, however, that system (bridge) wide fragilities be provided for use in loss estimation packages. The following sections propose a method for generating system fragilities using joint probabilistic seismic demand models and then present the bridge system fragilities derived in this study.

8.4.1 Combining Component Fragility Curves

One method for creating system level fragility curves is to use the seismic demand models developed for the various bridge components – as developed in 7. These models can then be convolved with the individual component limit state distributions.

As shown in Figure 8-5, once the n^{th} order joint probability density function, that describes the probabilistic seismic demand on the bridge is obtained, one must integrate it over all possible failure domains – domains which describe the designated limit states. This integration will result in the probability of failure for that particular system at a given value of the intensity measure. Depending on the complexity of the system and the number

of possible failure domains, performing this integration in closed form can be troublesome if not impossible. Another possibility is to perform this integration using numerical techniques. One particularly straight forward and simple numerical technique available for this task is Monte Carlo simulation.

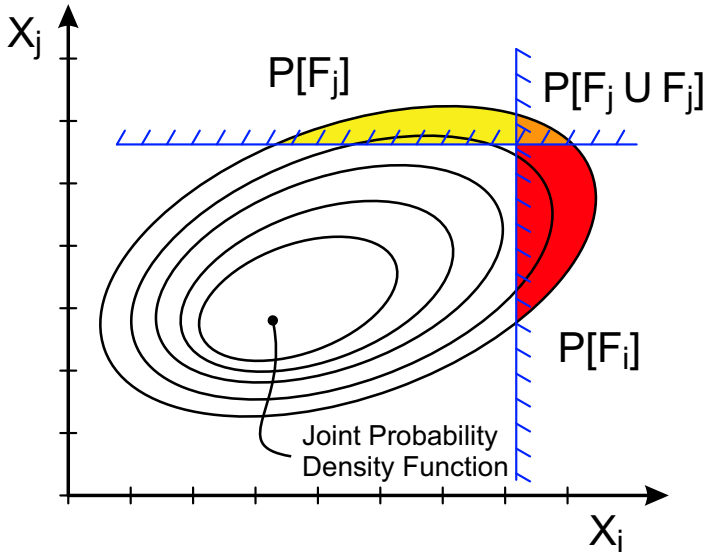

Figure 8-5: Bi-Variate Joint Probability Density Function Integrated Over All Failure Domains.

Monte Carlo simulation is a process in which *N* random samples are generated from the subject probability distributions. This is done for both the demand side and the capacity side. The paired realizations of these distributions are compared and evaluated for failure. Tracking of the system failure is accomplished through the use of an indicator function. The indicator function for the two dimensional case shown in Figure 8-5 is given in Equation 8.8.

$$I_F = \begin{cases} 1 & \text{if } (x_i, x_j) \in \mathrm{F}_{ij} \\ 0 & \text{if } (x_i, x_j) \notin \mathrm{F}_{ij} \end{cases} \tag{8.8}$$

where x_i and x_j are realizations of the i^{th} and j^{th} distributions and F_{ij} is defined by the i^{th} and j^{th} limit state.

The probability of being in the selected limit at a given value of the intensity measure ($P[LS|IM = a]$), is estimated by Equation 8.9

$$P[LS|IM = a] = \frac{\sum_{i=1}^{N} I_{F_i}}{N} \tag{8.9}$$

This numerical integration scheme is carried out for a reasonable range of the selected IM. The resulting probabilities are recognized as approximations to the CDF of the underlying distribution. Therefore, a simple linear regression is carried out to estimate the two parameters of the lognormal distribution. The resulting form matches that of Equation 8.7. An illustration of the creation of the CDF is given in Figure 8-6. An example of component and system fragility curves is given in Figure 8-7. This illustration is provided to show that the system as a whole is more fragile than any single component and thus justifies the procedures followed in this study.

An important note about the sampling of the demand and capacity distributions must be made. The correlation between the demands placed on the various bridge components must be incorporated into the sampling, as pointed out in Chapter 7. However, one must also take care when sampling on the four limit states for any given component. The numerical samples for each limit state must rank in the same order as their underlying limit states. This is to say that the sampled capacities (c) must satisfy $c_{slight} < c_{moderate} < c_{extensive} < c_{complete}$.

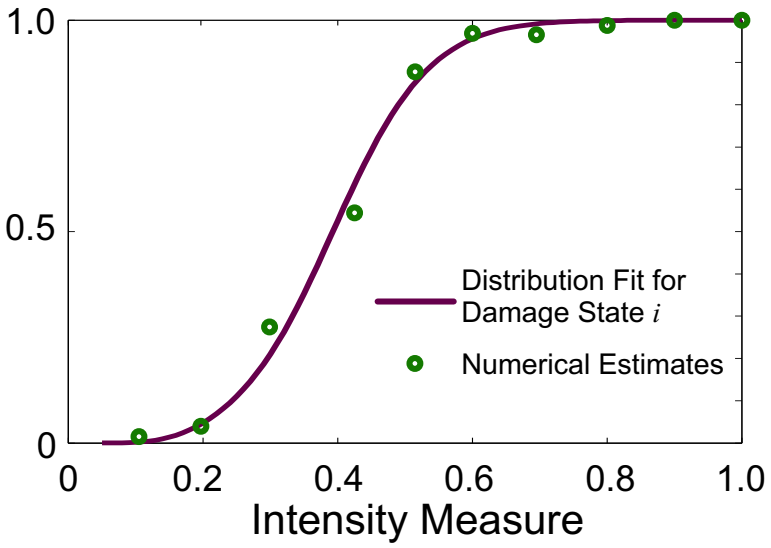

Figure 8-6: Illustration of Probability Distribution Estimation.

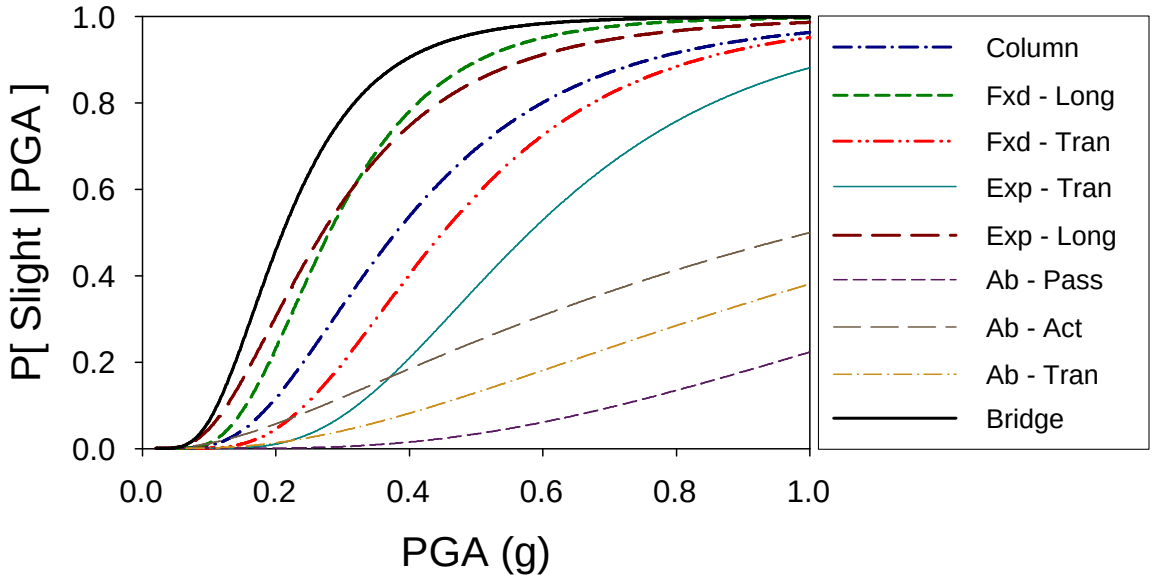

Figure 8-7: Component and System Fragility Curves for MSSS Steel Girder Bridge with Slight Damage.

This condition is simply accomplished by enforcing a 100 percent correlation between the limit states of a particular component.

8.4.2 Ground Motion Dependent Bridge System Fragility Curves

Following the methodology laid out in the previous section, the bridge system fragility curves are generated for the nine classes of bridges considered in this study. The fragility curves are presented for two different intensity measures (PGA, S_{a-gm}) and for two different ground motion suites (Rix, Wen). Tables 8-10 and 8-11 present the median PGAs and dispersions (β_{comp}) for the Rix and Wen ground motion suites respectively. Tables 8-12 and 8-13 give the same information for S_{a-gm} as the intensity measure.

Table 8-10: System Fragilities for Nine Bridge Types – PGA (Rix).

	Slight		Moderate		Extensive		Complete	
Bridge	**Med (g)**	**Disp**	**Med (g)**	**Disp**	**Med (g)**	**Disp**	**Med (g)**	**Disp**
MSC Concrete	0.13	0.91	0.53	0.69	0.75	0.68	1.04	0.71
MSC Slab	0.21	0.75	0.65	0.81	1.24	0.78	3.92	0.80
MSC Steel	0.14	0.50	0.25	0.45	0.32	0.48	0.40	0.49
MSSS Concrete	0.19	0.68	0.57	0.62	0.83	0.65	1.18	0.68
MSSS Concrete-Bx	0.26	0.77	0.80	0.80	1.49	0.80	3.27	0.83
MSSS Slab	0.19	0.81	0.54	0.79	1.00	0.78	2.40	0.81
MSSS Steel	0.21	0.49	0.39	0.45	0.50	0.47	0.70	0.51
SS Concrete	1.13	1.03	5.54	1.13	[a]99.00	0.00	[a]99.00	0.00
SS Steel	0.72	0.62	1.35	0.61	1.79	0.60	2.61	0.57

[a] Estimated medians larger than 6.0 g are reported as 99.00 as estimates this far beyond the regression limits have little meaning.

A closer look at the specific numbers presented in these tables is conducted in later sections. It is first necessary to look at some of the factors which affect these fragility curves before a final set of fragility curves is proposed.

Table 8-11: System Fragilities for Nine Bridge Types – PGA (Wen).

	Slight		Moderate		Extensive		Complete	
Bridge	**Med (g)**	**Disp**	**Med (g)**	**Disp**	**Med (g)**	**Disp**	**Med (g)**	**Disp**
MSC Concrete	0.17	0.75	0.53	0.65	0.74	0.62	0.99	0.62
MSC Slab	0.15	0.65	0.37	0.69	0.60	0.65	1.37	0.65
MSC Steel	0.24	0.53	0.41	0.49	0.51	0.52	0.63	0.53
MSSS Concrete	0.22	0.77	0.70	0.73	1.01	0.72	1.40	0.73
MSSS Concrete-Bx	0.19	0.74	0.59	0.80	1.14	0.79	3.51	0.82
MSSS Slab	0.16	0.76	0.48	0.72	0.84	0.68	1.58	0.60
MSSS Steel	0.27	0.49	0.51	0.43	0.66	0.46	1.00	0.50
SS Concrete	0.35	0.85	1.33	0.86	1.83	0.87	2.50	0.90
SS Steel	0.56	0.61	1.02	0.61	1.37	0.62	2.57	0.62

Table 8-12: System Fragilities for Nine Bridge Types – S_{a-gm} (Rix).

	Slight		Moderate		Extensive		Complete	
Bridge	**Med (g)**	**Disp**	**Med (g)**	**Disp**	**Med (g)**	**Disp**	**Med (g)**	**Disp**
MSC Concrete	0.28	0.88	1.08	0.69	1.55	0.70	2.16	0.69
MSC Slab	0.37	0.65	0.99	0.71	1.74	0.69	4.59	0.72
MSC Steel	0.29	0.62	0.53	0.57	0.67	0.60	0.86	0.64
MSSS Concrete	0.39	0.64	1.08	0.59	1.55	0.62	2.14	0.64
MSSS Concrete-Bx	0.42	0.60	1.09	0.61	1.83	0.61	3.62	0.62
MSSS Slab	0.35	0.67	0.95	0.70	1.67	0.69	3.70	0.72
MSSS Steel	0.38	0.52	0.70	0.48	0.88	0.50	1.27	0.57
SS Concrete	1.64	0.79	6.30	0.84	99.00	0.00	99.00	0.00
SS Steel	0.97	0.50	1.70	0.49	2.22	0.50	3.34	0.47

Table 8-13: System Fragilities for Nine Bridge Types – S_{a-gm} (Wen).

	Slight		Moderate		Extensive		Complete	
Bridge	**Med (g)**	**Disp**	**Med (g)**	**Disp**	**Med (g)**	**Disp**	**Med (g)**	**Disp**
MSC Concrete	0.13	1.12	0.82	1.06	1.52	1.05	2.65	1.05
MSC Slab	0.19	0.87	0.68	0.92	1.37	0.89	4.00	0.84
MSC Steel	0.26	0.88	0.69	0.84	1.02	0.86	1.51	0.87
MSSS Concrete	0.18	1.12	1.22	1.10	2.21	1.11	3.79	1.12
MSSS Concrete-Bx	0.27	1.09	1.52	1.21	3.81	1.18	99.00	0.00
MSSS Slab	0.19	1.13	1.01	1.10	2.23	1.03	5.04	0.80
MSSS Steel	0.44	0.66	1.16	0.61	1.70	0.65	3.27	0.70
SS Concrete	0.59	1.67	6.18	1.64	99.00	0.00	99.00	0.00
SS Steel	2.07	1.47	6.29	1.46	99.00	0.00	99.00	0.00

8.5 Impact of Ground Motion Suite on Fragility Curves

The analytical approach to generating seismic fragility curves using nonlinear time history analysis requires the assembly of a suite of ground motions appropriate for the region. As outlined in Chapter 3, two suites of synthetic ground motions were assembled for the CSUS. Ideally, one would hope that the fragility curves derived from each suite of ground motions would be nominally identical. However, the fragility curve estimates appear to be dependent on the ground motion suite selected. Figure 8-8 compares the medians of the system fragility curves for four representative bridges subjected to the two different ground motion suites where the IM of choice is PGA. Table 8-14 presents the percent difference between the medians.

Table 8-14: Percent Difference of Fragility Medians Derived From Different Ground Motion Suites.

	Percent Difference			
Damage State	**MSC Concrete**	**MSC Steel**	**MSSS Concrete**	**MSSS Steel**
Slight	24%	42%	14%	22%
Moderate	0%	39%	19%	24%
Extensive	1%	37%	18%	24%
Complete	5%	37%	16%	30%

It is seen for the MSC Concrete girder bridge that there is relatively little difference in the calculated medians. The slight damage state for this bridge shows a difference of 24 percent, yet five percent is the largest difference for the other three damage states. This apparent matching of medians does not hold for the other three bridge types highlighted in Table 8-14. The differences between the medians of the MSSS Concrete and MSSS Steel

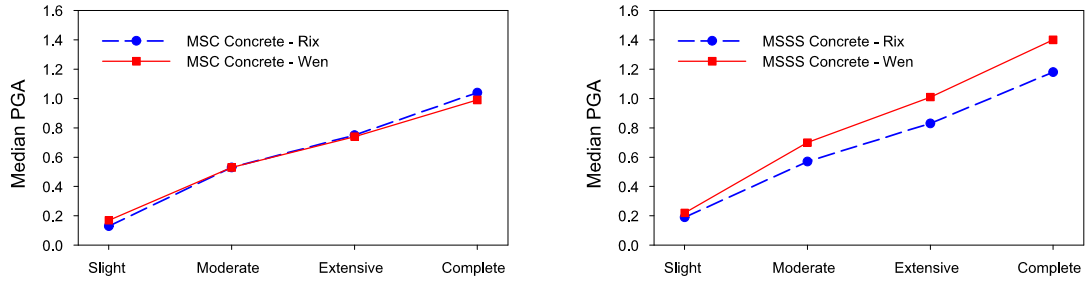

8-8(a):

8-8(b):

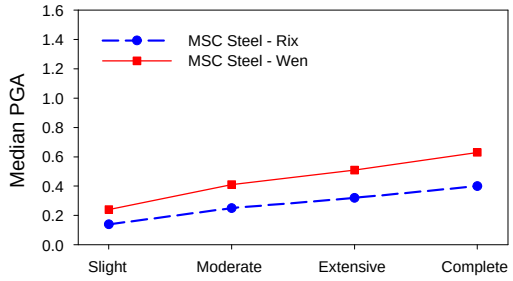

8-8(c):

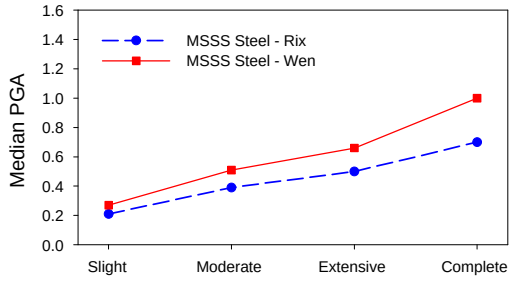

8-8(d):

Figure 8-8: Median Values of Fragility Curves Which are Ground Motion Specific (a) MSC Concrete (b) MSSS Concrete (c) MSC Steel (d) MSSS Steel.

bridges are around 20 to 25 percent while the differences for the MSC Steel bridge are even larger ranging from 37 to 42 percent. One may notice that these percent differences are even larger when S_{a-gm} is selected as the intensity measure. Thus, another motivation for using PGA is discovered.

With the observed dependence of fragility curves on the selected ground motion suite, one may ask which of the fragility curves in Tables 8-10 through 8-11 is correct. There is no evidence that would show preference of one set of fragility curves over another, thus making each set equally plausible. Therefore, it is proposed, that for the this study, both sets of fragility curves be combined to create a new set. In this way the influence of both sets of ground motions is incorporated.

8.5.1 Fragility Curve Combination

The effects of both suites of ground motions can be incorporated in a number of different ways. One may go back and modify the the probabilistic seismic demand models and then re-derive the fragility curves or one may combine the current system fragility curves directly. A method which follows the latter option is adopted in this study. A method looking at relative entropy (Kullback-Leibler-information) was introduced by Pulkkinen (1993). They showed that for N two-parameter lognormal distributions of equal weight, the new parameters of the aggregated lognormal distribution are calculated by Equations 8.10 and 8.11.

$$x_{m-agg} = \exp\left[\left(\sum_{i=1}^{N}\frac{1}{\zeta_i^2}\right)^{-1}\sum_{i=1}^{N}\frac{\ln x_{m-i}}{\zeta_i^2}\right] \tag{8.10}$$

$$\zeta_{agg} = \sqrt{N\left(\sum_{i=1}^{N}\frac{1}{\zeta_i^2}\right)^{-1}} \tag{8.11}$$

where x_{m-i} is the median value for the i^{th} distribution, ζ_i is the logarithmic standard deviation of the i^{th} distribution, x_{m-agg} and ζ_{agg} is the median and lognormal standard deviation of the aggregated distribution respectively. This method is implemented to aggregate the distributions from the two ground motion suites which results in the fragility curves presented in Tables 8-15 and 8-16. It should be noted that the fragility curves for the SS Concrete bridge are the same values as those for the Wen ground motions. This is because those derived from the Rix suite appear to be unreasonable.

Table 8-15: System Fragilities for Nine Bridge Types – PGA (Combined).

	Slight		Moderate		Extensive		Complete	
Bridge	**Med (g)**	**Disp**	**Med (g)**	**Disp**	**Med (g)**	**Disp**	**Med (g)**	**Disp**
MSC Concrete	0.16	0.81	0.53	0.67	0.75	0.65	1.01	0.66
MSC Slab	0.17	0.70	0.49	0.74	0.86	0.70	2.39	0.71
MSC Steel	0.19	0.51	0.32	0.47	0.41	0.50	0.51	0.51
MSSS Concrete	0.20	0.72	0.63	0.67	0.91	0.68	1.28	0.70
MSSS Concrete-Bx	0.22	0.76	0.69	0.80	1.31	0.79	3.39	0.82
MSSS Slab	0.17	0.79	0.51	0.76	0.91	0.72	1.87	0.68
MSSS Steel	0.24	0.49	0.45	0.44	0.58	0.47	0.85	0.50
SS Concrete	0.35	0.85	1.33	0.86	1.83	0.87	2.50	0.90
SS Steel	0.64	0.61	1.19	0.61	1.59	0.61	2.59	0.59

8.5.2 Proposed Bridge Fragility Curves

Looking at the bridge fragility curves in HAZUS, one may notice that only one dispersion is given for all damage states for all bridges (FEMA, 2003). The motivation is to simplify the dissemination of information. After looking at the dispersions listed in Tables 8-15

Table 8-16: System Fragilities for Nine Bridge Types – S_{a-gm} (Combined).

	Slight		Moderate		Extensive		Complete	
Bridge	**Med (g)**	**Disp**	**Med (g)**	**Disp**	**Med (g)**	**Disp**	**Med (g)**	**Disp**
MSC Concrete	0.22	0.98	1.00	0.82	1.54	0.82	2.31	0.82
MSC Slab	0.30	0.73	0.88	0.80	1.60	0.77	4.34	0.77
MSC Steel	0.28	0.71	0.58	0.67	0.79	0.69	1.09	0.73
MSSS Concrete	0.34	0.79	1.11	0.73	1.71	0.76	2.55	0.79
MSSS Concrete-Bx	0.38	0.74	1.18	0.77	2.25	0.77	6.86	0.82
MSSS Slab	0.31	0.81	0.97	0.84	1.84	0.81	4.30	0.76
MSSS Steel	0.41	0.57	0.87	0.53	1.18	0.56	2.07	0.63
SS Concrete	1.45	1.01	6.28	1.05	99.00	0.00	99.00	0.00
SS Steel	1.09	0.67	2.17	0.66	3.17	0.66	6.65	0.65

and 8-16, it is determined that this simplification is justified for each bridge. For example, the dispersions for the MSC Slab bridge for the slight through complete damage are calculated to be 0.70, 0.74, 0.70 and 0.71 respectively. Therefore, it is reasonable to assign a dispersion of 0.70 to all damage states of the MSC Slab bridge. Unlike HAZUS, this simplification does not appear to be appropriate going from one bridge type to another. The final proposed fragility curves for all nine bridge types, using PGA as the IM, are given in Table 8-17. The plots of these curves are subsequently given in Figures 8-9 through 8-11.

Table 8-17: Final Proposed System Fragilities for Nine Bridge Types – *PGA*.

	Median PGA Values (g)				
Bridge	**Slight**	**Moderate**	**Extensive**	**Complete**	**Dispersion**
MSC Concrete	0.16	0.53	0.75	1.01	0.7
MSC Slab	0.17	0.49	0.86	2.39	0.7
MSC Steel	0.19	0.32	0.41	0.51	0.5
MSSS Concrete	0.2	0.63	0.91	1.28	0.7
MSSS Concrete-Bx	0.22	0.69	1.31	3.39	0.8
MSSS Slab	0.17	0.51	0.91	1.87	0.8
MSSS Steel	0.24	0.45	0.58	0.85	0.5
SS Concrete	0.35	1.33	1.83	2.5	0.9
SS Steel	0.64	1.19	1.59	2.59	0.6

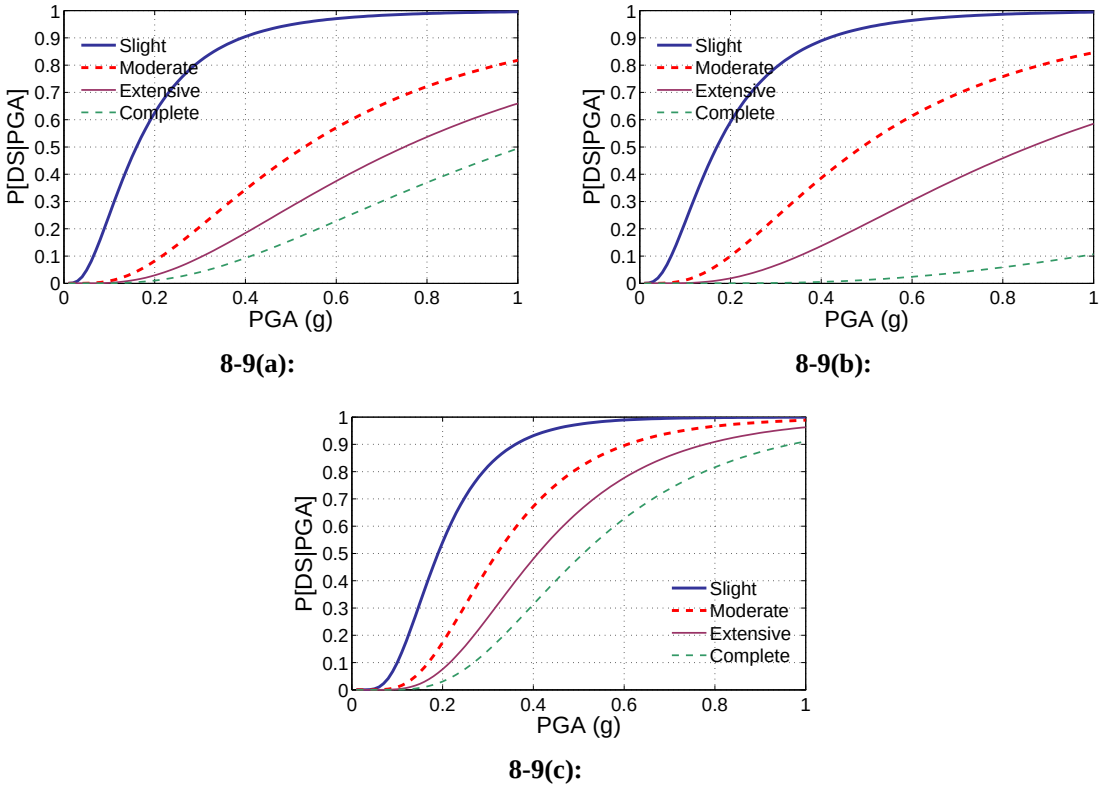

Figure 8-9: Proposed Fragility Curves for Three Multi-Span Continuous Bridge Classes (a) MSC Concrete (b) MSC Slab (c) MSC Steel.

The single span bridges appear to be the least vulnerable of all the bridge types considered. This appears to be the findings of other researchers as well (Basoz and Kiremidjian, 1999; Choi, 2002). A more complete comparison is facilitated by looking at just the medians of the various bridge types. Figure 8-12 compares the median values of all the multi-span bridges at each damage state.

Clearly in Figure 8-12, it is seen that the MSC Steel girder bridge is the most vulnerable of all bridge types. The columns and the steel rocker bearings appear to be the cause of this phenomenon. The deterministic response of the MSC Steel girder bridge, as discussed in

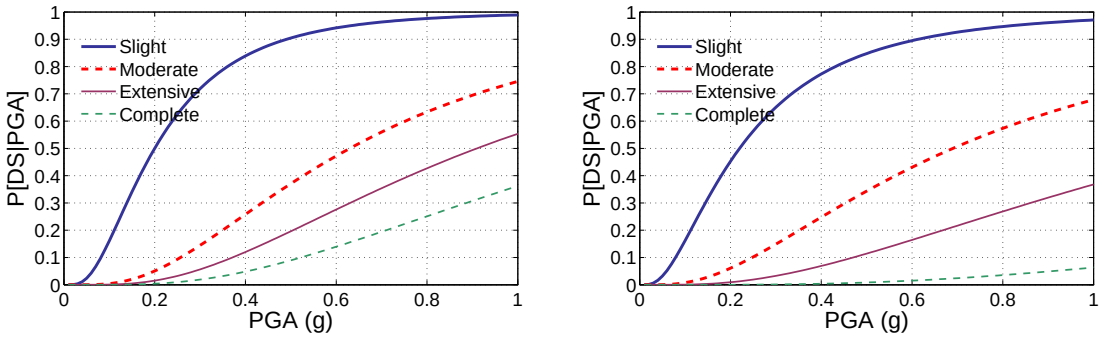

8-10(a): **8-10(b):**

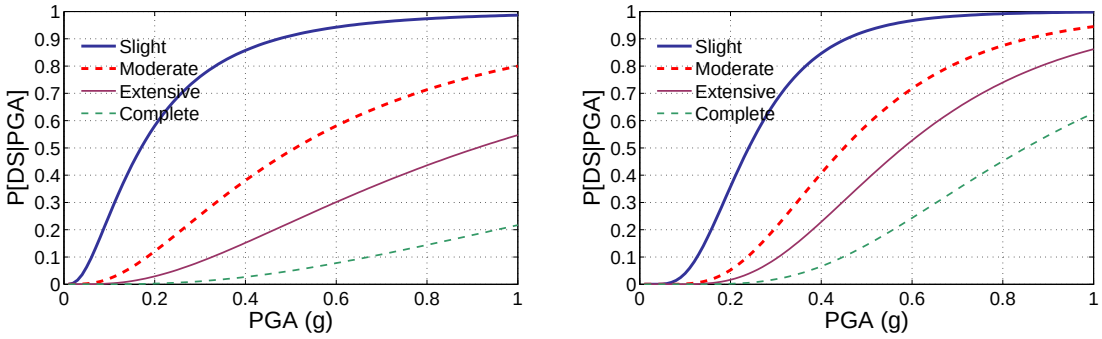

8-10(c): **8-10(d):**

Figure 8-10: Proposed Fragility Curves for Four Multi-Span Simply Supported Bridge Classes (a) MSSS Concrete (b) MSSS Concrete-Box (c) MSSS Slab (d) MSSS Steel.

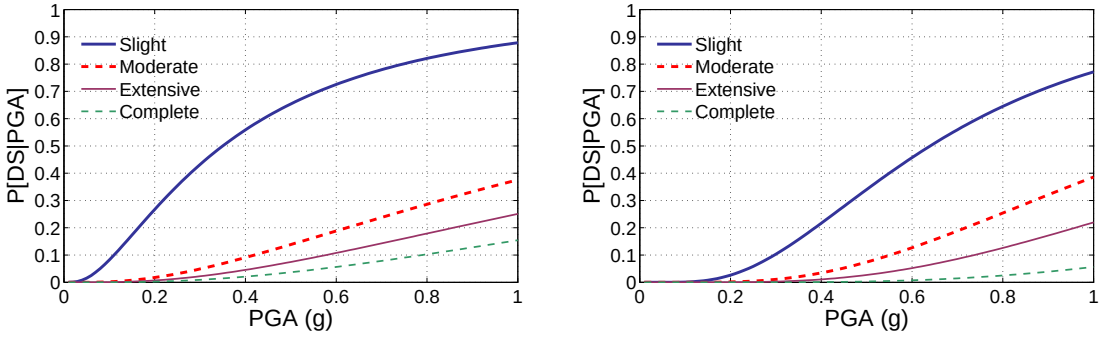

8-11(a): **8-11(b):**

Figure 8-11: Proposed Fragility Curves for Two Single Span Bridge Classes (a) SS Concrete (b) SS Steel.

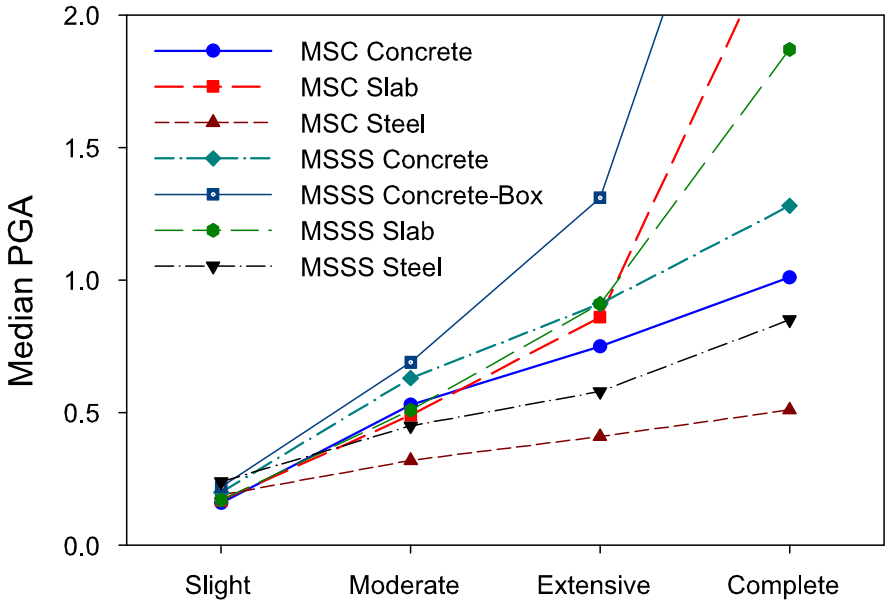

Figure 8-12: Comparison of Median PGA Values for Multi-Span Bridge Fragilities.

Chapter 5, showed that the majority of the longitudinal displacement of the bridge decks was due to deformation in these two components.

The second most fragile bridge is the MSSS Steel girder bridge. Once again the steel bearings – both fixed and rocker – influence the system fragility the most, followed closely by the columns. This trend with the steel bearings is expected because past experience has shown the steel bearings to be highly susceptible to seismic damage (Mander et al., 1996).

The MSC Concrete, MSC Slab and MSSS Slab bridges have very similar fragilities for the first two damage states. At the extensive and especially for the complete damage state, the slab bridges appear to be less vulnerable than the continuous concrete bridge. This phenomenon is due largely to the nature of the elastomeric bearings which are used. For the slab bridges and also the concrete-box girder bridge, very large thin elastomeric

pads are used, giving them large stiffnesses. The effect this has is to place the deformation demand on the abutments and the columns instead of the bearings thereby reducing the possibility of unseating.

8.6 Fragility Curve Comparison

In this section the fragility curves proposed as part of this study are compared with data from two sources. The first comparison conducted is with the fragility curves currently used by HAZUS. The second comparison is to empirical fragility curves developed from bridge damage resulting from the 1994 Northridge earthquake.

8.6.1 HAZUS Fragility Curve Comparison

The fragility curves which are currently used in HAZUS-MH were developed using the nonlinear static methodology discussed in Chapter 2. The underlying work for these fragility curves is presented in the work by Mander and Basoz (1999). These fragility curves were developed such that the information out of the National Bridge Inventory is all that is required for evaluation. The motivation is the recognition that any additional information for the bridges in a region would be very difficult to obtain. Thus, as with the fragility curves developed in this study, HAZUS' fragility curves are not applicable to a single bridge. The intent is that they be used for suites of bridges.

It is interesting to note that when the work is presented by Mander and Basoz (1999), the fragility curves are given in terms of median PGA. However, the same values are reported as median spectral accelerations at one second (S_{a-1}) in HAZUS (FEMA, 2003). The motive behind this shift is not altogether clear but is likely based on an assumption that the PGA is an approximation of the S_{a-1}.

The recommended dispersion values for all bridges, in the work by Mander and Basoz (1999), is 0.6 but this is changed to 0.4 in HAZUS (FEMA, 2003). It is believed that this adjustment is based on the belief that spectral intensity measures tend to reduce the dispersion. However as was already shown in Chapter 7 this is not necessarily the case when suites of bridges with varying periods are considered. The range of the dispersions developed in this study range from 0.5 to 0.9 with the majority being 0.7. In general, these dispersions are larger if spectral intensity measures are used. Hence, this supports more strongly the dispersion of 0.6 as was originally published.

The actual comparisons performed here are given in terms of the median PGA values. Table 8-18 shows the median values of the fragility curves from this study along with the fragility curves from Mander/HAZUS which are adjusted to represent three span bridges (see (Mander and Basoz, 1999)).

Graphical representations of the median comparisons for all nine sets of fragility curves are presented in Figures 8-13 through 8-15. Some obvious trends that are recognized from these figures is that the proposed fragility curves for the continuous span bridges are consistently more fragile than those proposed by HAZUS. However, in the case of the multi-span simply supported bridges, the HAZUS curves are consistently more fragile than the proposed curves. This trend seems to hold for the single span bridges as well.

The median values for the MSSS Steel girder bridge appear to compare the best, as seen in Figure 8-14(d). One of the reasons there is a discrepancy for the other MSSS bridge types, is that HAZUS assigns the same set of fragility curves to all MSSS bridges, regardless of their construction material. It is seen in Figure 8-14(a) that the concrete version of this bridge is less vulnerable than the steel one. This is largely due to the known

Table 8-18: Median Values of Proposed and HAZUS Fragility Curves – PGA.

Bridge	Source	Median PGA Values (g)			
		Slight	**Moderate**	**Extensive**	**Complete**
MSC Concrete	Proposed	0.16	0.53	0.75	1.01
	HAZUS	0.60	0.88	1.17	1.53
MSC Slab	Proposed	0.17	0.49	0.86	2.39
	HAZUS	0.60	0.88	1.17	1.53
MSC Steel	Proposed	0.19	0.32	0.41	0.51
	HAZUS	0.76	0.77	0.77	1.06
MSSS Concrete	Proposed	0.20	0.63	0.91	1.28
	HAZUS	0.26	0.39	0.50	0.73
MSSS Concrete-Box	Proposed	0.22	0.69	1.31	3.39
	HAZUS	0.26	0.39	0.50	0.73
MSSS Slab	Proposed	0.17	0.51	0.91	1.87
	HAZUS	0.26	0.39	0.50	0.73
MSSS Steel	Proposed	0.24	0.45	0.58	0.85
	HAZUS	0.26	0.39	0.48	0.72
SS Concrete	Proposed	0.35	1.33	1.83	2.50
	HAZUS	0.80	0.90	1.10	1.60
SS Steel	Proposed	0.64	1.19	1.59	2.59
	HAZUS	0.80	0.90	1.10	1.60

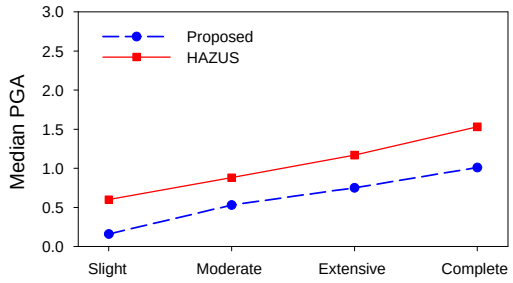

8-13(a): MSC Concrete

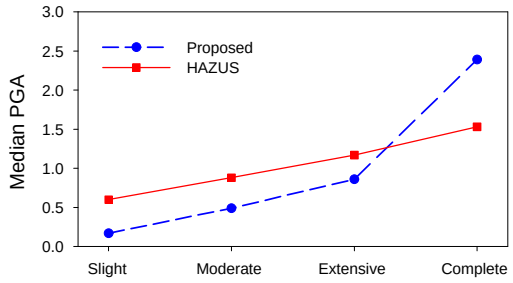

8-13(b): MSC Slab

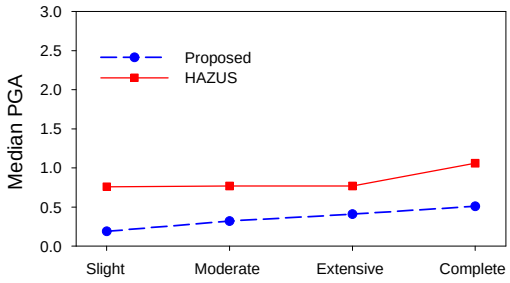

8-13(c): MSC Steel

Figure 8-13: Median Comparison of Proposed and HAZUS Fragility Curves for Multi-Span Continuous Bridge Classes.

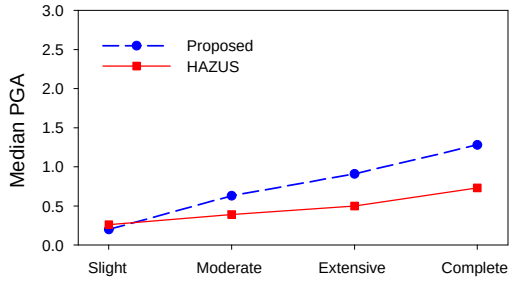

8-14(a): MSSS Concrete

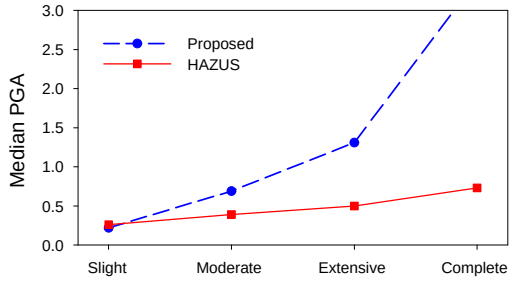

8-14(b): MSSS Concrete-Box

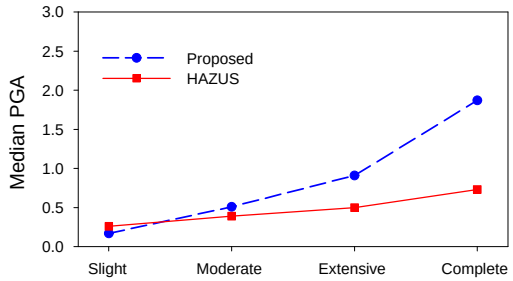

8-14(c): MSSS Slab

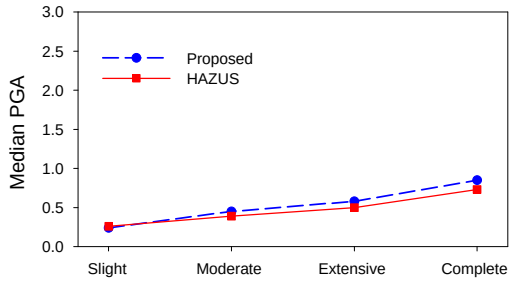

8-14(d): MSSS Steel

Figure 8-14: Median Comparison of Proposed and HAZUS Fragility Curves for Multi-Span Simply Supported Bridge Classes.

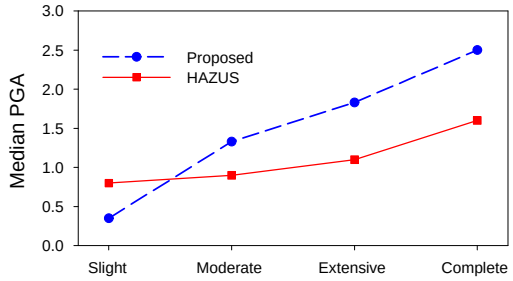

8-15(a): SS Concrete

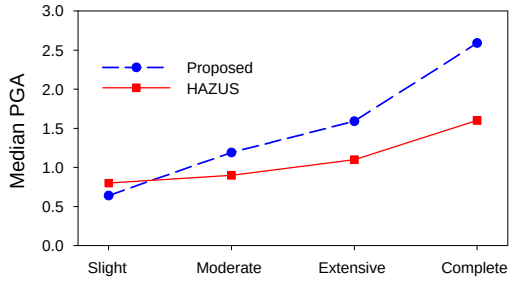

8-15(b): SS Steel

Figure 8-15: Median Comparison of Proposed and HAZUS Fragility Curves for Single Span Bridge Classes.

fragility of steel bearings. Looking at the concrete-box and slab bridges it is seen that the blanket fragility assigned by HAZUS is even less appropriate. Once again the largest factor for this difference is the types of bearings used in these bridge types.

As pointed out for the continuous span bridges, the proposed fragility curves are more fragile than those from HAZUS. The general cause for this discrepancy is with the responses of the concrete columns. The continuous nature of the bridges makes the superstructure more stiff than their simply supported counterparts, which often places less demand on the bearings. However, it is noticed in this study that the continuous nature of the bridges cause an increase in the demand placed on the substructure, including the columns and abutments. There are larger forces at the abutments due to pounding in these bridge types which is unaccounted for in static procedures like those used for HAZUS.

8.6.2 Empirical Fragility Curves

When a set of analytical fragility curves is developed, it is useful to validate them using damage data from previous earthquakes. This is most easily done by comparing the analytical fragility curves with empirical fragility curves. Following the 1994 Northridge California earthquake, Basoz and Kiremidjian (1997) compiled bridge damage data from which they developed empirical fragility curves, the results of which are presented in Tables 8-19 and 8-20 for two PGA intensity maps. The nature of these fragility curves does not lend itself to validation of the fragility curves proposed in this study – the reasoning for which will be provided hereafter. However, a comparison of similar bridge types is conducted to give some reference point for the proposed curves.

Table 8-19: Empirical Bridge Fragility Curves Based on Northridge Earthquake - (WCFS) (Basoz and Kiremidjian, 1997).

Bridge				Minor		Moderate		Major		Collapse	
Category	Abutment type	Pier type	Span cont.	Med(g)	Disp	Med(g)	Disp	Med(g)	Disp	Med(g)	Disp
C1S2	non-monolithic	N/A	N/A	0.80	0.67	0.80	0.67	1.21	0.66	-	-
C1M7	non-monolithic	multiple	continuous	0.39	0.34	0.43	0.31	0.63	0.23	0.82	0.25
C1M8	non-monolithic	multiple	discontinuous	0.32	0.46	0.32	0.46	0.38	0.41	-	-

Table 8-20: Empirical Bridge Fragility Curves Based on Northridge Earthquake - (USGS) (Basoz and Kiremidjian, 1997).

Bridge				Minor		Moderate		Major		Collapse	
Category	Abutment type	Pier type	Span cont.	Med(g)	Disp	Med(g)	Disp	Med(g)	Disp	Med(g)	Disp
C1S2	non-monolithic	N/A	N/A	0.99	0.51	0.99	0.51	1.40	0.49	-	-
C1M7	non-monolithic	multiple	continuous	0.73	0.55	0.85	0.52	1.66	0.51	3.18	0.62
C1M8	non-monolithic	multiple	discontinuous	0.58	0.91	0.58	0.91	0.79	0.83	-	-

8.6.2.1 Northridge Bridge Damage

During the 1994 Northridge earthquake 233 bridges were damaged. Of these damaged bridges, more than 85 percent of them were concrete bridges ranging from slab type to pre-cast box girder type bridges. Approximately one-third of these damaged bridges were seismically designed as per the post-1971 seismic codes. The damage states assigned to these bridges varied widely depending on the inspector (Basoz and Kiremidjian, 1997).

As mentioned previously, these empirical fragility curves are believed to not be appropriate for validation of the fragility curves proposed in this study. Basoz and Kiremidjian (1997) indicated that it is very difficult to get enough damaged bridges for each bridge type in each intensity range, a problem which was also highlighted by Shinozuka (1998). Therefore, bridge types must be aggregated to deal with this problem. For instance all multi-span continuous bridges with monolithic abutments and multi-column bents were aggregated. There was no discrimination regarding material type, thus treating steel, slab, box and concrete bridges alike.

Other factors which make using these fragility curves difficult are as follows. The empirical fragility curves are for California type bridges, whereas the proposed analytical curves are specific to the inventory of the CSUS. Also, the number of spans, skew and design consideration (seismic, non-seismic) is not clear for the empirical curves. However, the proposed curves were generated for very specific cases which allow for implementation in loss assessment programs.

Finally, there is a great degree of uncertainty pertaining to the actual PGA intensities felt by each bridge. Two different shaking intensity maps were used. One came from the

US Geological Survey (USGS) and the other came from Woodward-Clyde Federal Services (WCFS). The highest PGA value at any site for any bridge was 1.55 g and 0.66 g for USGS and WCFS respectively (Basoz and Kiremidjian, 1997). This disparity is significant and makes it difficult to build confidence in the information.

8.6.2.2 Empirical and Proposed Fragility Curves Compared

In spite of the apparent disconnects between the two, the empirical fragility curves are compared to the proposed analytical fragility curves. Figures 8-16, 8-17 and 8-18 compare the median values of the MSC, MSSS and SS bridges respectively. The empirical curves for each source of shaking intensity is provided. Once again, one may see the degree of disagreement for the two sets of empirical curves. It should also be noted that the steel type bridges are not compared because of their generalized absence in the damaged bridge inventory.

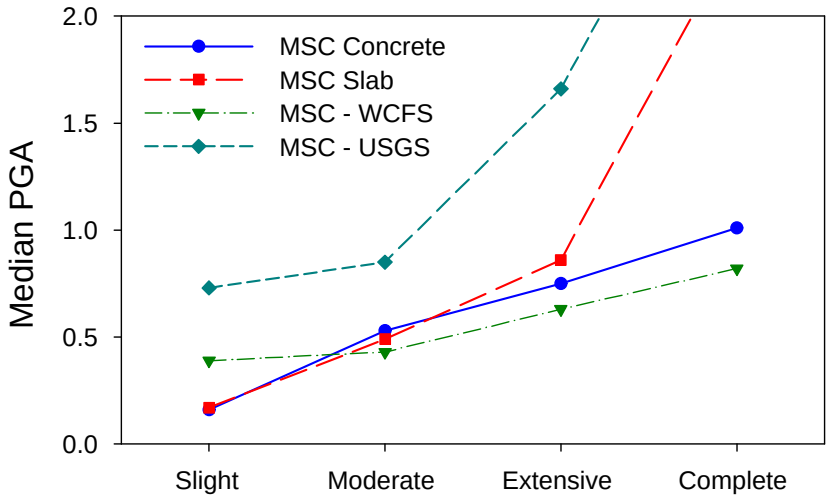

Figure 8-16: Median Comparison of Proposed and Empirical Northridge Fragility Curves for MSC Bridge Classes.

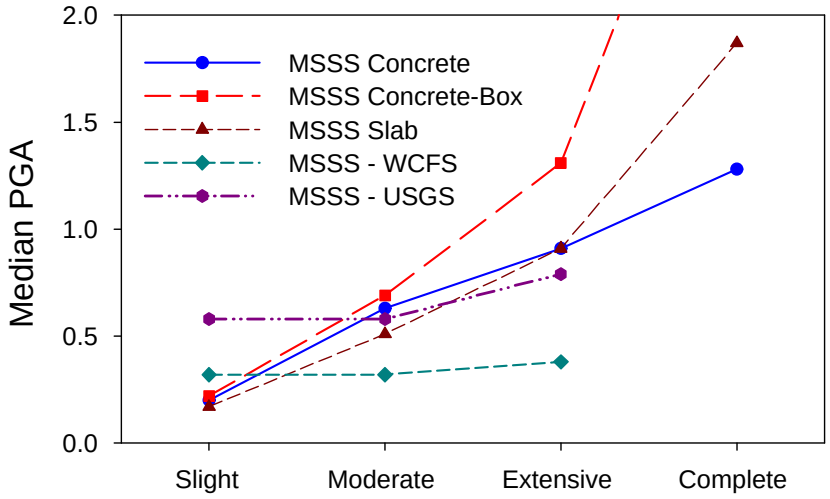

Figure 8-17: Median Comparison of Proposed and Empirical Northridge Fragility Curves for MSSS Bridge Classes.

Figure 8-16 shows that there is a relatively good agreement between the proposed MSC concrete and slab bridges and the WCFS bridges for the Moderate and Extensive damage states. For the slight damage state, both empirical curves show that the analytical curves may over estimate the bridge fragilities.

In the case of the MSSS bridges, the second and third damage states appear to agree well with the USGS fragility curves. Once again, the analytical fragility curves appear to overestimate the fragility at slight damage and underestimate at complete damage.

For the SS Concrete bridge, both the USGS and WCFS give lower median values for the moderate and extensive damage states. This is a very difficult result to interpret because no knowledge is possessed pertaining to the inventory make-up of the damaged bridges. One of the results of this study is a recognition that the shorter the length of a single span

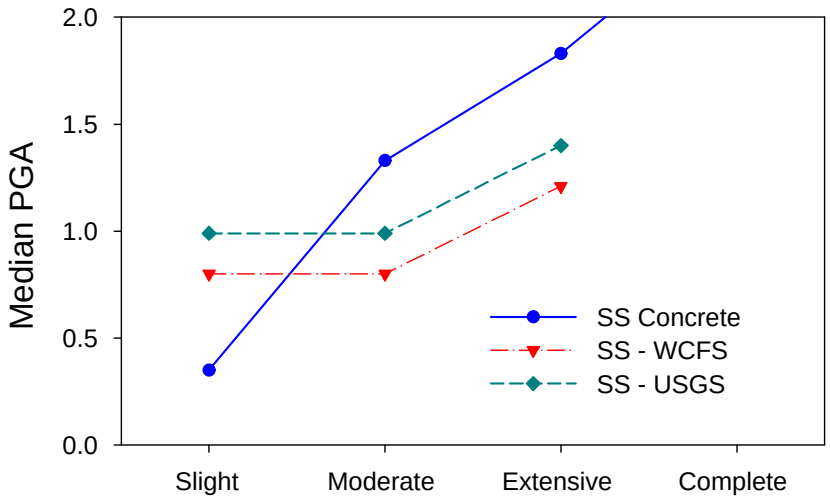

Figure 8-18: Median Comparison of Proposed and Empirical Northridge Fragility Curves for SS Bridge Classes.

bridge, the less vulnerable to ground shaking it becomes. The inventory of the CSUS shows a tendency of span lengths to the shorter side and thus explains why the analytical results show low vulnerabilities. The span length distribution for single span concrete bridges in the California inventory is likely not the same and would result in different findings.

In general, the proposed fragility curves follow the general trend of the empirically derived curves. This lends some measure of confidence to the curves developed in this study.

8.7 Closure

In this Chapter, seismic fragility curves are generated for nine classes of bridges common to the CSUS. These fragility curves are developed considering the entire inventory of the

region and are therefore appropriate only on a regional scale. Applying them to a single bridge is inappropriate because of the generalized bridge details required in this study.

These fragility curves were developed using the probabilistic seismic demand models created in Chapter 7 and the limit states set forth in this chapter. Using Monte Carlo simulation, the system (bridge) wide fragility were created by integrating over all failure domains and including all components of each bridge. The most fragile bridge types appear to be the steel bridges. This is largely due to the seismic vulnerability of the steel bearings used in steel bridges. As suspected, the concrete columns also proved to be significant contributors to the overall bridge fragilities.

In general, the continuous span bridges appear to be more fragile than their simply supported counter parts. This is somewhat surprising since pounding and unseating are larger concerns in the simply supported bridges. A reasonable explanation for this phenomenon is that the non-seismically detailed columns have a lot more demand placed on them in continuous bridges. Also, pounding and unseating are still a problem in continuous bridges but it is restricted to the regions around the abutments.

Of all the bridge types, the single span bridges appear to be the least vulnerable. This is in agreement with the findings of other similar studies (Basoz and Kiremidjian, 1999; Choi, 2002).

The following is a brief summary of the findings in this chapter.

- The selection of ground motion suite plays a significant role in the calculated fragility values. One reason for this is the difference in frequency content of the ground motion suites (see Chapter 3).

- HAZUS fragility curves compared well with the results of this study for the MSSS Steel girder bridge type. For the other bridge types, HAZUS has either higher or lower median values. It was noticed that this relationship depended on the selected damage state. Also, the dispersions calculated in this study tend to be larger than those assumed by HAZUS.

- The general trends of these fragility curves are consistent with the findings from the 1994 Northridge earthquake. Additional conclusions are difficult to draw because of the courseness and variability of the earthquake damage records.

CHAPTER IX

SUMMARY, CONCLUSIONS AND IMPACT

9.1 Summary and Conclusions

Prior to the 1990's, little consideration was given to the seismic design and detailing of highway bridges located in the Central and Southeastern United States (CSUS). This lack of attention to seismic design was due to an underestimation of the seismic hazard in the CSUS. Therefore, there are a large number of highway bridges that are vulnerable to seismic loads. The main objective of this study was to assess these vulnerabilities using a probabilistic framework. Considering both the uncertainty from the hazard and the uncertainty from the capacity of the bridges, seismic fragility curves are developed. The approach used in this study also considers the inherent variability present in each bridge class found in the CSUS.

Other studies have been conducted which developed fragility curves for specific bridges in the CSUS. However, none have treated the entire inventory in the region as was done in this study. Furthermore, not only does this study present fragility curves for many typical bridge classes, but also provides a customized frame work which may be used for further investigation of other bridge types which include the effects of retrofit strategies.

One of the first tasks of this study was to assemble some representation of the seismic hazard in the CSUS. This was accomplished through the compilation of two separate suites of synthetic ground motions which are specific to the region. Unfortunately, each time

history provided in the ground motion suites only contained a single component of the representative ground motion. Since the work in this study utilized 3-D analytical models it was required that each ground motion be represented by two orthogonal components. Thus, a methodology was proposed and implemented to simulate correlated orthogonal ground motion components from each existing time history.

The assembly of two time history suites allowed for the explicit investigation of the effect of ground motion suite on calculated bridge fragilities. In this study, it was observed that the ground motion suite used does indeed have a recognizable impact on the fragility results. Although the amplitude spectra of the ground motions are believed to play a role in this impact, it is believed that the content of the phase spectra is the major reason for discrepancies. Giving equal weight to the significance of the two ground motion suites used throughout this study, the effects of both were combined into composite bridge fragility curves. While the two assembled suites of ground motions do not cover all of the CSUS, they do contain some variability as to location, soil type/thickness, source models and site amplification models. This type of variability helps to generalize the fragility curves beyond a specific city.

The second major task of the study was to seek an understanding of the highway bridge inventory in the CSUS. This was accomplished through a detailed analysis of the National Bridge Inventory (NBI) database. It was determined that 88 percent of all highway bridges in the region could be assigned to one of nine general bridge classes. The largest of these bridge classes was found to be the multi-span simply supported concrete girder bridge

class, which accounts for approximately 19 percent of all bridges. Other common types include continuous and single span concrete girder bridges and equivalent steel girder bridge classes.

Using statistics of major geometric bridge descriptors, eight representative bridge configurations were developed for each class. Some of these descriptors are span length, deck width and column height. The eight representative bridge configurations were used throughout the remainder of the study accounting for the uncertainty in the inventory.

Three dimensional analytical models of all nine bridge classes were developed. These models were generated to incorporate a high degree of detail in the major bridge components that would lend themselves to act as damage indicators. Deterministic analyses indicated that the majority of the bridge classes were dominated by their fundamental longitudinal mode yet still showed some vulnerabilities under transverse loading.

An investigation of the predominant modeling parameters was carried out using a design-of-experiments framework. The intent of this investigation was to ascertain the impact these modeling parameters had on the response of the bridges and their components. Eight component responses were monitored for each investigation. It was found that different modeling parameters were deemed significant for the various monitored responses. However, there appeared to be a few modeling parameters which had more of a consistent impact on the seismic response of the subject bridges. These parameters include bearing stiffness and friction, abutment stiffness, damping ratio, loading direction and geometric configuration. This finding resulted in these parameters being treated probabilistically during the demand assessment studies.

Seismic demands on each bridge class were quantified through the development of probabilistic seismic demand models (PSDMs). The PSDM for each bridge class was represented in the form of a joint probability distribution function (JPDF) which captures the dependency that exists between the various components of the bridges. These JPDF were developed using a number of different intensity measures which are used to quantify the level of seismic excitation.

One question which has often arisen when developing PSDMs is which ground motion intensity measure should be used. For this reason, four different intensity measures were considered. The intensity measures include peak ground acceleration (PGA), spectral acceleration at the geometric mean of the fundamental period in each primary direction (S_{a-gm}), spectral acceleration at 0.2 seconds (S_{a-02}) and spectral acceleration at 1.0 seconds (S_{a-1}). Past studies have shown the spectral quantities are more ideal than non spectral quantities. However, only a single bridge (structure) with a particular configuration was used for these studies. It was found that when given an entire population of a particular bridge class – with varying dynamic characteristics – PGA appeared to be the most appropriate intensity measure.

The probabilistic seismic demand models were not enough to quantify the vulnerabilities of the various bridges and their components. Not only must demand be known and quantified but the capacities or the ability of the components to handle these demands must be quantified. The capacities or limit states used in this study were derived from a composite of experimental results, physics based assumptions and expert judgment relative to operational impacts.

Convolution of the demands and capacities resulted in the fragility functions of the bridges and their individual components. The multi-span continuous steel girder bridge appears to be the most fragile. This is primarily due to the vulnerability of steel bearings and the large demands placed on inadequate concrete columns. The second most vulnerable of the bridge types is the multi-span simply supported steel girder bridge, where once again the fragility of the steel bearings is significant. This finding is not particularly surprising since the vulnerable nature of the steel bearings has been known for some time (Mander et al., 1996). The bridge types that appear to be the most seismically resistant are the single span bridges. The vulnerabilities of the multi-span concrete bridges are typically not as high as they are for the steel-type bridges. However, their vulnerabilities are generally higher than those for the single span bridges.

Comparison of the proposed fragility curves with those developed for use in HAZUS-MH showed that for multi-span continuous bridges, HAZUS underestimates the bridge fragility. However, when simply supported bridges are considered, HAZUS overestimates the fragility of the bridges. The same holds true for single span bridges as well. This discrepancy is due in part to the generalized nature of HAZUS bridge classes. For example, four of the bridge classes considered in this study would fall into one bridge class for HAZUS. Another possible reason is that HAZUS used a static procedure for fragility curve development, which does not account for all of the dynamic effects in the response.

9.2 Impact

A rigorous methodology was used for the quantification of highway bridge vulnerabilities to seismic loading. This resulted in a number of significant contributions which include:

- Three-dimensional analytical models allowing for the study of the seismic response of the most common bridge types in the Central and Southeastern US.

- A better understanding of the modeling parameters which affect the seismic response of highway bridges, is provided. Two such parameters are the abutment stiffnesses and the bearing stiffnesses. This understanding points to the areas/components which should be further studied.

- The most significant contribution of this study is the development of seismic fragility curves for bridge classes common to the Central and Southeastern United States. These fragility curves, which assess the bridge seismic vulnerabilities, are provided as a direct input into seismic loss assessment packages such as HAZUS-MH, REDARS and MAEViz. This provides decision makers with some of the tools necessary to assess and appropriately address the weaknesses of the nation's transportation infrastructure.

9.3 Recommendations for Future Work

The work in the present study should be extended through additional research in the following areas:

- The effect of skew on the fragility of each bridge type should be investigated. HAZUS-MH currently has an equation providing for the modification of fragility medians to account for pier skew. This equation was developed based on static analyses and thus warrants a more thorough investigation and validation using dynamic analyses.

With 3-D bridge models already developed, incorporating the effects of skew is a straightforward modification to make.

- The effects of the number of spans a bridge has on its fragility should be investigated. The current study focused on three span bridges, as they are the most likely to occur. However, there is still a significant amount of the bridge inventory that does not have three spans. HAZUS-MH currently provides equations for median value modification but they need verification using dynamic approaches.

- Methodologies for the incorporation of liquefaction or ground deformation hazards should be developed. The work in this study considered explicitly the ground shaking hazard, however liquefaction was not considered. There is currently a lack of understanding of how the demands due to this type of hazard are to be assessed.

- Bridges which occur in major freeway interchanges often have a curved superstructure. The fragility of a particular curved bridge may be generated using the procedure laid out in this study. However, the feasibility of accounting for bridge curvature at a regional level must be investigated.

- Studies directed specifically at better understanding and quantifying bridge component capacities should be conducted. Specifically, the work should focus on the mapping of capacities to damage states and the mapping of damage states to losses. For example, limited experiments have been conducted on highway bridge abutments. Therefore, large scale experiments would be useful in generating better analytical

models and understanding the impact of damage on the perceived functionality of a bridge.

- A thorough in-depth study looking at simplified fragility generation methodologies should be conducted. This would require the adaptation of current simplified methodologies to incorporate the effects of all bridge components and not just generalized global bridge responses. If more confidence can be gained in simplified procedures, then larger studies on bridge fragilities will be facilitated.

- An extension of the proposed methodology to consider other hazards should be investigated. In the wake of recent natural and manmade disasters, it has become apparent that this nation's bridges are vulnerable to a number of different hazards.

APPENDIX A

SYNTHETIC GROUND MOTIONS

A.1 Wen and Wu Ground Motions

The methodology that Wen and Wu used in their research follows the procedure proposed by Herrmann and Akinci (1999), which uses a point-source model approach. Using the statistics of occurrence and magnitude information from the 1996 *USGS Open-File Report 96-532* (USGS, 1996), assuming the occurrence time as a Poisson process and that the epicenter location is uniformly distributed within the New Madrid fault zone, events of various magnitudes and distances were simulated for the region. This was done for a 10-year period of time and repeated $9,000$ times. Considering earthquakes with body wave magnitudes greater than or equal to five, $9,260$ events that are within the effective area for Memphis were created. This also resulted in $9,269$ events for Carbondale and $8,290$ events for St. Louis, giving moment magnitudes M_w ranging from 4.5 to 8.

The large number of ground motions generated allowed the authors to construct the uniform hazard response spectra (UHRS) for each of the cities. This is done by using the response spectrum for the individual ground motions, calculating probability distributions for the spectral acceleration at each period and then looking for the desired exceedance probabilities. For a more in-depth description of the procedure used, see (Wen and Wu, 2001).

A.1.1 Single Component Ground Motions

Once the uniform hazard response spectra were generated for each city at various hazard levels, specific ground motion suites were assembled. Using the UHRS for 10% and 2% in 50 years for each city as a baseline, the ten ground motions whose spectra most closely matched, in a least squares sense, were selected for each city and each hazard level. These ten ground motions were selected from amongst the $9,000\pm$ ground motions that were originally generated for each city. The response spectra were evaluated and compared at ten specific periods from 0 to 2 seconds. What resulted was ten ground motions for each of two hazard levels for each city, giving a total of 60 ground motion records. A ground motion time history sample for each city at each of the two hazard levels is presented in Figure A-1.

Amplitude, frequency and duration are parameters which are often used to define strong ground motions. Two of these parameters, namely amplitude and duration, are presented in Table A-1 for the six suites of ground motions. Peak ground acceleration (PGA) is often used to represent the amplitude of the ground motion and thus is presented in the table.

The frequency content of the ground motion suites is best seen through their respective response spectra. Figures A-2 through A-4 show the mean response spectra plus/minus one standard deviation for Carbondale, St. Louis and Memphis respectively at the 10% and 2% in 50 years hazard levels.

The mean response spectra for Memphis and Carbondale are very similar in shape. They both peak around 0.3-0.4 seconds and then taper off slowly as the period increases.

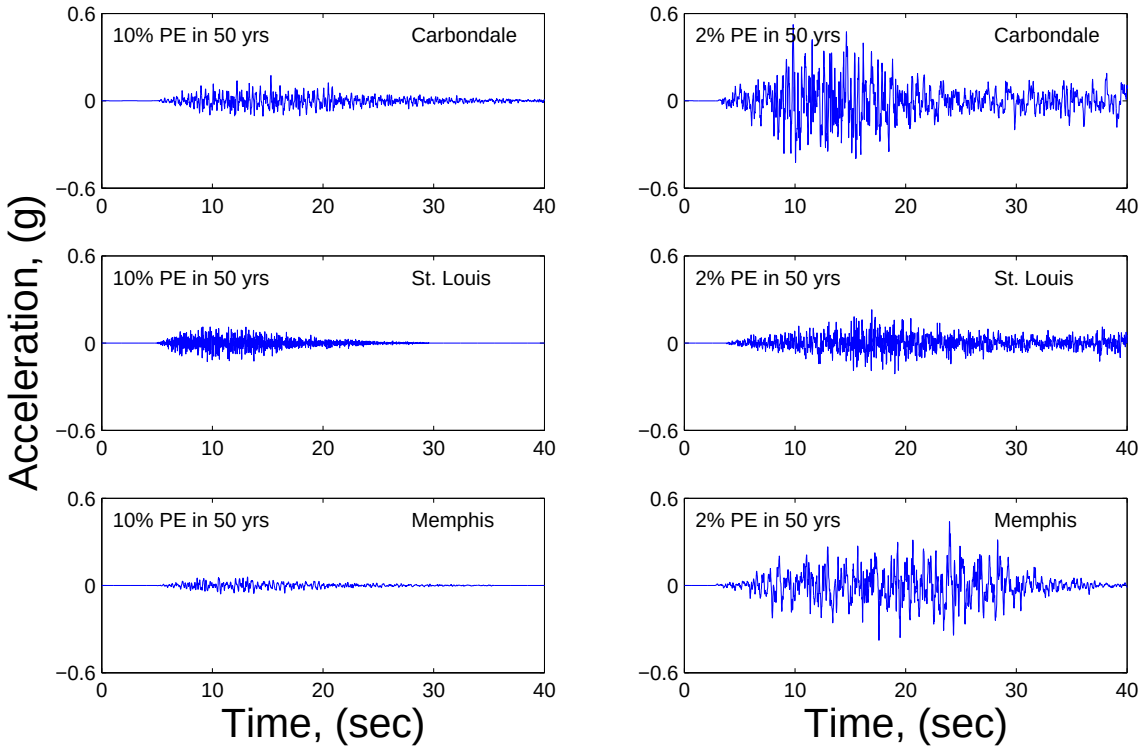

Figure A-1: Representative Time Histories of Ground Motions for 10% and 2% Probability of Exceedance in 50 Years for Carbondale, St. Louis and Memphis.

Table A-1: Mean Values of Ground Motion Parameters for Wen and Wu Suite of Synthetic Ground Motion Records.

Ground Motions for 10 % Probability of Exceedance in 50 Years

	Moment Magnitude (M_w)	Epicentral Distance (km)	Duration (sec)	PGA (g)	T_g (sec)
Carbondale	6.4	122	14.2	0.17	0.16
St. Louis	6.4	193	12.1	0.11	0.17
Memphis	6.4	88	4.4	0.08	0.45

Ground Motions for 2 % Probability of Exceedance in 50 Years

	Moment Magnitude (M_w)	Epicentral Distance (km)	Duration (sec)	PGA (g)	T_g (sec)
Carbondale	8.0	158	59.5	0.51	0.88
St. Louis	7.2	195	31.9	0.33	0.16
Memphis	8.0	151	31.2	0.38	0.99

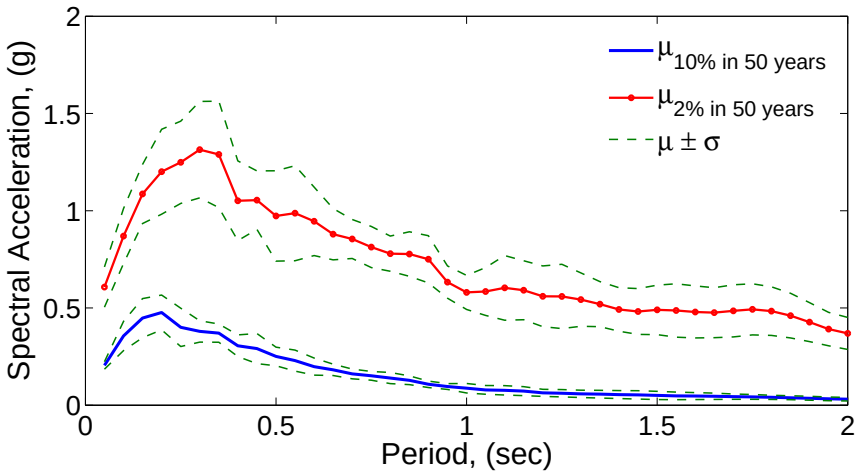

Figure A-2: Mean Response Spectra for 10% and 2% in 50 Years for Carbondale.

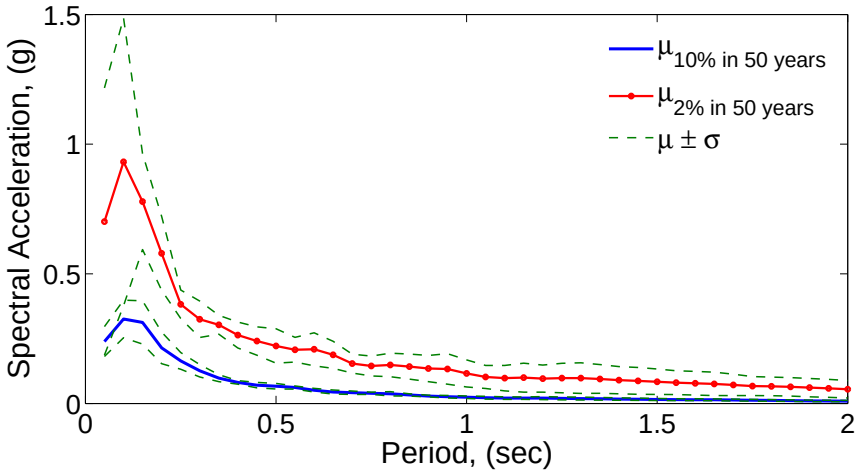

Figure A-3: Mean Response Spectra for 10% and 2% in 50 Years for St. Louis.

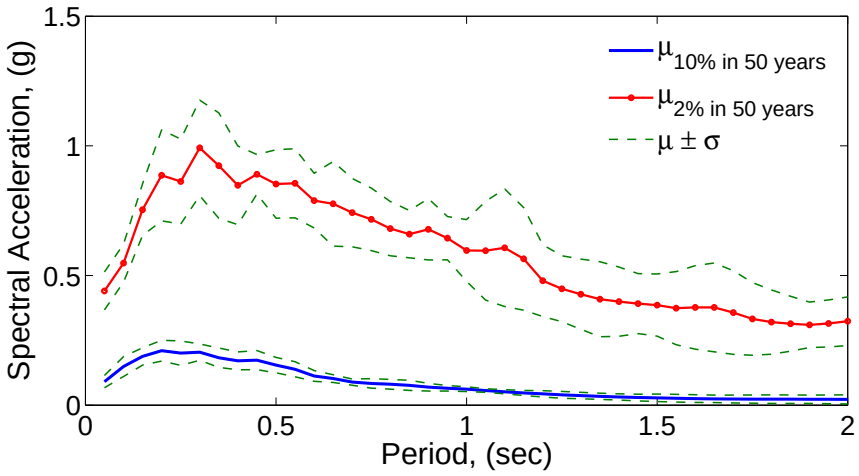

Figure A-4: Mean Response Spectra for 10% and 2% in 50 Years for Memphis.

The main difference between these two cities is that the amplitudes in Carbondale are approximately 30% and 100% greater than those in Memphis for the 2% and 10% in 50 years hazard levels respectively. The mean response spectrum for St. Louis, as seen in Figure A-3, shows that the majority of the energy content for these ground motions lies below 0.2 seconds. This happens to be outside the range in which the fundamental periods of most civil structures fall. Although the peak spectral acceleration values are similar to the other two cities, the frequency content is quite different.

A.1.2 Reduced Ground Motion Suite

A suite of 48 ground motions is needed for use in the probabilistic seismic demand analyses. Of the original ground motion suite, which consists of 60 ground motions (10 for each city-hazard combination), 48 are selected such that a good cross-section of PGA and S_a values is obtained. Therefore, after each of the 60 ground motions is divided into its associated components, eight ground motions are selected from each of the six city-hazard

Table A-2: Original File Names of 48 Seed Ground Motions Used From the 60 Wen and Wu (2001) Ground Motions.

Carbondale		**Memphis**		**St. Louis**	
10% in 50 yrs	2% in 50 yrs	10% in 50 yrs	2% in 50 yrs	10% in 50 yrs	2% in 50 yrs
c10_01s	c02_01s	m10_01s	m02_02s	l10_01s	l02_01s
c10_02s	c02_02s	m10_03s	m02_04s	l10_02s	l02_02s
c10_04s	c02_05s	m10_04s	m02_05s	l10_03s	l02_04s
c10_05s	c02_06s	m10_06s	m02_06s	l10_04s	l02_05s
c10_06s	c02_07s	m10_07s	m02_07s	l10_05s	l02_06s
c10_07s	c02_08s	m10_08s	m02_08s	l10_07s	l02_07s
c10_08s	c02_09s	m10_09s	m02_09s	l10_08s	l02_08s
c10_10s		m10_10s	m02_10s	l10_10s	l02_09s
					l02_10s

bins. Table A-2 gives the file names, as originally published by Wen and Wu (2001), of 48 seed ground motions used .

A.2 Rix and Fernandez Ground Motions

The methodology used by Rix and Fernandez-Leon (2004) to generate this suite of scenario ground motions follows the work done by Drosos (2003) and the procedure outlined in (Boore, 1983). The source models come from the work by Frankel et al. of the USGS (1996). Uncertainties in the source, path and site were incorporated in the Fourier Amplitude spectrum. The phase spectrum, however, contains Gaussian white noise which results in a phase spectrum which may not be representative of a real ground motion. A total of 220 ground motions were generated for three different magnitude levels (5.5, 6.5, 7.5) and four different epicentral distances (10, 20, 50, 100 km). Representative ground motions for the three magnitude levels are presented in Figure A-5.

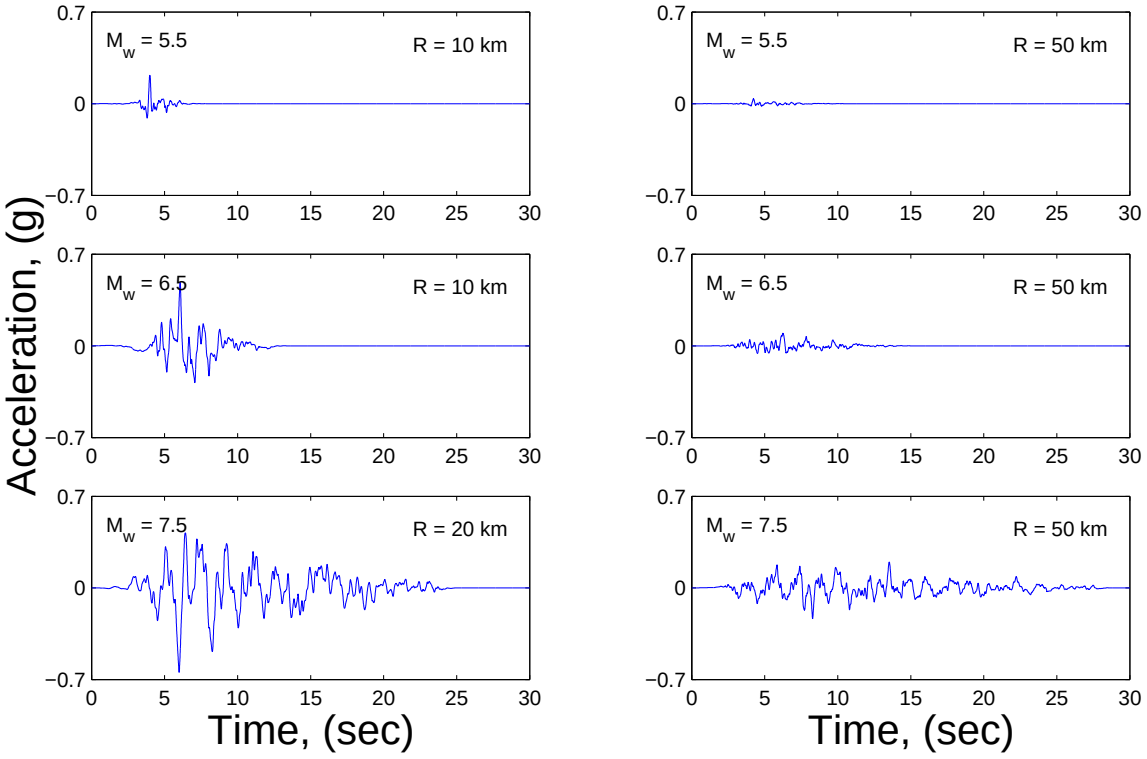

Figure A-5: Representative Time Histories of Ground Motions for M_w 5.5, 6.5 and 7.5 Events (Rix and Fernandez-Leon, 2004).

Table A-3: Original File Numbers of the 48 Seed Ground Motions Selected From the 220 Rix and Fernandez-Leon (2004) Ground Motions.

Epicentral Distance (km)	Magnitude	File Numbers
10	5.5	6, 9 10, 13, 14, 15, 16, 17
	6.5	4, 5, 7, 11, 13, 16, 17, 19
20	5.5	13,15,16,18
	6.5	9, 11, 13, 20
	7.5	2, 6, 10, 12, 16, 17, 18, 20
50	5.5	12, 13, 15, 17
	6.5	8, 9, 13, 17
	7.5	1, 2, 3, 12
100	7.5	4, 6, 12, 18

A.2.1 Reduced Ground Motion Suite

The 220 ground motions were reduced to 48 with the objective of obtaining a well distributed cross-section of PGA and S_a values. Table A-3 gives the record numbers of the files used for each magnitude-distance bin. Table A-4 gives the mean values of PGA, S_{a-02} and duration for the selected ground motions contained in each bin. The durations and peak accelerations for the magnitude 5.5 records are quite small. When intensities are this small the ground motion is not very informative regarding the seismic response of the subject bridge. The ground motion suite should induce responses in the structures ranging from the linear elastic range to the highly nonlinear range, thus allowing for a better description of structural behavior. Therefore, it is not useful to have many low intensity ground motions in the suite. As seen in Table A-3, few ground motions were selected from these small intensity bins while a larger number were selected from the higher intensity bins.

Table A-4: Mean Values of Identifying Properties of Reduced Rix and Fernandez-Leon (2004) Ground Motion Suite.

Epicentral Distance (km)	Magnitude	Mean Values		
		PGA (g)	S_{a-02} (g)	Duration (s)
10	5.5	0.16	0.30	8.19
	6.5	0.44	0.56	13.21
20	5.5	0.09	0.17	8.72
	6.5	0.26	0.37	13.22
	7.5	0.51	0.62	27.16
50	5.5	0.03	0.06	10.72
	6.5	0.09	0.17	16.09
	7.5	0.23	0.34	29.02
100	7.5	0.14	0.22	32.18

APPENDIX B

BRIDGE CLASSIFICATION

To facilitate and simplify the classification of the bridges in the CSUS, ten general bridge types were defined. To accomplish this task, the superstructure material and the superstructure construction types, as listed in the NBI database, where examined. The bridges with similar materials and/or construction types were grouped into the same bridge class. Materials that are similar such as “Concrete Continuous” and “Prestressed Concrete Continuous” were grouped into the more general category of “Continuous Concrete”. Both of these materials produce a superstructure of similar mass and would use similar bearing details. The bridges were also grouped using similar construction types. For example the “Stringer”, “Tee-Beam”, “Floor Girder” and “Channel Beam” were grouped into a more general group called “Girder”. These grouping assignments were made assuming that these construction types would produce structures with similar masses and use similar bearing details. The grouping assignments for each bridge classification used in this study are presented in Figure B-1

Table B-1: Construction Types Listed in NBI (FHWA, 1995a).

Name	Abbreviation	Material	Type	Spans
Multi-Span Continuous Concrete Girder	MSC Concrete	Concrete Continuous Prestressed Concrete Continuous	Stringer Tee-Beam Floor Girder Channel Beam	> 1
Multi-Span Continuous Steel Girder	MSC Steel	Continuous Steel	Stringer Tee-Beam Floor Girder Channel Beam	> 1
Multi-Span Continuous Slab	MSC Slab	Concrete Continuous Prestressed Concrete Continuous	Slab	> 1
Multi-Span Continuous Concrete Box Girder	MSC Concrete-Box	Concrete Continuous Prestressed Concrete Continuous	Box Beam - Multiple	> 1
Multi-Span Simply Supported Concrete Girder	MSSS Concrete	Concrete Prestressed Concrete	Stringer Tee-Beam Floor Girder Channel Beam	> 1
Multi-Span Simply Supported Steel Girder	MSSS Steel	Steel	Stringer Tee-Beam Floor Girder Channel Beam	> 1
Multi-Span Simply Supported Slab	MSSS Slab	Concrete Prestressed Concrete	Slab	> 1
Multi-Span Simply Supported Concrete Box Girder	MSSS Concrete-Box	Concrete Prestressed Concrete	Box Beam - Multiple	> 1
Single-Span Concrete Girder	SS_Concrete	Concrete Prestressed Concrete Concrete Continuous Prestressed Concrete Continuous	Stringer Tee-Beam Floor Girder Channel Beam Slab Box Beam - Multiple	< 2
Single-Span Steel Girder	SS_Steel	Steel Steel Continuous	Stringer Tee-Beam Floor Girder Channel Beam Slab Box Beam - Multiple	< 2

APPENDIX C

ANALYTICAL MODELS OF MAJOR HIGHWAY BRIDGE COMPONENTS

This Appendix is devoted to a discussion of the various components that are typical to the subject bridges. Accompanying this discussion is a presentation of the analytical *O*penSees models used to represent the behavior of the individual components.

C.1 Superstructure

The superstructure of a bridge refers to that portion of the bridge which is located above the bearings. In general, this consists of a set of girders with a thin concrete deck poured on top. The girders and deck are usually constructed such that they operate in composite action.

In this study, the deck elements are modeled using elastic beam column elements. This is because the superstructure is expected to remain linearly elastic under seismic loading. The section properties of each span are calculated for the composite section of the deck and girders – when applicable. The section properties are calculated for each bridge using the axes presented in Figure C-1. The properties are given in Table C-1 for the end spans and middle spans of each bridge. The the concrete bridge section properties are presented for concrete with a modulus of elasticity of 2.78e4 MPa while the steel bridges use a modulus equal to 2.0e5 MPa.

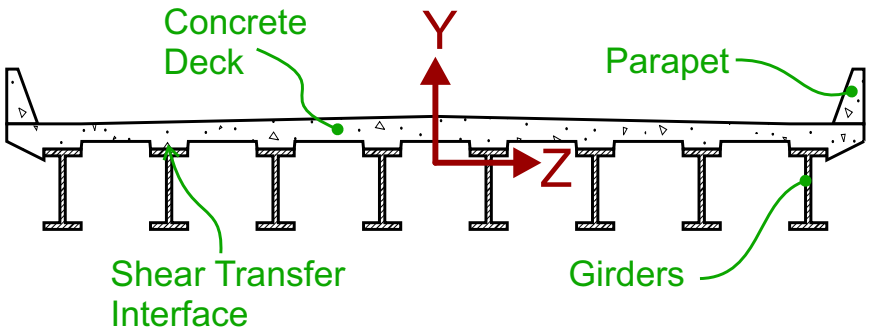

Figure C-1: Schematic of Typical Bridge Superstructure.

It should be noted that the stiffness of the superstructure does not play a significant role in the horizontal seismic response of the bridges whether it be loaded in the longitudinal or transverse direction. This is due to the fact that the composite deck sections are much more stiff than any of the other components and thereby behave much like rigid links. Although the response is not that sensitive to the stiffness, it is sensitive to the mass of the deck. Therefore, great care is given to accurately quantify the mass of each system.

C.2 Analytical Models of Bridge Steel Bearings

A bridge bearing is a mechanical system that permits movement or transfers loads from the superstructure (top) of the bridge to the substructure or support system of the bridge. They are typically responsible for transmitting both vertical and horizontal loads to the substructure. The forces applied to a bridge bearing mainly include superstructure self-weight, traffic loads, wind loads and earthquake loads. They become a significant factor in the overall response and functionality of a bridge before and after loading.

Table C-1: Deck Section Properties for Nine Bridge Class Models Presented in Section 5.2.

Bridge Class	E	End Spans				Main Span			
		I_z	I_y	Area	Weight	I_z	I_y	Area	Weight
	(MPa)	(m^4)	(m^4)	(m^2)	(kN/m)	(m^4)	(m^4)	(m^2)	(kN/m)
MSSS Concrete	2.78E+04	0.119	75.835	3.941	92.8	1.102	103.760	5.407	127.3
MSC Concrete	2.78E+04	0.119	75.835	3.941	92.8	1.102	103.760	5.407	127.3
MSSS Concrete_Box	2.78E+04	0.171	97.449	5.461	128.6	0.523	102.198	5.719	134.7
MSSS Slab	2.78E+04	0.069	35.371	3.523	82.9	0.069	35.371	3.523	82.9
MSC Concrete	2.78E+04	0.069	35.371	3.523	82.9	0.069	35.371	3.523	82.9
MSSS Steel	2.00E+05	0.027	9.776	0.508	39.0	0.113	12.992	0.676	52.0
MSC Steel	2.00E+05	0.236	17.028	0.888	68.3	0.236	17.028	0.888	68.3
SS Concrete	2.78E+04	0.000	0.000	0.000	0.0	0.350	20.528	2.763	65.1
SS Steel	2.00E+05	0.000	0.000	0.000	0.0	0.036	2.548	0.342	26.3

C.2.1 Overview of Steel Bearings

Steel bearings are a particular type of bearing that is commonly used in bridges. They can come in a variety of shapes and sizes but they all serve the same function. These bearings are divided into two main categories, fixed and expansion bearings. The classification is assigned by the type of movement they allow. A fixed bearing only permits rotational movement while an expansion bearing will permit both rotation and horizontal translation.

In the CSUS, there are six basic types of steel bearings used. They include roller, link, sliding, knuckle, leaf and rocker bearings (Choi, 2002). However, of those six types the rocker and sliding bearings were the most commonly used in the CSUS during the 1950's and 1960's (Mander et al., 1996). The high-type bearings have typically been used for bridges with spans greater than 20 m while the low-type bearings were used for bridges with span lengths under 20 m (Dutta, 1999). Figures C-2 and C-3 show the high-type rocker bearings and the low-type sliding bearings respectively.

The basic construction of these bearings attaches a masonry plate to the pier or abutment using anchor bolts. A sole plate is attached to the underside of the steel girders. These two plates are joined so as to enable the desired motions. For example, the low-type fixed bearing uses vertical dowels (pintles) through both the masonry and sole plates to restrict horizontal movement while still maintaining the capacity to rotate.

These bearing types are highly susceptible to corrosion and deterioration. They also have non-ductile properties. As a result, following the 1971 San Fernando earthquake, it was recognized that these types of bearings were highly vulnerable to seismic loading. As a consequence, they are no longer used in the design of new bridges or the renovation of

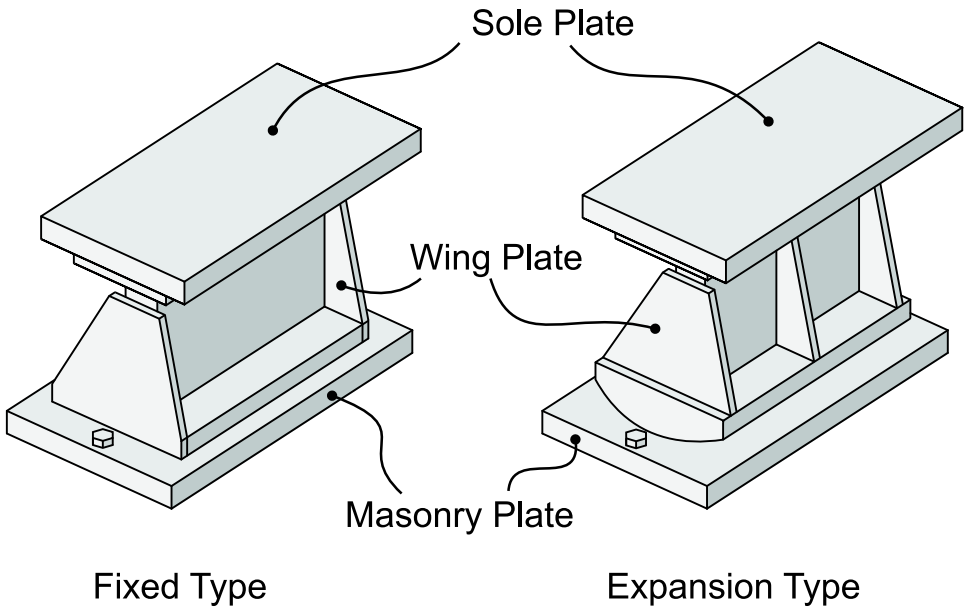

Figure C-2: High-Type Steel Rocker Bearings.

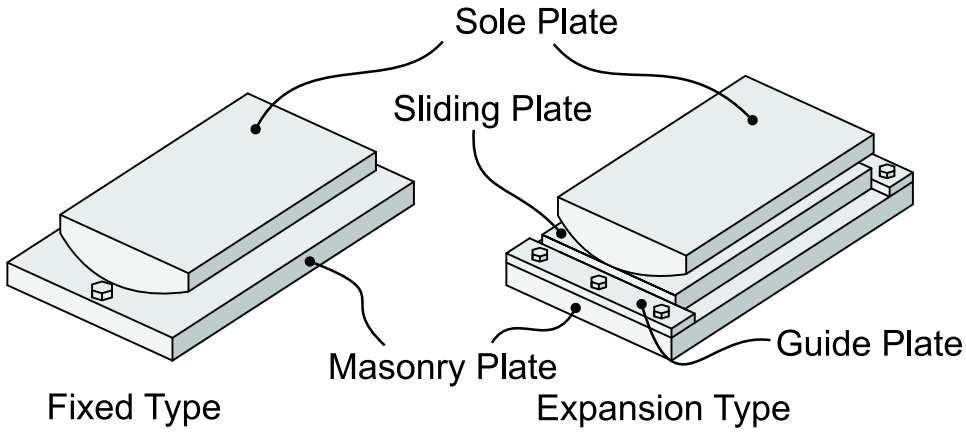

Figure C-3: Low-Type Steel Sliding Bearings.

old ones (Mander et al., 1996). Unfortunately, a very large part of the bridge inventory in the CSUS still has these types of bearings. Therefore, to appropriately model the bridge inventory, it is necessary to develop analytical models for these types of bearings. These bearing types will be used for the steel girder bridges in this study.

The analytical modeling of these bearings was aided greatly by the work of Mander et al. (1996). They fully recognized the need to better understand the response of these bearings to cyclic loading. In their study, they pulled a number of existing bearings from steel girder bridges located in New York and performed cyclic lateral load tests on them (Mander et al., 1996). These tests were performed in both the longitudinal and transverse directions with similar conditions to when they were installed in the bridge. They followed up the testing by proposing non-linear analytical models in Drain-2dx that closely approximate the behavior of each bearing type. These published models have been converted into *O*penSees for use in this study. The following subsections will present the longitudinal and transverse behavior of the high-type and low-type bearings and illustrate the *O*penSees models used to capture this.

C.2.2 High-Type Fixed Bearings

The high-type fixed bearing tests conducted by Mander et al. (1996) were performed under two scenarios. One scenario had the bearings mounted on a steel plate and the other scenario had the bearings mounted on a concrete pedestal. The results of the bearing tested on the concrete pedestal are used in this study because they are believed to better represent the typical conditions in the CSUS.

The bearing associated with this study is presented in Figure C-4. It has a base that is 559 mm wide and 406 mm deep. The overall height of the bearing from concrete pedestal to the bottom of the steel girder is 520 mm.

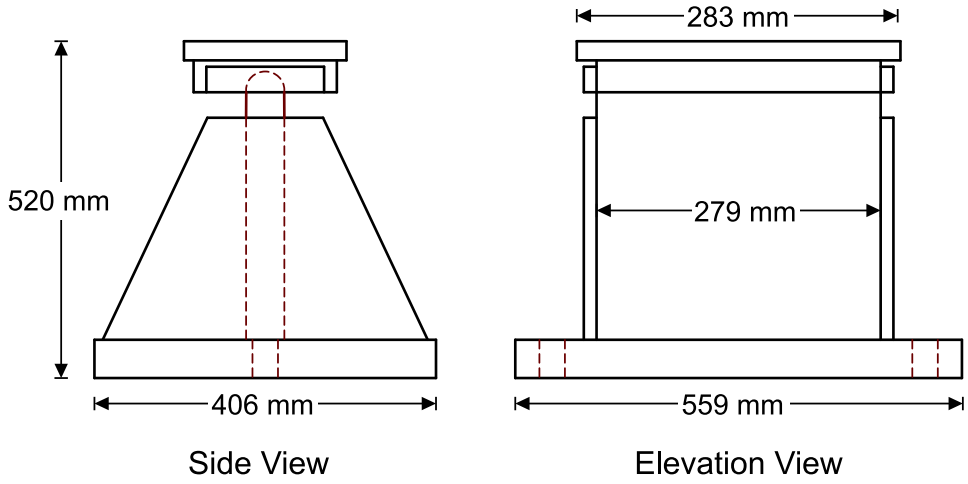

Figure C-4: Dimension of High-Type Fixed Bearing.

C.2.2.1 Longitudinal

The analytical model of the high type fixed bearing presented in Figure C-4 was originally developed by Mander using a number of different elements in Drain-2DX. These elements were a truss element and two link elements placed in parallel. The bilinear truss element was used to model the prying nature of the masonry plate while the link elements were implemented to capture rocking and stiffness degradation. These elements placed in parallel produced a composite element with a total initial elastic stiffness of 179 kN/mm. The *O*penSees model uses materials that are similar in behavior. A *Steel01* material and a *Hysteretic* material are used in parallel to get this composite behavior. Figure C-5 gives

a schematic and graphical description of the two materials used. This material is then assigned to a *zeroLength* element.

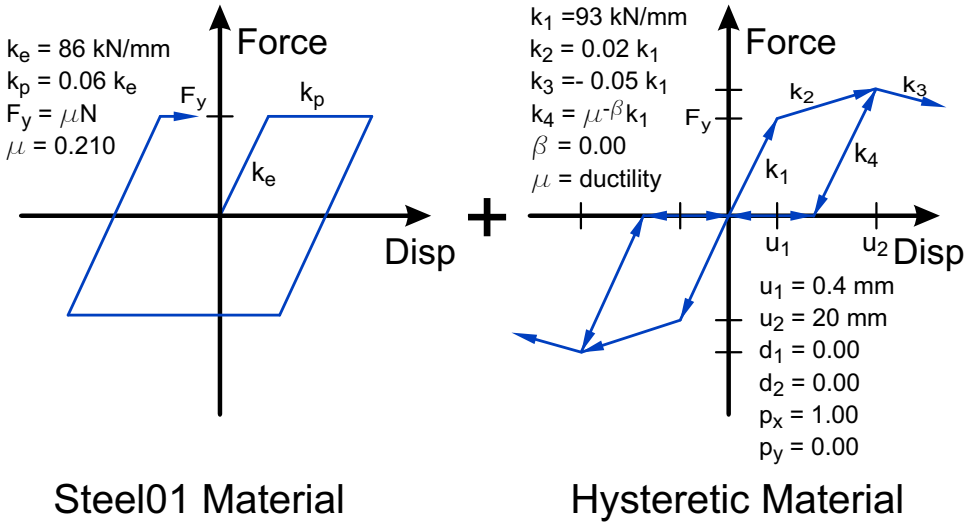

Figure C-5: OpenSees Model of High Type Fixed Bearing in Longitudinal Direction.

The model, as presented in Figure C-5, produces an initial stiffness of 167 kN/mm. The post yield stiffness is approximately 6% of the elastic stiffness. The displacement that occurs at yield is relatively small and is approximately 0.2 mm. The *Hysteretic* material in *O*penSees allows for the unloading stiffness of the material , k_4, to be a function of the deformation ductility, μ. This is written as $k_4 = \mu^{-\beta}k_1$ where $\beta = 0.0$. Pinching factors (p_x, p_y) and damage factors (d_1, d_2) can also be specified. The values used for this study can be found in Figure C-5. Using the experimental results provided by Mander et al., a comparative validation of the analytical model is given in Figure C-6. Although an exact overlay of the experimentally and analytically derived hystereses is desired, it is highly unlikely to be attained. This analytical model approximates well the experimental results

and will therefore be used hereafter. It should be noted that the concrete pedestal on which the bearing is mounted plays a very significant roll in the overall response of the bearing system. It is for this reason that it was included when performing the tests.

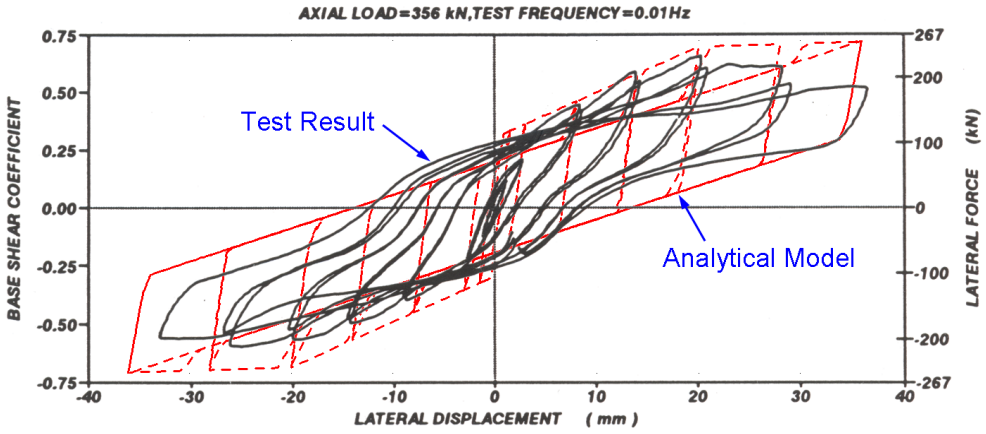

Figure C-6: Response of High Type Fixed Bearing in Longitudinal Direction, Experimental and Analytical (Mander et al., 1996).

C.2.2.2 Transverse

The high-type fixed bearing shown in Figure C-4 was also tested in the transverse direction. This means that the loading the bearing underwent during the experiment was the same it would see if a bridge was loaded in its transverse direction. By testing the bearing in two orthogonal directions, it enables analytical models to be generated with two orthogonal non-linear springs. The steel bearing loaded in the transverse direction exhibited similar behavior to the bearing under longitudinal loading. It saw the same type of prying of the masonry plate and a bending of the anchor bolts.

The modeling for this bearing behavior is accomplished using a bilinear steel material (*Steel01*) and a *Hysteretic* material placed in parallel. This model which closely follows the model proposed by Mander et al is graphically presented in Figure C-7. The bilinear steel material, which has a perfectly plastic range, is used to simulate the sliding of the bearing. The coefficient of friction, μ plays a direct role in determining the force required for sliding to occur. This material has an initial stiffness of 216 kN/mm and a coefficient of friction $\mu = 0.375$. The rocking and degradation are captured through the hysteretic material, which has an initial stiffness $k_1 = 5$ kN/mm.

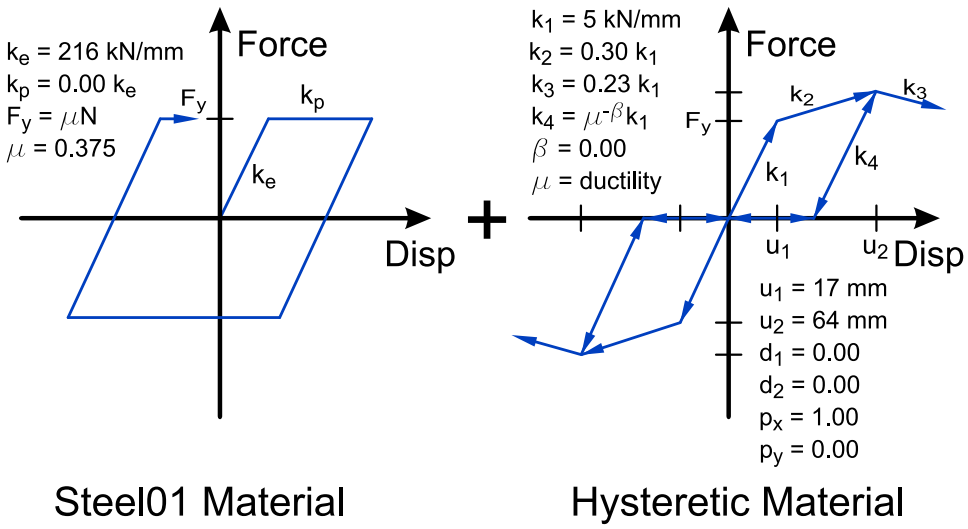

Figure C-7: OpenSees Model of High Type Fixed Bearing in Transverse Direction.

Figure C-8 presents the experimental results of the transverse loading overlain with the analytical results. This shows that the analytical model approximates the experiment reasonably well. Although it does not capture all of the apparent nonlinearities, the analytical model does capture well the pinching of the hysteresis or lack thereof.

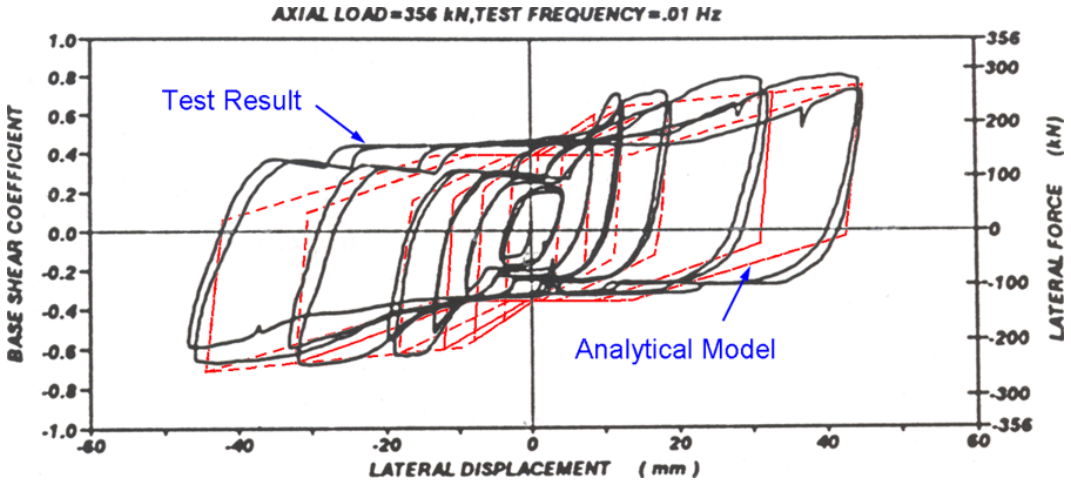

Figure C-8: Response of High Type Fixed Bearing in Transverse Direction, Experimental and Analytical (Mander et al., 1996).

C.2.3 High-Type Rocker Bearings

When the high-type fixed bearings, presented in Figure C-4, are used, they are typically used in conjunction with a rocker-type bearing, as shown in Figure C-9. The base part of the rocker is locked against horizontal translation using pintles or dowels. Thus, the horizontal motion of this expansion type bearing is accommodated through a rocking, rather than a sliding, motion. Although effective in allowing horizontal translations, this bearing type is highly susceptible to instability. As the displacement gets large the bearing has a tendency to topple. This phenomenon can be seen in Figure C-10.

The subject bearing given in Figure C-9 has very similar dimensions as its fixed counterpart. It has a width and depth of 610 mm and 432 mm respectively. The total vertical height is 520 mm.

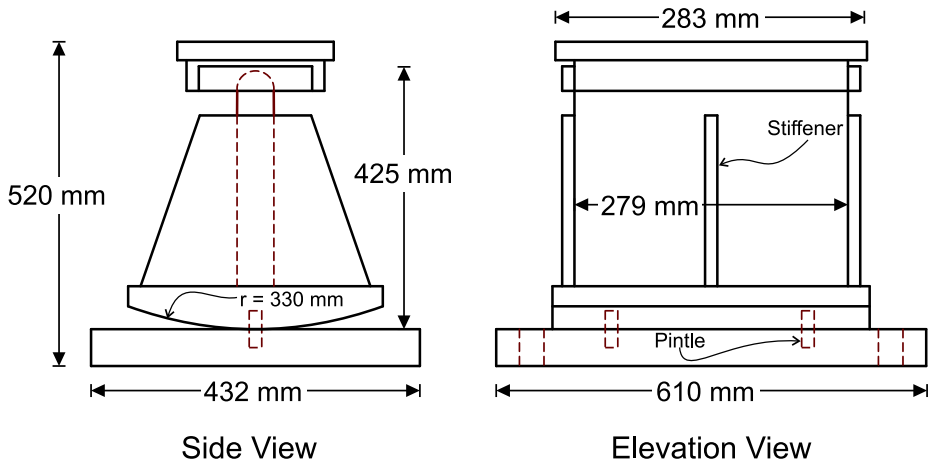

Figure C-9: Dimension of High-Type Expansion Bearing.

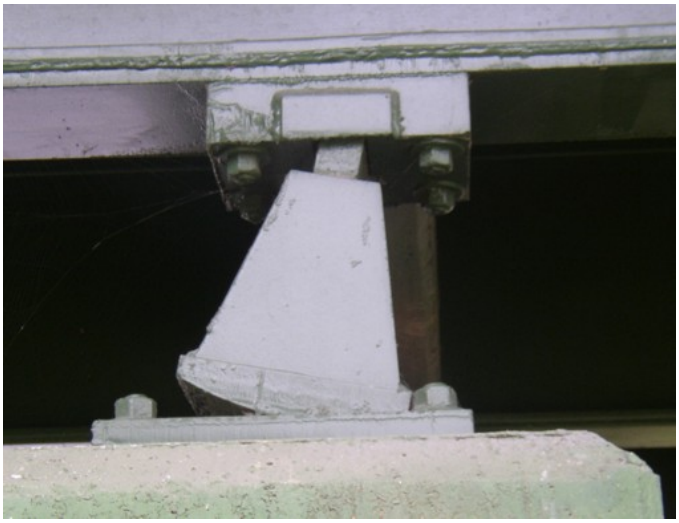

Figure C-10: High-Type Rocker Bearing Motion.

C.2.3.1 Longitudinal

As pointed out previously, the motion of this bearing when loaded in the longitudinal direction is a rocking motion. This motion causes friction that results from rolling resistance at the base and Coloumb friction at the top hinge. Although one would expect the hysteresis loops to be regular, debris and uneven wear cause the experimental hysteresis loops to be irregular (Mander et al., 1996).

The *O*penSees model for this behavior consists of the bilinear material *Steel01* as shown in Figure C-11. The initial stiffness of this bearing, k_e, is 14 kN/mm with a post-yield stiffness, $k_p = 0.018k_e$. The post-yield stiffness would ideally be perfectly plastic but the buildup of debris causes some plastic stiffness to exist. The yield force, F_y, is once again a function of the frictional coefficient $\mu = 0.04$. Figure C-12 shows a comparison between the analytical and experimental results.

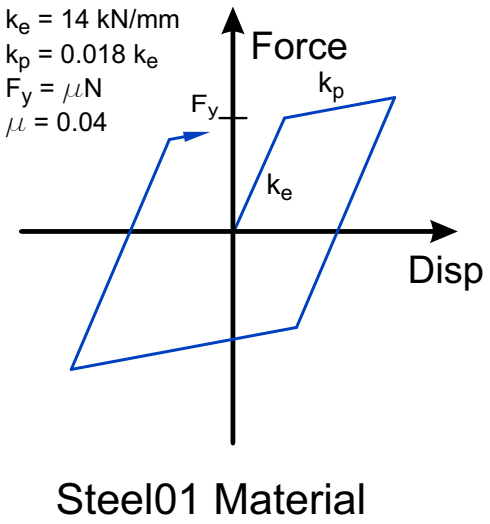

Figure C-11: OpenSees Model of High Type Rocker Bearing in Longitudinal Direction.

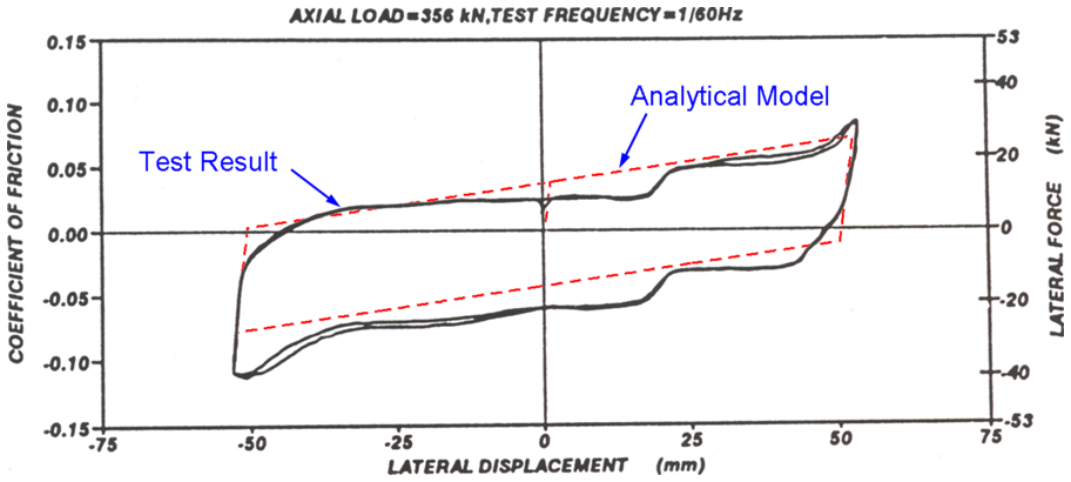

Figure C-12: Response of High Type Rocker Bearing in Longitudinal Direction, Experimental and Analytical (Mander et al., 1996).

C.2.3.2 Transverse

The transverse motion for the high-type rocker bearing is not as simple and straight forward as the longitudinal motion. The *O*penSees model, shown in Figure C-13, uses two materials, *Steel01* and *Hysteretic*, in parallel to capture this more complex behavior. There is still a sliding frictional component present which is modeled using the *Steel01* bilinear material. This has an initial stiffness of 252 kN/mm and a perfectly plastic behavior. The yield force, $F_y = \mu N$, uses a coefficient of friction $\mu = 0.10$.

As the rocker is loaded transversely it comes in contact with a keeper plate. This plate causes an increase in the stiffness and strength of the bearing until it fractures. The *Hysteretic* material is used to simulate the loading and fracture sequence of the keeper plate. The initial stiffness of this material is 22 kN/mm. The rest of its parameters are outlined in Figure C-13.

Figure C-14 shows a comparison between the analytical and experimental results. It is important to note that the experimental test was run for just one side of the hysteresis. Since, however, there is a keeper plate on both sides of the bearing one would expect the same behavior when loaded in the opposite direction. The *Hysteretic* material in Figure C-13 captures this response.

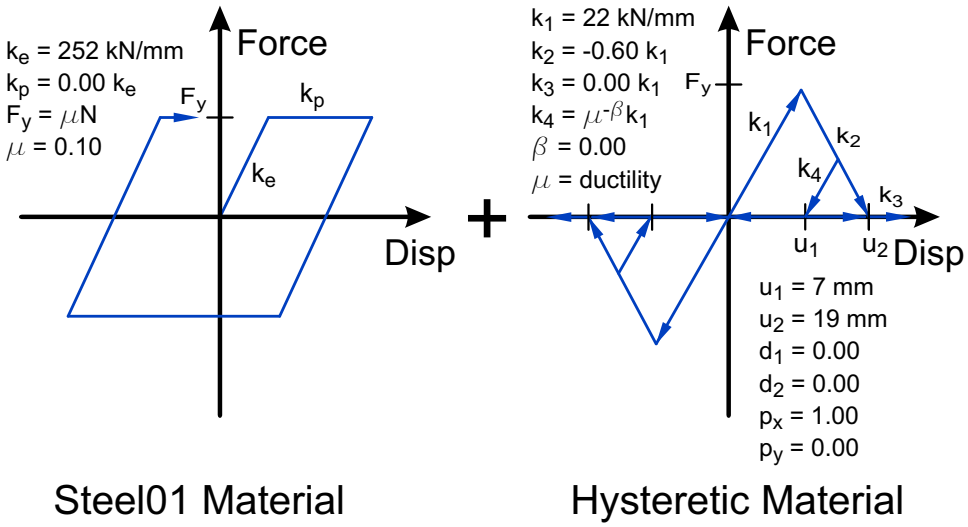

Figure C-13: OpenSees Model of High Type Rocker Bearing in Transverse Direction.

C.2.4 Low-Type Fixed Bearings

Another type of steel bearing used for steel girder bridges are the low-type sliding bearings shown in Figure C-3. The fixed version of this bearing allows for rotation while restricting horizontal translation. Figure C-15 gives a schematic along with dimensions for the low-type fixed bearing tested by Mander et al. and which is used in this study. This bearing has

a masonry plate that is 152 mm by 533 mm and is approximately 38 mm thick. The convex sole plate is approximately 152 mm by 358 mm and is also 38 mm thick.

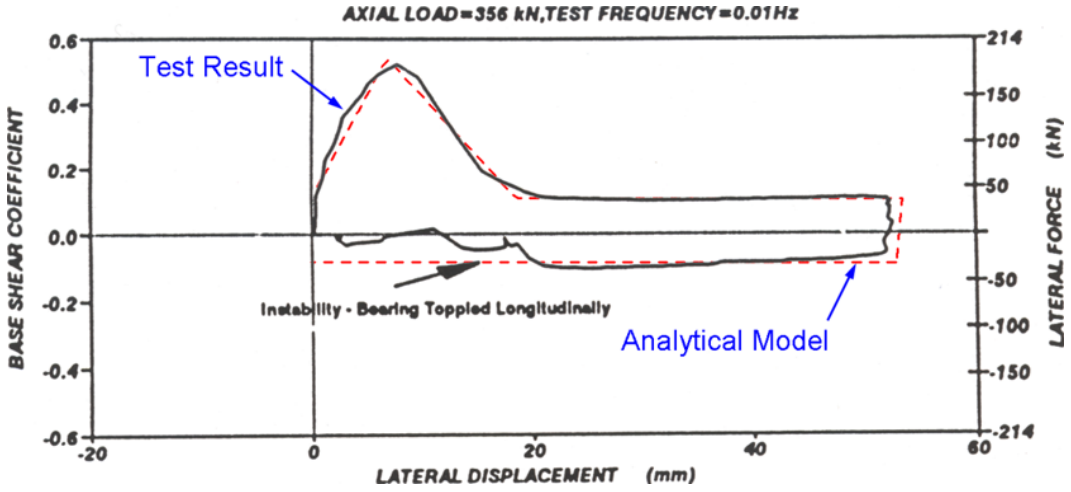

Figure C-14: Response of High Type Rocker Bearing in Transverse Direction, Experimental and Analytical (Mander et al., 1996).

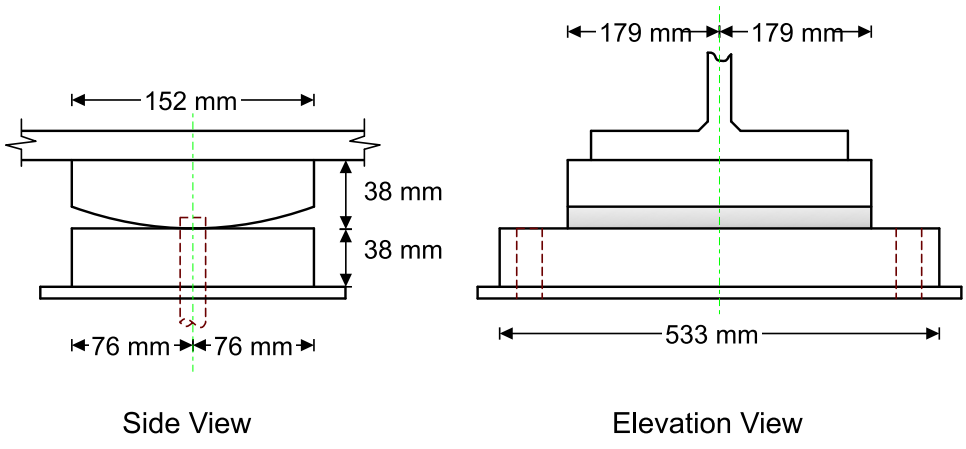

Figure C-15: Dimensions of Low-Type Fixed Bearing.

C.2.4.1 Longitudinal

The longitudinal behavior of the fixed bearing is modeled in *O*penSees using a *Steel01* and a *Hysteretic* material in parallel, as shown in Figure C-16. The *Steel01* material, as before, simulates the frictional component of the bearing response. It has an initial stiffness, k_e of 356.0 kN/mm, a frictional coefficient of $\mu = 0.37$ and a perfectly plastic behavior.

The pintles or dowels that are used to restrict horizontal translation are actually inserted into slotted holes in the sole plate. This allows for some movement prior to engaging the pintles in the bearing response. The movement in this model is plus or minus 2.0 mm. The additional effect of the pintles is handled by the *Hysteretic* material. It allows for the gap to close before engaging at which point an additional stiffness of 210 kN/mm is added.

Figure C-17 compares the analytical and experimental hystereses for this bearing. Some of the discrepancy is due to pintle not being centered in the slot during the experimental setup. Otherwise, the analytical model is a very reasonable approximation to the real bearing.

C.2.4.2 Transverse

The behavior of the low-type fixed bearing in the transverse direction is similar to the response of the longitudinal direction. The analytical modeling of the bearing behavior can be obtained using a *Steel01* and *Hysteretic* material in parallel (Figure C-18). The *Steel01* (bilinear) material has an initial stiffness k_e of 356 kN/mm and a perfectly plastic behavior to model the sliding component. The coefficient of friction μ equals 0.37.

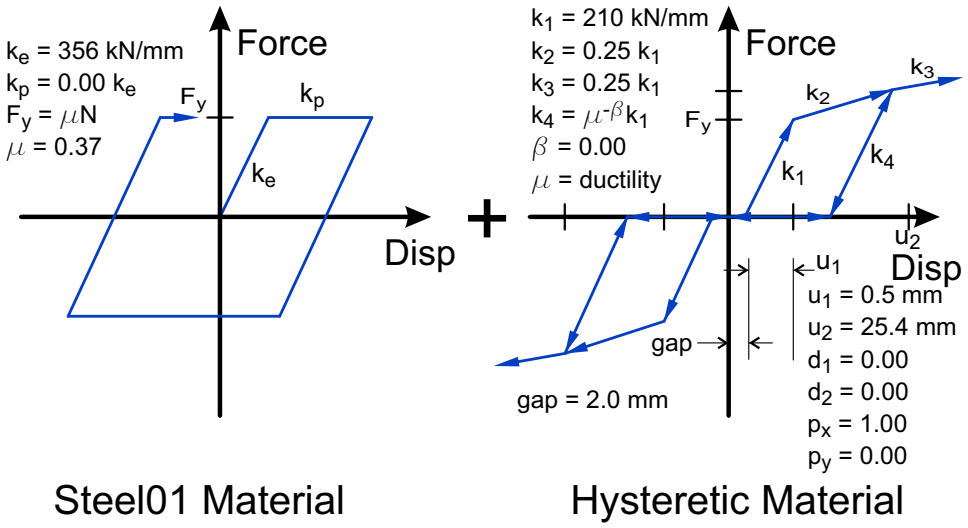

Figure C-16: OpenSees Model of Low Type Fixed Bearing in Longitudinal Direction.

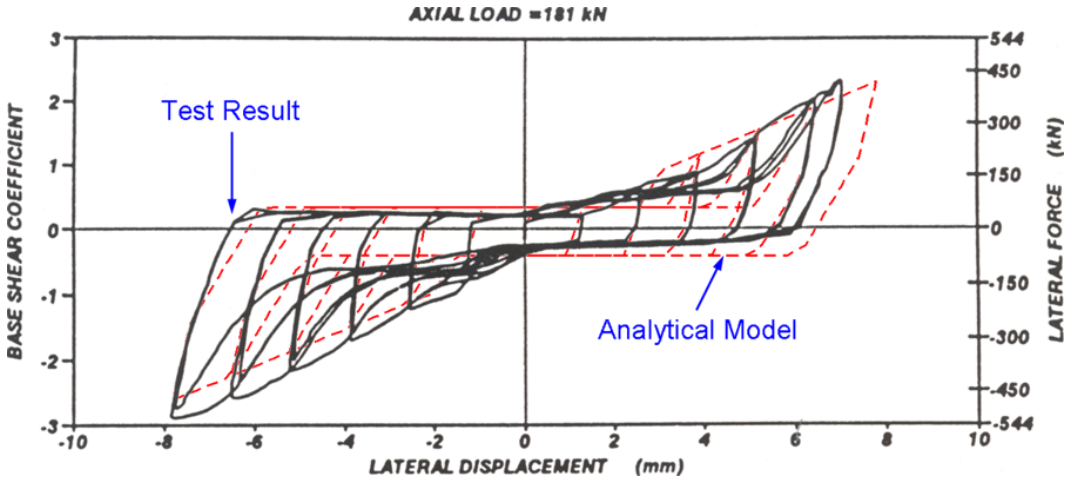

Figure C-17: Response of Low Type Fixed Bearing in Longitudinal Direction, Experimental and Analytical (Mander et al., 1996).

Once again the contribution of the pintle is added through the*Hysteretic* material. The initial stiffness of this material is 350 kN/mm but it has to close a gap of 1.5 mm before engaging.

The composite behavior is presented in Figure C-19. There is a slight irregularity on each side of the hysteresis which, as previously mentioned, is attributed to the pintle not being centered in the hole. Overall, the analytical model is able to simulate the experimental results.

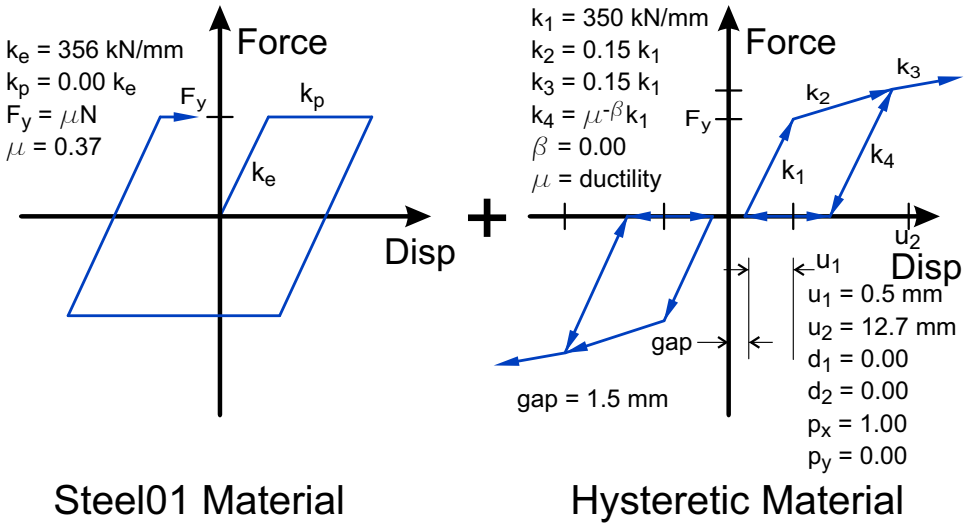

Figure C-18: OpenSees Model of Low Type Fixed Bearing in Transverse Direction.

C.2.5 Low-Type Sliding Bearings

The low-type sliding bearings presented in this section are designed to be an expansion type bearing when loaded in the longitudinal direction. This bearing type is shown in Figure C-20. It can be seen that a convex sole plate that is 152 mm by 358 mm by 38 mm thick

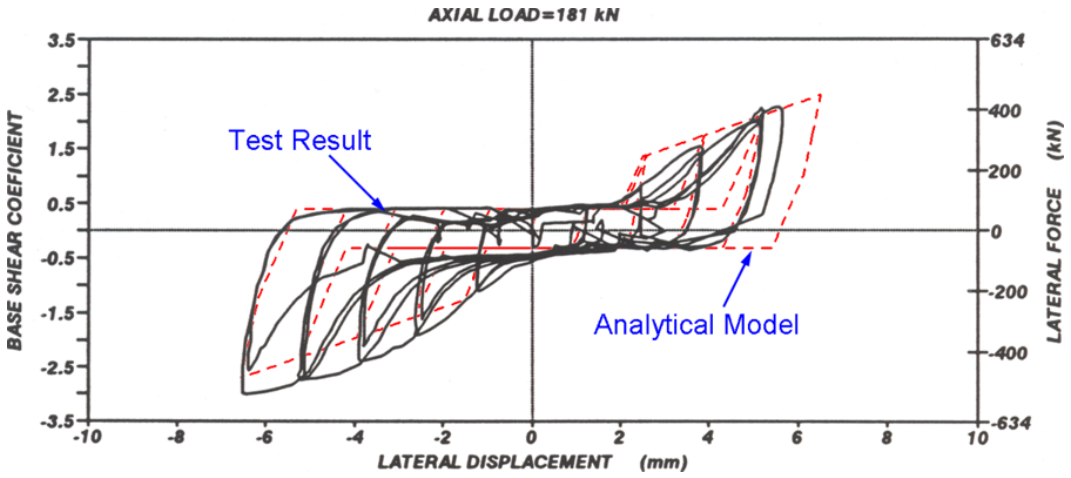

Figure C-19: Response of Low Type Fixed Bearing in Transverse Direction, Experimental and Analytical (Mander et al., 1996).

is paired with a flat sliding plate of the same size. This allows for rotation of the bearing about the transverse axis while still accommodating translation in the longitudinal direction. There are guide plates bolted onto the masonry plate to allow sliding longitudinally but provide restraint transversely.

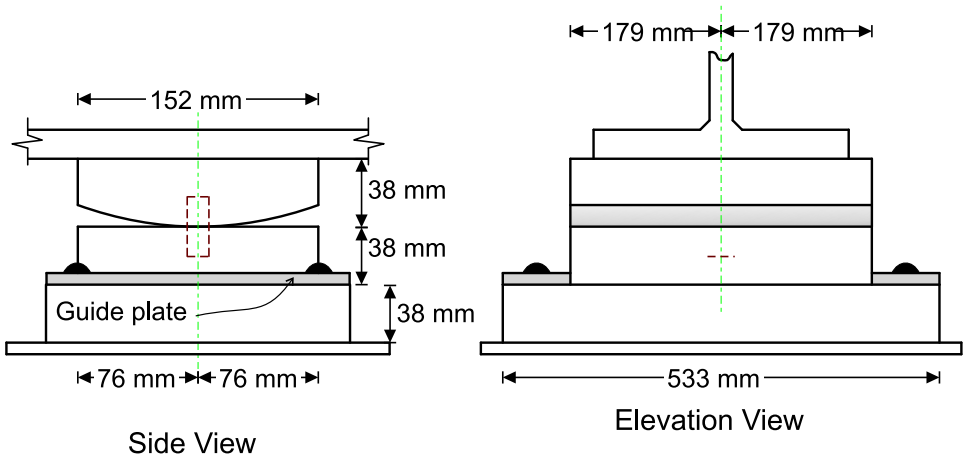

Figure C-20: Dimensions of Low-Type Expansion Bearing.

C.2.5.1 Longitudinal

Loading the low-type expansion bearing in the longitudinal direction shows an initial stiffness which drops close to zero once the frictional force is overcome. This is best modeled using a *Steel01* material with an elastic perfectly plastic range as shown in Figure C-21. The initial stiffness, k_e, is 123 kN/mm and the associated coefficient of friction, μ, is 0.20. Figure C-22 compares this analytical model with the experimental results. It is seen that this is not a perfect representation of the bearing behavior but it still provides a valid approximation. This is due to some corrosion and debris that is present in the bearing.

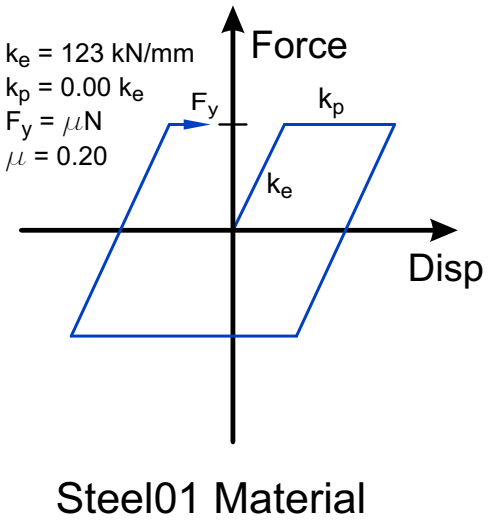

Figure C-21: OpenSees Model of Low-Type Sliding Bearing in Longitudinal Direction.

C.2.5.2 Transverse

The transverse behavior of the expansion bearing is a little more complex than the longitudinal behavior. In fact, it is much closer to the behavior seen in the fixed bearing. This

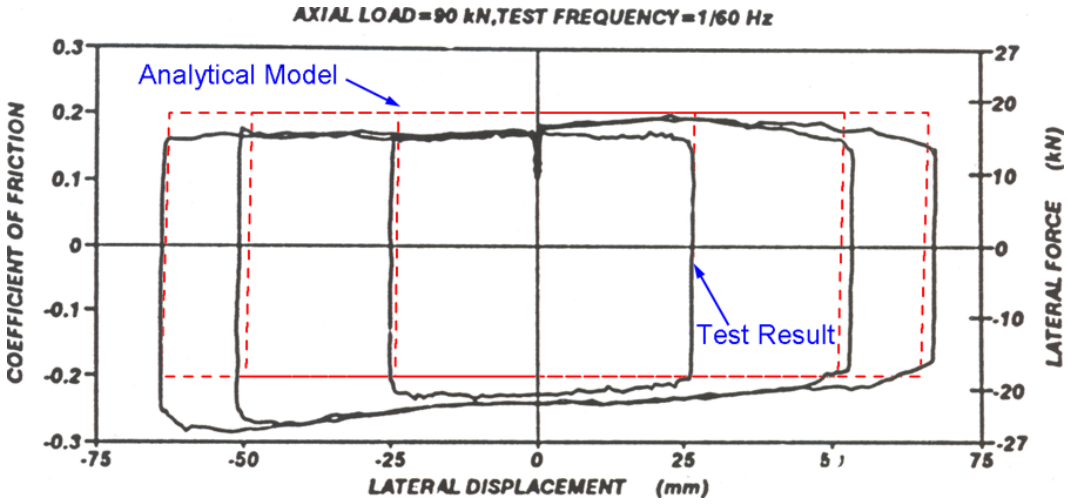

Figure C-22: Response of Low-Type Sliding Bearing in Longitudinal Direction, Experimental and Analytical (Mander et al., 1996).

is because it has transverse guide plates which provide additional stiffness and strength to the bearing. It still has the frictional component modeled by the *Steel01* material where $k_e = 123kN/mm$ and $\mu = 0.35$. The transition from sliding to striking is handled with a *Hysteretic* material and an associated gap. As seen in Figure C-23, the initial stiffness, k_1, is 35 kN/mm and the gap before the engagement of this material is 3 mm. Figure C-24 shows that the hysteresis of this bearing is not quite anti-symmetric with respect to the origin. This is probably due to debris and corrosion in the bearing.

C.3 Elastomeric Bridge Bearings

Elastomeric bridge bearings have been a very common bearing used on concrete girder and slab type bridges. These types of bearings consist of an elastomeric rubber pad and some steel dowels for restraint. They have traditionally performed well under seismic loading but have also been known to “walk-out” if not properly secured (Imbsen and Nutt, 1981).

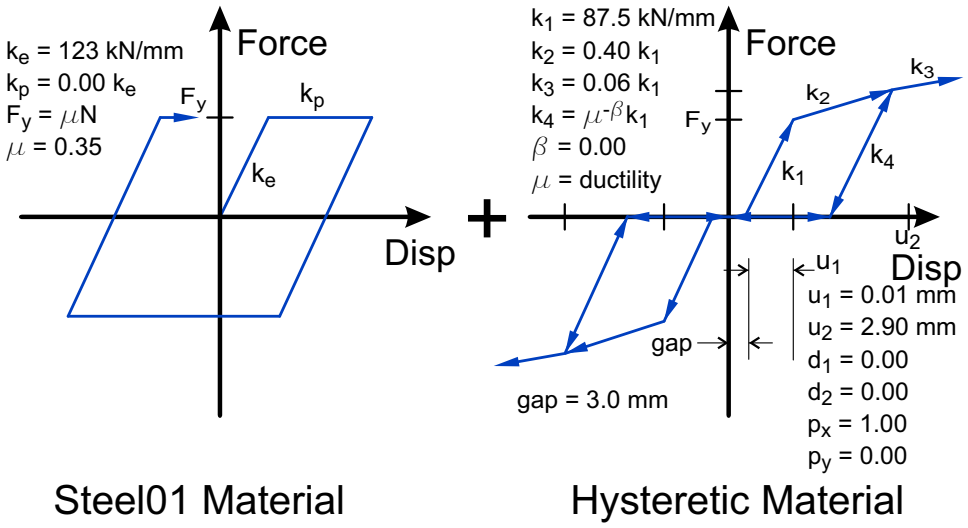

Figure C-23: OpenSees Model of Low-Type Sliding Bearing in Transverse Direction.

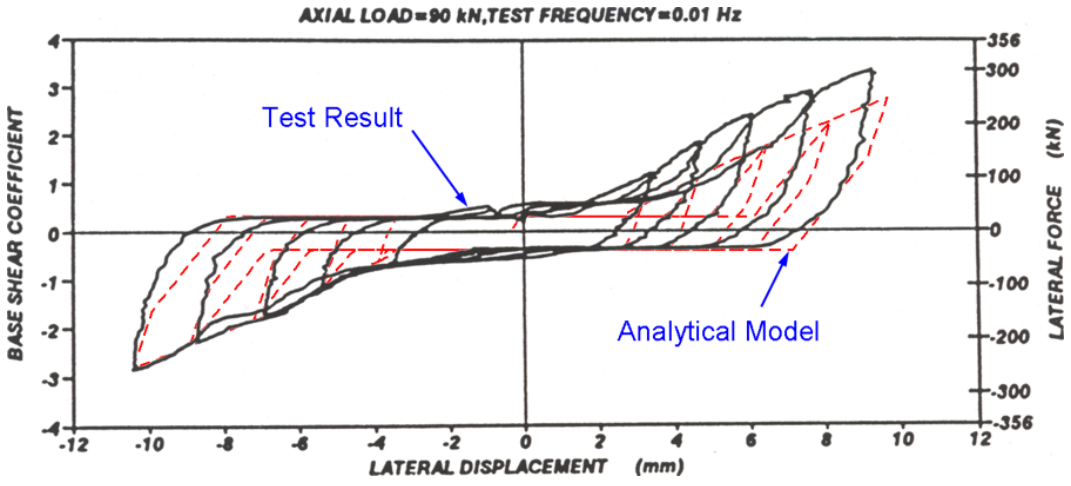

Figure C-24: Response of Low-Type Sliding Bearing in Transverse Direction, Experimental and Analytical (Mander et al., 1996).

These types of bearings will be used for all of the bridge types in this study which have concrete superstructures.

As mentioned, the bearing system consists of an elastomeric rubber pad and some steel dowels that embed into the pier cap and project through the pad into the underside of the concrete girder/slab. Each component of the bearing system provides a distinct contribution in the transfer of forces. The elastomeric pad transfers horizontal load by developing a frictional force while the steel dowels provide resistance through a beam type action. It is therefore justified that a model of each component, the pad and the dowels, be developed separately and then combined in parallel to get the appropriate composite action.

A typical bearing size and configuration used throughout this study is presented in Figure C-25. It is a typical bearing size for a AASHTO Type I pre-stressed concrete girder. It consists of a neoprene pad that is 152 mm wide by 406 mm long and 25.4 mm thick. It also has two 1“ diameter steel dowels that project into the girder 76.2 mm. For a fixed type bearing the dowels are inserted into a hole that is 31.8 mm in diameter, as seen in Figure C-25. To create an expansion bearing, this hole is swapped for a slot that is 31.8 mm wide by 76.2 mm long. This bearing configuration will be used for illustration purposes in later sections.

C.3.1 Overview of Elastomeric Pad and Dowel

C.3.1.1 Elastomeric Pad

As pointed out previously, the behavior of the elastomeric pad is characterized by sliding. As was seen during the discussion of the steel sliding bearings, this sliding behavior is characterized by the initial stiffness which accepts load until the coefficient of friction is

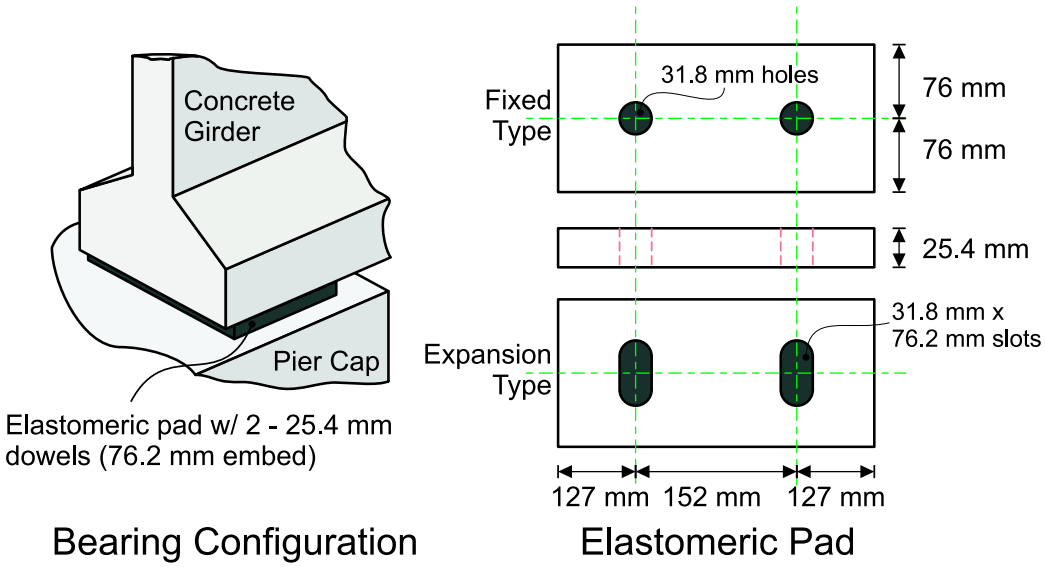

Figure C-25: Typical Elastomeric Bearing Used for Concrete Bridge Girders.

exceeded. Once it is exceeded, the stiffness changes to a value that is nearly zero (Schrage, 1981).

The modeling of the elastomeric pad can be accomplished through the use of an elastic perfectly plastic material. The chore lies in determining the initial shear stiffness of the bearing and also the calculation of an appropriate coefficient of friction. The initial stiffness, k_o, can be calculated by equation C.1 (Choi, 2002).

$$k_o = \frac{GA}{h_r} \tag{C.1}$$

Where A is the area of the elastomeric bearing, G is the shear modulus of the elastomer and h_r is the thickness of the elastomeric pad. A and h_r are a result of the size of the bearing and can be pulled from a set of plans but G needs to assume some typical value. Shear values for elastomers in bridge bearings range between 0.66 MPa and 2.07 MPa depending

on their hardness (**?**). Since this value can vary over the bridge inventory, an average value of 1.38 MPa is assumed as a typical value for this study. This may be a slightly higher value than would be typical for new rubber, but a large majority of these types of bearings are 20 - 30 years old and have likely hardened.

The frictional coefficient for concrete bridges takes into account the interface between the elastomeric rubber and a concrete surface. Some experimental tests have shown that the coefficient of friction for an elastomeric bearing is a function of the normal stress on the bearing, σ_m, and is given by equation C.2 (Schrage, 1981).

$$\mu = 0.05 + \frac{0.4}{\sigma_m} \tag{C.2}$$

where μ is the coefficient of friction and σ_m is the normal stress on the bearing given in MPa. For the bearing given in Figure C-25 and when the normal stress, $\sigma_m = 1.29 MPa$, the coefficient of friction is $\mu = 0.36$ and the initial stiffness is 3.35 kN/mm.

C.3.1.2 Steel Dowels

The steel dowels, used to prevent excessive movement between the girders and the piers on which they bear, are 25.4 mm in diameter. A typical girder will require two dowels at each end. The dowels are embedded into the top of the concrete pier/bent and projected loosely 76.2 mm into the bottom of the girder. Under working loads the response of these dowels is expected to remain linear. However, for moderate earthquakes, a non-linear behavior is expected.

In work performed by Vintzeleou and Tassios (1987), it was shown that there is extreme pinching in the hysteresis when a dowel is loaded as a cantilever, as is the case for

elastomeric type bearings. There was also an obvious drop off in strength as the dowels fractured. In an attempt to capture this behavior, Choi (2002) used an ABAQUS model of a steel dowel to assist in developing and verifying a Drain-2DX model. The estimated yield and ultimate strength for each dowel is approximately 56.0 kN and 58.0 kN respectively. The initial stiffness of each dowel is calculated at 46 kN/mm. Figure C-26 shows the analytical model developed by Choi and is subsequently used in this study.

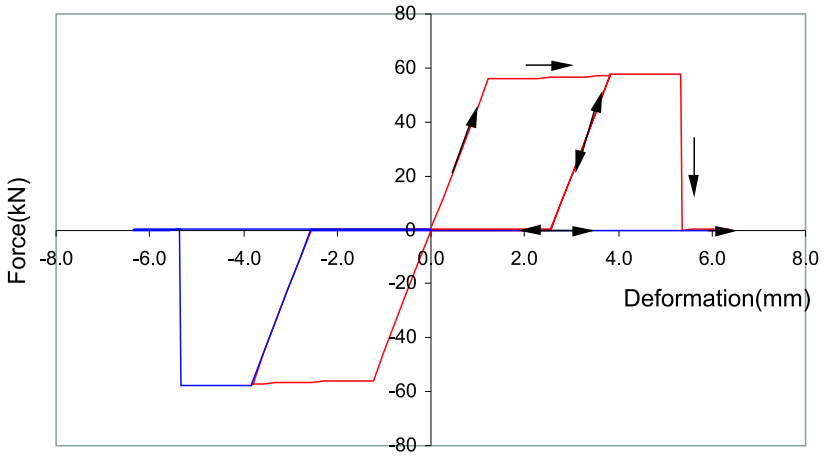

Figure C-26: Analytical Model of Steel Dowel Behavior Under Cyclic Loading (Choi, 2002).

C.3.2 Analytical Model of Elastomeric Bearing with Fixed Dowels

The composite behavior of an elastomeric bridge bearing is achieved by combining the behavior of the elastomeric pad and two steel dowels in parallel. The elastomeric pad is modeled using a *Steel01* material with an initial stiffness of 3.35 kN/mm and a yield force, $F_y = \mu N$. The dowel behavior is modeled using a *Hysteretic* material using an initial

stiffness of 92 kN/mm, as seen in Figure C-27. For the fixed bearing the 25.4 mm dowels are inserted into a 31.8 mm hole. This allows a total of 6.4 mm of movement without initiating the effects of the dowels. The condition is simulated by placing a 3.1 mm gap on each side of the hysteresis, as shown in Figure C-27. Figure C-28 shows the composite behavior of the elastomeric bridge bearing. It should be noted that the behavior of this bearing is the same in both the longitudinal and transverse directions.

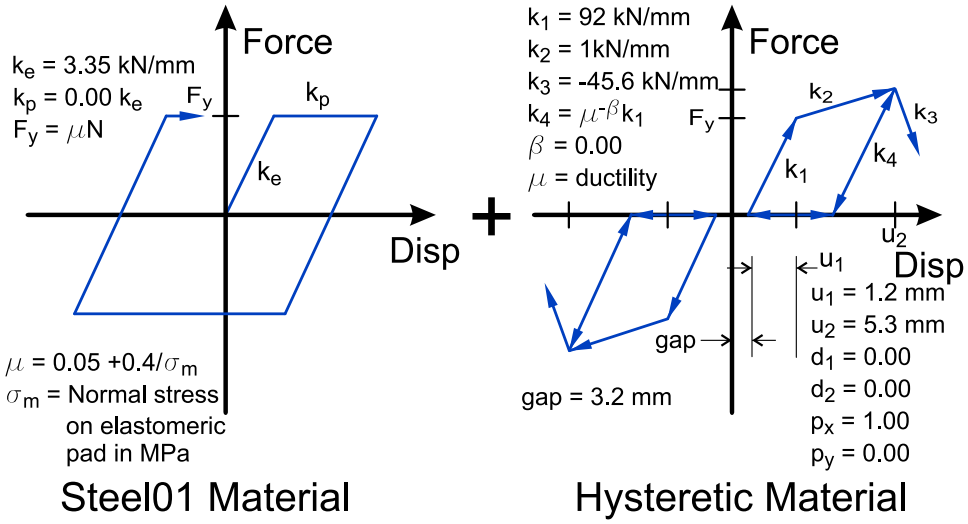

Figure C-27: OpenSees Model of Elastomeric Bearing with Fixed Dowels.

C.3.3 Analytical Model of Elastomeric Bearing with Expansion Dowel

Figure C-29 shows the *O*penSees analytical model used for the expansion bearings. The only difference between the expansion bearing and the fixed bearing is the size of the gap that must be closed before the dowels are engaged. The gap for this bearing is 25.4 mm. This model simulates the bearing behavior when loaded in the longitudinal direction and

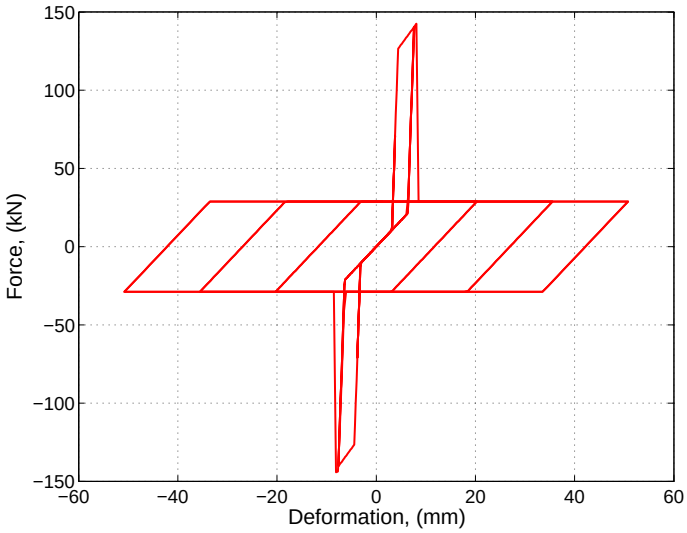

Figure C-28: Hysteretic Behavior of Elastomeric Bearing with Fixed Dowels.

is shown in Figure C-30. The response in the transverse direction is identical to that of the fixed bearing with only a 3.2 mm gap.

C.4 Abutments

Abutments are a vital component of highway bridges. They provide vertical support of the bridge superstructure at the bridge ends and connect the bridge with the roadway approaches. They also provide lateral restraint, both longitudinal and transverse, to the bridge superstructure when the bridge undergoes loading in those directions. There are various types of abutments used in bridge design. Figure C-31 shows four of these types, namely a gravity abutment, a U-shape abutment, a spill through abutment and a pile bent abutment. These all belong to a special class of abutments called “seat-type” abutments (Wang, 2000).

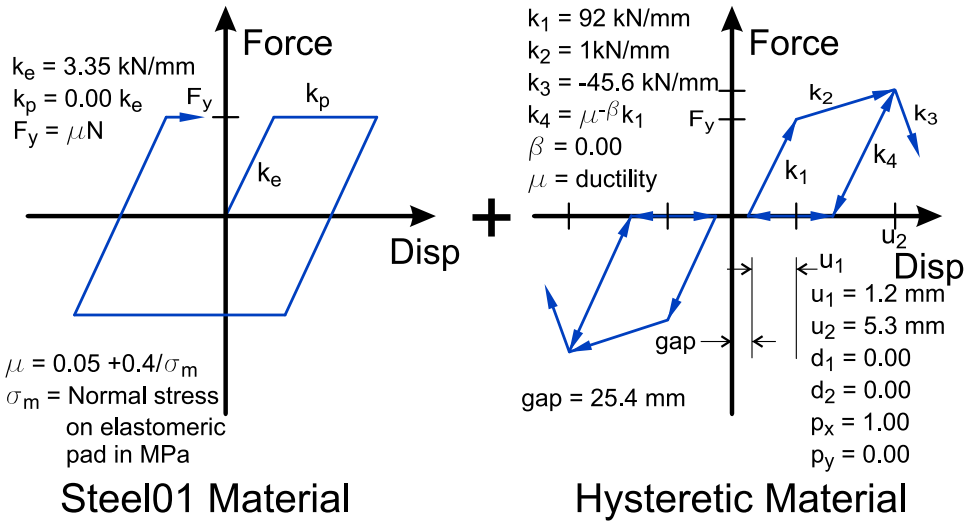

Figure C-29: OpenSees Model of Elastomeric Bearing with Expansion Dowels.

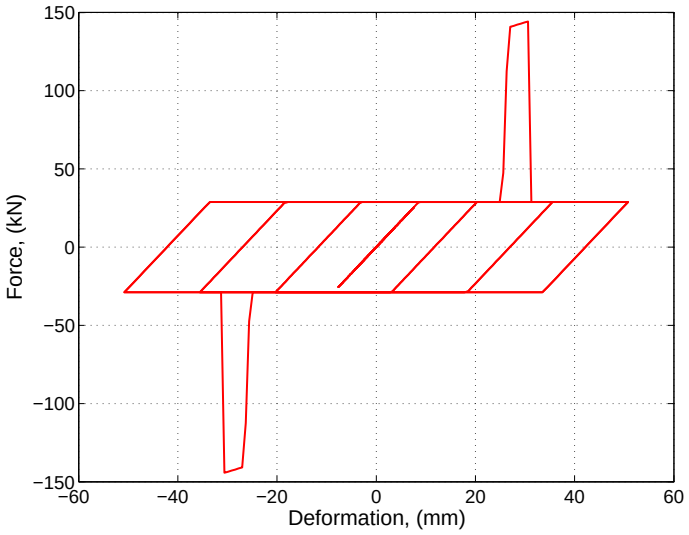

Figure C-30: Hysteretic Behavior of Elastomeric Bearing with Expansion Dowels.

This is in contrast to monolithic abutments which are built integral with the bridge superstructure. This study uses the pile bent type abutment in all the bridge models as it is a very common type in the CSUS (Hwang et al., 2000).

C.4.1 Overview of Abutments

As stated previously, bridge abutments primarily resist vertical loads but they also must take horizontal loads. Horizontal loading of abutments can occur as a result of traffic loads due to acceleration and braking. Seismic loads can also place great demands on bridge abutments. For instance, the longitudinal response of a bridge during seismic loading can increase the earth pressures on the abutment. Impact of the deck with the abutment can further increase these pressures.

In the longitudinal direction there are two types of resistance that are present. The first is a passive resistance which is developed as the abutment wall is pressed into the soil back-fill, as shown in Figure C-32. Thus, passive resistance is partially provided by the soil and partially provided by the piles. The other type is active resistance which occurs as the abutment is pulled away from the backfill. During this motion the piles provide most of the horizontal resistance. For the pile-bent abutment type, wing walls may not be very large, and therefore may not contribute much to the transverse horizontal resistance of the abutment. Therefore, for all practical purposes, this study considers that transverse resistance is provided solely by the piles.

As previously mentioned, seismic loads can place great demands on a bridge abutment. Past earthquakes have shown that there are essentially two types of abutment damage that

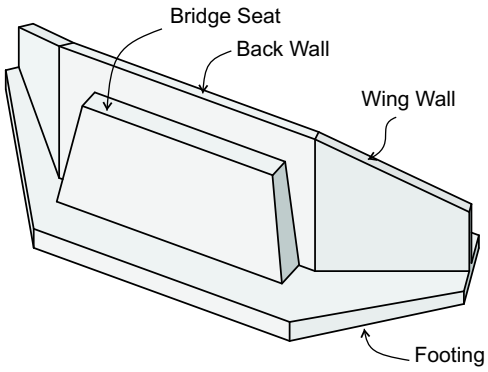

C-31(a): Gravity - type

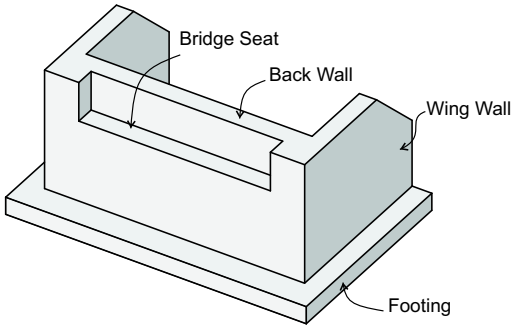

C-31(b): U - type

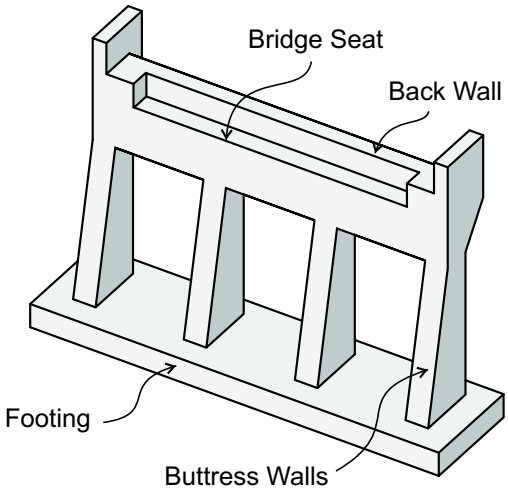

C-31(c): Spill-through - type

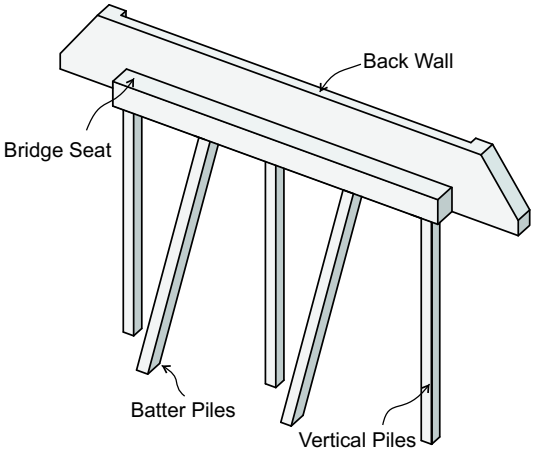

C-31(d): Pile Bent - type

Figure C-31: Girder Seat Abutment Types (Tonias, 1995).

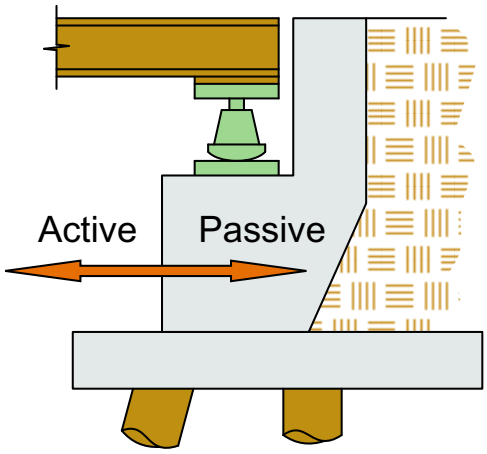

Figure C-32: Definition of Longitudinal Abutment Behavior.

can occur during seismic loading. The first, stability damage, is mainly caused by foundation failure due to excessive ground deformation or loss of bearing capacity of the soil. This type of damage is made evident through tilting, sliding, settling and overturning of the abutment. This type of failure can cause a serious disruption in the use of the bridge. The other type of damage is component damage or in other words actual damage to the abutment itself. This type of damage is caused by excessive soil pressures as the relative displacement between the abutment and the soil gets large. This type of damage is more easily repaired than the stability damage (Wang, 2000).

Past experience has shown that abutments play an important role in the overall behavior of bridges under seismic loading. This fact has been reinforced numerous times as researchers have attempted to ascertain the contribution that abutments make (Goel, 1997; Karantzikis and Spyrakos, 2000; Wilson and Tan, 1990). As a result, it has been recognized that abutment seismic response models need to be developed and implemented in both the analysis and design of bridges. The following subsection discusses further the development of the models used in this study.

C.4.2 Analytical Models of Abutments

A common implementation of the effect of the abutments is the addition of discrete linear springs. A guideline for the stiffness of this linear spring was published by Caltrans (1990). Their recommendation was to assume the passive soil-abutment stiffness was 115 kN/mm/m. This was to be valid for a standard 2.4 m tall back-wall. This value could then be multiplied by the actual width of the abutment to obtain a total passive stiffness for the spring. The effects of the piles could be added in both the active and passive directions

allowing for 7 kN/mm per each 45 ton, 70 ton and 406.4 mm Cast-In-Drilled-Hole (CIDH) piles. The transverse direction once again accounted for the piles and then also allowed for the 115 kN/mm/m for 2/3 of the wing-wall width. If the bridge width is over about 15 m, the wing-walls appear to contribute little and are therefore ignored (Caltrans, 1990). Although a linear spring is used, an ultimate soil pressure of 0.37 MPa is used to limit the amount of load taken by the abutment. This value represents the maximum stress the back-fill can take under cyclic loading. Static loading permits a value of 0.24 MPa.

A half-scale abutment experiment was performed at UC Davis to investigate further the stiffness of abutments in both the longitudinal and transverse direction (Maroney et al., 1993). These tests showed that the initial stiffness of 115 kN/mm/m used by Caltrans appears to significantly overestimate the actual passive stiffness present in the abutment (Maroney et al., 1994). Further abutment modeling work by Goel and Chopra (1997) found that the Caltrans procedures proposed for modeling the abutment in the transverse direction produced good results. When it came to the passive stiffness of the abutment it was shown that the Caltrans value was indeed too large, just as the half-scale tests had found. Caltrans later modified their initial stiffness estimate for the passive resistance of the soil giving a possible range of 11.5 kN/mm/m to 28.8 kN/mm/m (Caltrans, 1999). They maintain that the ultimate soil pressure remains at 0.37 MPa and the pile stiffnesses remain at 7 kN/mm/pile.

C.4.2.1 Longitudinal Model

This study assumes a pile stiffness value of of 7 kN/mm/pile, as recommended by Caltrans (1990). It also assumes, that for typical bridges, the passive soil stiffness can be calculated

using a value of 20.2 kN/mm/m. This is the median value of the recommended range. The ultimate passive soil pressure of 0.37 MPa is also accepted for this study.

It was noticed in the work performed by Maroney et al. (1994), that the passive stiffness of the abutment decreased as the tip displacement of the abutment increased. By the time the ultimate soil pressure was reached, the passive stiffness fell to zero. It is thus apparent that a non-linear model of the passive behavior is needed to appropriately capture the abutment behavior. In a study by Martin and Yan (1995), they found that the ultimate soil pressure was reached at relative tip displacements of 6 % to 10 % of the back-wall height depending on whether there were cohesionless or cohesive soils present. This information, in addition to a few key assumptions, allows the generation of a quad-linear model for passive abutment stiffness. A development of this model is presented in the following subsection and the actual model is presented in Figure C-33 and Table C-4.

C.4.2.2 Modeling of Passive Soil Stiffness at Abutment

Following the results of the previously mentioned studies, Caltrans presented some basic recommendations pertaining to the modeling of passive stiffness of abutments (Caltrans, 1990, 1999). This study accepts these recommendations which are given in Table C-2. Some simple assumptions are made to facilitate the conversion of the linear Caltrans model into an equivalent non-linear model.

As noted in Table C-2 the ranges for possible values of initial stiffness and ultimate deformation are 11.5 - 28.8 kN/mm/m (K_{1p}) and 6% - 10% (Δ_{3p}) respectively. However, the ultimate passive soil pressure is assumed to be 0.37 MPa for all cases. To generate the non-linear model, as shown in Figure C-33, some relationships must be drawn between the

Table C-2: Passive Abutment-Soil Behavior Parameters (Caltrans, 1999; Martin and Yan, 1995).

Soil Type	Initial Stiffness	Ultimate Deformation[1]
Cohesionless	11.5	6%
Cohesive	28.8	10%
All Soil Types		
Ultimate Soil Pressure, (MPa)		0.37

[1] Δ/h, Abutment tip displacement (Δ) as a percentage of abutment height (h)

initial stiffness, ultimate deformation and ultimate soil pressure. It is therefore assumed that there is a linear relationship between the initial stiffness and the ultimate deformation. This relationship is given in Equation C.3.

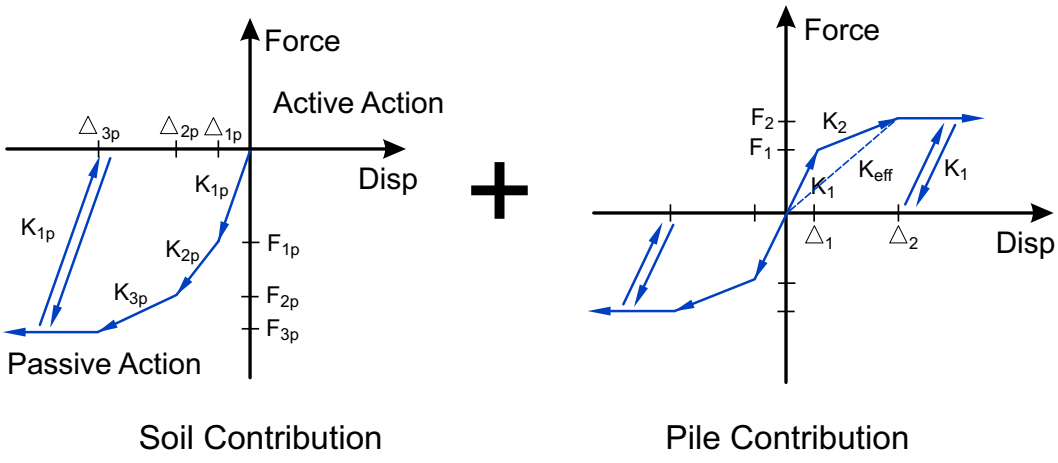

Figure C-33: Analytical Model of Abutment in Longitudinal Direction.

$$\Delta_{3p} = \left(0.06 + \left(\frac{K_{1_p} - 11.5}{28.8 - 11.5}\right)(0.04)\right)(h) = (0.0334 + 0.00231K_{1p})h \qquad \text{(C.3)}$$

Where K_{1p} is initial stiffness, Δ_{3p} is ultimate deformation and h is the total height of the abutment back-wall. Equation C.3 gives $\Delta_{3p}/h = 0.06$ when $K_{1p} = 11.5$ kN/mm/m and $\Delta_{3p}/h = 0.10$ when $K_{1p} = 28.8$ kN/mm/m.

The deformation at first yield Δ_{1p} is assumed to be 10% Δ_{3p} and while Δ_{2p} is assumed to be 35% of Δ_{3p}. The yield force for each meter of wall width, F_{1p}, is simply taken as the product of K_{1p} and Δ_{1p}. The ultimate force per unit width of wall, F_{3p}, is $0.37MPa \cdot h$. And finally F_{2p} is assumed to be F_{1p} plus 55% of the difference between F_{1p} and F_{3p}. This is clarified in equation C.4.

$$F_{2p} = F_{1p} + 0.55(F_{3p} - F_{1p}) \tag{C.4}$$

With the anchor points of the model, the deformations (Δ_{ip}) and corresponding forces (F_{ip}), defined it is now a simple task to calculate the two remaining stiffnesses, K_{2p} and K_{3p}. Although this model may seem complex, it is relatively simple to implement in OpenSees. Figure C-34 gives an example of the model backbone for three different initial stiffness values, namely 11.5 kN/mm/m, 20.2 kN/mm/m and 28.8 kN/mm/m.

C.4.2.3 Modeling of Pile Stiffness at Abutment

The abutment piles are assumed to act in both active and passive loading of the abutment. The Caltrans recommendation of 7 kN/mm/pile is accepted for this study with an ultimate strength of 119 kN/pile (Caltrans, 1990). The behavior of the pile, however, is not linear up to the ultimate strength. The initial stiffness degrades with soil surface yielding. This study assumes the tri-linear model implemented by Choi (2002), which is also presented in Figure C-33 and Table C-4. He assumed that the piles become plastic at a deformation of

Table C-3: Values for Passive Abutment-Soil Behavior Parameters.

Parameter	Equation[2]	Alternate Form
K_{1p}	11.5 - 28.5 kN/mm	
K_{2p}	$\frac{0.55(F_{3p}-F_{1p})}{0.25\Delta_{3p}}$	
K_{3p}	$\frac{0.45(F_{3p}-F_{1p})}{0.65\Delta_{3p}}$	
F_{1p}	$K_{1p}\Delta_{1p}$	
F_{2p}	$F_{1p} + 0.55(F_{3p} - F_{1p})$	$0.45F_{1p} + 0.55F_{3p}$
F_{3p}	$(0.37\text{ MPa})h$	
Δ_{1p}	$0.10\Delta_{3p}$	
Δ_{2p}	$0.35\Delta_{3p}$	
Δ_{3p}	$\left(0.06 + \left(\frac{K_{1p}-11.5}{28.8-11.5}\right)(0.04)\right)h$	$\left[3.34(10)^{-2} + 2.31(10)^{-3}K_{1p}\right]h$

[2]Values for each meter width of wall.

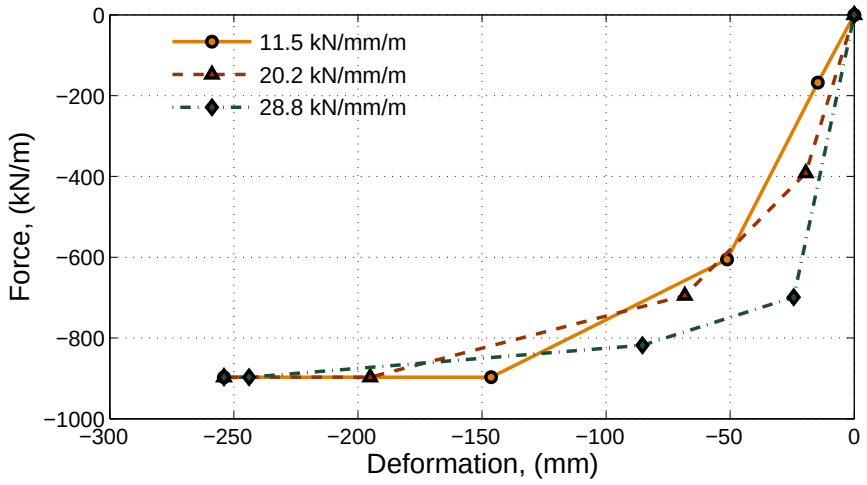

Figure C-34: Abutment Behavior Modeling for Three Levels of Initial Stiffness

Table C-4: Model Properties of Abutment.

Properties	Notations	Values
Soil Behavior (Passive Action)		
Initial Stiffness	K_{1p}	11.5 - 28.8 kN/mm/m
Displacement 1 at top	Δ_{1p}/h	$0.1(\Delta_{3p}/h)$
Second Stiffness	K_{2p}	[1]95% - 6% K_{1p}
Displacement 2 at top	Δ_{2p}/h	$0.35(\Delta_{3p}/h)$
Third Stiffness	K_{3p}	[1]30% - 2% K_{1p}
Displacement 3 at top	Δ_{3p}/h	8.0%
Pile Behavior (Dual Action)		
Effective Stiffness	K_{eff}	7 kN/mm/pile x # of piles
Initial Stiffness	K_1	$2.333xK_{eff}$
Displacement 1 at top	Δ_1/h	7.62 mm
Second Stiffness	K_2	$0.428K_{eff}$
Displacement 2 at top	Δ_2/h	25.4 mm

[1]See Appendix C for Clarifications.

25.4 mm. It was also assumed that first yielding occurs at 30 % of the ultimate deformation. This corresponds to a yielding force equal to 70 % of the ultimate force.

The overall model used to simulate abutment behavior in the longitudinal direction is created by placing the soil model and the pile model in parallel as seen in Figure C-33. Figure C-35 shows the hysteretic behavior of an abutment section that is 1.91 m wide and has the equivalent of 1.2 piles. There is a noticeable difference between the passive behavior and the active behavior.

C.4.2.4 Transverse Model

The components of an abutment system that contribute to its transverse stiffness are the piles and the wing walls. Caltrans pointed out that the effect of wing-walls decreases as the width of the abutment increases. It is therefore their recommendation that only the piles be considered when modeling the transverse direction. The effective stiffness contributed

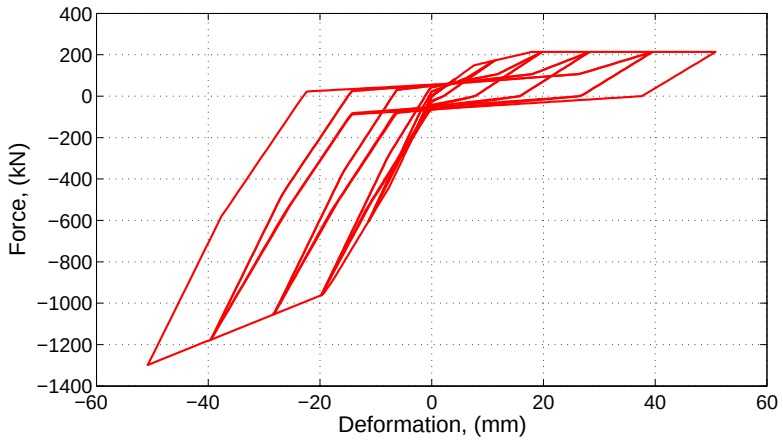

Figure C-35: Hysteretic Behavior of Abutment in Longitudinal Direction.

by the piles is approximately the same, whether the abutment is loaded longitudinally or transversely. Therefore, the pile portion of the longitudinal model is also used for the transverse modeling. Figure C-36 shows the analytical model once again and Table C-4 defines the values. Figure C-37 shows the hysteretic transverse behavior of a 1.91 m wide abutment section with the equivalent of 1.2 piles.

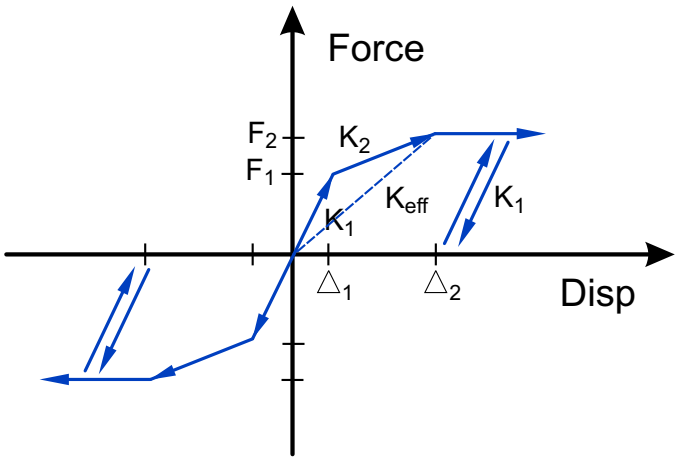

Figure C-36: Analytical Model of Abutment in Transverse Direction.

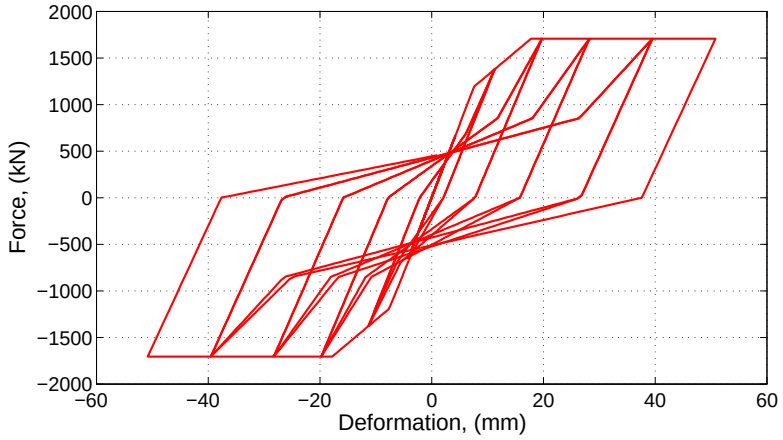

Figure C-37: Hysteretic Behavior of Abutment in Transverse Direction.

C.5 Impact Elements

Some bridge types, such as those considered in this study, are prone to have impact occur between their adjacent decks or between the decks and the abutments when loaded seismically. In particular, those bridge types that don't possess adequate continuity along the length of the bridge, such as the multi-span simply supported girder bridge types, are susceptible to this phenomenon. Relatively recent earthquakes, such as the 1994 Northridge and the 1995 Kobe earthquakes, have highlighted the damaging effects of adjacent deck pounding in bridges (EERI, 1995a,b). Damage such as crushing and spalling of the deck as well as unseating of the girders were evidence of this phenomenon.

C.5.1 Overview of Impact Elements

It is recognized that the pounding of decks can affect the way a bridge responds to seismic loading. It is therefore incumbent upon researchers to include the effects of pounding when

generating analytical bridge models. A common way of implementing this phenomenon is by using a contact element in the model. Essentially the element monitors the gap between adjacent sections of the bridge and is engaged once the associated gap is closed. This setup is illustrated in Figure C-38 where the contact element is a nonlinear spring with a gap.

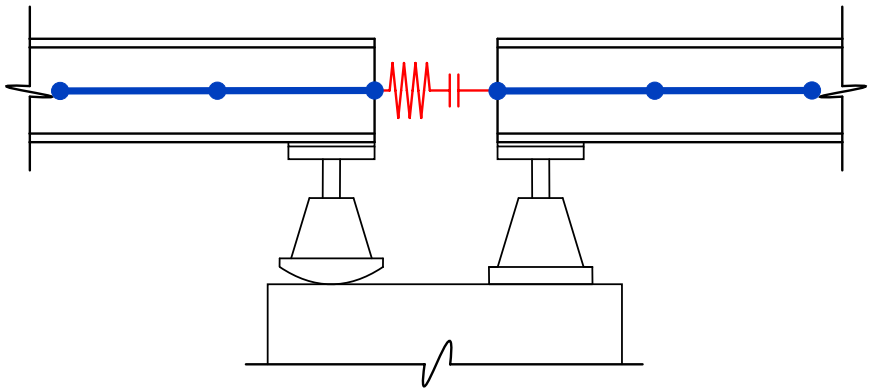

Figure C-38: Pounding of Bridge Decks.

C.5.2 Analytical Model of Impact Elements

The concept of the contact element is quite simple but the actual modeling of its behavior can be more cumbersome. Muthukumar (2003) performed a study looking at the pounding in bridges and recommended a procedure for generating appropriate contact elements. This study showed impact models that do not allow for energy dissipation such as linear models tend to over estimate the system response due to impact. It was therefore recommended that a bilinear spring be used to capture the effects of impact including energy dissipation. Figure C-39 shows the model recommended by Muthukumar (2003), which is used in this study.

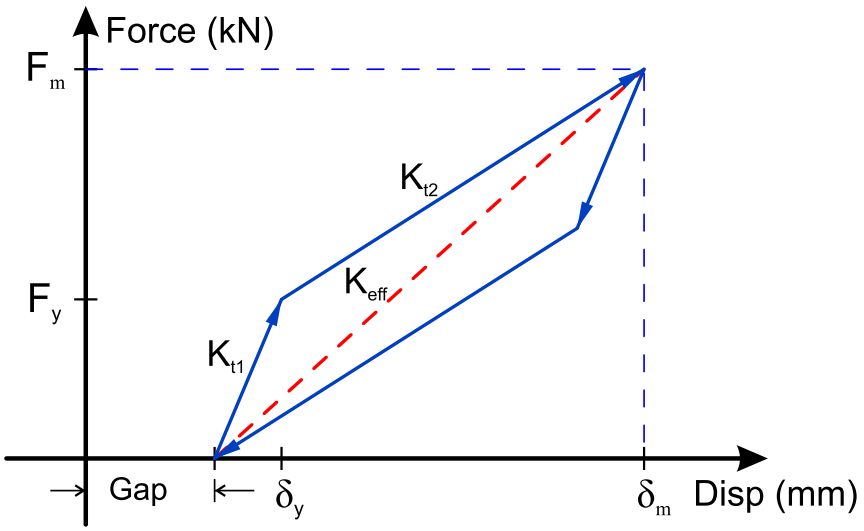

Figure C-39: Analytical Model of Impact Between Decks (Muthukumar, 2003).

The derivation of the parameters K_{t1} and K_{t2} uses the energy dissipated upon impact in comparison with the area in the hysteresis. By equating these two values and assuming a maximum deformation, δ_m, these stiffnesses are calculated. The presentation of the equations and assumptions for this model has been included in subsection C.5.2.1. In this study the maximum deformation or penetration δ_m is assumed to be 25.4 mm and δ_y is assumed to be $(0.10)(\delta_m)$. Following this assumption, $K_{t1} = 1,116$ kN/mm and $K_{t2} = 384$ kN/mm. The hysteresis of this model is presented in Figure C-40.

C.5.2.1 Modeling of Deck Pounding Using Contact Elements

The parameters , K_{t1}, K_{t2}, δ_y and δ_m for the impact model are calibrated to the total expected energy loss, ΔE, during an impact event. Using a stereomechanical approach the energy dissipated during impact can be derived and written as shown in equation C.5.

$$\Delta E = \frac{k_h \delta_m^{n+1}\left(1 - e^2\right)}{n+1} \tag{C.5}$$

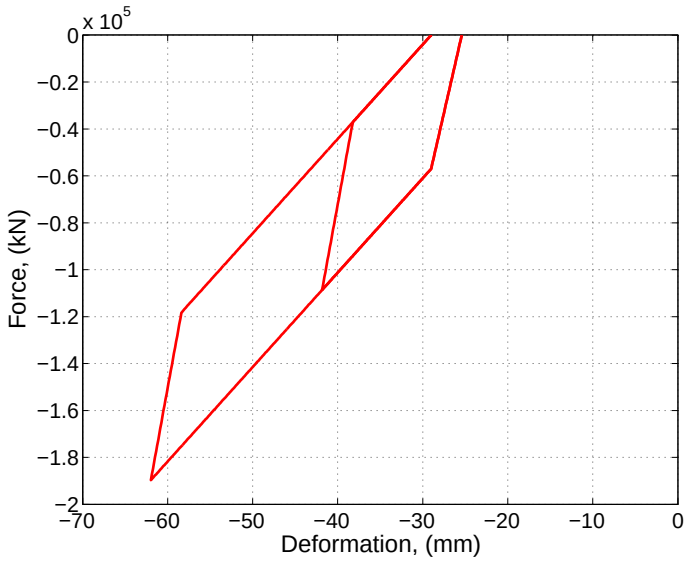

Figure C-40: Hysteretic Behavior of Impact Between Decks.

Where ΔE is the energy dissipated, k_h is an impact stiffness parameter with a typical value in English units of 25,000 k-in$^{-3/2}$, n is the Hertz coefficient typically taken as 3/2, e is the coefficient of restitution with a typical range of 0.6 - 0.8 and δ_m is the maximum penetration of the two decks.

With the dissipated energy estimated, the parameters for the bilinear model are adjusted to yield the same energy dissipation. The first step is to limit the penetration to some maximum value δ_m. The effective stiffness, K_{eff}, as seen in Figure C-39 is then obtained as:

$$K_{eff} = k_h \sqrt{\delta_m} \tag{C.6}$$

After some manipulation the remaining impact model parameters are obtained using equations C.7 through C.9.

Table C-5: Impact Element Modeling Parameters.

Parameter	Value
k_h	2,608 kip-in$^{-3/2}$/1.9 m
n	3/2
e	0.8
δ_m	25.4 mm
a	0.1
δ_y	2.54 mm
K_{eff}	456 kN/mm (per 1.9 m width)
K_{t1}	1,116 kN/mm (per 1.9 m width)
K_{t2}	384 kN/mm (per 1.9 m width)

$$\delta_y = a\delta_m \tag{C.7}$$

$$K_{t1} = K_{eff} + \frac{\Delta E}{a\delta_m^2} \tag{C.8}$$

$$K_{t2} = K_{eff} - \frac{\Delta E}{(1-a)\delta_m^2} \tag{C.9}$$

Where K_{t1} is the initial stiffness, K_{t2} is the post-yield stiffness, a is a yield parameter taken in this study as 0.1, δ_y is the yield penetration and the rest of the parameters are as previously defined. The impact model used in this study is developed using some typical recommended values and will be used for all bridges throughout this study. Table C-5 gives a concise presentation of the values used in this study.

C.6 Multi-Column Concrete Bents

Bridge piers are substructure components which act as intermediate vertical and horizontal supports for bridge decks. There are a number of different pier types used in CSUS bridges

including pier walls, hammerhead piers and multi-column rigid frame piers. The multi-column rigid frame piers, commonly referred to as multi-column bents, appear to be the most prevalent type of pier used in the CSUS and will therefore be used in all analytical models used throughout this study (Hwang et al., 2000). Figure C-41 shows a typical bridge bent configuration which consists of multiple concrete columns which are supported on reinforced concrete footings which are in turn supported on multiple piles. The tops of the columns are joined by a reinforced concrete bent beam, used to provide support for the bridge girders.

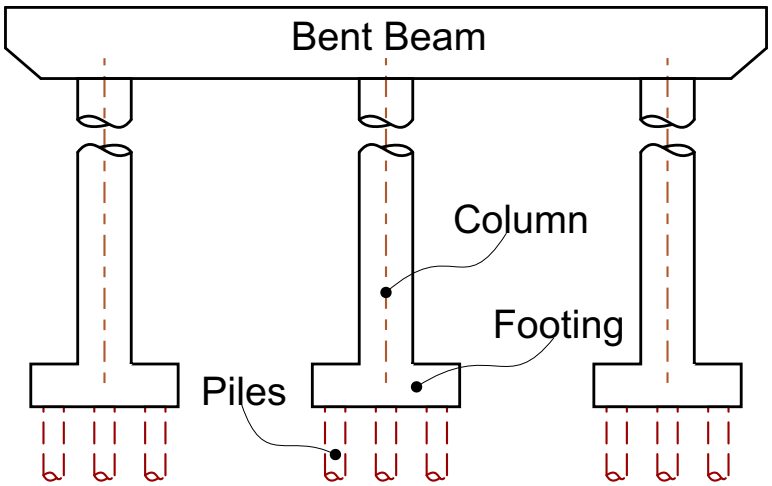

Figure C-41: Typical Multi-Column Concrete Bridge Bent Configuration.

C.7 Analytical Modeling of Concrete Bents

The concrete bents are modeled in *O*penSees using a combination of displacement beam-column elements and rigid links. A representative discretization of the bent is presented

in Figure C-42. The section properties for the columns and the bent beams are created using fiber elements with appropriate constitutive models for both the concrete and the steel reinforcement. The following sections will present the material models and section models for both the columns and the beams.

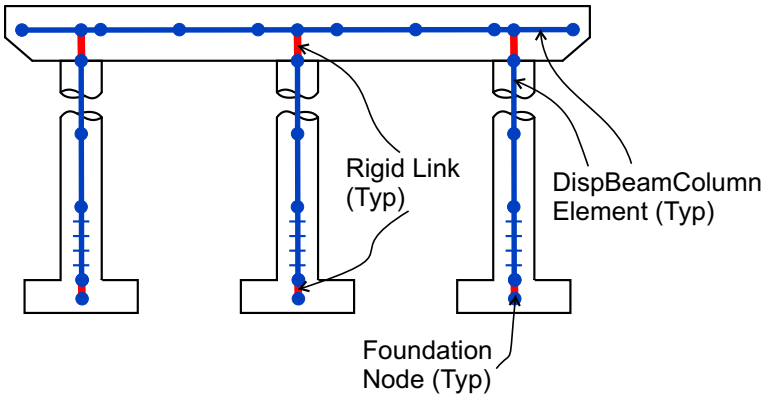

Figure C-42: Discretization of Multi-Column Concrete Bridge Bent.

C.7.1 Material Models

Reinforced concrete sections are constructed from three materials, namely unconfined concrete, confined concrete and reinforcing steel. The unconfined concrete behavior is modeled using the *Concrete01* material as provided in *O*penSees. This material uses the Kent-Scott-Park model which utilizes a degraded linear uploading/reloading stiffness and a residual stress. The behavior of this material is depicted in Figure C-43. In this figure, a concrete peak compressive stress of 27.6 MPa occurs at an associated strain $\epsilon_o = 0.002$.

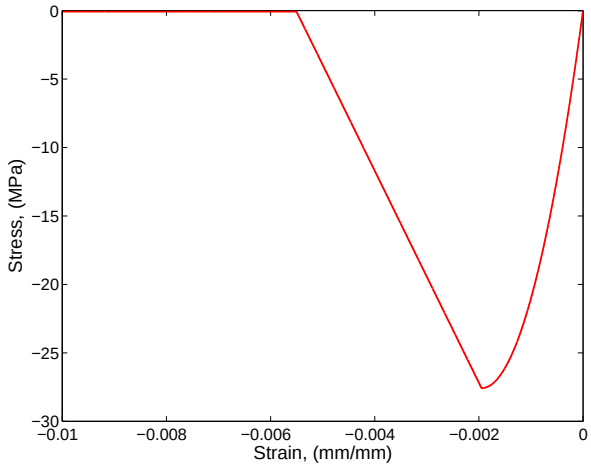

Figure C-43: Analytical Behavior of Unconfined Concrete.

The model for the confined concrete, that which is inside the transverse reinforcing steel cage, is slightly different from that of the unconfined (cover) concrete. Previous researchers have shown that confinement of concrete by transverse reinforcement results in a significant increase in both the strength and ductility of compressed concrete (Mander et al., 1988). The maximum stress and associated strain for the confined concrete is given as Kf_c' and $\epsilon_0 = 0.002K$ respectively, where K is given in Equation C.10, f_c' is the unconfined compressive cylinder strength, ρ_s is the ratio of volume of steel hoops to volume of concrete core measured to the outside of the peripheral hoop and f_{yh} is the yield strength of the steel hoops (Park et al., 1982).

$$K = 1 + \frac{\rho_s f_{yh}}{f_c'} \tag{C.10}$$

For the columns in the CSUS, it is assumed that typical transverse reinforcement is provided by 12.7 mm bars spaced at 307 mm from center to center with grade 60 steel. For

a 906 mm diameter circular column, $\rho_s = 2.04e-3$, which results in a K value of 1.031. Therefore, the confined compressive strength and associated strain are equal to 28.5 MPa and 2.062e-3 respectively. This material behavior is given in Figure C-44. It is clearly seen that both the strength and ductility of the concrete has increased.

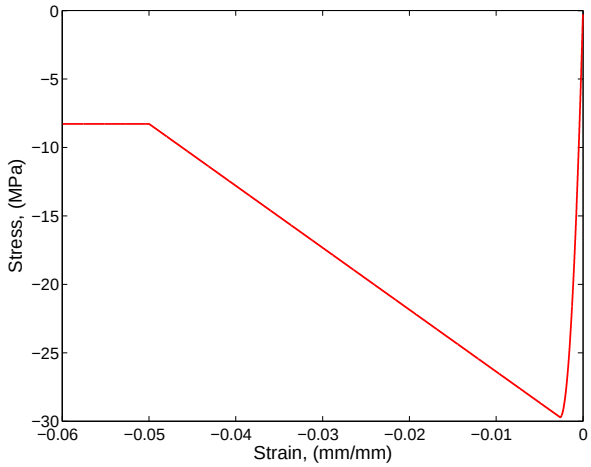

Figure C-44: Analytical Behavior of Confined Concrete.

The reinforcing steel is assumed to have a yield strength, $f_{ys} = 414MPa$, and an elastic modulus, $E_s = 200GPa$, and is modeled as a bilinear material using *O*penSees *Steel01* material. A strain hardening ratio of 0.018 is used for this material. This bilinear behavior is seen in Figure C-46.

C.7.2 Analytical Model of Concrete Columns

The elements for the columns are generated using displacement beam-column elements that have an associated fiber section being representative of the true column section. Fiber

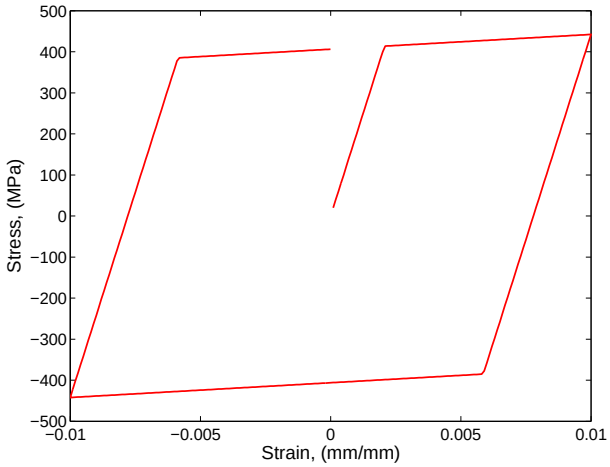

Figure C-45: Analytical Behavior of Reinforcing Steel.

elements allow the creation of a composite section which consists of different materials located at various spacial locations. There are two main column types which are used in this study. The slab bridges, as listed in Table 4-5, use a 762 mm square column with eight 25.4$mm\phi$ bars and the remainder of the bridge types use a 914.4 mm diameter circular column with 12 28.58$mm\phi$ bars. The actual configuration and dimensions of the columns will be presented later when each individual bridge type is discussed. For illustration purposes, the discretization of the circular columns is given in Figure C-46.

For verification purposes, a moment-curvature analysis of the reinforced concrete section is performed. The results of this analysis are compared under monotonic loading with those created by a commercial software package UCFyber. As shown in Figure C-47, there is an excellent agreement between the two software packages.

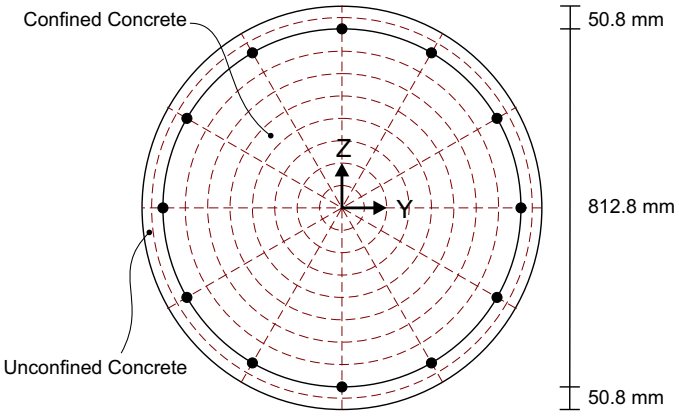

Figure C-46: Fiber Discretization of Circular Reinforced Concrete Column.

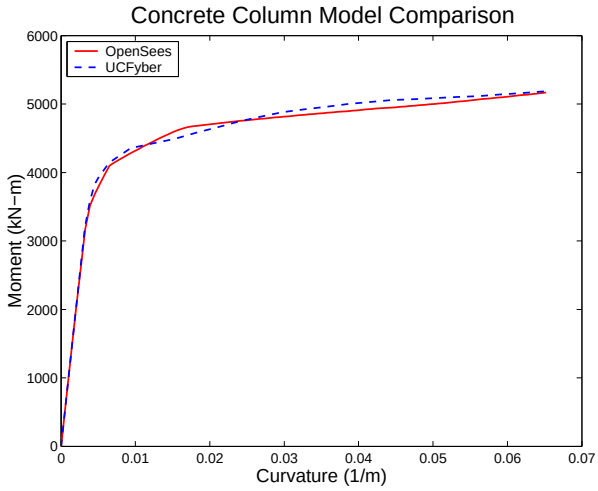

Figure C-47: Moment-Curvature Relationship of Reinforced Concrete Column Comparing OpenSees and UCFyber.

C.7.3 Analytical Model of Concrete Beam

The section for the concrete bent beam is created in the same way as for the circular columns. The bent beam is a rectangular section which is 1067 mm wide by 1220 mm tall and employs 14 – 28.6 *mm* ϕ reinforcing bars. Figure C-48 shows the discretization of the beam section while Figure C-49 shows its hysteretic behavior under cyclic loading. The non-symmetric behavior of the beam is clearly seen, as would be expected due to the non-symmetric distribution of the reinforcing steel. It should be noted that this beam section is valid for all bridge types, listed in Table 4-5, except for the slab type bridges. These slab type bridges have beam sections that are 762 mm wide x 1219.2 mm tall which use ten 31.75*mm*ϕ bars

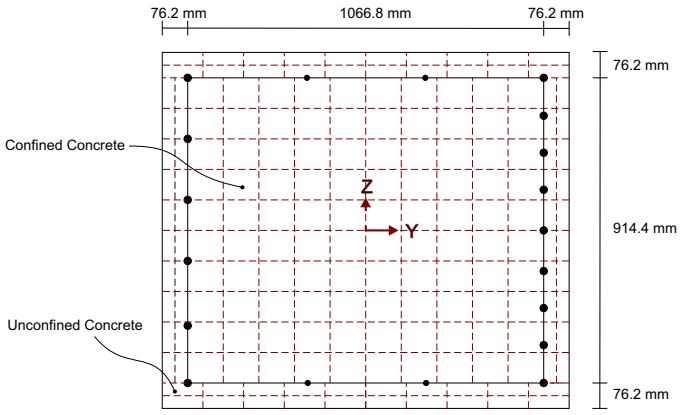

Figure C-48: Fiber Discretization of Reinforce Concrete Bent Beam.

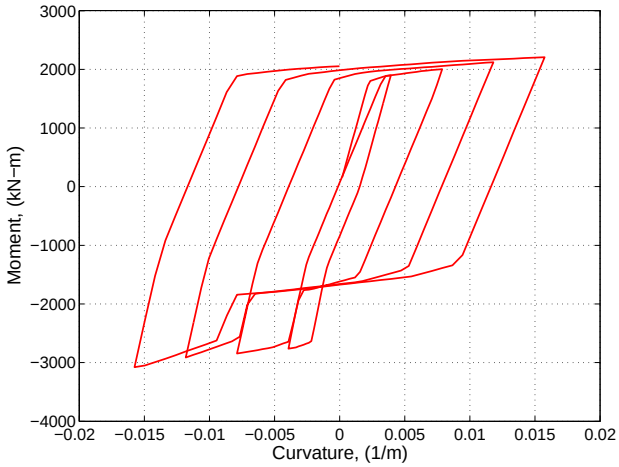

Figure C-49: Hysteretic Moment-Curvature Behavior of Reinforced Concrete Bent Beam.

C.8 Foundations

Foundations are a critical part of the substructure of a bridge system since all inertial forces must be transferred to them. For most highway bridges in the CSUS, deep foundations employing a pile system are used (Hwang et al., 2000). The following subsections will give a brief overview of pile foundations and their analytical models used throughout this study.

C.8.1 Overview of Pile Foundations

A pile foundation system, as shown in Figure C-50, consists of a group of piles, some vertical and some battered, tied together at the top with a concrete pile-cap. The piles, which are slender structural elements, are typically driven deep into the ground with the primary purpose of resisting horizontal and vertical loads. The load resisting mechanisms utilized by pile foundations include the skin resistance occurring between the pile and the

soil or they rely on the end bearing on a firm or dense soil. Often a combination of these two mechanisms is employed in pile foundation design (Ezeldin, 2001). Pile foundations are used for a variety of reasons, among which are (Fellenius, 1991):

- The need to locate a competent layer of soil to which loads can be transferred.
- Distribute loads to soils that are out of danger of scour.
- The structure may be sensitive to differential settlements.
- Loads transmitted to the soil are too large to be transmitted to the soil through typical shallow foundations.

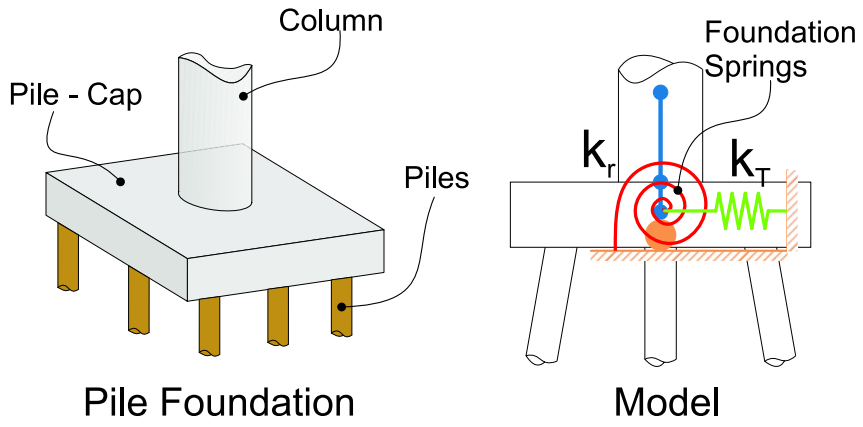

Figure C-50: Typical Pile Foundation and Associated Model.

When structures are subjected to seismic loads, one of the main tasks is to analyze how the loads are distributed through the structure. Traditionally, the effects of the foundation on the response of bridges was neglected in analytical models but has now been

recognized as a significant contributor to the response of the entire system (Ma and Deng, 2000). The analytical models that have since been developed range from very complex finite element models which explicitly treat the soil-structure interaction (direct method) to a more simplified approach which treat the effects of the soil with a set of simple rotational and translational springs (substructure method) (Wolf, 1985). The direct method can be computationally expensive in that these models generally contain a very large number of degrees-of-freedom and therefore, are not suitable for the large number of simulations required by this study. The substructure method is a more simplistic approach but allows for more economical analysis times while still considering the effects of the surrounding soil. Thus, this simplified method is used throughout this study.

C.8.2 Analytical Models of Pile Foundations

The analytical models for the pile foundations are created by deriving simple linear or non-linear springs that capture both the translational and rotational behavior of the foundation. This is done by considering the stiffness of an individual pile and then modifying these values to account for geometric effects of the pile group. The two pile stiffnesses required for the derivation of the pile cap stiffness are the vertical stiffness and the horizontal stiffness of each individual pile. The rotational stiffness at the top of each pile is not incorporated in this study as it is often considered to have a negligible contribution (Ma and Deng, 2000).

The estimate of vertical stiffness of an individual pile is developed by considering both its frictional and tip resistance. The rigidity of the pile itself plays a role but is difficult to calculate. Therefore, a solution for a rigid pile and a solution for a flexible pile are created and the estimate comes from their average. This procedure was conducted in the work

by Choi (2002) for typical piles in the CSUS. He concluded that an appropriate vertical stiffness for a single pile is approximately 175 kN/mm, which is the value that will be used in this study.

The horizontal stiffness of a single pile is assumed to follow the same behavior as the piles in the abutments. This assumes an effective stiffness of 7.0 kN/mm/pile and uses the nonlinear model as presented in Table C-4 and Figure C-36.

The composite pile behavior is computed following some basic geometry based equations presented by Ma and Deng (2000). The equations for horizontal and rotational stiffness of the pile cap are presented in Equations C.11a and C.11b respectively.

$$K_{G,h} = \sum_{i=1}^{N} K_{hh,i} \tag{C.11a}$$

$$K_{G,r} = \sum_{i=1}^{N} K_{vv,i} \cdot x_i^2 \tag{C.11b}$$

Where $K_{hh,i}$ is the horizontal stiffness and $K_{vv,i}$ is the vertical stiffness of the i^{th} pile and x_i is the distance from the centroid of the pile group measured in the direction perpendicular to axis of rotation. The aggregate stiffnesses of the pile group in the horizontal and rotational directions are represented by $K_{G,h}$ and $K_{G,r}$ respectively.

The bridges in this study use two different sizes of footings. The footings used in the slab bridges are 1.57 m wide by 2.34 m long and use six piles. All other bridge types have footings which are 2.44 m square and use eight piles. The configuration of these footings are given in Figure C-51. The calculated footing stiffnesses are presented in Table C-6.

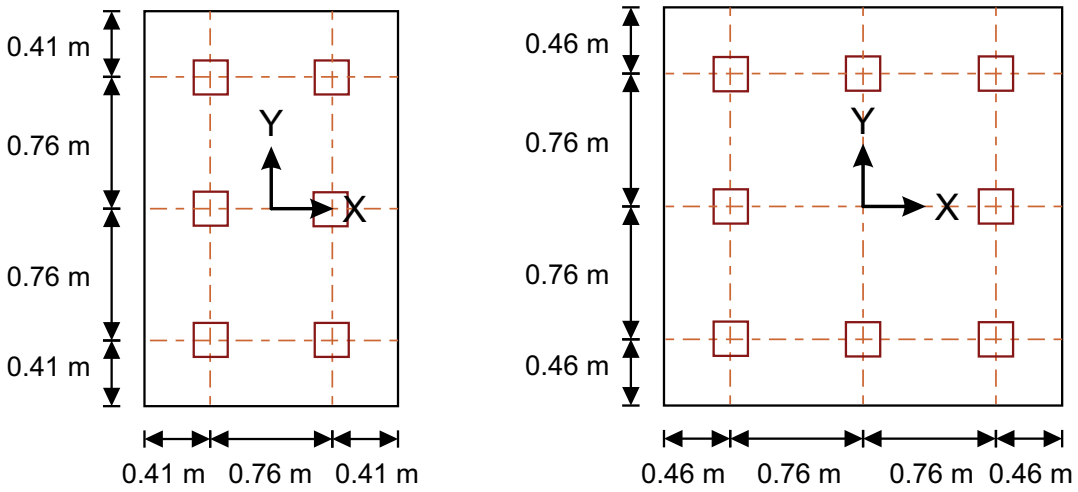

C-51(a): Slab Bridges

C-51(b): All Other Bridge Types

Figure C-51: Configuration of Bridge Footings.

Table C-6: Stiffnesses of Pile Foundations.

Bridge Type	Horizontal (kN/mm)		Rotational (kN-m/rad)	
	x	y	x - x	y - y
Slab	98	98	$4.04 \cdot (10)^5$	$1.52 \cdot (10)^5$
Multi-Span	130.5	130.5	$6.06 \cdot (10)^5$	$6.06 \cdot (10)^5$

APPENDIX D

MODAL PROPERTIES OF TYPICAL HIGHWAY BRIDGE CLASSES

The modal properties of bridges are a useful way to classify their general characteristics. Tables D-1, D-2, D-3 present the modal properties including period and effective modal mass for the multi-span simply supported, multi-span continuous and single span bridges. The fundamental period of all the multi-span bridge types has a longitudinal mode except for the slab type bridges whose fundamental modes are transverse.

The period range of all simply supported bridges is from 0.28 - 0.62 seconds. These bridges represent the most flexible of the bridge classes as is evidenced by there periods. The continuous span bridges have periods that range from 0.28 for the slab bridge to 0.54 for the concrete girder bridge. The single span bridges represent the shortest periods with the concrete bridge having a period of 0.32 seconds and the steel bridge with low-type bearings having a period of 0.17 seconds.

Table D-1: Modal Properties of Multi-Span Simply Supported Bridges.

MSSS Concrete				
Mode	Period	Effective Modal Mass (%)		
No.	(sec)	Longitudinal	Transverse	Vertical
1^{st}	0.6192	84.3	0	0
2^{nd}	0.4611	0	78.3	0
3^{rd}	0.3359	0	0	0
4^{th}	0.3288	0	0	0
5^{th}	0.3101	0	13.3	0
MSSS Concrete Box				
Mode	Period	Effective Modal Mass (%)		
No.	(sec)	Longitudinal	Transverse	Vertical
1^{st}	0.3064	93.7	0	0
2^{nd}	0.2244	0	0	31.4
3^{rd}	0.1657	0	0	0
4^{th}	0.1657	0	0	34.7
5^{th}	0.1352	0	20.7	0
MSSS Slab				
Mode	Period	Effective Modal Mass (%)		
No.	(sec)	Longitudinal	Transverse	Vertical
1^{st}	0.2798	0.3	93.2	0
2^{nd}	0.1926	91.9	0.3	0
3^{rd}	0.1562	0.4	0	0
4^{th}	0.1173	0	0	10.7
5^{th}	0.1173	0	0	36.3
MSSS Steel (High-Bearing)				
Mode	Period	Effective Modal Mass (%)		
No.	(sec)	Longitudinal	Transverse	Vertical
1^{st}	0.2952	84.6	1	0
2^{nd}	0.2535	1	89.6	0
3^{rd}	0.2337	0	0	31.5
4^{th}	0.1787	0	0.4	0
5^{th}	0.1439	0.8	0.1	0

Table D-2: Modal Properties of Multi-Span Continuous Bridges.

MSC Concrete				
Mode	Period	Effective Modal Mass (%)		
No.	(sec)	Longitudinal	Transverse	Vertical
1^{st}	0.5434	93.1	0	0
2^{nd}	0.4218	0	91.5	0
3^{rd}	0.3038	0	0	0
4^{th}	0.2287	0	0	18
5^{th}	0.1262	0	0	0
MSC Slab				
Mode	Period	Effective Modal Mass (%)		
No.	(sec)	Longitudinal	Transverse	Vertical
1^{st}	0.2798	0.3	93.2	0
2^{nd}	0.1926	91.9	0.3	0
3^{rd}	0.1562	0.4	0	0
4^{th}	0.1173	0	0	6.2
5^{th}	0.1173	0	0	0
MSC Steel (High-Bearing)				
Mode	Period	Effective Modal Mass (%)		
No.	(sec)	Longitudinal	Transverse	Vertical
1^{st}	0.4407	96.2	0	0
2^{nd}	0.3071	0	94.9	0
3^{rd}	0.2726	0	0	7.7
4^{th}	0.2127	0	0	0
5^{th}	0.179	0	0	0

Table D-3: Modal Properties of Single-Span Bridges.

SS Concrete				
Mode	Period	Effective Modal Mass (%)		
No.	(sec)	Longitudinal	Transverse	Vertical
1^{st}	0.3242	0	100	0
2^{nd}	0.317	100	0	0
3^{rd}	0.1794	0	0	80.7
4^{th}	0.1759	0	0	0
5^{th}	0.044	0	0	0
SS Steel				
Mode	Period	Effective Modal Mass (%)		
No.	(sec)	Longitudinal	Transverse	Vertical
1^{st}	0.1732	0	0	80.7
2^{nd}	0.096	0	99.5	0
3^{rd}	0.0757	100	0	0
4^{th}	0.0512	0	0.5	0
5^{th}	0.0433	0	0	0

APPENDIX E

ANOVA TABLE CALCULATIONS

The analysis of variance table for a fractional factorial design with blocking is moderately different from that for a full factorial as introduced by Hayter (2002). The general form of the table is given in Table E-1. The notations are given as follows.

Where:

y	=	response of interest		
n_b	=	number of blocks per replicate	=	8
n_{bb}	=	number of trials per block	=	4
n	=	number of replicates	=	3
n_T	=	total trials	=	$(2^5)n = 96$
k	=	number of parameters		

The sums of squares are calculated as outlined in equations E.1 through E.4.

$$SSF_i = (n)2^{k-p-1}\sum_{j=1}^{2}\left(\bar{y}_{j.....} - \bar{y}_{.....}\right)^2 \quad \text{(E.1)}$$

Where $\bar{y}_{1.....}$ is the mean of all response values where parameter i is (+), $\bar{y}_{1.....}$ is the mean of all response values where parameter i is (-), $\bar{y}_{.....}$ is the mean of all response values and $p = k - 5$.

$$SSb = n_{bb}\sum_{b=1}^{n_T/n_{bb}}(\bar{y}_{.....b} - \bar{y}_{.....})^2 \quad \text{(E.2)}$$

Where $\bar{y}_{\ldots\ldots b}$ is the mean of all response values for block number b.

$$SST = \sum_{j=1}^{(n)2^5} \left(y_j - \bar{y}_{\ldots\ldots} \right)^2 \tag{E.3}$$

Where y_j is the response of the j^{th} trial.

$$SSE = SST - \sum_{i=1}^{k} SSF_i - SSb \tag{E.4}$$

Table E-1: ANOVA for Fractional Factorial Design with Blocking.

Source	DOF	Sums of Squares	Mean Squares	F-Stat	p-value
Factor 1	1	SSF_1	$MSF_1 = \frac{SSF_1}{1}$	$F_1 = \frac{MSF_1}{MSE}$	$P[F_{1,n_T-(n_b(n)-1)-k-1} > F_1]$
$\vdots$	$\vdots$	$\vdots$	$\vdots$	$\vdots$	$\vdots$
Factor k	1	SSF_k	$MSF_k = \frac{SSF_k}{1}$	$F_k = \frac{MSF_k}{MSE}$	$P[F_{1,n_T-(n_b(n)-1)-k-1} > F_k]$
Blocks	$n_b(n) - 1$	SSb	$MSb = \frac{SSb}{n_b(n)-1}$	$F_b = \frac{MSb}{MSE}$	$P[F_{n_b(n)-1,n_T-(n_b(n)-1)-k-1} > F_b]$
Error	$n_T - (n_b(n) - 1) - k - 1$	SSE	$MSE = \frac{SSE}{n_T-(n_b(n)-1)-k-1}$		
Total	$n_T - 1$	SST			

APPENDIX F

BAYESIAN UPDATING OF CAPACITY CURVES

F.1 Introduction to Bayesian Theory

The Bayesian framework assumes that the parameters which estimate a distribution are random variables. For example, the probability density function for the random variable X, given in Equation F.1, is not only a function of x but is also a function of its parameters $\underline{\theta} = \{\theta_1, \ldots, \theta_n\}$.

$$f_X(x) = p(x|\underline{\theta}) \tag{F.1}$$

Bayesian theory asserts that the true values of $\underline{\theta}$ are random variables. This is in contrast to classical statistics where it is the estimates of the parameters ($\hat{\underline{\theta}}$) which are random variables.

Following this assumption regarding the distribution parameters, it is possible to update the parameter distribution whenever new information becomes available $f'_{\underline{\Theta}}(\underline{\theta}) \rightarrow f''_{\underline{\Theta}}(\underline{\theta})$. The framework for accomplishing this is update is Bayes' theorem, as given in Equation F.2 where both A and B are events.

$$P[B_i|A] = \frac{P[A|B_i]P[B_i]}{\sum_{j=1}^{n} P[A|B_j]P[B_j]} \tag{F.2}$$

This idea is then extended to probability distributions, the form of which is given in Equation F.3.

$$f''_{\underline{\Theta}}(\underline{\theta}) = \frac{L(x|\underline{\theta})\, f'_{\underline{\Theta}}(\underline{\theta})}{\int_{\theta_n} \dots \int_{\theta_1} L(\underline{\theta}|x)\, f'_{\underline{\Theta}}(\underline{\theta}) d\theta_1 \dots d\theta_n} \tag{F.3}$$

where

$f'_{\underline{\Theta}}(\underline{\theta})$ ≡ the analysts' prior state of knowledge about the unknown quantities $\underline{\theta}$.

x ≡ the set of additional information (e.g. expert's opinions)

$L(\underline{\theta}|x)$ ≡ the likelihood of the evidence x given that the true values of the unknown quantities are $\underline{\theta}$.

$f''_{\underline{\Theta}}(\underline{\theta})$ ≡ the analysts' posterior state of knowledge about the unknown quantities $\underline{\theta}$ given that they have received the set of additional information x.

Equation F.3 can be more concisely represented as shown in Equation F.4.

$$f''_{\underline{\Theta}}(\underline{\theta}) = k^{-1} L(x|\underline{\theta})\, f'_{\underline{\Theta}}(\underline{\theta}) \tag{F.4}$$

where k is a normalizing constant given as $\int_{\theta_n} \dots \int_{\theta_1} L(x|\underline{\theta})\, f'_{\underline{\Theta}}(\underline{\theta}) d\theta_1 \dots d\theta_n$. The normalizing constant is an important part of the formulation as it ensures that a proper distribution is derived.

Extending the second axiom of probability theory, one can recognize that a necessary requirement of the posterior distribution is given as Equation F.5.

$$\int_{\theta_n} \dots \int_{\theta_1} f''_{\underline{\Theta}}(\underline{\theta}))d\theta_1 \dots d\theta_n = 1.0 \tag{F.5}$$

At times this condition is not met resulting in what is referred to as an improper distribution. Therefore it becomes necessary to adjust k such that the posterior distribution, $f''_{\underline{\Theta}}(\underline{\theta})$, is normalized to a proper distribution.

Once the posterior distribution of the parameters is defined, the uncertainty can be included in the probability calculation of the underlying variable Y (see Equation F.6).

$$P[Y \leq a] = \int_{-\infty}^{\infty} \dots \int_{-\infty}^{\infty} P[Y \leq a|\underline{\theta}] f''_{\underline{\Theta}}(\underline{\theta})d\underline{\theta} \tag{F.6}$$

Thus, the distribution of Y now includes the influence of the additional information x.

F.2 Derivation for Lognormal Distribution When Given Percentiles

Often when working with experts it is convenient for them to provide information in terms of percentiles. For example, the analyst may request that expert i provide the value y_i for which they believe represents the 10^{th} percentile. This may be repeated for m percentiles and n experts giving the responses y_{ji} for $i = 1, \dots, n$ and $j = 1, \dots, m$.

When the data is given in this type of format, the form of the posterior distribution of the parameters must be re-derived. Following the work of Mosleh and Apostolakis (1986), the derivation proceeds as follows.

The PDF for the i^{th} expert and j^{th} percentile is given in Equation F.7.

$$f_Y(y_{ji}) = \frac{1}{\sqrt{2\pi}\sigma_{ji}y_{ji}} e^{-\frac{1}{2}\left(\frac{\ln y_{ji} - \ln y_j^t}{\sigma_{ji}}\right)^2} \tag{F.7}$$

Where y_j^t is the true value of the j^{th} percentile. σ_{ji} is a value assessed subjectively by the analyst which implies the degree of confidence the analyst has in the i^{th} expert's ability to assess the j^{th} percentile.

The parameters for the lognormal distribution are related to the true value of the j^{th} percentile (y_j^t) through the standard normal distribution. This is shown in Equation F.8.

$$\ln y_j^t = \zeta Z_j + \lambda \tag{F.8}$$

where ζ and λ are the parameters for the lognormal distribution. Z_j is the appropriate value of the standard normal distribution for the j^{th} percentile.

Substituting Equation F.8 into Equation F.7 gives Equation F.9.

$$f_Y(y_{ji}) = \frac{1}{\sqrt{2\pi}\sigma_{ji}y_{ji}} e^{-\frac{1}{2}\left(\frac{\ln y_{ji}-(\zeta Z_j+\lambda)}{\sigma_{ji}}\right)^2} \tag{F.9}$$

If the responses between every expert at every percentile are considered to be independent, then the likelihood function is given by Equation F.10.

$$L(\lambda,\zeta|y_1\cdots y_n) = \prod_{i=1}^{n}\prod_{j=1}^{m} \frac{1}{\sqrt{2\pi}\sigma_{ji}y_{ji}} e^{-\frac{1}{2}\left(\frac{\ln y_{ji}-(\zeta Z_j+\lambda)}{\sigma_{ji}}\right)^2} \tag{F.10}$$

This likelihood expression results in an expression for the joint posterior distribution of λ and ζ as shown in Equation F.11. The prior joint distribution of λ and ζ, $f_{\lambda,\zeta}(\lambda,\zeta)$, is unknown in this case. It has been suggested by some that the unknown prior is best represented by a uniform distribution Mosleh and Apostolakis (1986). However, it is argued that since the uniform distribution is not invariant under reparameterizations, that it does not truly represent a complete lack of knowledge Harney (2003). It is suggested that a true

lack of knowlege on parameter distributions is best represented by constants ($\lambda_c \equiv$ constant, $\zeta_c \equiv$ constant).

$$f''_{\Lambda,Z}(\lambda,\zeta) = \frac{\prod_{i=1}^{n}\prod_{j=1}^{m}\frac{1}{\sqrt{2\pi}\sigma_{ji}y_{ji}}e^{-\frac{1}{2}\left(\frac{\ln y_{ji}-(\zeta Z_j+\lambda)}{\sigma_{ji}}\right)^2}\lambda_c\zeta_c}{\iint\prod_{i=1}^{n}\prod_{j=1}^{m}\frac{1}{\sqrt{2\pi}\sigma_{ji}y_{ji}}e^{-\frac{1}{2}\left(\frac{\ln y_{ji}-(\zeta Z_j+\lambda)}{\sigma_{ji}}\right)^2}\lambda_c\zeta_c d\zeta d\lambda} \tag{F.11}$$

Canceling out the constants from both the numerator and denominator results in Equation F.12.

$$f''_{\Lambda,Z}(\lambda,\zeta) = \frac{\prod_{i=1}^{n}\prod_{j=1}^{m}e^{-\frac{1}{2}\left(\frac{\ln y_{ji}-(\zeta Z_j+\lambda)}{\sigma_{ji}}\right)^2}}{\iint\prod_{i=1}^{n}\prod_{j=1}^{m}e^{-\frac{1}{2}\left(\frac{\ln y_{ji}-(\zeta Z_j+\lambda)}{\sigma_{ji}}\right)^2}d\zeta d\lambda} \tag{F.12}$$

The appearance of the equation simplifies even further by recognizing that the denominator is a constant k'.

$$f''_{\Lambda,Z}(\lambda,\zeta) = k'^{-1}\prod_{i=1}^{n}\prod_{j=1}^{m}e^{-\frac{1}{2}\left(\frac{\ln y_{ji}-(\zeta Z_j+\lambda)}{\sigma_{ji}}\right)^2} \tag{F.13}$$

Equation F.13 can be rewritten in terms of summations by pulling the products up into the exponent. Equation F.14 shows the modified equation where $\sum_{ji}$ represents the double summation over all *n* and *m*.

$$f''_{\Lambda,Z}(\lambda,\zeta) = k'^{-1}e^{-\frac{1}{2}\sum_{ji}\left(\frac{\ln y_{ji}-(\zeta Z_j+\lambda)}{\sigma_{ji}}\right)^2} \tag{F.14}$$

It is now beneficial to rewrite the term in the exponent to make it more usable. Following a series of algebraic manipulations, Equation F.14 can be rewritten as Equation F.15.

$$f''_{\Lambda,Z}(\lambda,\zeta) = k'^{-1}e^{-\frac{1}{2}\left[\left(\frac{\lambda-\hat{\lambda}(\zeta)}{\sigma_\lambda}\right)^2+\left(\frac{\zeta-\hat{\zeta}}{\sigma_\zeta}\right)^2\right]} \tag{F.15}$$

where k' is calculated by Equation F.16.

$$k' = \int_{-\infty}^{\infty} \int_{0}^{\infty} e^{-\frac{1}{2}\left[\left(\frac{\lambda-\hat{\lambda}(\zeta)}{\sigma_\lambda}\right)^2+\left(\frac{\zeta-\hat{\zeta}}{\sigma_\zeta}\right)^2\right]} d\zeta d\lambda \tag{F.16}$$

The parameters of Equation F.15 are defined in the Equations F.17 through F.20.

$$\hat{\lambda}(\zeta) = \frac{\sum_{ji} \sigma_{ji}^{-2} \ln y_{ji} - \zeta \sum_{ji} \sigma_{ji}^{-2} Z_j}{\sum_{ji} \sigma_{ji}^{-2}} \tag{F.17}$$

$$\sigma_\lambda^2 = \left(\sum_{ji} \sigma_{ji}^{-2}\right)^{-1} \tag{F.18}$$

$$\hat{\zeta} = \frac{\left(\sum_{ji} \sigma_{ji}^{-2} Z_j \ln y_{ji}\right)\left(\sum_{ji} \sigma_{ji}^{-2}\right) - \left(\sum_{ji} \sigma_{ji}^{-2} Z_j\right)\left(\sum_{ji} \sigma_{ji}^{-2} \ln y_{ji}\right)}{\left(\sum_{ji} \sigma_{ji}^{-2} Z_j^2\right)\left(\sum_{ji} \sigma_{ji}^{-2}\right) - \left(\sum_{ji} Z_j \sigma_{ji}^{-2}\right)^2} \tag{F.19}$$

$$\sigma_\zeta^2 = \frac{\sum_{ji} \sigma_{ji}^{-2}}{\left(\sum_{ji} \sigma_{ji}^{-2} Z_j^2\right)\left(\sum_{ji} \sigma_{ji}^{-2}\right) - \left(\sum_{ji} Z_j \sigma_{ji}^{-2}\right)^2} \tag{F.20}$$

Equation F.15 now describes the posterior joint probability distribution for λ and ζ. This equation can now be used to calculate the updated distribution of each limit state by using it with Equation F.6. The expected value for the CDF ($F_X(x)$) of the limit state distribution is given in Equation F.21.

$$E\left[F_X(x)\right] = \int_0^x \int_{-\infty}^{\infty} \int_0^{\infty} \frac{1}{\sqrt{2\pi} x' \zeta} e^{\left(-\frac{1}{2}\left(\frac{\ln x' - \lambda}{\zeta}\right)^2\right)} f''_{\Lambda,Z}(\lambda, \zeta) \mathrm{d}\zeta \mathrm{d}\lambda \mathrm{d}x' \tag{F.21}$$

This equation must then be solved numerically. At the same time, percentiles of the distribution $F_X(x)$ may be calculated as shown in Figure 8-3. Assuming all σ_{ji} values to be

equal to 0.5, the resulting lognormal distributions for each limit state of each component is given in Table 8-9.

APPENDIX G

COMPONENT FRAGILITY CURVES

The fragility curves for the components of each of the nine bridge types are presented in this Appendix. The medians are given in terms of gravitational acceleration g. Whenever the estimated median is larger than 4.0, the median and dispersion values are replaced by 99.00 and 0.00 respectively. This indicates that this particular component is not significant for that limit state. The curves are presented for intensity measure of PGA and S_{a-gm}, as derived using both the Rix and Fernandez ground motion suite and also the Wen and Wu ground motion suite.

G.1 MSC Concrete

This section contains the component fragility curves for the multi-span continuous concrete girder bridge.

Table G-1: Component Fragilities for MSC Concrete Bridge Components - PGA (Rix).

	Slight		Moderate		Extensive		Complete	
Component	**Med (g)**	**Disp**	**Med (g)**	**Disp**	**Med (g)**	**Disp**	**Med (g)**	**Disp**
Column	0.51	0.71	0.77	0.66	1.21	0.74	1.70	0.74
Fxd-Long	0.29	0.83	0.97	0.80	1.25	0.83	1.67	0.87
Fxd-Tran	3.12	1.81	99.00	0.00	99.00	0.00	99.00	0.00
Exp-Long	0.27	0.81	1.04	0.77	1.38	0.80	1.92	0.85
Exp-Tran	3.23	1.80	99.00	0.00	99.00	0.00	99.00	0.00
Ab-Pass	0.99	0.70	3.03	0.70	99.00	0.00	99.00	0.00
Ab-Act	0.48	2.29	99.00	0.00	99.00	0.00	99.00	0.00
Ab-Tran	0.56	1.06	2.63	1.25	99.00	0.00	99.00	0.00

Table G-2: Component Fragilities for MSC Concrete Bridge Components - S_{a-gm} (Rix).

	Slight		Moderate		Extensive		Complete	
Component	**Med (g)**	**Disp**	**Med (g)**	**Disp**	**Med (g)**	**Disp**	**Med (g)**	**Disp**
Column	1.01	0.65	1.53	0.60	2.38	0.68	3.35	0.69
Fxd-Long	0.62	0.82	2.04	0.79	2.62	0.81	3.51	0.85
Fxd-Tran	99.00	0.00	99.00	0.00	99.00	0.00	99.00	0.00
Exp-Long	0.57	0.84	2.29	0.80	3.06	0.83	99.00	0.00
Exp-Tran	99.00	0.00	99.00	0.00	99.00	0.00	99.00	0.00
Ab-Pass	2.22	0.75	99.00	0.00	99.00	0.00	99.00	0.00
Ab-Act	0.96	2.26	99.00	0.00	99.00	0.00	99.00	0.00
Ab-Tran	1.12	1.03	99.00	0.00	99.00	0.00	99.00	0.00

Table G-3: Component Fragilities for MSC Concrete Bridge Components - PGA (Wen).

	Slight		Moderate		Extensive		Complete	
Component	**Med (g)**	**Disp**	**Med (g)**	**Disp**	**Med (g)**	**Disp**	**Med (g)**	**Disp**
Column	0.50	0.69	0.73	0.66	1.08	0.72	1.45	0.72
Fxd-Long	0.34	0.64	0.92	0.61	1.14	0.63	1.45	0.67
Fxd-Tran	1.24	1.33	99.00	0.00	99.00	0.00	99.00	0.00
Exp-Long	0.35	0.76	1.17	0.72	1.50	0.75	2.01	0.79
Exp-Tran	1.34	1.32	99.00	0.00	99.00	0.00	99.00	0.00
Ab-Pass	2.08	0.92	99.00	0.00	99.00	0.00	99.00	0.00
Ab-Act	0.46	1.49	3.91	1.74	99.00	0.00	99.00	0.00
Ab-Tran	0.46	1.00	1.83	1.16	3.77	1.12	99.00	0.00

Table G-4: Component Fragilities for MSC Concrete Bridge Components - S_{a-gm} (Wen).

	Slight		Moderate		Extensive		Complete	
Component	**Med (g)**	**Disp**	**Med (g)**	**Disp**	**Med (g)**	**Disp**	**Med (g)**	**Disp**
Column	0.76	1.05	1.42	0.97	2.74	1.09	99.00	0.00
Fxd-Long	0.41	1.20	2.75	1.15	99.00	0.00	99.00	0.00
Fxd-Tran	99.00	0.00	99.00	0.00	99.00	0.00	99.00	0.00
Exp-Long	0.39	1.21	3.07	1.14	99.00	0.00	99.00	0.00
Exp-Tran	99.00	0.00	99.00	0.00	99.00	0.00	99.00	0.00
Ab-Pass	99.00	0.00	99.00	0.00	99.00	0.00	99.00	0.00
Ab-Act	0.52	2.08	99.00	0.00	99.00	0.00	99.00	0.00
Ab-Tran	0.66	1.81	99.00	0.00	99.00	0.00	99.00	0.00

G.2 MSC Slab

This section contains the component fragility curves for the multi-span continuous slab bridge.

Table G-5: Component Fragilities for MSC Slab Bridge Components - PGA (Rix).

	Slight		Moderate		Extensive		Complete	
Component	**Med (g)**	**Disp**	**Med (g)**	**Disp**	**Med (g)**	**Disp**	**Med (g)**	**Disp**
Column	1.10	0.76	1.72	0.71	2.76	0.79	3.98	0.80
Fxd-Long	99.00	0.00	99.00	0.00	99.00	0.00	99.00	0.00
Fxd-Tran	99.00	0.00	99.00	0.00	99.00	0.00	99.00	0.00
Exp-Long	2.86	0.95	99.00	0.00	99.00	0.00	99.00	0.00
Exp-Tran	99.00	0.00	99.00	0.00	99.00	0.00	99.00	0.00
Ab-Pass	99.00	0.00	99.00	0.00	99.00	0.00	99.00	0.00
Ab-Act	0.37	1.01	1.55	1.18	3.26	1.13	99.00	0.00
Ab-Tran	0.26	0.77	0.91	0.93	1.73	0.89	99.00	0.00

Table G-6: Component Fragilities for MSC Slab Bridge Components - S_{a-gm} (Rix).

	Slight		Moderate		Extensive		Complete	
Component	**Med (g)**	**Disp**	**Med (g)**	**Disp**	**Med (g)**	**Disp**	**Med (g)**	**Disp**
Column	1.51	0.69	2.23	0.65	3.37	0.72	99.00	0.00
Fxd-Long	99.00	0.00	99.00	0.00	99.00	0.00	99.00	0.00
Fxd-Tran	99.00	0.00	99.00	0.00	99.00	0.00	99.00	0.00
Exp-Long	99.00	0.00	99.00	0.00	99.00	0.00	99.00	0.00
Exp-Tran	99.00	0.00	99.00	0.00	99.00	0.00	99.00	0.00
Ab-Pass	99.00	0.00	99.00	0.00	99.00	0.00	99.00	0.00
Ab-Act	0.62	0.82	2.18	0.97	99.00	0.00	99.00	0.00
Ab-Tran	0.44	0.70	1.31	0.84	2.32	0.80	99.00	0.00

Table G-7: Component Fragilities for MSC Slab Bridge Components - PGA (Wen).

	Slight		Moderate		Extensive		Complete	
Component	**Med (g)**	**Disp**	**Med (g)**	**Disp**	**Med (g)**	**Disp**	**Med (g)**	**Disp**
Column	0.58	0.70	0.82	0.67	1.20	0.73	1.60	0.73
Fxd-Long	0.92	0.69	2.23	0.67	2.68	0.68	3.34	0.71
Fxd-Tran	99.00	0.00	99.00	0.00	99.00	0.00	99.00	0.00
Exp-Long	0.69	0.64	1.51	0.62	1.78	0.63	2.16	0.65
Exp-Tran	99.00	0.00	99.00	0.00	99.00	0.00	99.00	0.00
Ab-Pass	2.06	0.81	99.00	0.00	99.00	0.00	99.00	0.00
Ab-Act	0.20	0.67	0.51	0.77	0.82	0.74	99.00	0.00
Ab-Tran	0.20	0.80	0.66	0.94	1.22	0.90	99.00	0.00

Table G-8: Component Fragilities for MSC Slab Bridge Components - S_{a-gm} (Wen).

	Slight		Moderate		Extensive		Complete	
Component	**Med (g)**	**Disp**	**Med (g)**	**Disp**	**Med (g)**	**Disp**	**Med (g)**	**Disp**
Column	1.21	0.84	1.92	0.80	3.13	0.87	99.00	0.00
Fxd-Long	2.66	1.00	99.00	0.00	99.00	0.00	99.00	0.00
Fxd-Tran	99.00	0.00	99.00	0.00	99.00	0.00	99.00	0.00
Exp-Long	1.71	0.90	99.00	0.00	99.00	0.00	99.00	0.00
Exp-Tran	99.00	0.00	99.00	0.00	99.00	0.00	99.00	0.00
Ab-Pass	99.00	0.00	99.00	0.00	99.00	0.00	99.00	0.00
Ab-Act	0.29	0.95	1.11	1.10	2.23	1.06	99.00	0.00
Ab-Tran	0.29	1.04	1.47	1.24	3.43	1.19	99.00	0.00

G.3 MSC Steel

This section contains the component fragility curves for the multi-span continuous steel girder bridge.

Table G-9: Component Fragilities for MSC Steel Bridge Components - PGA (Rix).

	Slight		Moderate		Extensive		Complete	
Component	**Med (g)**	**Disp**	**Med (g)**	**Disp**	**Med (g)**	**Disp**	**Med (g)**	**Disp**
Column	0.21	0.49	0.28	0.46	0.38	0.51	0.47	0.52
Fxd-Long	0.85	0.72	2.00	0.72	3.29	0.78	99.00	0.00
Fxd-Tran	0.67	0.76	1.49	0.76	2.36	0.81	99.00	0.00
Exp-Long	0.17	0.56	0.35	0.54	0.42	0.56	0.53	0.59
Exp-Tran	0.24	0.59	0.47	0.59	0.69	0.63	1.61	0.67
Ab-Pass	0.63	0.71	1.08	0.71	2.32	0.69	2.32	0.69
Ab-Act	99.00	0.00	99.00	0.00	99.00	0.00	99.00	0.00
Ab-Tran	0.72	0.94	3.07	1.12	99.00	0.00	99.00	0.00

Table G-10: Component Fragilities for MSC Steel Bridge Components - S_{a-gm} (Rix).

	Slight		Moderate		Extensive		Complete	
Component	**Med (g)**	**Disp**	**Med (g)**	**Disp**	**Med (g)**	**Disp**	**Med (g)**	**Disp**
Column	0.44	0.60	0.59	0.58	0.81	0.62	1.04	0.63
Fxd-Long	1.82	0.77	99.00	0.00	99.00	0.00	99.00	0.00
Fxd-Tran	1.10	0.52	2.20	0.52	3.29	0.57	99.00	0.00
Exp-Long	0.34	0.79	0.79	0.77	0.98	0.79	1.27	0.82
Exp-Tran	0.47	0.46	0.90	0.46	1.29	0.51	2.94	0.56
Ab-Pass	1.56	0.95	2.94	0.95	99.00	0.00	99.00	0.00
Ab-Act	99.00	0.00	99.00	0.00	99.00	0.00	99.00	0.00
Ab-Tran	1.36	0.87	99.00	0.00	99.00	0.00	99.00	0.00

Table G-11: Component Fragilities for MSC Steel Bridge Components - PGA (Wen).

	Slight		Moderate		Extensive		Complete	
Component	**Med (g)**	**Disp**	**Med (g)**	**Disp**	**Med (g)**	**Disp**	**Med (g)**	**Disp**
Column	0.36	0.52	0.46	0.50	0.60	0.53	0.74	0.54
Fxd-Long	0.76	0.58	1.44	0.58	2.08	0.61	99.00	0.00
Fxd-Tran	0.59	0.66	1.16	0.66	1.70	0.70	99.00	0.00
Exp-Long	0.31	0.60	0.58	0.58	0.69	0.59	0.84	0.62
Exp-Tran	0.33	0.56	0.66	0.56	0.98	0.61	2.38	0.66
Ab-Pass	1.24	0.76	2.21	0.76	99.00	0.00	99.00	0.00
Ab-Act	99.00	0.00	99.00	0.00	99.00	0.00	99.00	0.00
Ab-Tran	0.89	1.03	99.00	0.00	99.00	0.00	99.00	0.00

Table G-12: Component Fragilities for MSC Steel Bridge Components - S_{a-gm} (Wen).

	Slight		Moderate		Extensive		Complete	
Component	**Med (g)**	**Disp**	**Med (g)**	**Disp**	**Med (g)**	**Disp**	**Med (g)**	**Disp**
Column	0.57	0.92	0.91	0.87	1.49	0.94	2.17	0.95
Fxd-Long	2.91	1.19	99.00	0.00	99.00	0.00	99.00	0.00
Fxd-Tran	2.42	1.45	99.00	0.00	99.00	0.00	99.00	0.00
Exp-Long	0.41	0.89	1.22	0.85	1.63	0.88	2.28	0.93
Exp-Tran	0.44	1.14	1.52	1.14	3.10	1.21	99.00	0.00
Ab-Pass	99.00	0.00	99.00	0.00	99.00	0.00	99.00	0.00
Ab-Act	99.00	0.00	99.00	0.00	99.00	0.00	99.00	0.00
Ab-Tran	99.00	0.00	99.00	0.00	99.00	0.00	99.00	0.00

G.4 MSSS Concrete

This section contains the component fragility curves for the multi-span simply supported concrete girder bridge.

Table G-13: Component Fragilities for MSSS Concrete Bridge Components - PGA (Rix).

	Slight		Moderate		Extensive		Complete	
Component	**Med (g)**	**Disp**	**Med (g)**	**Disp**	**Med (g)**	**Disp**	**Med (g)**	**Disp**
Column	0.50	0.69	0.79	0.63	1.27	0.72	1.84	0.73
Fxd-Long	0.52	0.85	1.76	0.81	2.27	0.84	3.07	0.88
Fxd-Tran	99.00	0.00	99.00	0.00	99.00	0.00	99.00	0.00
Exp-Long	0.27	0.78	0.97	0.73	1.26	0.76	1.72	0.81
Exp-Tran	99.00	0.00	99.00	0.00	99.00	0.00	99.00	0.00
Ab-Pass	1.83	0.60	99.00	0.00	99.00	0.00	99.00	0.00
Ab-Act	0.43	0.98	1.97	1.18	99.00	0.00	99.00	0.00
Ab-Tran	0.83	0.86	3.14	1.03	99.00	0.00	99.00	0.00

Table G-14: Component Fragilities for MSSS Concrete Bridge Components - S_{a-gm} (Rix).

	Slight		Moderate		Extensive		Complete	
Component	**Med (g)**	**Disp**	**Med (g)**	**Disp**	**Med (g)**	**Disp**	**Med (g)**	**Disp**
Column	0.93	0.64	1.42	0.58	2.23	0.68	3.16	0.68
Fxd-Long	0.89	0.79	2.70	0.76	3.40	0.78	99.00	0.00
Fxd-Tran	99.00	0.00	99.00	0.00	99.00	0.00	99.00	0.00
Exp-Long	0.54	0.75	1.90	0.71	2.46	0.74	3.35	0.79
Exp-Tran	99.00	0.00	99.00	0.00	99.00	0.00	99.00	0.00
Ab-Pass	3.71	0.63	99.00	0.00	99.00	0.00	99.00	0.00
Ab-Act	0.90	0.92	99.00	0.00	99.00	0.00	99.00	0.00
Ab-Tran	1.57	0.79	99.00	0.00	99.00	0.00	99.00	0.00

Table G-15: Component Fragilities for MSSS Concrete Bridge Components - PGA (Wen).

	Slight		Moderate		Extensive		Complete	
Component	**Med (g)**	**Disp**	**Med (g)**	**Disp**	**Med (g)**	**Disp**	**Med (g)**	**Disp**
Column	0.72	0.82	1.14	0.78	1.86	0.86	2.71	0.86
Fxd-Long	0.53	0.77	1.50	0.74	1.87	0.76	2.41	0.80
Fxd-Tran	1.19	1.34	99.00	0.00	99.00	0.00	99.00	0.00
Exp-Long	0.38	0.78	1.31	0.74	1.71	0.77	2.32	0.82
Exp-Tran	0.92	1.32	3.21	1.25	99.00	0.00	99.00	0.00
Ab-Pass	3.52	0.89	99.00	0.00	99.00	0.00	99.00	0.00
Ab-Act	0.56	1.17	2.91	1.36	99.00	0.00	99.00	0.00
Ab-Tran	0.98	1.10	99.00	0.00	99.00	0.00	99.00	0.00

Table G-16: Component Fragilities for MSSS Concrete Bridge Components - S_{a-gm} (Wen).

	Slight		Moderate		Extensive		Complete	
Component	**Med (g)**	**Disp**	**Med (g)**	**Disp**	**Med (g)**	**Disp**	**Med (g)**	**Disp**
Column	1.16	1.18	2.42	1.09	99.00	0.00	99.00	0.00
Fxd-Long	0.76	1.27	99.00	0.00	99.00	0.00	99.00	0.00
Fxd-Tran	99.00	0.00	99.00	0.00	99.00	0.00	99.00	0.00
Exp-Long	0.41	1.17	3.28	1.10	99.00	0.00	99.00	0.00
Exp-Tran	2.38	2.32	99.00	0.00	99.00	0.00	99.00	0.00
Ab-Pass	99.00	0.00	99.00	0.00	99.00	0.00	99.00	0.00
Ab-Act	0.88	1.89	99.00	0.00	99.00	0.00	99.00	0.00
Ab-Tran	2.11	1.73	99.00	0.00	99.00	0.00	99.00	0.00

Table G-17: Component Fragilities for MSSS Concrete Bridge Components - PGA (No Rot).

	Slight		Moderate		Extensive		Complete	
Component	**Med (g)**	**Disp**	**Med (g)**	**Disp**	**Med (g)**	**Disp**	**Med (g)**	**Disp**
Column	0.52	0.65	0.81	0.59	1.30	0.69	1.87	0.69
Fxd-Long	0.48	0.87	1.58	0.84	2.02	0.86	2.70	0.90
Fxd-Tran	99.00	0.00	99.00	0.00	99.00	0.00	99.00	0.00
Exp-Long	0.30	0.76	1.12	0.72	1.46	0.75	2.02	0.80
Exp-Tran	99.00	0.00	99.00	0.00	99.00	0.00	99.00	0.00
Ab-Pass	2.25	0.66	99.00	0.00	99.00	0.00	99.00	0.00
Ab-Act	0.41	0.86	1.62	1.04	3.35	0.99	99.00	0.00
Ab-Tran	0.94	0.98	3.92	1.15	99.00	0.00	99.00	0.00

Table G-18: Component Fragilities for MSSS Concrete Bridge Components - S_{a-gm} (No Rot).

	Slight		Moderate		Extensive		Complete	
Component	**Med (g)**	**Disp**	**Med (g)**	**Disp**	**Med (g)**	**Disp**	**Med (g)**	**Disp**
Column	0.96	0.61	1.46	0.55	2.27	0.65	3.20	0.65
Fxd-Long	0.96	0.85	3.09	0.82	3.93	0.84	99.00	0.00
Fxd-Tran	99.00	0.00	99.00	0.00	99.00	0.00	99.00	0.00
Exp-Long	0.58	0.72	1.98	0.68	2.56	0.71	3.48	0.76
Exp-Tran	99.00	0.00	99.00	0.00	99.00	0.00	99.00	0.00
Ab-Pass	3.95	0.67	99.00	0.00	99.00	0.00	99.00	0.00
Ab-Act	0.84	0.82	3.34	1.01	99.00	0.00	99.00	0.00
Ab-Tran	1.72	0.89	99.00	0.00	99.00	0.00	99.00	0.00

Table G-19: Component Fragilities for MSSS Concrete Bridge Components - PGA (Longitudinal).

	Slight		Moderate		Extensive		Complete	
Component	**Med (g)**	**Disp**	**Med (g)**	**Disp**	**Med (g)**	**Disp**	**Med (g)**	**Disp**
Column	0.74	0.33	0.92	0.30	1.16	0.34	1.38	0.35
Fxd-Long	0.71	0.45	1.28	0.43	1.45	0.44	1.67	0.46
Exp-Long	0.54	0.35	0.97	0.33	1.10	0.34	1.27	0.37
Ab-Pass	1.40	0.31	2.44	0.31	99.00	0.00	99.00	0.00
Ab-Act	0.63	0.40	1.16	0.47	1.60	0.45	99.00	0.00

Table G-20: Component Fragilities for MSSS Concrete Bridge Components - S_{a-gm} (Longitudinal).

	Slight		Moderate		Extensive		Complete	
Component	**Med (g)**	**Disp**	**Med (g)**	**Disp**	**Med (g)**	**Disp**	**Med (g)**	**Disp**
Column	1.01	0.60	1.53	0.54	2.36	0.63	3.30	0.64
Fxd-Long	1.03	0.90	3.36	0.87	99.00	0.00	99.00	0.00
Exp-Long	0.57	0.65	1.85	0.61	2.36	0.64	3.15	0.69
Ab-Pass	3.59	0.61	99.00	0.00	99.00	0.00	99.00	0.00
Ab-Act	0.90	0.79	3.25	0.95	99.00	0.00	99.00	0.00

G.5 MSSS Concrete-Box

This section contains the component fragility curves for the multi-span simply supported concrete-box girder bridge.

Table G-21: Component Fragilities for MSSS Concrete-Box Bridge Components - PGA (Rix).

	Slight		Moderate		Extensive		Complete	
Component	**Med (g)**	**Disp**	**Med (g)**	**Disp**	**Med (g)**	**Disp**	**Med (g)**	**Disp**
Column	0.87	0.82	1.41	0.77	2.36	0.86	3.52	0.86
Fxd-Long	99.00	0.00	99.00	0.00	99.00	0.00	99.00	0.00
Fxd-Tran	99.00	0.00	99.00	0.00	99.00	0.00	99.00	0.00
Exp-Long	1.68	0.76	99.00	0.00	99.00	0.00	99.00	0.00
Exp-Tran	99.00	0.00	99.00	0.00	99.00	0.00	99.00	0.00
Ab-Pass	3.45	0.71	99.00	0.00	99.00	0.00	99.00	0.00
Ab-Act	0.30	0.86	1.16	1.04	2.38	0.99	99.00	0.00
Ab-Tran	0.74	1.02	3.68	1.23	99.00	0.00	99.00	0.00

Table G-22: Component Fragilities for MSSS Concrete-Box Bridge Components - S_{a-gm} (Rix).

	Slight		Moderate		Extensive		Complete	
Component	**Med (g)**	**Disp**	**Med (g)**	**Disp**	**Med (g)**	**Disp**	**Med (g)**	**Disp**
Column	1.15	0.60	1.75	0.55	2.70	0.64	3.79	0.65
Fxd-Long	99.00	0.00	99.00	0.00	99.00	0.00	99.00	0.00
Fxd-Tran	99.00	0.00	99.00	0.00	99.00	0.00	99.00	0.00
Exp-Long	2.28	0.63	99.00	0.00	99.00	0.00	99.00	0.00
Exp-Tran	99.00	0.00	99.00	0.00	99.00	0.00	99.00	0.00
Ab-Pass	99.00	0.00	99.00	0.00	99.00	0.00	99.00	0.00
Ab-Act	0.46	0.69	1.45	0.84	2.65	0.80	99.00	0.00
Ab-Tran	1.07	0.80	99.00	0.00	99.00	0.00	99.00	0.00

Table G-23: Component Fragilities for MSSS Concrete-Box Bridge Components - PGA (Wen).

	Slight		Moderate		Extensive		Complete	
Component	**Med (g)**	**Disp**	**Med (g)**	**Disp**	**Med (g)**	**Disp**	**Med (g)**	**Disp**
Column	0.87	0.85	1.49	0.79	2.65	0.90	99.00	0.00
Fxd-Long	99.00	0.00	99.00	0.00	99.00	0.00	99.00	0.00
Fxd-Tran	99.00	0.00	99.00	0.00	99.00	0.00	99.00	0.00
Exp-Long	1.33	0.80	99.00	0.00	99.00	0.00	99.00	0.00
Exp-Tran	99.00	0.00	99.00	0.00	99.00	0.00	99.00	0.00
Ab-Pass	99.00	0.00	99.00	0.00	99.00	0.00	99.00	0.00
Ab-Act	0.21	0.81	0.74	0.97	1.45	0.93	99.00	0.00
Ab-Tran	0.56	0.92	2.39	1.10	99.00	0.00	99.00	0.00

Table G-24: Component Fragilities for MSSS Concrete-Box Bridge Components - S_{a-gm} (Wen).

	Slight		Moderate		Extensive		Complete	
Component	**Med (g)**	**Disp**	**Med (g)**	**Disp**	**Med (g)**	**Disp**	**Med (g)**	**Disp**
Column	2.35	1.13	99.00	0.00	99.00	0.00	99.00	0.00
Fxd-Long	99.00	0.00	99.00	0.00	99.00	0.00	99.00	0.00
Fxd-Tran	99.00	0.00	99.00	0.00	99.00	0.00	99.00	0.00
Exp-Long	99.00	0.00	99.00	0.00	99.00	0.00	99.00	0.00
Exp-Tran	99.00	0.00	99.00	0.00	99.00	0.00	99.00	0.00
Ab-Pass	99.00	0.00	99.00	0.00	99.00	0.00	99.00	0.00
Ab-Act	0.32	1.21	2.06	1.44	99.00	0.00	99.00	0.00
Ab-Tran	1.43	1.41	99.00	0.00	99.00	0.00	99.00	0.00

G.6 MSSS Slab

This section contains the component fragility curves for the multi-span simply supported slab bridge.

Table G-25: Component Fragilities for MSSS Slab Bridge Components - PGA (Rix).

	Slight		Moderate		Extensive		Complete	
Component	**Med (g)**	**Disp**	**Med (g)**	**Disp**	**Med (g)**	**Disp**	**Med (g)**	**Disp**
Column	0.68	0.76	1.05	0.71	1.69	0.79	2.42	0.80
Fxd-Long	99.00	0.00	99.00	0.00	99.00	0.00	99.00	0.00
Fxd-Tran	99.00	0.00	99.00	0.00	99.00	0.00	99.00	0.00
Exp-Long	2.55	1.05	99.00	0.00	99.00	0.00	99.00	0.00
Exp-Tran	99.00	0.00	99.00	0.00	99.00	0.00	99.00	0.00
Ab-Pass	99.00	0.00	99.00	0.00	99.00	0.00	99.00	0.00
Ab-Act	0.30	1.03	1.50	1.24	3.52	1.18	99.00	0.00
Ab-Tran	0.27	0.83	0.82	0.96	1.49	0.92	99.00	0.00

Table G-26: Component Fragilities for MSSS Slab Bridge Components - S_{a-gm} (Rix).

	Slight		Moderate		Extensive		Complete	
Component	**Med (g)**	**Disp**	**Med (g)**	**Disp**	**Med (g)**	**Disp**	**Med (g)**	**Disp**
Column	1.13	0.69	1.71	0.64	2.67	0.72	3.75	0.73
Fxd-Long	99.00	0.00	99.00	0.00	99.00	0.00	99.00	0.00
Fxd-Tran	99.00	0.00	99.00	0.00	99.00	0.00	99.00	0.00
Exp-Long	3.18	0.84	99.00	0.00	99.00	0.00	99.00	0.00
Exp-Tran	99.00	0.00	99.00	0.00	99.00	0.00	99.00	0.00
Ab-Pass	99.00	0.00	99.00	0.00	99.00	0.00	99.00	0.00
Ab-Act	0.51	0.82	2.04	1.01	99.00	0.00	99.00	0.00
Ab-Tran	0.49	0.76	1.50	0.90	2.69	0.86	99.00	0.00

Table G-27: Component Fragilities for MSSS Slab Bridge Components - PGA (Wen).

	Slight		Moderate		Extensive		Complete	
Component	**Med (g)**	**Disp**	**Med (g)**	**Disp**	**Med (g)**	**Disp**	**Med (g)**	**Disp**
Column	0.59	0.64	0.86	0.60	1.29	0.67	1.77	0.68
Fxd-Long	1.84	0.71	99.00	0.00	99.00	0.00	99.00	0.00
Fxd-Tran	99.00	0.00	99.00	0.00	99.00	0.00	99.00	0.00
Exp-Long	0.79	0.57	1.76	0.55	2.09	0.56	2.54	0.59
Exp-Tran	99.00	0.00	99.00	0.00	99.00	0.00	99.00	0.00
Ab-Pass	3.79	0.83	99.00	0.00	99.00	0.00	99.00	0.00
Ab-Act	0.19	0.86	0.69	1.02	1.37	0.98	99.00	0.00
Ab-Tran	0.36	0.94	1.48	1.11	3.08	1.06	99.00	0.00

Table G-28: Component Fragilities for MSSS Slab Bridge Components - S_{a-gm} (Wen).

	Slight		Moderate		Extensive		Complete	
Component	**Med (g)**	**Disp**	**Med (g)**	**Disp**	**Med (g)**	**Disp**	**Med (g)**	**Disp**
Column	1.28	0.80	2.15	0.73	3.74	0.84	99.00	0.00
Fxd-Long	99.00	0.00	99.00	0.00	99.00	0.00	99.00	0.00
Fxd-Tran	99.00	0.00	99.00	0.00	99.00	0.00	99.00	0.00
Exp-Long	2.09	0.88	99.00	0.00	99.00	0.00	99.00	0.00
Exp-Tran	99.00	0.00	99.00	0.00	99.00	0.00	99.00	0.00
Ab-Pass	99.00	0.00	99.00	0.00	99.00	0.00	99.00	0.00
Ab-Act	0.24	1.47	1.80	1.70	99.00	0.00	99.00	0.00
Ab-Tran	0.63	1.26	99.00	0.00	99.00	0.00	99.00	0.00

G.7 MSSS Steel

This section contains the component fragility curves for the multi-span simply supported steel girder bridge.

Table G-29: Component Fragilities for MSSS Steel Bridge Components - PGA (Rix).

	Slight		Moderate		Extensive		Complete	
Component	**Med (g)**	**Disp**	**Med (g)**	**Disp**	**Med (g)**	**Disp**	**Med (g)**	**Disp**
Column	0.38	0.54	0.53	0.50	0.76	0.56	1.00	0.57
Fxd-Long	0.28	0.46	0.47	0.46	0.64	0.49	1.25	0.53
Fxd-Tran	0.45	0.48	0.83	0.48	1.19	0.53	2.64	0.57
Exp-Long	0.27	0.59	0.57	0.56	0.70	0.59	0.89	0.62
Exp-Tran	0.58	0.46	1.32	0.46	2.12	0.54	99.00	0.00
Ab-Pass	1.64	0.65	99.00	0.00	99.00	0.00	99.00	0.00
Ab-Act	1.00	1.02	99.00	0.00	99.00	0.00	99.00	0.00
Ab-Tran	1.29	0.84	99.00	0.00	99.00	0.00	99.00	0.00

Table G-30: Component Fragilities for MSSS Steel Bridge Components - S_{a-gm} (Rix).

	Slight		Moderate		Extensive		Complete	
Component	**Med (g)**	**Disp**	**Med (g)**	**Disp**	**Med (g)**	**Disp**	**Med (g)**	**Disp**
Column	0.70	0.65	0.99	0.61	1.43	0.67	1.90	0.67
Fxd-Long	0.49	0.42	0.80	0.42	1.07	0.45	2.02	0.49
Fxd-Tran	0.70	0.39	1.21	0.39	1.65	0.43	3.31	0.47
Exp-Long	0.48	0.68	1.06	0.66	1.30	0.68	1.65	0.71
Exp-Tran	0.95	0.37	2.03	0.37	3.13	0.45	99.00	0.00
Ab-Pass	2.98	0.70	99.00	0.00	99.00	0.00	99.00	0.00
Ab-Act	1.67	0.96	99.00	0.00	99.00	0.00	99.00	0.00
Ab-Tran	1.99	0.76	99.00	0.00	99.00	0.00	99.00	0.00

Table G-31: Component Fragilities for MSSS Steel Bridge Components - PGA (Wen).

	Slight		Moderate		Extensive		Complete	
Component	**Med (g)**	**Disp**	**Med (g)**	**Disp**	**Med (g)**	**Disp**	**Med (g)**	**Disp**
Column	0.54	0.52	0.76	0.47	1.09	0.54	1.43	0.55
Fxd-Long	0.32	0.43	0.58	0.43	0.81	0.47	1.72	0.52
Fxd-Tran	0.41	0.48	0.70	0.48	0.95	0.51	1.91	0.55
Exp-Long	0.39	0.64	0.88	0.61	1.09	0.63	1.39	0.67
Exp-Tran	0.60	0.50	1.48	0.50	2.50	0.58	99.00	0.00
Ab-Pass	3.04	0.69	99.00	0.00	99.00	0.00	99.00	0.00
Ab-Act	0.96	1.08	99.00	0.00	99.00	0.00	99.00	0.00
Ab-Tran	2.37	1.08	99.00	0.00	99.00	0.00	99.00	0.00

Table G-32: Component Fragilities for MSSS Steel Bridge Components - S_{a-gm} (Wen).

	Slight		Moderate		Extensive		Complete	
Component	**Med (g)**	**Disp**	**Med (g)**	**Disp**	**Med (g)**	**Disp**	**Med (g)**	**Disp**
Column	1.53	0.86	2.67	0.79	99.00	0.00	99.00	0.00
Fxd-Long	0.56	0.66	1.40	0.66	2.36	0.73	99.00	0.00
Fxd-Tran	0.81	0.60	1.80	0.60	2.84	0.66	99.00	0.00
Exp-Long	0.78	0.77	2.41	0.72	3.23	0.75	99.00	0.00
Exp-Tran	2.18	1.02	99.00	0.00	99.00	0.00	99.00	0.00
Ab-Pass	99.00	0.00	99.00	0.00	99.00	0.00	99.00	0.00
Ab-Act	99.00	0.00	99.00	0.00	99.00	0.00	99.00	0.00
Ab-Tran	99.00	0.00	99.00	0.00	99.00	0.00	99.00	0.00

Table G-33: Component Fragilities for MSSS Steel Bridge Components - PGA (No Rot).

	Slight		Moderate		Extensive		Complete	
Component	**Med (g)**	**Disp**	**Med (g)**	**Disp**	**Med (g)**	**Disp**	**Med (g)**	**Disp**
Column	0.39	0.52	0.54	0.48	0.78	0.55	1.02	0.55
Fxd-Long	0.27	0.46	0.46	0.46	0.63	0.49	1.26	0.53
Fxd-Tran	0.43	0.58	0.79	0.58	1.12	0.62	2.43	0.66
Exp-Long	0.27	0.57	0.57	0.55	0.69	0.57	0.87	0.60
Exp-Tran	0.60	0.50	1.44	0.50	2.38	0.58	99.00	0.00
Ab-Pass	1.70	0.65	99.00	0.00	99.00	0.00	99.00	0.00
Ab-Act	0.92	0.96	99.00	0.00	99.00	0.00	99.00	0.00
Ab-Tran	1.27	0.86	99.00	0.00	99.00	0.00	99.00	0.00

Table G-34: Component Fragilities for MSSS Steel Bridge Components - S_{a-gm} (No Rot).

	Slight		Moderate		Extensive		Complete	
Component	**Med (g)**	**Disp**	**Med (g)**	**Disp**	**Med (g)**	**Disp**	**Med (g)**	**Disp**
Column	0.71	0.63	1.00	0.59	1.46	0.65	1.93	0.66
Fxd-Long	0.48	0.50	0.82	0.50	1.11	0.53	2.20	0.56
Fxd-Tran	0.72	0.39	1.27	0.39	1.75	0.43	3.57	0.48
Exp-Long	0.49	0.69	1.07	0.67	1.31	0.68	1.66	0.72
Exp-Tran	0.95	0.39	2.04	0.39	3.18	0.46	99.00	0.00
Ab-Pass	3.14	0.71	99.00	0.00	99.00	0.00	99.00	0.00
Ab-Act	1.66	0.98	99.00	0.00	99.00	0.00	99.00	0.00
Ab-Tran	2.02	0.80	99.00	0.00	99.00	0.00	99.00	0.00

Table G-35: Component Fragilities for MSSS Steel Bridge Components - PGA (Longitudinal).

	Slight		Moderate		Extensive		Complete	
Component	**Med (g)**	**Disp**	**Med (g)**	**Disp**	**Med (g)**	**Disp**	**Med (g)**	**Disp**
Column	0.63	0.25	0.73	0.23	0.87	0.27	0.99	0.27
Fxd-Long	0.57	0.27	0.73	0.27	0.83	0.28	1.13	0.30
Exp-Long	0.53	0.29	0.77	0.28	0.85	0.29	0.96	0.30
Ab-Pass	1.30	0.33	2.05	0.33	3.88	0.29	3.88	0.29
Ab-Act	1.04	0.48	2.13	0.57	3.10	0.55	99.00	0.00

Table G-36: Component Fragilities for MSSS Steel Bridge Components - S_{a-gm} (Longitudinal).

	Slight		Moderate		Extensive		Complete	
Component	**Med (g)**	**Disp**	**Med (g)**	**Disp**	**Med (g)**	**Disp**	**Med (g)**	**Disp**
Column	0.71	0.60	0.98	0.56	1.39	0.62	1.82	0.63
Fxd-Long	0.57	0.58	0.93	0.58	1.22	0.60	2.25	0.63
Exp-Long	0.50	0.64	1.07	0.61	1.30	0.63	1.64	0.66
Ab-Pass	3.13	0.72	99.00	0.00	99.00	0.00	99.00	0.00
Ab-Act	1.98	1.00	99.00	0.00	99.00	0.00	99.00	0.00

G.8 SS Concrete

This section contains the component fragility curves for the single-span concrete girder bridge.

Table G-37: Component Fragilities for SS Concrete Bridge Components - PGA (Rix).

	Slight		Moderate		Extensive		Complete	
Component	**Med (g)**	**Disp**	**Med (g)**	**Disp**	**Med (g)**	**Disp**	**Med (g)**	**Disp**
Fxd-Long	99.00	0.00	99.00	0.00	99.00	0.00	99.00	0.00
Fxd-Tran	99.00	0.00	99.00	0.00	99.00	0.00	99.00	0.00
Exp-Long	99.00	0.00	99.00	0.00	99.00	0.00	99.00	0.00
Exp-Tran	99.00	0.00	99.00	0.00	99.00	0.00	99.00	0.00
Ab-Pass	99.00	0.00	99.00	0.00	99.00	0.00	99.00	0.00
Ab-Act	2.16	1.10	99.00	0.00	99.00	0.00	99.00	0.00
Ab-Tran	2.45	1.06	99.00	0.00	99.00	0.00	99.00	0.00

Table G-38: Component Fragilities for SS Concrete Bridge Components - S_{a-gm} (Rix).

	Slight		Moderate		Extensive		Complete	
Component	**Med (g)**	**Disp**	**Med (g)**	**Disp**	**Med (g)**	**Disp**	**Med (g)**	**Disp**
Fxd-Long	99.00	0.00	99.00	0.00	99.00	0.00	99.00	0.00
Fxd-Tran	99.00	0.00	99.00	0.00	99.00	0.00	99.00	0.00
Exp-Long	99.00	0.00	99.00	0.00	99.00	0.00	99.00	0.00
Exp-Tran	99.00	0.00	99.00	0.00	99.00	0.00	99.00	0.00
Ab-Pass	99.00	0.00	99.00	0.00	99.00	0.00	99.00	0.00
Ab-Act	2.94	0.86	99.00	0.00	99.00	0.00	99.00	0.00
Ab-Tran	3.13	0.81	99.00	0.00	99.00	0.00	99.00	0.00

Table G-39: Component Fragilities for SS Concrete Bridge Components - PGA (Wen).

	Slight		Moderate		Extensive		Complete	
Component	**Med (g)**	**Disp**	**Med (g)**	**Disp**	**Med (g)**	**Disp**	**Med (g)**	**Disp**
Fxd-Long	0.66	0.93	2.10	0.90	2.67	0.92	3.56	0.95
Fxd-Tran	99.00	0.00	99.00	0.00	99.00	0.00	99.00	0.00
Exp-Long	0.62	0.94	2.11	0.91	2.72	0.93	3.68	0.97
Exp-Tran	1.46	1.41	99.00	0.00	99.00	0.00	99.00	0.00
Ab-Pass	99.00	0.00	99.00	0.00	99.00	0.00	99.00	0.00
Ab-Act	2.62	1.38	99.00	0.00	99.00	0.00	99.00	0.00
Ab-Tran	1.38	1.04	99.00	0.00	99.00	0.00	99.00	0.00

Table G-40: Component Fragilities for SS Concrete Bridge Components - S_{a-gm} (Wen).

	Slight		Moderate		Extensive		Complete	
Component	**Med (g)**	**Disp**	**Med (g)**	**Disp**	**Med (g)**	**Disp**	**Med (g)**	**Disp**
Fxd-Long	1.82	1.69	99.00	0.00	99.00	0.00	99.00	0.00
Fxd-Tran	99.00	0.00	99.00	0.00	99.00	0.00	99.00	0.00
Exp-Long	1.48	1.60	99.00	0.00	99.00	0.00	99.00	0.00
Exp-Tran	99.00	0.00	99.00	0.00	99.00	0.00	99.00	0.00
Ab-Pass	99.00	0.00	99.00	0.00	99.00	0.00	99.00	0.00
Ab-Act	99.00	0.00	99.00	0.00	99.00	0.00	99.00	0.00
Ab-Tran	99.00	0.00	99.00	0.00	99.00	0.00	99.00	0.00

G.9 SS Steel

This section contains the component fragility curves for the single-span steel girder bridge.

Table G-41: Component Fragilities for SS Steel Bridge Components - PGA (Rix).

	Slight		Moderate		Extensive		Complete	
Component	**Med (g)**	**Disp**	**Med (g)**	**Disp**	**Med (g)**	**Disp**	**Med (g)**	**Disp**
Fxd-Long	0.81	0.60	1.43	0.60	1.99	0.63	99.00	0.00
Fxd-Tran	1.72	0.73	3.43	0.73	99.00	0.00	99.00	0.00
Exp-Long	1.34	0.54	2.13	0.53	2.41	0.54	2.78	0.55
Exp-Tran	1.01	0.75	2.07	0.75	3.12	0.79	99.00	0.00
Ab-Pass	99.00	0.00	99.00	0.00	99.00	0.00	99.00	0.00
Ab-Act	2.11	0.86	99.00	0.00	99.00	0.00	99.00	0.00
Ab-Tran	2.80	1.06	99.00	0.00	99.00	0.00	99.00	0.00

Table G-42: Component Fragilities for SS Steel Bridge Components - S_{a-gm} (Rix).

	Slight		Moderate		Extensive		Complete	
Component	**Med (g)**	**Disp**	**Med (g)**	**Disp**	**Med (g)**	**Disp**	**Med (g)**	**Disp**
Fxd-Long	1.05	0.47	1.78	0.47	2.42	0.50	99.00	0.00
Fxd-Tran	1.97	0.55	3.66	0.55	99.00	0.00	99.00	0.00
Exp-Long	1.78	0.46	2.79	0.44	3.13	0.45	3.60	0.47
Exp-Tran	1.26	0.60	2.41	0.60	3.51	0.64	99.00	0.00
Ab-Pass	99.00	0.00	99.00	0.00	99.00	0.00	99.00	0.00
Ab-Act	2.70	0.80	99.00	0.00	99.00	0.00	99.00	0.00
Ab-Tran	2.93	0.85	99.00	0.00	99.00	0.00	99.00	0.00

Table G-43: Component Fragilities for SS Steel Bridge Components - PGA (Wen).

	Slight		Moderate		Extensive		Complete	
Component	**Med (g)**	**Disp**	**Med (g)**	**Disp**	**Med (g)**	**Disp**	**Med (g)**	**Disp**
Fxd-Long	0.71	0.57	1.27	0.57	1.77	0.60	3.70	0.64
Fxd-Tran	1.63	1.05	3.60	1.05	99.00	0.00	99.00	0.00
Exp-Long	1.51	0.62	2.56	0.61	2.94	0.62	3.46	0.63
Exp-Tran	0.62	0.63	1.14	0.63	1.61	0.66	3.49	0.69
Ab-Pass	99.00	0.00	99.00	0.00	99.00	0.00	99.00	0.00
Ab-Act	1.47	0.81	3.88	0.91	99.00	0.00	99.00	0.00
Ab-Tran	3.60	1.34	99.00	0.00	99.00	0.00	99.00	0.00

Table G-44: Component Fragilities for SS Steel Bridge Components - S_{a-gm} (Wen).

	Slight		Moderate		Extensive		Complete	
Component	**Med (g)**	**Disp**	**Med (g)**	**Disp**	**Med (g)**	**Disp**	**Med (g)**	**Disp**
Fxd-Long	3.63	1.44	99.00	0.00	99.00	0.00	99.00	0.00
Fxd-Tran	99.00	0.00	99.00	0.00	99.00	0.00	99.00	0.00
Exp-Long	99.00	0.00	99.00	0.00	99.00	0.00	99.00	0.00
Exp-Tran	2.76	1.46	99.00	0.00	99.00	0.00	99.00	0.00
Ab-Pass	99.00	0.00	99.00	0.00	99.00	0.00	99.00	0.00
Ab-Act	99.00	0.00	99.00	0.00	99.00	0.00	99.00	0.00
Ab-Tran	99.00	0.00	99.00	0.00	99.00	0.00	99.00	0.00

References

AASHTO (1998). *AASHTO LRFD Bridge Design Specifications*. American Association of State Highway and Transportation Officials, Washington, D.C.

Abrahamson, N. A. (1988). "Statistical Properties of Peak Ground Accelerations Recorded by the SMART 1 Array." *Bulletin of the Seismological Society of America*, 78(1), 26–41.

Ala Saadeghvaziri, M. and Rashidi, S. (1998). "Effect of Steel Bearings on Seismic Response of Bridges in Eastern United States." *6th US National Conference on Earthquake Engineering*, Seattle, WA. EERI.

Ang, A. H.-S. and Tang, W. H. (1975). *Probability Concepts in Engineering Planning and Design*, Vol. I. John Wiley and Sons, New York.

ATC (1985). "Earthquake Damage Evaluation Data for California." *Report No. ATC-13*, Applied Technology Council.

ATC (1991). "Seismic Vulnerability and Impact of Disruption of Lifelines in the Conterminous United States." *Report No. ATC-25*, Applied Technology Council.

Atkinson, G. M. and Boore, D. M. (1995). "Ground motion relations for Eastern North America." *Bulletin of the Seismological Society of America*, 85(1), 17.

Ayyub, B. M. and Lai, K.-L. (1989). "Structural Reliability Assessment Using Latin Hypercube Sampling." *Proceedings of ICOSSAR '89, the 5th International Conference on Structural Safety and Reliability, Part II*, Vol. Part II, San Francisco, CA, USA. ASCE, p 1177–1184.

Baker, J. and Cornell, A. C. (2005a). "Correlation of response spectral values for multicomponent ground motions." *Bulletin of the Seismological Society of America* (In Press).

Baker, J. and Cornell, A. C. (2005b). "A Vector-Valued Ground Motion Intensity Measure Consisting of Spectral Acceleration and Epsilon." *Earthquake Engineering and Structural Dynamics*, 34(10), 1193–1217.

Baker, J. and Cornell, A. C. (2005c). "Which Spectral Acceleration Are You Using?." *Earthquake Spectra* (In Press).

Basoz, N. and Kiremidjian, A. S. (1999). "Development of Empirical Fragility Curves for Bridges." *5th US Conference on Lifeline Earthquake Engineering*, Seattle, WA, USA. ASCE.

Basoz, N. and Kiremidjian, Anne, S. (1996). "Risk Assessment for Highway Transportation Systems." *Report No. NCEER-118*, JohnA. Blume Earthquake Engineering Center.

Basoz, N. and Kiremidjian, Anne, S. (1997). "Evaluation of Bridge Damage Data From the Loma Prieta and Northridge, CA Earthquakes." *Report No. MCEER-98-0004*, MCEER.

Bavirisetty, R., Vinayagamoorthy, M., and Duan, L. (2000). "Dynamic Analysis." *Bridge Engineering Handbook*, W.-F. Chen and L. Duan, eds., CRC Press.

Bignell, J. L., Lafave, J. M., Wilkey, J. P., and Hawkins, N. M. (2004). "Seismic Evaluation of Vulnerable Highway Bridges with Wall Piers on Emergency Routes in Southern Illinois." *13th World Conference on Eartquake Engineering*, Vancouver, B.C. Canada.

Boore, D. M. (1983). "Stochastic Simulation of High-Frequency Ground Motions Based on Seismological Models of the Radiated Spectra." *Bulletin of the Seismological Society of America*, 73(6), 1865–1894.

Caltrans (1990). *Caltrans Structures Seismic Design References*. California Department of Transportation, Sacramento, CA, first edition.

Caltrans (1999). *Caltrans Seismic Design Criteria*. California Department of Transportation, Sacramento, CA, first edition.

Chang, S. E. and Nojima, N. (1998). "Measuring Lifeline System Performance: Highway Transportation Systems in Recent Earthquakes." *6th US National Conference on Earthquake Engineering*, Seattle, WA. EERI.

Cheng, F. Y., Lou, K. Y., and Sheng, L. H. (1998). "Collapse Studies of Freeway Bridges During the Northridge Earthquake." *6th US National Conference on Earthquake Engineering*, Seattle, WA. EERI.

Choi, E. (2002). "Seismic Analysis and Retrofit of Mid-America Bridges," PhD thesis, Georgia Institute of Technology.

Choi, E., DesRoches, R., and Nielson, B. (2004). "Seismic Fragility of Typical Bridges in Moderate Seismic Zones." *Engineering Structures*, 26(2), 187–199.

Chopra, A. K. (2000). *Dynamics of Structures*. Prentice Hall, Upper Saddle River, NJ, second edition.

Cornell, A. C., Jalayer, F., and Hamburger, R. O. (2002). "Probabilistic Basis for 2000 SAC Federal Emergency Management Agency Steel Moment Frame Guidelines." *Journal of Structural Engineering*, 128(4), 526–532.

Der Kiureghian, A. (2002). "Bayesian Methods for Seismic Fragility Assessment of Lifeline Components." *Acceptable Risk Processes: Lifelines and Natural Hazards, Monograph No. 21*, A. D. Kiureghian, ed., Technical Council on Lifeline Earthquake Engineering, ASCE, Reston VA USA.

Drosos, V. A. (2003). "Synthesis of Earthquake Groundmotions for the New Madrid Seismic Zone," Master's, Georgia Institute of Technology.

Dutta, A. (1999). "On Energy Based Seismic Analysis And Design of Highway Bridges," PhD thesis, State University of New York at Buffalo.

EERI (1995a). "The Hyogo-Ken Nanbu Earthquake Reconnaissance Report." *Report No. 95-04*, Earthquake Engineering Research Institute.

EERI (1995b). "Northridge Earthquake of January 17, 1994 - Reconnaissance Report." *Report No. 95-03*, Earthquake Engineering Research Institute.

Ellingwood, B. and Hwang, H. (1985). "Probabilistic Descriptions of Resistance of Safety-Related Structures in Nuclear Plants." *Nuclear Engineering and Design*, 88(2), 169–178.

Ellingwood, B. R. and Wen, Y.-K. (2005). "Risk-Benefit-Based Design Decisions for Low-Probability/High Consequence Earthquake Events in Mid-America." *Progress in Structural Engineering and Materials*, 7(2), 56–70.

Elnashai, A., Borzi, B., and Vlachos, S. (2004). "Deformation-Based Vulnerability Functions for RC Bridges." *Structural Engineering and Mechanics*, 17(2), 215–244.

Ezeldin, A. S. (2001). "Pile Foundations." *Practical Foundation Engineering Handbook*, R. W. Brown, ed., McGraw-Hill.

Fang, J., Li, Q., Jeary, A., and Liu, D. (1999). "Damping of Tall Buildings: Its Evaluation and Probabilistic Characteristics." *Structural Design of Tall Buildings*, 8(2), 145–153.

Fellenius, B. H. (1991). "Pile Foundations." *Foundation Engineering Handbook*, H.-Y. Fang, ed., Van Nostrand Reinhold.

FEMA (1997). *HAZUS 97: Technical Manual*. Federal Emergency Management Agency, Washington DC.

FEMA (2003). *HAZUS-MH MR1: Technical Manual*, Vol. Earthquake Model. Federal Emergency Management Agency, Washington DC.

FHWA (1994). "National Bridge Inspection Standards." *Report No. Sec. 650.301*, Federal Highway Administration.

FHWA (1995a). *Recording and Coding Guide for the Structure Inventory and Appraisal of the Nation's Bridges*, Vol. FHWA-PD-96-001. Office of Engineering Bridge Devision, Federal Highway Administration, McLean, VA.

FHWA (1995b). *Seismic Retrofitting Manual for Highway Bridges*, Vol. FHWA-RD-94-052. Office of Engineering and Highway Operations R&D, Federal Highway Administration, McLean, VA.

FHWA (2002). "National Bridge Inventory Data.

Giovenale, P., Cornell, A. C., and Esteva, L. (2004). "Comparing the Adequacy of Alternative Ground Motion Intensity Measures for the Estimation of Structural Responses." *Earthquake Engineering & Structural Dynamics*, 33, 951979.

Goel, R. K. (1997). "Earthquake Characteristics of Bridges with Integral Abutments." *Journal of Structural Engineering*, 123(11), 1435–1443.

Goel, R. K. and Chopra, A. K. (1997). "Evaluation of Bridge Abutment Capacity and Stiffness During Earthquake." *Earthquake Spectra*, 13(1), 1–21.

Harney, H. L. (2003). *Bayesian Inference: Parameter Estimation and Decisions*. Springer, Berlin, Germany, first edition.

Haukaas, T. (2003). "Finite Element Reliability and Sensitivity Methods for Performance-Based Engineering," PhD thesis, University of California, Berkeley.

Hayter, A. (2002). *Probability and Statistics for Engineers and Scientists*. Duxbury, Pacific Grove, second edition.

Herrmann, R. B. and Akinci, A. (1999). "Mid-America Ground Motion Models" `http://www.eas.slu.edu/People/RBHerrmann/MAEC/maecgnd.html`, Date Accessed: August 15, 2005.

Hwang, H. and Huo, J. R. (1998). "Probabilistic Seismic Damage Assessment of Highway Bridges." *6th US National Conference on Earthquake Engineering*, Seattle, WA. EERI.

Hwang, H., Jernigan, J. B., and Lin, Y.-W. (2000). "Evaluation of Seismic Damage to Memphis Bridges and Highway Systems." *Journal of Bridge Engineering*, 5(4), p 322–330.

Hwang, H., Liu, J. B., and Chiu, Y.-H. (2000). "Seismic Fragility Analysis of Highway Bridges." *Report No. MAEC RR-4*, Center for Earthquake Research Informaion.

Iman, R. L. and Conover, W. J. (1980). "Small Sample Sensitivity Analysis Techniques for Computer Models, With an Application to Risk Assessment." *Communication Statistics*, A9(17), 1749–1842.

Imbsen, R. A. and Nutt, R. V. (1981). "Increased Seismic Resistance of Highway Bridges Using Improved Bearing Design Concepts." *Dynamic Response of Structures–Experimentation, Observation, Prediction, and Control*, Atlanta, GA. ASCE, pages 416–430.

Jacob, K. H. (1992). "Seismic Hazards in the Eastern U.S. and the Impact on Transportation Lifelines." *Lifeline Earthquake Engineering in the Central and Eastern U.S., Monograph No. 5*, New York, NY. ASCE.

Jernigan, J. B. and Hwang, H. (2002). "Development of Bridge Fragility Curves." *7th US National Conference on Earthquake Engineering*, Boston, Mass. EERI.

Johnston, A. C. and Schweig, E. S. (1996). "Enigma of the New Madrid Earthquakes of 1811-1812." *Annual Review of Earth and Planetary Sciences*, 24, 339.

Kameda, H. (2000). "Engineering Management of Lifeline Systems Under Earthquake Risk." *12th World Conference on Eartquake Engineering*, Auckland, New Zealand. New Zealand Society for Earthquake Engineering.

Karantzikis, M. J. and Spyrakos, C. C. (2000). "Seismic Analysis of Bridges Including Soil-Abutment Interaction." *12th World Conference on Earthquake Engineering*, Vol. 33.

Karim, K. R. and Yamazaki, F. (2001). "Effect of Earthquake Ground Motions on Fragility Curves of Highway Bridge Piers Based on Numerical Simulation." *Earthquake Engineering and Structural Dynamics*, 30(12), 1839–1856.

Keaton, J. R., Zeng, Y., and Anderson, J. G. (2000). "Procedure for Scaling Earthquake Records to Match Acceleration Response Spectra for Engineering Design." *Proceedings, 6th International Conference on Seismic Zonation*. Earthquake Engineering Research Institute.

Kim, S.-H. and Shinozuka, M. (2004). "Development of Fragility Curves of Bridges Retrofitted by Column Jacketing." *Proabilistic Engineering Mechanics*, 19, 105–112.

King, S. A., Kiremidjian, A. S., Basoz, N., Law, K., Vucetic, M., Doroudian, M., Olson, R. A., Eidinger, J. M., Goettel, K. A., and Horner, G. (1997). "Methodologies for Evaluating the Socio-Economic Consequences of Large Earthquakes." *Earthquake Spectra*, 13(4), 565–584.

Kottegoda, N. T. and Rosso, R. (1997). *Statistics, Probability, and Reliability for Civil and Environmental Engineers*. The McGraw-Hill Companies, Inc.

Ma, Y. and Deng, N. (2000). "Deep Foundations." *Bridge Engineering Handbook*, W.-F. Chen and L. Duan, eds., CRC Press.

Mackie, K. and Stojadinovic, B. (2001). "Probabilistic Seismic Demand Model for California Bridges." *Journal of Bridge Engineering*, 6(6), 468–480.

Mackie, K. and Stojadinovic, B. (2003). "Seismic Demands for Performance-Based Design of Bridges." *Report No. PEER 312*.

Mackie, K. and Stojadinovic, B. (2004). "Fragility Curves for Reinforced Concrete Highway Overpass Bridges." *13th World Conference on Eartquake Engineering*, Vancouver, B.C. Canada.

Mander, J. B. and Basoz, N. (1999). "Seismic Fragility Curve Theory for Highway Bridges." *5th US Conference on Lifeline Earthquake Engineering*, Seattle, WA, USA. ASCE.

Mander, J. B., Kim, D. K., Chen, S. S., and Premus, G. J. (1996). "Response of Steel Bridge Bearings to the Reversed Cyclic Loading." *Report No. NCEER 96-0014*, NCEER.

Mander, J. B., Priestley, M. J. N., and Park, R. (1988). "Observed Stress-Strain Behavior of Confined Concrete." *Journal of Structural Engineering*, 114(8), 1827–1849.

Maroney, B., Kutter, B., Romstad, K., Chai, Y. H., and Vanderbilt, E. (1994). "Interpretation of Large Scale Bridge Abutment Test Results." *Proceedings of 3rd Annual Seismic Research Workshop*, Sacramento, CA. Caltrans.

Maroney, B., Romstad, K., and Kutter, B. (1993). "Experimental Testing of Laterally Loaded Large Scale Bridge Abutments." *Structural Engineering in Natural Hazards Mitigation*, Irvine, CA. ASCE.

Martin, G. R. and Yan, L. (1995). "Modeling Passive Earth Pressure for Bridge Abutments." *Earthquake-Induced Movements and Seismic Remediation of Existing Foundations and Abutments, ASCE 1995 Annual National Convention*, Vol. Geotechnical Special Publication 55, San Diego, CA. ASCE.

Mathworks (2004). *Matlab: Language of Technical Computing*. Mathworks, New York, NY, r14 edition.

MCEER (1999). "Highway Bridge Retrofit Manual." *Report No. 106-G-2.2*, Multidisciplinary Center for Earthquake Engineering Research.

McKenna, F. and Feneves, G. L. (2005). "Open System for Earthquake Engineering Simulation" Pacific Earthquake Engineering Research Center, Version 1.6.2.

Melchers, R. E. (2001). *Structural Reliability Analysis and Prediction*. John Wiley & Sons Ltd., West Sussex, England, second edition.

Mosleh, A. and Apostolakis, G. (1986). "The Assessment of Probability Distributions from Expert Opinions with an Application to Seismic Fragility Curves." *Risk Analysis*, 6(4), 447–461.

Muthukumar, S. (2003). "A Contact Element Approach with Hysteresis Damping for the Analysis and Design of Pounding in Bridges," Dissertation, Georgia Institute of Technology.

Nateghi, F. and Shahsavar, V. L. (2004). "Development of Fragility and Reliability Curves for Seismic Evaluation of a Major Prestressed Concrete Bridge." *13th World Conference on Eartquake Engineering*, Vancouver, B.C. Canada.

Nielson, B. G. and DesRoches, R. (2004). "Improved Methodology for Generation of Analytical Fragility Curves for Highway Bridges." *9th ASCE Specialty Conference on Probabilistic Mechanics and Structural Reliability*, Albuquerque, NM. ASCE.

Padgett, J. E. and DesRoches, R. (2005). "Survey of Bridge Inspectors for Highway Bridge Damage-Functionality Relationships." Georgia Institute of Technology, (Unpublished Work).

Park, D. and Hashash, Y. M. A. (2005). "Evaluation of Seismic Site Factors in the Mississippi Embayment. II. Probabilistic Seismic Hazard Analysis with Nonlinear Site Effects." *Soil Dynamics and Earthquake Engineering*, 25(2), 145.

Park, R., Priestley, M. J. N., and Gill, W. D. (1982). "Ductility of Square-Confined Concrete Columns." *Journal of Structural Engineering*, 108(ST4), 929–950.

Phares, B. M., Rolander, D. D., Graybeal, B. A., and Washer, G. A. (2000). "Studying the Reliability of Bridge Inspection." *Public Roads*, 64(3).

Porter, K. (2003). "An Overview of PEER's Performance-Based Earthquake Engineering Methodology." *Applications of Statistics and Probability in Civil Engineering*, San Francisco, CA. CERRA.

Pulkkinen, U. (1993). "Methods for Combination of Expert Judgements." *Reliability Engineering and System Safety*, 40, 111–118.

Ranf, R. T., Eberhard, M. O., and Malone, S. (2003). "Post-Earthquake Prioritization of Bridge Inspections." *Earthquake Spectra*.

Rashidi, S. and Ala Saadeghvaziri, M. (1997). "Seismic Modeling of Multi-Span Simply-Supported Bridges Using ADINA." *Computers and Structures*, 64(5-6), 1025–1039.

Rix, G. J. (2003). "Matlab Script for Spectral Matching a Ground Motion to a Target Response Spectrum" Georgia Insitute of Technology, (Unpublished Work).

Rix, G. J. and Fernandez-Leon, J. A. (2004). "Synthetic Ground Motions for Memphis, TN" `http://www.ce.gatech.edu/research/mae_ground_motion`, Date Accessed: July 2, 2004.

Rojahn, C., Scawthorn, C., Khater, M., and Ballantyne, D. B. (1992). "Transportation Lifeline Losses in Large Eastern Earthquakes." *Lifeline Earthquake Engineering in the Central and Eastern US*, New York, NY, USA. ASCE, p 87–101.

Rossetto, T. and Elnashai, A. (2004). "A New Analytical Procedure for the Derivation of Displacement-Based Vulnerability Curves for Populations of Structures." *13th World Conference on Eartquake Engineering*, Vancouver, B.C. Canada.

SAS (2004). "JMP: Statistical Discovery Software" Cary, NC.

Schrage, I. (1981). "Anchoring of Bearings by Friction." *Joint Sealing and Bearing Systems for Concrete Structures, World Congress on Joints and Bearings*, Vol. 1, Niagara Falls, NY, USA. American Concrete Inst.

Seed, H. B. and Whitman, R. V. (1970). "Design of Earth Retaining Structures for Dynamic Loads." *ASCE, Specialty Conf on Lateral Stresses in Ground and Design of Earth-Retaining Structures*, Ithaca, NY. ASCE, 47.

Sewell, R. T., Toro, G. R., and McGuire, R. K. (1996). "Impact of Ground Motion Characterization on Conservatism and Variability in Seismic Risk Estimates." *Report No. NUREG/CR-6467*, Office of Nuclear Regulatory Research, U.S. Nuclear Regulatory Commission.

Shinozuka, M. (1998). "Development of Bridge Fragility Curves" University of Southern California, (Unpublished Work).

Shinozuka, M., Chang, S., Eguchi, R. T., Abrams, D. P., Hwang, H., and Rose, A. (1997). "Advances in Earthquake Loss Estimation and Application to Memphis, Tennessee." *Earthquake Spectra*, 13(4), 739–758.

Shinozuka, M., Feng, M. Q., Kim, H., Uzawa, T., and Ueda, T. (2003). "Statistical Analysis of Fragility Curves." *Report No. MCEER-03-0002*, MCEER.

Shinozuka, M., Feng, Maria, Q., Kim, H.-K., and Kim, S.-H. (2000). "Nonlinear Static Procedure for Fragility Curve Development." *Journal of Engineering Mechanics*, 126(12), 1287–1296.

Shinozuka, M., Feng, Maria, Q., Lee, J., and Naganuma, T. (2000). "Statistical Analysis of Fragility Curves." *Journal of Engineering Mechanics*, 126(12), 1224–1231.

Song, J. and Ellingwood, B. R. (1999). "Seismic reliability of special moment steel frames with welded connections: II." *Journal of Structural Engineering*, 125(4), 372.

Tonias, D. E. (1995). *Bridge Engineering: Design, Rhabilitation, and Maintenance of Modern Highway Bridges*. McGraw-Hill, Inc., New York, NY.

Tuttle, M. P., Schweig, E. S., Sims, J. D., Lafferty, R. H., Wolf, L. W., and Haynes, M. L. (2002). "The earthquake potential of the New Madrid seismic zone." *Bulletin of the Seismological Society of America*, 92(6), 2080.

USGS (1996). "National Seismic-Hazard Maps: Documentation." *Report No. OFR-96-532*, U.S. Geological Survey.

USGS (2002). "Earthquake Hazard in the Heart of the Homeland." *Fact Sheet FS-131-02*, U.S. Geological Survey.

USGS (2004). "Earthquake Hazards Program Website." `http://earthquake.usgs.gov/`, Date Accessed: August 15, 2005.

Vamvatsikos, D. and Cornell, A. C. (2002). "Incremental Dynamic Analysis." *Earthquake Engineering & Structural Dynamics*, 31, 491–514.

Veneziano, D., Sussman, J. M., Gupta, U., and Kunnumkal, S. M. (2002). "Eartquake Loss Under Limited Transportation Capacity: Assessment, Sensitivity and Remediation." *7th US National Conference on Earthquake Engineering*, Boston, Mass. EERI.

Vintzeleou, E. N. and Tassios, T. P. (1987). "Behavior of Dowels Under Cyclic Deformations." *ACI Structural Journal (American Concrete Institute)*, 84(1), 18–30.

Wald, D., Oppenheimer, D., Gee, L., Benz, H., Leith, W., McCarthy, J., Simpson, R., Schwarz, S., Worden, B., Quitoriano, V., Rico, H., Hauksson, E., Earle, P., and Lystoka, L. (2004). "New Tools from the California Integrated Seismic Network (CISN) and Advanced National Seismic System (ANSS)." *2004 Disaster Resistant California Conference*, Sacramento, CA. The Governor's Office of Emergency Services, California.

Wang, J. (2000). "Piers and Columns." *Bridge Engineering Handbook*, W.-F. Chen and L. Duan, eds., CRC Press.

Wen, Y. K., Ellingwood, B. R., Veneziano, D., and Bracci, J. (2003). "Uncertainty Modeling in Earthquake Engineering." *Report No. MAE-FD-2*, Mid-America Earthquake Center.

Wen, Y. K. and Wu, C. L. (2001). "Uniform Hazard Ground Motions for Mid-America Cities." *Earthquake Spectra*, 17(2), 359–384.

Werner, S. D., Lavoie, J.-P., Eitzel, C., Cho, S., Huyck, C., Ghosh, S., Eguchi, R. T., Taylor, C. E., and Moore II, J. E. (2003). "REDARS 1: Demonstration Software for Seismic Risk Analysis of Highway Systems" `http://mceer.buffalo.edu/publications/resaccom/03-SP01/02werner.pdf`, Date Accessed: November 16, 2005.

Werner, S. D., Taylor, C., and Moore, J. (1997). "Loss Estimation Due to Seismic Risks to Highway Systems." *Earthquake Spectra*, 13(4), 585–604.

Werner, S. D. and Taylor, C. E. (2002). "Component Vulnerability Modeling Issues for Analysis of Seismic Risks to Transportation Lifeline Systems." *Acceptable Risk Processes: Lifelines and Natural Hazards, Monograph No. 21*, S. D. Werner and C. E. Taylor, eds., Technical Council on Lifeline Earthquake Engineering, ASCE, Reston VA USA.

Whitman, R. V., Biggs, J. M., Brennan III, J. E., Cornell, C. A., de Neufville, R. L., and Vanmarcke, E. H. (1975). "Seismic Design Decision Analysis." *Journal of the Structural Division, ASCE*, 101(ST5), 1067–1084.

Wilson, J. C. and Tan, B. S. (1990). "Bridge Abutments. Formulation of Simple Model for Earthquake Response Analysis." *Journal of Engineering Mechanics*, 116(8), 1828–1837.

Wolf, J., P. (1985). *Dynamic Soil-Structure Interaction*. Prentice-Hall, Inc, Englewood Cliffs, N.J.

Wu, C.-F. J. and Hamada, M. (2000). *Experiments: Planning, Analyisis, and Parameter Design Optimization*. John Wiley & Sons, Inc., New York.

Yamazaki, F., Hamada, T., Motoyama, H., and Yamauchi, H. (1999). "Earthquake Damage Assessment of Expressway Bridges in Japan." *Technical Council on Lifeline Earthquake Engineering Monograph*, (16), p 361–370.

Yashinsky, M. (1999). "New Developments in CALTRANS Seismic Analysis and Design Procedures for Bridges." *Seismic Response of Concrete Bridges*, M. Yashinsky, ed., ACI, Farmington Hills, Michigan, 89–130.

Yu, O., Allen, D. L., and Drnevich, V. P. (1991). "Seismic Vulnerability Assessment of Bridges on Earthquake Priority Routes in Western Kentucky." *3rd US Conference on Lifeline Earthquake Engineering*, Los Angeles, CA, USA. ASCE.

VITA

Bryant G. Nielson was born on February 16, 1973 in Cedar City, Utah. Immediately on graduation from High School, he began his undergraduate work at Utah State University. After his first year, there was a hiatus in his studies at USU as he served a two year mission for his church in Los Angeles California. Bryant's undergraduate studies at USU resumed in 1994 resulting in a Bachelor's of Science degree in 1998. He stayed on at USU for graduate work and received his Master's of Science degree in 2000. After working for a small structural design firm – Reeve and Associates – for two years, Bryant continued his graduate work by pursuing a Ph.D. at the Georgia Institute of Technology.